Delayed local delivery of synthetic prostacyclin to modulate inflammatory processes in support of bone regeneration

vorgelegt von

Diplom-Ingenieur, Master of Science

Sebastian Wendler

von der Fakultät III – Prozesswissenschaften

der Technischen Universität Berlin

zur Erlangung des akademischen Grades

Doktor der Ingenieurwissenschaften

– Dr.-Ing. –

genehmigte Dissertation

Promotionsausschuss:

Vorsitzender: Prof. Dr. Peter Neubauer

Gutachter: Prof. Dr. Roland Lauster

Gutachter: Prof. Dr. Georg N. Duda

Gutachter: Prof. Dr. Jens Kurreck

Tag der wissenschaftlichen Aussprache: 18. Oktober 2019

Berlin 2019

Table of contents

I. Danksagung

Allen voran bedanke ich mich bei Prof. Dr. Georg N. Duda für die Möglichkeit meine Doktorarbeit extern an seinem Julius Wolff Institut der Charité durchzuführen. In dieser Zeit konnte ich mich stark weiter entwickeln und bin dankbar für die bedeutsamen Erfahrungen und der Lehre in der Graduiertenschule BSRT, in der er auch mein erster Betreuer war. Ich bedanke mich für konstruktive Diskussionen und die Möglichkeit sogar Einblicke in das Patentwesen zu erhalten.

Mein besonderer Dank gilt auch meinem Doktorvater an der TU-Berlin Prof. Dr. Roland Lauster. Er hat meinen wissenschaftlichen Werdegang stets mit voller Unterstützung begleitet vom Studium der medizinischen Biotechnologie, über die Betreuung meiner Diplomarbeit und nun bis hin zu meiner Doktorarbeit.

Ich bin meinem zweiten Betreuer an der BSRT Prof. Hans-Dieter Volk zutiefst dankbar für die Unterstützung in der immunologischen Fragestellung meines Projekts. Als Direktor des Instituts für Medizinische Immunologie an der Charité war sein unerschöpfliches Wissen essenziel für das Gelingen dieser Arbeit.

Meiner Gruppenleiterin und Mentorin der BSRT Dr. Katharina „Kate“ Schmidt-Bleek kann ich nicht dankbar genug sein. Mit ihrem Optimismus und ihrer Kreativität konnten wir zusammen viele Herausforderung meistern. Ich habe unsere wissenschaftlichen Diskussionen stets mit Freude genossen.

Ein großer Dank gilt auch meiner Arbeitsgruppe – AG Schmidt-Bleek. Nicht nur zahlenmäßig ist die Gruppe über die Jahre gewachsen. Ich bin stolz, dass unser Teamwork sich in vielen gemeinsamen Publikationen zeigt. Insbesondere danke ich für jegliche Unterstützung von Claudia, Christian, Henrik, Norma und Hanna.

Die interdisziplinäre Verzahnung des JWI war beeindruckend und ich danke der AG Wildemann für Benutzung und Unterstützung in der Zellkultur; der AG Petersen im Großraumlabor und beim Staffellauf durch den Tiergarten; AG Geissler, insbesondere Martin für das geduldige Beibringen des Arbeitens mit MSCs; dem Chirurgen Dr. Tobias Winkler für die translationelle Erfahrung in der Zuarbeit für seinen Antrag eines klinischen Versuchs aus meinem Projekt heraus; und Dag für Unterstützung bei der Materialforschung.

Dr. Sabine Bartosch, Janet und Bianca danke ich für die Organisation meiner Bildung in der BSRT.

Mit Rat und Tat sowie einer tollen Arbeitsatmosphäre haben mich durch die herausfordernden Jahre außerdem noch gebracht: Gabriella, Agnes, Evi, die Thiele-Brüder, Paul, Katrein, Eduardo, Clemens, Aline und Julia.

Diese Arbeit war allerdings auch auf externe Kooperationspartner angewiesen, denen mein Dank gilt. Die HPLC-Analyse ermöglichten Prof. Dr. Lorenz Adrian und Jan Birkigt am UFZ in Leipzig und mein

alter Studienfreund Christian Schipp von der TU-Berlin. AG Hauser am DRFZ, Berlin gestattete mir die Nutzung des LSM.

Ohne die Finanzierung der Friede Springer Stiftung und der BSRT wäre das Gelingen dieser Arbeit ebenfalls nicht möglich gewesen und ich bin stolz von diesen Organisationen unterstützt worden zu sein.

Ich bin auch dankbar dafür, dass ich die Studenten Moritz, Tyas und René in ihren ersten wissenschaftlichen Schritten betreuen durfte.

Meine Freunde haben mir auch immer wieder Kraft gegeben. Insbesondere Sandra, Jessi, Christian, Laurent und Emma.

Meine lieben Eltern und meine gesamte Familie hat mir Rückhalt gegeben wann immer ich ihn brauchte und auf den ich mich immer verlassen konnte. Ich danke Euch!

II. Selbständigkeitserklärung

Hiermit erkläre ich, dass ich die hier vorliegende Dissertation selbstständig und eigenhändig und nur unter Verwendung der angegebenen Hilfsmittel und Literaturquellen angefertigt habe.

Ich versichere, dass ich diese Arbeit weder in gleicher noch in ähnlicher Form in anderen Prüfungsverfahren vorgelegt habe.

Ich habe die dem Prüfungsverfahren zu Grunde liegende Promotionsordnung der Fakultät III Prozesswissenschaften der Technischen Universität Berlin zur Kenntnis genommen.

III. Competing interests

On the basis of this work, the Charité *Universitätsklinikum* Berlin, my colleagues and myself have submitted a patent application PCT/EP2018/073453, “Immunmodulation for prevention of poor healing of musculoskeletal injuries in compromised patients”, which is published under WO/2019/043148.

I declare no competing financial interests.

IV. List of abbreviations

%	percent
-/-	homozygous knockout
°C	degrees Celsius
µ	micro
µCT	micro computed tomography
AChE	acetylcholinesterase
AF	Alexa Fluor
ALP	alkaline phosphatase
AM	adipoinductive media or acetoxymethyl ester
APC	allophycocyanin
BM	bone marrow
BMP	bone morphogenic protein
BSA	bovine serum albumin
BV	bone volume
bw	bodyweight
cAMP	cyclic adenosine monophosphate
CD	cluster of differentiation
CM	conditioned media
cmm	cubic millimeters
CO2	carbon dioxide
CSF	colony-stimulating factor
CXCL	C-X-C motif ligand
CXCR	C-X-C motif receptor
DAD	diode array detector
DAPI	4',6-diamidino-2-phenylindole
ddH_2O	double distilled water
DMEM	Dulbecco's modified Eagle's medium
DMSO	dimethyl sulfoxide
dpo	days post osteotomy
e.g.	exempli gratia = for example
ECM	extracellular matrix
EDTA	ethylenediaminetetraacetic acid

eF	eFluor
ELISA	enzyme-linked immunosorbent assay
EM	expansion media
em	emission
et al.	et alii = and others
EtOH	ethanol
ex	excitation
f.	and following
FACS	fluorescence-activated cell sorting
FCS	fetal calf serum
FELASA	Federation of Laboratory Animal Science Associations
h	hours
HA	hydroxyapetite
i.e.	id est = that is
IBMX	3-isobutyl-1-methylxanthine
IFN-γ	interferon gamma
IL	interleukin
IP	prostaglandin I_2 receptor
k	kilo
K	Kelvin
L	liters
Lam	laminin
LPS	lipopolysaccharide
m	milli
M	molar
MACS	magnetic activated cell sorting
mg/kg b.w.	milligram per kilogram body weight
min	minutes
MMPs	matrix metalloproteases
mMSCs	mouse MSCs
MSC	mesenchymal stromal cell
mTOR	mammalian target of rapamycin
n	nano
NaCl	sodium chloride

NSAIDs	nonsteroidal anti-inflammatory drugs
O/N	overnight
OCN	osteocalcin
OM	osteoinductive media
OSX	osterix
P/S	penicillin and streptomycin
Pa	Pascal
PBS	phosphate buffered saline
PBSTW	PBS supplemented with Tween-20
PE	phycoerythrin
PEG	polyethylene glycol
PFA	paraformaldehyde
PGI_2	prostacyclin
PGIS	prostacyclin synthase
PLGA	poly-D, L-lactic-co-glycolic acid
rcf	relative centrifugal force
rh	recombinant human
rm	recombinant murine
ROI	region of interest
RP-HPLC/UV	reversed phase high performance liquid chromatography with UV-detector
RPMI	Roswell Park Memorial Institute medium
RT	room temperature
sec	seconds
TNF-α	tumor necrosis factor alpha
TRIS	tris(hydroxymethyl)aminomethane
TV	total callus volume
UHPLC	ultra high performance liquid chromatography
UV	ultra violet
v/v	volume per volume
VOI	volume of interest

V. List of figures

VI. List of tables

VII. List of formulas

VIII. Abstract

Delayed fracture healing or non-unions are relevant challenges in the clinical setting with a prevalence of more than 10 % of the regeneration outcomes. Autologous bone grafting or local application of growth factors such as bone morphogenic protein 2 (BMP-2) are considered to be current therapeutic gold standards. However, BMP-2 is expansive and over-dosage led to reports of negative side effects resulting in a more restricted application of such additive factors. In particular, for non-critical size defects, alternative methods might be to target those cells that block or alter healing cascades instead of focusing only onto boosting the positive elements of bone formation. A brief and highly regulated secretion of pro-inflammatory molecules is critical to initiate tissue regeneration, which is followed by an anti-inflammatory phase. Only afterwards, the tissue restoration can take place. Hence, elongation of inflammation can lead to delayed fracture healing or even non-unions, indicating immune cells as alternative therapeutic targets.

The hypothesis of this doctoral thesis was that the delayed local application of an anti-inflammatory molecule, such as prostacyclin (PGI_2), shortens the inflammatory phases of bone healing and therefore accelerates the regenerative process.

Application of the synthetic PGI_2 analog Iloprost on CD3/CD28-activated T cells revealed a reduction of pro-inflammatory cytokines such as interferon γ (INF-γ) or tumor necrosis factor α (TNF-α) in a dose dependent manner. In particular, the PGI_2 analog suppressed isolated CD8+ proliferation and cytokine secretion. Furthermore, pro-inflammatory M1-type macrophages were reduced in their activity in response to synthetic PGI_2, whereas anti-inflammatory M2-type macrophages could be further stimulated. Activated T regulatory cells (Treg) could not be stimulated significantly further with the drug. On the contrary, non-stimulated Treg showed higher anti-inflammatory interleukin 10 (IL-10) secretion as a pharmacologic response. Conditioned media were harvested from activated T cells within bone marrow cultures, and from isolated and activated CD8+ cells and Treg. Applied onto osteogenic differentiating mesenchymal stromal cells (MSCs), inhibitory effects of the cytokine-enriched media were detected on mineralization capacity and cell viability. Prior PGI_2-treatment on the immune cell cultures could significantly reduce these inflammatory effects and in particular on cytokine-induced apoptosis. Furthermore, no negative effects of Iloprost were observed neither in osteogenic nor chondrogenic differentiation when directly applied on bone marrow derived MSCs (BM-MSCs). However, proliferative activity was reduced and sporadic adipogenic differentiation occurred with the highest applied dose.

These *in vitro* data indicated that the pro-inflammatory phase at its peak constitutes the optimal pharmacologic target for time-dependent PGI_2 application to accelerate the bone healing process. Since the initial inflammation is necessary to induce the regenerative process, a delayed drug application after fracture was considered crucial for modulating the inflammatory phases. Moreover, the anti-coagulative

PGI_2 could lead to an interference with the early endogenous hematoma formation. To achieve this, a local drug delivery approach was chosen and investigated with medical grade fibrin as a hydrogel-based carrier material. The fibrin matrix was loaded with PGI_2 and a non-loaded shell of fibrin was modulated around it. *In vitro* drug release with *in vivo*-like conditions (37 °C and proteinase K in physiologic solution) was performed and liquid-liquid extracted samples were analyzed with reversed phase high performance liquid chromatography with ultra violet detector (RP-HPLC/UV). Obtained kinetics revealed a delayed drug release of 24 hours with the core-shell system compared to core alone. After complete release of Iloprost, the fibrin matrices collapsed due to degradation.

A non-critical size defect mouse model was used for the proof of concept, which is characterized by a defined fracture gap into which the drug release system was placed. Indeed, significantly increased volumes of newly formed bone were detected in the mouse osteotomy model after 21 days post osteotomy (dpo). Histology revealed more advanced endochondral phases in the PGI_2 treatment group compared to the control. At an earlier time point of 3 dpo fibrin material of the release system was not degraded yet in the fracture gap. In this osteotomy model, 3 dpo is considered subsequent of the peak pro-inflammatory phase, and after 3 days a major amount of PGI_2 was presumably released into the observed area – according to the *in vitro* release kinetics. In fact, at 3 dpo, significantly reduced numbers of CD8+ cells were detected with decelerated PGI_2 release. Moreover, CD8+ cells were inhibited in activity, indicated by double staining for IFN-γ. CD4+ cells, which comprise the Treg fraction, were additionally decreased at 3 dpo after treatment. Analysis of the response of the innate immune cells was again carried out onto macrophage polarization. The impact onto polarization with delayed PGI_2 release was suppression and increase in M1 and M2 macrophages, respectively. Additionally, delayed release of synthetic PGI_2 diminished CD68+ cell fraction, which contains macrophages. Moreover, CD68+TNF-α+ cells were pharmacologically reduced as well.

Taken together, delayed release of synthetic PGI_2 can support fracture healing via immune modulation and constitutes a viable alternative to growth factor applications.

IX. Zusammenfassung

Verzögerte Frakturheilung oder Pseudoarthrosen sind relevante klinische Herausforderungen mit einer Prävalenz von mehr als 10 % in den regenerativen Ergebnissen. Autologe Knochentransplantation oder lokale Applikation von Wachstumsfaktoren, wie *bone morphogenic protein 2* (BMP-2) werden als aktuelle therapeutische Goldstandards angesehen. Jedoch führten die hohen Kosten und Berichte über negative Nebenwirkungen insbesondere bei Überdosierung von BMP-2 zu einer vorsichtigeren Anwendung solch additiver Faktoren. Insbesondere bei nicht-kritischen Defekten könnten alternative Methoden auf diejenigen Zellen abzielen, die die Heilungskaskaden blockieren oder verändern, anstatt lediglich auf die positiven Elemente zur Verstärkung der Knochenbildung zu fokussieren. Eine knappe und stark regulierte Sekretion von proinflammatorischen Molekülen ist kritisch für die Initiierung der Geweberegeneration, welche von einer antiinflammatorischen Phase gefolgt wird. Erst anschließend kann die Geweberestauration geschehen. Deshalb kann eine Verlängerung der Entzündung zu verzögerter Frakturheilung oder gar Nichtvereinigung führen, was Immunzellen als therapeutische Alternative indiziert.

Die Hypothese dieser Doktorarbeit war, dass die verzögerte lokale Freisetzung eines anti-inflammatorischen Moleküls, wie Prostacyclin (PGI_2), die inflammatorische Phasen der Knochenheilung verkürzt und deshalb den regenerativen Prozess beschleunigt.

Anwendung des synthetischen PGI_2-Analogs Iloprost auf CD3/CD28-aktivierte T-Zellen offenbarte eine dosisabhängige Reduktion proinflammatorischer Moleküle, wie Interferon-γ (INF-γ) oder Tumornekrosefaktor-α (TNF-α). Insbesondere unterdrückte das PGI_2-Analog die Proliferation und die Zytokinsekretion isolierter CD8+ Zellen. Darüber hinaus waren proinflammatorische Makrophagen vom M1-Typ in Reaktion auf synthetisches PGI_2 in ihrer Aktivität reduziert, während antiinflammatorische Makrophagen vom M2-Typ zusätzlich stimuliert werden konnten. Aktivierte T-regulatorische Zellen (Treg) konnten mit dem Wirkstoff nicht weiter signifikant stimuliert werden. Im Gegensatz dazu zeigten nicht stimulierte Treg eine höhere entzündungshemmende Sekretion von Interleukin 10 (IL-10) als pharmakologische Reaktion. Konditionierte Medien wurden von aktivierten T-Zellen innerhalb von Knochenmarkskulturen gewonnen, sowie von isolierten CD8+ Zellen und Treg. Auf osteogene Differenzierung von mesenchymalen Stromazellen (MSCs) angewendet, wurden inhibitorische Wirkungen der mit Zytokinen angereicherten Medien auf Mineralisierungskapazität und Zellvitalität nachgewiesen. PGI_2-Vorbehandlung der Immunzellkulturen konnte diese entzündlichen Wirkungen und insbesondere die Zytokin-induzierte Apoptose signifikant reduzieren. Außerdem wurden keine negativen Wirkungen von Iloprost beobachtet, weder in osteogener noch in chondrogener Differenzierung, wenn direkt auf aus Knochenmark stammenden MSCs angewendet. Jedoch war die proliferative Aktivität verringert und sporadische adipogene Differenzierung trat auf mit der höchsten angewendeten Dosis.

Diese *in vitro* Daten zeigten, dass im Knochenheilungsprozess die proinflammatorische Phase zu ihrem Höhepunkt das optimale pharmakologische Ziel für die zeitabhängige Anwendung von PGI_2 darstellt. Da die initiale Entzündung nötig für die Induzierung des regenerativen Prozesses ist, wurde eine verzögerte Wirkstoffapplikation nach der Fraktur als entscheidend für die Modulation der Entzündungsphasen angesehen. Zudem könnte das anti-koagulative PGI_2 zu einer Störung der frühen endogenen Hämatombildung führen. Um dies zu erreichen, wurde ein lokaler Ansatz zur Medikamentenabgabe gewählt und mit medizinischem Fibrin als Trägermaterial auf Hydrogelbasis untersucht. Die Fibrinmatrix wurde mit PGI_2 beladen und um sie herum wurde eine nicht beladene Hülle aus Fibrin moduliert. Die Arzneimittelfreisetzung wurde *in vitro* durchgeführt mit *in-vivo*-ähnlichen Zuständen (37 ° C und Proteinase K in physiologischer Lösung), und flüssig-flüssig extrahierte Proben wurden mit Umkehrphasen-Hochleistungsflüssigkeitschromatographie mit einem Ultraviolett-Detektor (RP-HPLC/UV) analysiert. Die erhaltene Kinetik ergab eine um 24 Sunden verzögerte Medikamentenfreisetzung des Kern-Hülle-Systems im Vergleich zum Kern allein. Nach vollständiger Freisetzung von Iloprost kollabierten die Fibrinmatrizen aufgrund von Auflösungsprozessen.

Für den *Proof-of-Concept* wurde ein nicht kritisches Defektmausmodell verwendet, das durch eine definierte Bruchlücke gekennzeichnet ist, in die das Wirkstofffreisetzungssystem eingebracht wurde. Tatsächlich wurden im Mausosteotomiemodell 21 Tage nach Osteotomie (dpo) signifikant erhöhte Volumina neu gebildeten Knochens nachgewiesen. Die Histologie zeigte im Vergleich zur Kontrolle weiter fortgeschrittene endochondrale Phasen in der PGI_2-Behandlungsgruppe. Zu einem früheren Zeitpunkt von 3 dpo war das Fibrinmaterial des Freisetzungssystems im Frakturspalt noch nicht abgebaut. In diesem Osteotomiemodell wird 3 dpo als Folge der maximalen proinflammatorischen Phase betrachtet, und nachdem vermutlich eine größere Menge an PGI_2 in den beobachteten Bereich freigesetzt worden war – hinsichtlich der *in vitro* Freisetzungskinetik. In der Tat wurde nach 3 dpo eine signifikant verringerte Anzahl von CD8+ Zellen mit verlangsamter PGI_2-Freisetzung nachgewiesen. Darüber hinaus wurde die Aktivität von CD8+ Zellen gehemmt, was durch Doppelfärbung mit IFN-γ angezeigt wird. CD4+ Zellen, die die Treg-Fraktion umfassen, wurden nach der Behandlung bei 3 dpo zusätzlich verringert. Die Analyse der Reaktion der angeborenen Immunzellen wurde erneut anhand von Makrophagenpolarisation durchgeführt. Der Einfluss auf die Polarisation mit verzögerter PGI_2-Freisetzung war entweder Unterdrückung oder Zunahme der M1- oder M2-Makrophagen. Zusätzlich verringerte die verzögerte Freisetzung von synthetischem PGI_2 die CD68+ Zellfraktion, welche Makrophagen beinhaltet. Darüber hinaus wurden CD68+TNF-α+ Zellen auch pharmakologisch reduziert.

Zusammengenommen kann die verzögerte Freisetzung von synthetischem PGI_2 die Frakturheilung durch Immunmodulation unterstützen und stellt eine praktikable Alternative zu Wachstumsfaktoranwendungen dar.

1. Introduction

Regeneration of fractures is the most efficient regenerative process in the human body and does not even leave a scar on the bone tissue. However, in the clinical situation more than 10 % of the patients suffer from delayed fracture healing or even non-unions (Einhorn & Lane 1998; Ryaby 1998; Haas 2000). Especially aged patients show reduced regenerative capacity of fractures (Gruber *et al.* 2006). The geriatric group of fracture patients also bear osteoporosis, which is characterized by reduced bone mass and lower quality in bone structure, which can lead to fractures caused by fragility (Holroyd et al, 2008). Half of these fractures are located in the femoral neck and the patients can be permanently incapacitated. The regeneration time is excessive and during the first year of healing, mortality rates are high as 21 – 36 % in those weak and aged patients (Eisman *et al.* 2012). Current treatment of such medical conditions is often time consuming, painful and leads to a high socioeconomic impact (Pountos *et al.* 2008; Boursinos *et al.* 2009; Zeckey *et al.* 2011). Also in young and healthy patients, extended healing times for injuries of the musculoskeletal apparatus decrease the quality of life, frequently require second interventions, augmented costs for medical care and lead to an increase of absent days from work. Since musculoskeletal injuries, like fractures, represent such a significant burden on society and economy, a better understanding of the underlying processes guiding regeneration is needed for new therapeutic approaches that improve the endogenous healing process of these incidents.

Therapeutic gold standards to support impaired fracture healing are mainly growth factor application and autologous bone grafting for bone fusion or large defects. Regarding pharmacology, bone morphogenic protein 2 (BMP-2) application in bone tissue is approved by the Food and Drug Administration (FDA). However, reports of severe negative side effects are accumulating, i.e. surgical site infections and other wound complications, heterotopic bone formation, erythema, edema, pseudarthrosis and local inflammation (Argintar *et al.* 2011; Woo 2013). Strikingly, a high dose of recombinant human BMP-2/CRM (BMP-2/compression resistant matrix) in lumbar spinal arthrodesis was associated with an increased carcinogenic risk (Carragee *et al.* 2013; Lad *et al.* 2013). In consequence, the FDA had excluded the use of BMPs in patients with a history of cancer. Thus, alternatives are needed that allow to enable bone healing in critical situations or even to prevent delayed healing in challenged patients. Also in case of fragility fractures in osteoporotic bone, there is currently no approved therapy available for enhancement of regeneration (Kanakaris *et al.* 2009). Promising drugs are for instance neutralizing antibodies specific for endogenous inhibitors of Wnt/β-catenin signaling, such as dickkopf-1 and sclerostin. However, the administration is restricted to systemic injections, which can cause severe non-specific mineralized depositions. Moreover, patient's safety could be compromised regarding carcinogenesis and the sealing of osteal foramina (Baron & Hesse 2012).

In recent years, the interplay of the immune system with bone tissue has gained more attention. Historically, the term osteoimmunology derived from research on rheumatoid arthritis (Takayanagi 2005). Recently, lessons from this chronic inflammatory disease motivated studies in fracture healing

with the discovery of surprisingly significant impacts of immune cells and their cytokines onto this regenerative process (Toben *et al.* 2011; Reinke *et al.* 2013; Chan *et al.* 2015).

Therefore, this doctoral thesis aims at describing the design and investigation of an alternative localized approach to accelerate bone healing – immune modulation. Moreover, bone healing can be viewed as a prototype of regeneration and insights into the interaction of steering of inflammation and fracture repair might be applied on other healing processes.

1.1 Bone tissue

Bone is composed of cortical and trabecular bone, cartilage, hematopoietic and connective tissues. In particular, trabecular or spongy bone consists of a lattice of fine bone plates filled with hematopoietic marrow also known as medulla, fat containing marrow or blood vessels (Fig. 1.1 A). Small capillaries and arterioles from arterial vessels span throughout the bone marrow and supply sinusoids, which are interconnected by intersinusoidal capillaries (Kopp *et al.* 2005). In higher vertebrates, the bones are categorized by their shape, i.e. short, long, sesamoid and irregular. During body growth, the diaphysis is primarily elongating with an epiphysis at each end. Long bones, like the femur and tibia in our legs, bear most of the load of healthy skeletal mobility. To enable mobility with connected joints, each epiphysis is covered with hyaline cartilage (articular cartilage).

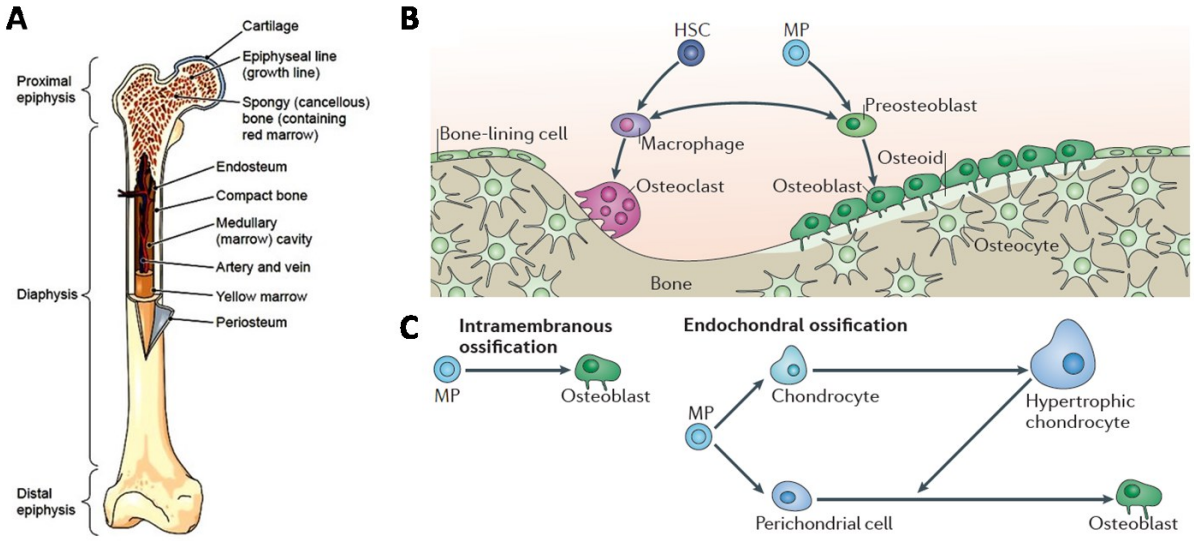

Figure 1.1: Physiology of the femur long bone and biology of key player cells. (A) The outer shell of the long bone is made of cortical bone also known as compact bone. This is covered by connective tissue termed the periosteum. The main shaft is the diaphysis with an epiphysis at each end consisting of spongy cancellous bone filled with red bone marrow. The cylinder-like inside of the long bone is called medullary cavity and contains in young individuals red bone marrow, which transforms to yellow marrow with age. (B) Constant bone remodeling is achieved by osteoblasts and osteoclasts. Osteoblasts have their origin in mesenchymal progenitors (MPs) and produce not yet mineralized extracellular matrix – the osteoid. When incorporated into compact bone a subset of

osteoblasts can become osteocytes, or bone-lining cells. Osteoclasts in turn are multinucleated resorptive cells derived from macrophages, which have their origin in hematopoietic stem cells (HSCs). For proper homeostasis of the bones, the numbers of osteoblasts and osteoclasts need to be balanced. (C) In particular, in homeostasis or regeneration osteoblasts can differentiate from MPs through either intramembranous or endochondral ossification. Intramembranous ossification requires MPs to condense and subsequently differentiate into osteoblasts. On the contrary, during endochondral ossification, MPs condense and differentiate into perichondrial cells and chondrocytes. Afterwards, cartilage producing hypertrophic chondrocytes trigger their transdifferentiation or differentiation of perichondrial cells to osteoblasts. For (A) adapted from www.encyclopedia.lubopitko-bg.com, and for (B) and (C) adapted from Long 2011.

1.1.1 Compact bone

In higher vertebrates, like humans, the skeleton is in a constant state of remodeling to adapt to changing loading demands. This is achieved by the balanced activity of bone-forming osteoblasts and bone-resorbing osteoclasts (Fig. 1.1 B). Osteoblast lineage cells comprise their mesenchymal progenitors (MPs), pre-osteoblasts, osteoblasts, bone-lining cells and osteocytes. To produce compact bone, osteoblasts secrete a unique combination of extracellular proteins, including osteocalcin (OCN), alkaline phosphatase (ALP) and type I collagen. The resulting extracellular matrix is called osteoid when first deposited and not yet mineralized. When mineralized through the accumulation of calcium phosphate in the form of hydroxyapatite the unique features of this biomaterial is a certain weight-bearing rigidity, which comes along as a lightweight composition at the same time (Long 2011).

To achieve homeostasis in the characteristic adaptive properties the compact bone requires constant resorption by osteoclasts (Fig. 1.1 B). Interestingly, osteoclasts are multinucleated cells derived from macrophages, which are in turn progenitors of hematopoietic stem cells (HSCs) in the BM (Jain & Weinstein 2009). The resorption of compact bone of this cell type is achieved by the releases of hydrogen ions through the action of carbonic anhydrase and by matrix degrading hydrolytic enzymes like cathepsins and matrix metalloproteases (MMPs). Most characteristic in this regard is cathepsin K (CTSK) (Wilson *et al.* 2009).

95 % of cells within the compact bone material are osteocytes, which are derived from osteoblasts (Fig. 1.1 B) (Bonewald 2011). Osteocytes regulate the remodeling of bone in response to both mechanical and hormonal signals. Therefore, they form an extensive network with each other, with osteoblasts and with the bone lining cells. The regulation is partly mediated by osteocytes via secreted sclerostin (Powell *et al.* 2011). Sclerostin inhibits Wnt signaling and in this way differentiation in osteoblast lineage cells, and also suppresses BMP signaling (Krause *et al.* 2010).

1.1.2 Bone marrow

Bone marrow (BM) is a tissue type that is not only filling the bones and maintaining them, but it is the location of blood cell production and therefore contains hematopoietic stem cells (HSCs) and

hematopoietic progenitor cells (Fig. 1.2) (Kopp *et al.* 2005). Furthermore, it harbors innate and adaptive immune cells (Zhao *et al.* 2012b) and also multipotent progenitor cells, which can differentiate into tissue types of mesenchymal origin, like the osteoblasts, adipocytes, fibroblasts, endothelial cells and reticular cells. BM even displays structural similarities to primary lymphoid organs, i.e. lymph nodes and spleen, however, in a less organized manner (Tripp *et al.* 1997). In particular, 8 – 20 % of the BM mononuclear population are lymphocytes (Schirrmacher *et al.* 2003; Feuerer *et al.* 2004). Furthermore, the BM microenvironment provides appropriate support for further development of T cells after maturation in the thymus (Dejbakhsh-Jones *et al.* 1995).

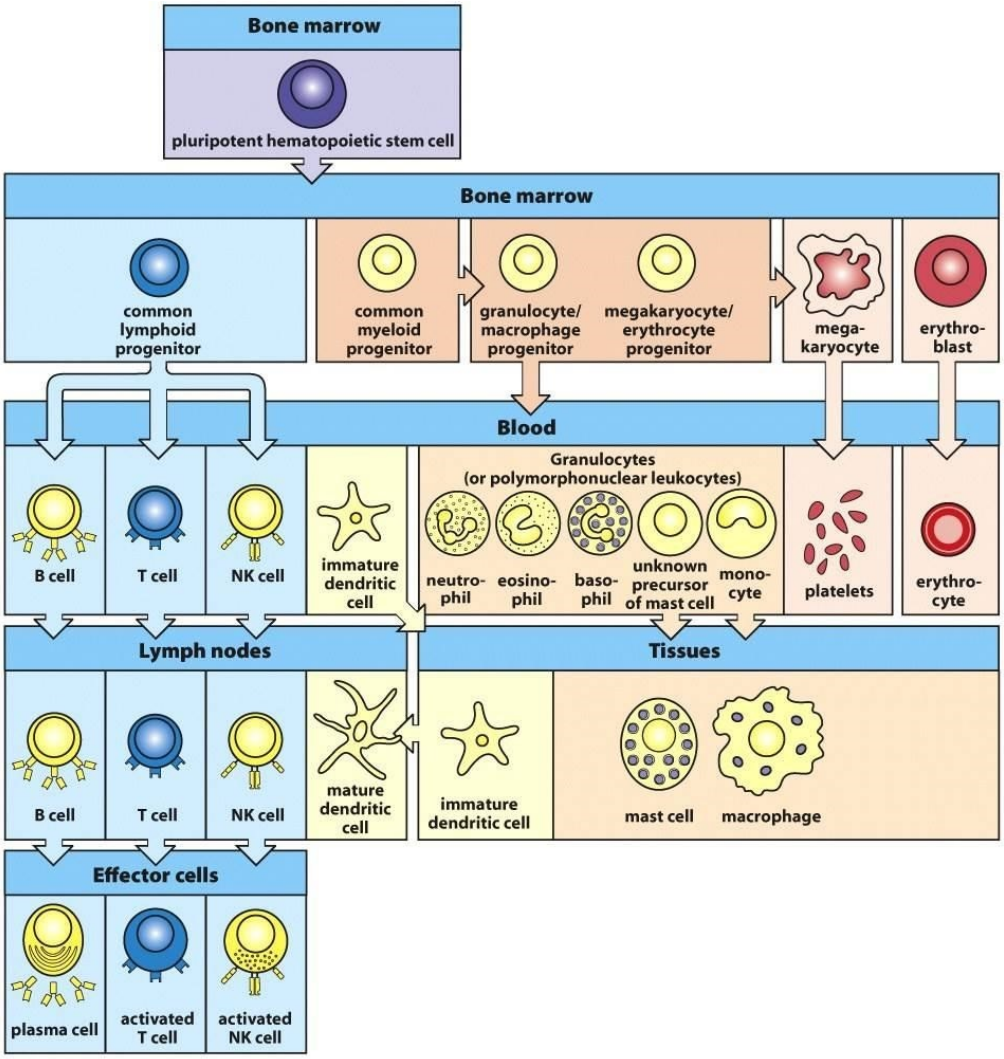

Figure 1.2: Hematopoiesis in higher vertebrates as simplified overview of the immune system. In the bone marrow, hematopoietic stem cells produce lymphoid and myeloid progenitors, of which the latter differentiate to immune cells, platelets and erythrocytes of the blood stream. Adaptive immune cells such as B, T, and NK cells further migrate and mature in lymph nodes from which they can be send out to fight invading pathogens as effector cells or eventually modulate bone healing. Innate immune cells also mature to patrol the blood as neutrophils, eosinophils or basophils. Monocytes further differentiate into macrophages to fulfill versatile roles in various tissues. Most immune cell types can be further classified into complex subtypes, for instance into CD8+ T cells and CD25++CD4+FoxP3+ T cells (Scheme from Janeway's immunobiology 2012).

Rodents such as mice and rats are unique in hematopoiesis as a significant proportion of this process is additionally taking places in the spleen as well (Reagan *et al.* 2011). In this thesis, mice were used for the investigations *in vivo* as model organism. However, the focus is laid on the bone marrow, since it is the organ, which is injured during fractures and the primary source of inflammatory cells upon which local therapeutic treatments are directed to. Additionally, the results of this thesis are meant to support pre-clinical science and not to investigate distinct specifications of the mouse model further.

1.1.2.1 Immune cells in bone marrow

T cells are characterized by their antigen-detecting T cell receptor (TCR) consisting in general of TCR-α and TCR-β chains, CD3 (cluster of differentiation 3) and ζ-chain accessory molecules. (A minority of T cells express a TCR with γ and δ chains instead of α and β chains.) In this way, T cells "read" body foreign antigens when presented by antigen presenting cells (APCs) via their MHC-I or -II complex, respectively, depending on the APC-type. Furthermore, 1 – 5 % of mononuclear cells in this tissue are CD3+ T cells (Feuerer *et al.* 2004). Overall, there are 1.5 % CD4+ T cells and 2.0 – 2.5 % CD8+ T cells (Zeng *et al.* 2002; Mazo *et al.* 2005). Notably, this leads to a CD4/CD8 ratio in the BM of 1:2, which is inverted as compared to both peripheral lymph nodes and the blood.

Moreover, the BM constitutes a war museum of victorious T cell encounters with pathogenic invaders. The majority of T cells express surface markers, which indicate antigen experience, such as CD44++ and CD122+, whereas most T cells in spleen and peripheral lymph nodes have naïve phenotypes (Mazo *et al.* 2005). Bone marrow also contains relatively high numbers of memory T cells, which are CD45R0+ in humans and CD44++ in mice (Sallusto *et al.* 2004; Mazo *et al.* 2005). On the contrary, naïve T cells are CD45RA+ and CD44- in human and mice, respectively.

Memory T cells do not represent a homogenous population but can be divided according to their activation and differentiation state into less differentiated, long-lived memory-stem T_{SCM} and central memory T cells (T_{CM}) to more differentiated effector memory T cells (T_{EM}) (Sallusto *et al.* 2004). The ladder can also re-express the naïve marker CD45RA and are therefore defined as T_{EMRA}. Furthermore, T_{EM} are CD62L-, reside in the peripheral circulation and tissues, and if necessary migrate to inflamed peripheral tissues, such as skin, lungs, and other mucosal tissues, and conduct immediate effector function. In contrast, the central memory is mediated by CD62L+ T_{CM}, which are found in the lymph nodes and peripheral circulation. In response to antigenic stimulation T_{CM} home to T cell areas of secondary lymphoid organs, and at first proliferate and differentiate into effector cells.

CD8+ is located mainly on antigen-specific cytotoxic T cells and keeps their TCR and the antigen-presenting MHC I molecule of the target cell bound closely together (Devine *et al.* 1999). Once "bitten their prey", the CD8+ cells kill e.g. cancer cells or infected cells. Antigen specific memory CD8+ T cells prefer to reside in BM where they receive proliferative signals by IL-7 and/or IL-15 (Becker *et al.*

2005). Furthermore, the BM can be regarded as a niche for the antigen-independent proliferation of memory CD8+ T cells. These lymphocyte are CD44+ and HLA-DR++, which suggests that CD8+ T cells in BM are in a rather pre-activated state in humans. Furthermore, after acute infection or tumor development tumor associated antigen-specific CD8+ T cells are still present in high quantities in BM even for several months (Masopust *et al.* 2001). Interestingly, the CD8+ T_{EMRA} cells are a new diagnostic tool for the outcome prediction of fracture healing (see below,1.3). Furthermore, memory CD8+ T cells proliferate faster in BM compared to standard secondary lymphoid or extra-lymphoid organs and also undergo basal proliferation (Becker *et al.* 2005; Parretta *et al.* 2005). BM also provides specific signals for recruitment of T_{CM} from the blood (Mazo *et al.* 2005). Especially in mice, T_{CM} constitute the largest endogenous subset of CD8+ T cells in BM (Weninger *et al.* 2001).

CD4+ T cells differentiate into several effector subtypes, e.g. T helper (Th) cells (Ziegler 2016). Th1 cells secrete interferon-γ (IFN-γ) and are involved in responses to intracellular pathogens. Whereas Th2 cells produce interleukin-4 (IL-4), IL-5 and IL-13, and respond to helminth (worm) infections. The Th17 CD4+ helper T cells defend against extracellular pathogens and are characterized by their effector cytokines IL-17A, IL-17F, IL-21 and IL-22 (Zou & Restifo 2010). Development of Th17 cells is dependent on IL-1 and IL-23 and additionally, in concurrence with regulatory T cells (Treg) for differentiation and function, dependent on IL-6 and TGF-β (Prabhala *et al.* 2010). Another strong producer of IL-17A and initiator of inflammation are the closely related γδ T cells, which also contribute to protective immune responses in case of infections (Papotto *et al.* 2017).

Treg also comprise a subpopulation of T helper cells. They are specialized in suppression of T cell-mediated immune responses, and characteristically express the transcription factor forkhead box P3 (FoxP3) (Fontenot *et al.* 2003). Treg cells secrete high levels of anti-inflammatory master regulator IL-10 and transforming growth factor β (TGF-β) (Kingsley *et al.* 2002). In addition, they secrete immunosuppressive IL-35 (Geem *et al.* 2015). Hence, Treg can even reduce the inflammatory severity of graft-versus-host disease (GVHD) (Feuerer *et al.* 2004) or reduce the number of neutrophils and macrophages in ischemia-reperfusion injury (Kingsley *et al.* 2002). There are two main subsets of Treg including a population of FoxP3+ natural Treg (nTreg), which are thymus derived and specific for self-antigens, and induced or adaptive Treg (iTreg) that are derived from mature CD4+CD25-Foxp3- precursors in the periphery following inflammatory stimuli (Chaudhry & Rudensky 2013).

Almost one-third of CD4+ T cells in BM are CD4+CD25+ Treg, in contrast to their smaller fractions in primary lymphoid organs of 5 – 10 % of the CD4+ T cells (Zeng *et al.* 2002; Zou *et al.* 2004). However, the overall fraction of Treg in BM cells is only 0.5 %. In particular, C-X-C motif ligand 12 (CXCL12) mediates Treg cell trafficking to BM by their C-X-C motif receptor 4 (CXCR4). CXCL12 is also known as stromal cell-derived factor-1 (SDF-1). Mechanistically, antigen presentation to the T cell receptor by BM dendritic cells can induce cell division of Treg while in parallel activating their ability to suppress effector T cells. However, the persistent strong immune suppressive function of Treg cells can lead to

cancer induction. In patients with prostate cancer the numbers of BM Treg cells are much higher (Zhao *et al.* 2012a). Furthermore, these patients often have bone metastases with bone precipitation as a pathological characteristic.

Macrophages are part of the large and heterogeneous population of the myeloid-derived cells. 20 – 30 % of mononuclear cells in the BM belong to this group, which comprises also myeloid progenitors and immature myeloid cells (Gabrilovich & Nagaraj 2009). Macrophages act as phagocytic cells clearing cell debris and possible pathogenic invaders (Leibovich & Ross 1975). Furthermore, macrophages are key players in initiating and controlling inflammation (Mantovani *et al.* 2013).

Approximately 1 % of BM's mononuclear cells represent mature B cells, which are capable of producing pathogen specific antibodies as plasma cells. B cells derive from HSCs and develop in BM before they migrate into peripheral blood to move into peripheral lymphoid organs (Sandel *et al.* 2001). Furthermore, BM is a reservoir for long-lived plasma cells and is involved in the maintenance of long immunity (Manz *et al.* 1997).

In addition, there are 0.4 – 4 % natural killer T (NKT) cells in BM (Higuchi *et al.* 2002) and 1.5 % CD11c1 dendritic cells (Banchereau *et al.* 2000; Feuerer *et al.* 2004). NKT cells are a subset of T cells, which express common natural killer cell markers such as NK1.1 and are positive for IL-2Rb (CD122), Ly49 family receptors and of course for TCR (Kronenberg 2005). NK and NKT cells are the innate counterpart to the cytotoxic T cells, whereas NKT cells recognize further CD1, which binds self and foreign lipids and glycolipids.

Neutrophils are an essential component of the innate immune system and link it with the adaptive counterpart (Nathan 2006). They are the most abundant granulocyte type and differentiate from HSCs in the BM, where the majority of neutrophils is also reserved. Characterized is this cell type by the granulocyte surface marker Ly6G (Daley *et al.* 2008).

Dendritic cells (DCs) play additionally a key role in linking innate and adaptive immune responses (Banchereau *et al.* 2000). Circulating DCs home to the BM where they are retained better than in spleen, liver and lung tissues. In BM, DCs are able to trigger T_{CM}-mediated responses with antigen-dependent contacts (Sallusto *et al.* 2004). This cell type takes up blood-derived antigens, processes them and induce antigen-specific systemic protective T cells-mediated immunity (Schirrmacher *et al.* 2003).

1.1.2.2 Mesenchymal stromal cells

Mesenchymal stromal cells (MSCs) resembling morphologically fibroblasts, are mainly found in the BM, and reported numbers vary from 0.001 – 0.1 % of MSCs in total BM cells (Bernardo & Fibbe 2013). They reside in an undifferentiated (adult) state, but are multipotent. Hence, MSCs are able of differentiating into cell types of mesodermal origin, such as osteoblasts, chondrocytes, myocytes and

adipocytes (Friedenstein *et al.* 1974; Pittenger *et al.* 1999). Moreover, MSCs are capable of producing cytokines and growth factors for hematopoiesis and can attract hematopoietic cells to the BM by inducing expression of homing receptors (Cheng *et al.* 2003).

Crucially, MSCs can exert profound immunoregulatory activity without the requirement of antigen-presenting cells (Krampera *et al.* 2003). In particular, MSCs can inhibit T cell proliferation in responses to polyclonal stimuli and to their cognate peptide in a MHC-independent manner (Le Blanc *et al.* 2003). Furthermore, MSCs can also induce T cell anergy, i.e. tolerance or inactivity (Glennie *et al.* 2005), as well as, T cell apoptosis (Plumas *et al.* 2005), suppress T cell IFN-γ production and increase IL-4 secretion. In addition to that versatility, MSCs can even enhance the Treg cell compartment (Aggarwal & Pittenger 2005). However, the expression of early activation markers such as CD25 and CD69 on T cells is unaffected in the presence of MSCs, but IFN-γ production is reduced. The inhibitory effect of MSCs is directed mainly at the level of cell proliferation without interfering with early T cell activation. Concerning B cells, MSCs can inhibit proliferation and affect their differentiation, antibody production and chemotactic behavior (Glennie *et al.* 2005). MSCs also act suppressive onto innate immune cells, like DCs (Nauta *et al.* 2006) and NKs (Spaggiari *et al.* 2008).

Taken together, the bone marrow is a versatile tissue type, which is not just filling material for the skeleton. Among the many so far known functions, it provides the cells to maintain the compact bones, is producing constantly new blood cells and is a reservoir for the cellular memory of the immune system. Hence, it already provides all necessary cell types in case of regeneration after fracture of the bone, especially immune cells, which are ready to initiate inflammation and are a target for immunomodulatory approaches.

1.2 Bone healing process

Fracture healing is a regenerative process rather than a repair process. Hence, it results in remodeled bone and not in inferior scar tissue, which can occur e.g. in injured muscle or skin. The process can commence either directly or most commonly indirectly. Direct (primary) formation of new mineralized bone is a process called intramembranous healing and is the goal after open reduction and internal fixation surgery (Marsell & Einhorn 2011) (see above, Fig. 1.1 C). However, it does not naturally occur since it requires a precise anatomical reduction of the fracture ends, without any gap formation, and an absolute stable fixation.

Indirect (secondary) fracture healing is the most common form and contains an endochondral phase (Gerstenfeld *et al.* 2006; Marsell & Einhorn 2011). Fascinatingly, it does not require anatomical reduction or rigidly stable conditions, because a chondrogenic matrix is formed. The cartilage material can absorb mechanical strains better during this step-wise re-connecting of the bone compared to rigid but still weak early mineral bone. However, endochondral regeneration is enhanced by micro-motion

and weight-bearing and can explain how skeletal beings in the wild open nature can have a chance to regenerate, without medical treatment. In this thesis, the common endochondral process is further described and investigated.

As a complex multistage healing process, endochondral bone regeneration proceeds in well-orchestrated phases, which are initiated in response to injury. The main phases can be broken down into hematoma formation, pro-inflammation, anti-inflammation, soft callus formation, mineralization of hard callus, resorption and remodeling (Fig. 1.3 A). Participating in this process are various tissues, such as bone marrow, periosteum, endosteum, muscle, and blood vessels (Ozaki *et al.* 2000; Colnot *et al.* 2006). These tissue types are the source of specific cells, such as immune cells, progenitor cells, and MSCs (Andrew *et al.* 1994; Colnot *et al.* 2006; Schmidt-Bleek *et al.* 2009) and signaling factors, i.e. cytokines, growth factors, and chemokines (Gerstenfeld *et al.* 2003b; Ai-Aql *et al.* 2008).

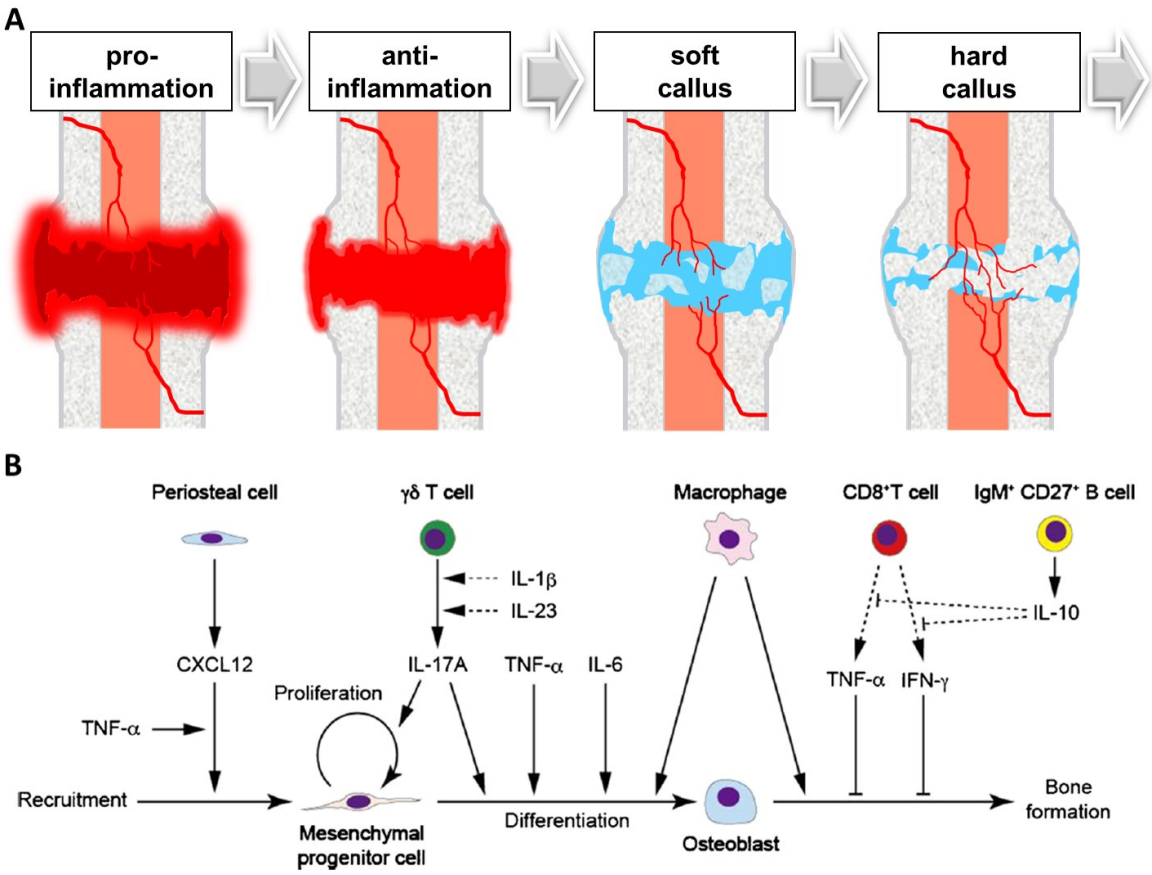

Figure 1.3: The interplay of immune cells and osteolineage cells during the phases of endochondral fracture healing is highly complex. However, basic principles that help understanding of new therapeutic approaches can be broken down with describing only key player cell types and signaling factors. (A) After hematoma formation in the fracture callus, the process is initiated by a strong pro-inflammatory phase, which is followed by an anti-inflammatory phase. Only afterwards a tissue restauration can take place with the establishment of a soft callus, which consists of cartilage. This in turn is transformed into a mineralized hard callus. After subsequent remodeling phases, the bone is regenerated. (B) The scientific field of osteoimmunology is studying the interplay of immune and bone cells, e.g. during the regulation of bone formation. For instance, mesenchymal cells are recruited to the

injury site by interaction of CXCL12–CXCR4. TNF-α stimulates the responsiveness of mesenchymal progenitor cells to CXCL12 (also known as SDF-1), which is expressed by periosteal cells. Furthermore, proliferation and osteoblastogenesis of MSCs are enhanced by IL-17A, which is mainly produced by γδ T cells, but also by Th17 cells. Low doses of TNF-α and IL-6 promote osteoblast differentiation from MSCs. Additionally, macrophages promote osteoblastogenesis and bone formation. CD8+ T cells suppress bone fracture healing by producing high doses of pro-inflammatory cytokines, such as TNF-α and IFN-γ, which inhibit bone formation. Among other cell types like Treg, for instance also IgM+CD27+ B cells produce anti-inflammatory IL-10, which suppresses pro-inflammatory processes. Hence, the suppression of pro-inflammation can indirectly support bone formation. For (B) adapted from Ono & Takayanagi 2017.

1.2.1 Hematoma formation

Immediately after trauma, a primary hematoma is generated by coagulation of blood, which builds a scaffold of the structural protein complex fibrin (Bolander 1992; Einhorn 1998). Obviously, it harbors cells derived from both peripheral and intramedullary blood, as well as BM cells. The hematoma is located in between and around the fracture ends and within the medulla forming a template for callus formation (Gerstenfeld *et al.* 2003b). Subsequently, the fibrin content is increased in the following days after fracture injury to form a granulation tissue (Marsell & Einhorn 2011). A stable hematoma is crucial for initial bone healing. This could be proven in a sheep tibial osteotomy model, when fracture hematomas were removed at 4 and 7 days, the result was a significant delay of early fracture healing (Schell *et al.* 2017). Furthermore, the hematoma is characterized by low levels of oxygen and glucose as well as high concentrations of lactate and reductive metabolites. This specific bioenergetic situation results in biological signals, which have a strong influence on recruiting immune cells, which are capable of adaptation to the hypoxic micro milieu to the site of injury (Krauss *et al.* 2001; Cramer *et al.* 2003).

On the one hand, inflammatory cytokines can have negative effects on bone, joints and implanted materials when prolonged or chronic expression occur as seen in rheumatoid arthritis. On the other hand, a brief and highly regulated secretion of pro-inflammatory molecules following the acute injury is critical for initiating tissue regeneration (Andrew *et al.* 1994; Gerstenfeld *et al.* 2003b; Kolar *et al.* 2010). Further studies in humans and rodents of the fracture hematoma, which is rich in pro-inflammatory factors and immune cells, suggest that the early inflammatory events following fracture are critical to the outcome of fracture healing (Grundnes & Reikeras 1993; Chung *et al.* 2006b; Kolar *et al.* 2010; Kolar *et al.* 2011; Hoff *et al.* 2013).

In particular, within hours after the onset of inflammation, molecules associated with tissue injury are recognized by Toll-like receptors (TLRs) present on innate effector cells. TLR ligation triggers the release of inflammatory mediators, which initiate innate immune responses mainly through the activation of phagocytic cells, including macrophages and neutrophils (Gordon & Mantovani 2011). Neutrophils migrate toward the site of inflammation where they accumulate within minutes (Kolaczkowska & Kubes 2013), and mount a host defensive response, including phagocytosis and the release of reactive oxygen species, anti-microbial peptides, and serine proteinases (Soehnlein &

Lindbom 2010). Additionally, TLR ligation activates stromal cells, including MSCs, thus creating an inflammatory environment (Waterman *et al.* 2010; Mantovani *et al.* 2013).

MSCs express a number of distinct and overlapping TLRs and stimulation of specific TLRs affects the subsequent immune modulating responses of MSCs (Nemeth *et al.* 2010; Waterman *et al.* 2010). Under the hypoxic conditions of the hematoma, MSCs are stimulated by pro-inflammatory, yet low concentrated cytokines, e.g. TNF-α, IL-17A, IL-6 and IFN-γ (see above, Fig. 1.3 B) (Ono & Takayanagi 2017). These factors up-regulate the expression of TLR2 and TLR4, thus, increasing the sensitivity of MSCs towards a pro-inflammatory M1-type to the inflammatory milieu (Raicevic *et al.* 2010). However, prolonged stimulation with TLR ligands causes downregulation of TLR2 and TLR4 (Mo *et al.* 2008), most likely as a self-regulatory mechanism to control the immune response.

As mentioned above, macrophages are important initiators and controllers of inflammation, and MSCs can influence macrophage function depending on the inflammatory context (Mantovani *et al.* 2013). As we have shown, monocytes arriving at the inflammatory environment develop into activated pro-inflammatory M1 macrophages, which are CD80+ and stimulate local inflammation by releasing pro-inflammatory cytokines (Schlundt *et al.* 2015). Macrophages further appear to be crucial for the degradation of the initial fibrin-rich matrix, as their chemical depletion led to an arrest in fracture regeneration at the chondrogenic phase. Furthermore, fracture repair arrested as well at any time of Fas-induced apoptosis in macrophages in transgenic mice (Raggatt *et al.* 2014).

1.2.2 Pro-inflammatory phase

The pro-inflammatory phase is necessary to initiate reparative responses following injury (Nathan 2006; Soehnlein & Lindbom 2010) and especially to initiate the endochondral cascade in fracture healing (Schmidt-Bleek *et al.* 2012b; Schmidt-Bleek *et al.* 2014) (see above, Fig. 1.3 A). Crucially, the early inflammatory phase is even a key rate-controlling step in fracture healing. During the established initial pro-inflammatory phase, pro-inflammatory cells, like M1 macrophages and CD8+ T cells release cytokines, which comprise TNF-α, IFN-γ, IL-1, IL-6, IL-11 and IL-18 (Einhorn *et al.* 1995; Gerstenfeld *et al.* 2003b). These factors further recruit other inflammatory cells, which induce secondary inflammatory signals, and act as a chemotactic agent to recruit further necessary cells, enhance extracellular matrix (ECM) synthesis and promote angiogenesis (Kon *et al.* 2001; Lee & Lorenzo 2006; Yang *et al.* 2007; Schmidt-Bleek *et al.* 2015). For instance, TNF-α is promoting migration of muscle-derived stromal cells (MDSC) (Glass *et al.* 2011). Furthermore, TNF-α potentiates BM-MSCs to chemotaxis toward high concentrations of SDF-1 (Egea *et al.* 2011).

Moreover, the pro-inflammatory activities of M1 MSCs are beneficial in the early phase of inflammation and help attract various immune cells. Therefore, MSCs increase production of growth factors, such as IL-6, IL-8, granulocyte macrophage colony-stimulating factor (GM-CSF), and macrophage migration

inhibitory factor (MIF), that recruit neutrophils and enhance their pro-inflammatory activity (Brandau *et al.* 2010). In addition to neutrophils, immune responses are enhanced by MSCs through the production of chemokines that recruit lymphocytes to sites of inflammation, such as CXCL-9, CXCL-10, and CXCL-11 (Ren *et al.* 2008; Li *et al.* 2012). Recently, my colleagues could highlight the strong chemoattraction of CXCL12 (SDF-1) toward BM immune cells (Cipitria *et al.* 2017).

1.2.3 Anti-inflammatory phase

After initiating the healing process, the pro-inflammatory phase needs to cease via the anti-inflammatory phase (see above, Fig. 1.3 A). Therefore, the inflammatory milieu changes from pro- to anti-inflammatory signaling (Schmidt-Bleek *et al.* 2012b). Otherwise, a prolonged pro-inflammatory phase is negatively influencing the outcome of bone regeneration (Lienau *et al.* 2009; Schmidt-Bleek *et al.* 2009; Chan *et al.* 2015). For instance, an enrichment of CD8+ T cells in the hematoma and adjacent BM was observed in a delayed fracture healing model in sheep (Schmidt-Bleek *et al.* 2012b). Although pro-inflammatory cells, like M1 macrophages, are crucial for the initiation of the regenerative process, chronic inflammation and unsuccessful healing are associated with a prolonged inflammation (Parihar *et al.* 2010; Claes *et al.* 2012). In this regard, a fundamental concept of biochemical regulation are feedback loops. Hence, pro-inflammatory CD8+ cells start to secrete IL-10 at their peak activity levels (Trandem *et al.* 2011). IL-10 is an anti-inflammatory master regulator in human and mouse (Couper *et al.* 2008; Shouval *et al.* 2014). Moreover, this regulation of activation and deactivation of powerful biochemical processes is also orchestrated by the communication of different cell types with each other back and forth. Therefore, peak levels of pro-inflammatory cytokines secreted by M1 macrophages or activated T cells stimulate MSCs and trigger the release of mediators that switch the differentiation of monocytes toward an anti-inflammatory profile and ultimately towards CD206+ M2 macrophages (Gordon & Martinez 2010; Le Blanc & Mougiakakos 2012; Mantovani *et al.* 2013). M2 macrophages are also called regenerative macrophages, since they are essential for tissue remodeling as well (Brown *et al.* 2012a; Raggatt *et al.* 2014).

In analogy, when exposed to these high levels of pro-inflammatory cytokines, MSCs themselves adopt an immune-suppressive M2 phenotype to release anti-inflammatory signals and promote tissue homeostasis. In particular, this mechanism is dependent on cellular contact and also soluble factors, including prostaglandin E_2 (PGE_2) and catabolites of indoleamine 2,3 dioxygenase (IDO) activity such as kynurenine (Ghannam *et al.* 2010; Eggenhofer & Hoogduijn 2012). Moreover, activation of MSCs with high concentrations of IFN-γ, and TNF-α increases the expression of cyclooxygenase 2 (COX2) and IDO in BM-MSCs, thereby further promote a homeostatic response towards M2 macrophage polarization (Francois *et al.* 2012).

Additionally, this polarizing effect of MSCs on macrophages is closely linked with the ability of MSCs to secrete TGF-β and PGE_2, which supports the emergence of the strong immunosuppressive Treg from CD4+ T cells upon cell-cell contact (Burr *et al.* 2013). In particular, the generation of Treg was reported to be monocyte dependent (Melief *et al.* 2013). Adding to this, MSCs can also generate regulatory APCs characterized by their Treg-promoting activity. A mechanism that could further stimulate a suppressor response of Treg constitutes the IL-2 feedback loop (Sakaguchi *et al.* 2008). It is described for antigen-activated T cells to produce IL-2, which in turn activates Tregs to prevent inflammatory overreactions.

Similarly, M2 macrophages secrete a combination of cytokines, including high levels of IL-10 and TGF-β1 that together exert an anti-inflammatory effect and allow tissue regeneration following inflammation. M2 polarized macrophages also produce CCL18, a factor that in conjunction with TGF-β further promotes the generation of Treg.

Moreover, TLR3-activated human M2 MSCs promote survival of resting and activated neutrophils with secretion of IL-6, IFN-β, and GM-CSF (Cassatella *et al.* 2011). MSCs are additionally able to suppress effector T cell proliferation induced by cellular or nonspecific mitogenic stimuli (Di Nicola *et al.* 2002). This is again achieved through the secretion of soluble factors including TGF-β, hepatocyte growth factor (HGF), PGE_2, IDO (in humans), NO (in mice), and hemoxygenase (HO) (Stagg & Galipeau 2013). In human cells, IDO promotes the degradation of tryptophan into kynurenine and other catabolites that do not only suppress T cell proliferation, but also induce Treg differentiation. The suppression of T cell proliferation involves both CD4+ and CD8+ T cells. Furthermore, IFN-γ production and cytotoxicity are also inhibited in a dose-dependent manner (Krampera *et al.* 2003; Aggarwal & Pittenger 2005). In murine MSCs, secreted NO is mainly suppressing T cell proliferation (Li *et al.* 2012). While MSCs directly produce soluble factors that suppress T cell proliferation, it appears that this ability is dependent on the presence of monocytes (Cutler *et al.* 2010; Francois *et al.* 2012; Melief *et al.* 2013). MSC's immunosuppressive influence by a variety of so far identified factors extends to further multiple cell types of the innate and adaptive immune system, including DCs, NKs and B cells (Burr *et al.* 2013).

1.2.4 MSC recruitment

After the initial inflammatory phases are completed, the reconstruction of the tissue is conducted by specific MSCs, which have to be further recruited, proliferate and differentiate into chondrogenic and in later phases into osteogenic cells (see above, Fig. 1.3 B). Exactly where these cells are migrating from is not fully understood, but most data indicate that these MSCs are derived from BM and surrounding soft tissues, like periosteum and muscles (Ozaki *et al.* 2000; Barry & Murphy 2004; Colnot *et al.* 2006; Schindeler *et al.* 2009; Maes *et al.* 2010; Zhou *et al.* 2017). The potential contribution of circulating progenitor cells from blood supply in bone healing is a matter of debate (Feehan *et al.* 2019). In a parabiotic mouse model between a transgenic mouse constitutively expressing enhanced GFP (eGFP)

and a syngenic counterpart, only 5 – 6 % of osteogenic connective tissue progenitors in the counterpart were eGFP expressing cells from the donor (Kumagai *et al.* 2008). This study indicated that circulating cells make a relative minor cellular contribution to closed fracture repair in mice.

BMP-2 is known to be indispensable for bone regeneration (Tsuji *et al.* 2006). However, among the BMPs, BMP-7 is more vital in recruitment of progenitor cells (Bais *et al.* 2009). Key regulators of recruiting and homing specific MSCs to the site of trauma are SDF-1 and its G-protein-coupled receptor CXCR-4, which form an axis (SDF-1/CXCR-4) (Ma *et al.* 2005; Granero-Molto *et al.* 2009; Kitaori *et al.* 2009). SDF-1 expression is increased at the fracture site, and especially in the periosteum at the edges of the fracture. Hence, besides attracting immune cells, SDF-1 has additionally a role in recruiting CXCR-4 expressing MSCs to the injured site during endochondral fracture healing (Granero-Molto *et al.* 2009; Kitaori *et al.* 2009). Further important chemokine receptors involved in MSCs recruitment to sites of inflammation and injury include also C-X-C chemokine receptor type (CXCR) -5 and -6, as well as, C-C chemokine receptor type (CCR) -1, -7 and -9 (Honczarenko *et al.* 2006). Hypoxia inducible factor-1a (HIF-1a) has also an important role in this regard and its induction of vascular endothelial growth factor (VEGF) in the revascularization process shows that hypoxic gradients regulate MSC progenitor cell trafficking by HIF-1 (Ceradini *et al.* 2004; Wan *et al.* 2008).

1.2.5 Soft and hard callus

Following containment of inflammation, a fibrin-rich granulation tissue forms and endochondral formation occurs in between the fracture ends, and external to periosteal sites (Marsell & Einhorn 2011). Newly generated cartilage tissue forms a soft callus (see above, Fig. 1.3 A), which gives the fracture a stable structure (Dimitriou *et al.* 2005). Hence, it contains both proteoglycan and type II procollagen (Einhorn 1998). This soft callus is than transformed into a hard callus, which consists of a first immature bony tissue with a semi-rigid structure, which allows weight bearing (Gerstenfeld *et al.* 2006). These intermediate temporal tissue types are dependent on recruited and differentiated MSCs, which produce collagen-I and collagen-II matrices. In this process, the TGF-β superfamily members are of great importance. TGF-β2, -β3 and GDF-5 are key signaling factors in the subsequent chondrogenesis and endochondral ossification (Cho *et al.* 2002; Marsell & Einhorn 2009). Whereas, BMP-5 and -6 induce at periosteal sites the proliferation of cells during intramembranous ossification. In addition, BMP-2 is crucial for initiation of the reconstructing phases (Tsuji *et al.* 2006; Marsell & Einhorn 2011).

After more than a week in the process an abundance of chondrogenic progenitors is present, which undergo mitosis. Usually, after two weeks proliferation declines and enlarged, matrix producing hypertrophic chondrocytes become the dominant cell type in the chondroidic callus. Subsequently, chondrocytes are removed in an ordered transition of tissue types in which the cellular mechanisms are genetically programmed to involve proliferation, maturation, and apoptotic cell death. However, some

non-programmed cell removal, including necrosis does occur. Interestingly, cells derived from hypertrophic chondrocytes contribute to the osteoblast pool in trabecular bones via transdifferentiation in development, postnatal growth and fracture healing (Yang *et al.* 2014; Zhou *et al.* 2014). This was proven by genetically labeled chondrocytes and hypertrophic chondrocytes.

1.2.6 Blood vessel formation

Fracture healing requires blood supply, as homeostatic tissue does. Hence, revascularization is vital for the process of bone regeneration (Keramaris *et al.* 2008; Schmidt-Bleek *et al.* 2015). During endochondral fracture repair, chondrocyte apoptosis and cartilaginous degradation is necessary to make way for blood vessel in-growth at the repair site (Ai-Aql *et al.* 2008). The process of vascularization is primarily regulated by both an angiopoietin-dependent pathway, and a VEGF-dependent pathway (Tsiridis *et al.* 2007). The initial vascular in-growth originates from the already present vessels in the periosteum via angiogenesis, which is stimulated by angiopoetin-1 and -2 (Ang-1, -2) (Lehmann *et al.* 2005). In contrast, vasculogenesis generates completely new blood vessels by endothelial MSCs, which aggregate and proliferate to form an initial vascular plexus. VEGF promotes both angiogenesis and vasculogenesis (Kanczler & Oreffo 2008).

Another promoter of angiogenesis and vasculogenesis is laminin (Simon-Assmann *et al.* 2011). Laminins are heterotrimeric proteins, which contain an α-, β- and γ-chain. This composition allows for different genetic variants, which affects their distinct role during blood vessel growth by interacting with cell surface receptors on endothelial cells and pericytes to influence their behavior. In general, the function of laminin in blood vessel growth is remodeling of the vascular basement membrane (Patarroyo *et al.* 2002).

Several other pro-angiogenic factors are also involved in these responses, such as the synergistic interactions of the BMPs with VEGF and the role of mechanical stimuli to enhance angiogenic activities in a VEGFR2-dependent manner (Ai-Aql *et al.* 2008; Kanczler & Oreffo 2008). However, VEGF signaling is the key regulating mechanism of vascular regeneration (Keramaris *et al.* 2008). Moreover, hypertrophic chondrocytes as well as osteoblasts secrete high levels of VEGF. Hence, via VEGF these cells support the ingrowth of blood vessels and the avascular soft callus can be transformed into vascularized osseous tissue (Keramaris *et al.* 2008). Furthermore, sprouting new blood vessels are following the migration of VEGF secreting MSC-derived osteoblast precursors into the late-hypertrophic cartilage of the soft callus (Maes *et al.* 2010).

1.2.7 Mineralization and resorption

Chondrocytes in the fracture callus proliferate and secrete collagen and other proteoglycans. Subsequently, they become hypertrophic and switch to the production of ALP to calcify the extracellular matrix. Afterwards, the resorption of this mineralized cartilage is mounted by several signaling factors, such as TNF-α, osteoprotegerin (OPG), macrophage colony-stimulating factor (M-CSF), and receptor activator of nuclear factor kappa B ligand (RANKL) (Barnes *et al.* 1999; Gerstenfeld *et al.* 2003b). Woven bone is generated by bone cells and osteoclasts, which are both recruited by OPG, osteopontin (OPN), M-CSF, and RANKL. The Wnt pathway regulates the differentiation of pluripotent MSCs into the osteoblastic lineage and positively regulates osteoblastic bone formation (Chen & Alman 2009). TNF-α further promotes the recruitment of MSCs with osteogenic potential but its most important role may be to initiate chondrocyte apoptosis (Gerstenfeld *et al.* 2003b).

The calcification mechanism requires mitochondria. In addition to energy conversion, they gather granules filled with calcium, which were produced in the hypoxic fracture environment. After elaboration into the cytoplasm of fracture callus chondrocytes, the calcium granules are transferred into the extracellular matrix. There, the calcium precipitates in combination with phosphate to form mineral deposits (Ketenjian & Arsenis 1975). The peak of the hard callus formation is defined by mineralized tissue and extracellular matrix markers such as type I procollagen, OCN, ALP and osteonectin (Einhorn 1998). As the hard callus formation progresses and the calcified cartilage of the hard callus exchanges with woven bone, the callus becomes more solid and mechanically rigid (Gerstenfeld *et al.* 2006).

1.2.8 Bone remodeling

The temporary hard callus is a stiff structure and provides biomechanical stability. However, it is not completely restoring the biomechanical characteristics of uninjured, healthy bone. Hence, a second phase of resorption is commencing during the bone regeneration cascade. In particular, the hard callus is remodeling into a lamellar bone structure with a central medullary cavity (Gerstenfeld *et al.* 2003b). This phase is regulated by highly expressed TNF-α and IL-1, compared to the other members of the TGF-β family (Ai-Aql *et al.* 2008; Mountziaris & Mikos 2008). However, some BMPs such as BMP-2, are also involved in this phase with strong expression (Marsell & Einhorn 2009). The process of remodeling is conducted by a balance between lamellar bone deposition and hard callus resorption by osteoblasts and osteoclasts, respectively (Wendeberg 1961). The external callus is slowly replaced by lamellar bone. Whereas the internal callus remodeling re-establishes a medullar cavity, which is typical for diaphyseal bone (Marsell & Einhorn 2011).

Also at this later phase of the bone healing process, immune cells are involved. Monocytes and macrophage are entangled in osteogenesis (Guihard *et al.* 2012; Nicolaidou *et al.* 2012) and fracture callus remodeling (Alexander *et al.* 2011). Interestingly, adaptive immune cells appear to be involved

in governing the quality of the new formed bone (Toben *et al.* 2011). After Wolff's law, the bone in a healthy person or animal will then further adapt to the loads under which it is placed. Recently, we have shown for the first time that T cells are also guiding the remodeling process and determine bone quality (El Khassawna *et al.* 2017). In particular, T cells are regulating collagen deposition and osteoblast distribution. Therefore, in a healthy system, T cells do not only enhance the initial pro-inflammatory phase but also contribute to proper bone elasticity for optimal absorbance of mechanical loading.

1.3 Impaired bone healing conditions

Many insides into osteoimmunology are derived from the findings on rheumatoid arthritis (RA). These basic principles are often used to describe the impact of inflammatory processes at the onset of bone healing. However, there are fundamental difference in those two clinical situations. On the one hand, rheumatoid arthritis is a chronic inflammation whereas bone healing is characterized by distinct phases of inflammation. On the other hand, there are clinical cases of impaired healing or even permanent non-unions, which could be explained by potential chronic inflammation appearing at the early stages of the healing process (Parihar *et al.* 2010; Claes *et al.* 2012). For instance, chronically high levels of TNF-α impaired fracture healing in a murine diabetes model (Alblowi *et al.* 2009). In particular, diabetes-enhanced TNF-α levels increased the expression of resorptive factors in chondrocytes through a process that involves activation of forkhead box protein O1 (FOXO1). Furthermore, the TNF-α dysregulation lead to enhanced osteoclast formation and accelerated loss of cartilage, which is a symptom in RA and detrimental in condrogenic stages of impaired fracture healing.

Moreover, using a bone defect model in rats it was found that the hematoma in the delayed healing group expressed significantly increased levels of pro-inflammatory IL-1β (Wang *et al.* 2016). The delayed bone healing resulted from a larger defect and was in line with findings that inflammatory cytokines influence blood coagulation. In particular, the clotting rate is accelerated by facilitating the γ–γ cross-linking of fibrinogen between protofibrils (Sahni *et al.* 2004). However, this, in particular, leads to decreased hematoma permeability (Sjoland *et al.* 2007).

Classically, reasons for delayed fracture healing or non-unions are critical gap size (Clements *et al.* 2008; Reichert *et al.* 2009), or suboptimal fixation (Schell *et al.* 2008; Lienau *et al.* 2010; Mehta *et al.* 2010). However, besides blaming the surgeons, emerging knowledge in the field of bone healing in the recent years has indicated several underlying biological deficits within the body of the patients, e.g. in angiogenesis together with the formation of atrophic pseudarthrosis (Keramaris *et al.* 2008; Lienau *et al.* 2009; Fassbender *et al.* 2011). Moreover, the importance of the signaling and cellular factors of the hematoma has profound implications in the clinical setting. During surgical treatment of open fractures, surgeons often lavage the wound extensively to reduce the risk of infections. However, this also depletes

the wound bed of crucial mediators as well as immune and osteoprogenitor cells, which can lead to unfavorable regenerative outcomes (Chan *et al.* 2015).

Especially, an elongation of the pro-inflammatory phase results in delayed healing conditions (Kolar *et al.* 2011; Schmidt-Bleek *et al.* 2012a; Schmidt-Bleek *et al.* 2012b). The immediate localized inflammatory reaction should be short-lived and leading to the desired regenerative responses. However, it can be prolonged or too excessive and resulting in tissue damage. In particular, delayed bone healing in a sheep model revealed a prolonged pro-inflammatory reaction (Schmidt-Bleek *et al.* 2012b), which had a negative influence on the revascularization of the injured region (Lienau *et al.* 2009) and subsequently delayed the chondrogenic and osteogenic processes (Lienau *et al.* 2010). A clinical study confirmed the association between the individual immune responsiveness and bone healing outcome (Hoff *et al.* 2011). Immune-suppressed fracture patients suffering from autoimmune disease or other conditions of an impaired immune system compared to healthy fracture patients showed a pronounced inflammatory reaction. This accented inflammation coupled with an inadequate response to the hypoxic conditions after injury results in a delayed or ineffective bone healing. Recently, my colleagues could show that the local application of SDF-1 is not significantly beneficial to femoral fracture healing, although it is a strong chemoattractant for osteogenic progenitor cells (Cipitria *et al.* 2017). However, due to the additional potent triggering of migration of immune cells by SDF-1, a potential unbeneficial ratio of recruited BM-MSCs to inflammatory cells was discussed.

Furthermore, specific immune cell subsets are correlated to a negative influence on regeneration. Decades ago it was suggested by studies on wound repair, that specific inflammatory cells, i.e. CD8+ T cells, might have negative effects on the healing process (Barbul *et al.* 1989). Therefore, the initial inflammatory phase of bone healing was investigated in sheep (Schmidt-Bleek *et al.* 2012a). A delayed healing situation correlated with an increased fraction of $CD8^+$ T cells in the fracture area 60 hours after osteotomy (Schmidt-Bleek *et al.* 2012b). In the clinics, delayed fracture healing in patients significantly correlated with enhanced levels of terminally differentiated CD8+ T_{EMRA} cells in peripheral blood (Reinke *et al.* 2013). The high titer of CD8+ T_{EMRA} cells reflected individual immune profiles rather than a post-fracture reaction. Furthermore, CD8+ T_{EMRA} cells were condensed in fracture hematoma and strong producers of the pro-inflammatory cytokines INF-γ and TNF-α. For instance, subcutaneous implantation of 200 ng of TNF-α in a BMSC-treated critical-sized defect model suppressed BM-MSC regeneration of bone (Suzawa *et al.* 2003). Additionally, IFN-γ was subcutaneously implanted at the site of a BM-MSC scaffold in a cranial defect in mice and reversed the ability for BM-MSCs to heal the defect (Liu *et al.* 2011).

The decline in regenerative capacity during the aging process is a phenomenon observed in all vertebrates as I have discussed in a previous publication (Wendler *et al.* 2015). In addition to stem cell aging, the risk for cancer is growing with age. On the one hand, this is due to a decrease of proto-oncogenic signals accompanied by an increase in gate-keeping tumor suppressor signals with age, to

counteract the increasing risk of cancer incidences (Nakada *et al.* 2011). This negatively affects stem cell self-renewal, and hence, regenerative capacity and tissue growth decline during aging. On the other hand, the above mentioned immunogenic age-related positive correlation with CD8+ T_{EMRA} cell titers and the duration of fracture healing in patients is even discussed as new diagnostic tool for the prediction of impaired healing (Reinke *et al.* 2013).

Besides the age-dependent changes in stem and progenitor cell pools, the generation and expansion of an immune memory is another factor diminishing regenerative capacity of bone in the aged. This fact could additionally be confirmed by an improved healing outcome after rejuvenation of the immune system (Xing *et al.* 2010). In addition, immunocompromised mice develop increased bone density (Sjogren *et al.* 2012).

The immune system has developed during evolution into a highly efficient system to protect the organism from invading pathogens. However, from the osteoimmunologic perspective it appears that this might was paid with decreased regenerative capacity. During lifetime, the immune systems grows more experienced, which is apparent in the change of its cellular composition, behavior and cytokine production (Fulop *et al.* 2017). In general, these age-related changes are found in several immunologic parameters, which are summarized as immunosenescence. Over the years, this leads to a cumulative up-regulation of pro-inflammatory factors. A parallel process is called inflamm-aging, which is related to a lower, but still chronic inflammation in the elderly. We could show recently that also the experience level of the adaptive immune system in particular, has an impact on bone regeneration and homeostasis (Bucher *et al.* 2019).

1.4 Immune modulation

1.4.1 Time independent modulation

The regenerative process should be initiated by a strong but timely sharp pro-inflammatory phase. If this is not the case, T cells represent a steering tool to reach desired parameters, i.e. the absence of mature adaptive immune cells accelerated fracture healing, in particular, earlier mineralization and remodeling (Toben *et al.* 2011). However, adaptive immune cells are involved in supporting the quality of the new formed bone. As we have shown, this is in particular due to T cell functions (El Khassawna *et al.* 2017). T cells secret inflammatory cytokines that promote bone resorption, as well as, Wnt ligands that stimulate bone formation and regulate bone homeostasis by cross talking with bone marrow stromal cells and osteoblasts. Furthermore, in the mouse osteotomy model, which was also used in this thesis project, a depletion of CD8+ T cells via specific antibodies prior to fracture resulted in enhanced endogenous regeneration (Reinke *et al.* 2013). In contrast, a transfer of CD8+ T cells impaired the healing process, i.e. mimicking the clinical situation of patients with high CD8+ T_{EMRA} titers.

Studies on wound healing indicated already a positive effect of CD8+ cell depletion 24 h prior or starting at the time point of wound incision (Barbul *et al.* 1989). Interestingly, these studies did not find any effects of depletion of $CD4^+$ T cells on wound healing. However, reports about the relationship between high bone mass and decreased bone resorption in mice with high Treg numbers led to the assumption that this subpopulation could promote bone healing (Zaiss *et al.* 2010; Pacifici 2013). The tolerogenic capacity of Tregs to counteract transplant rejection (van Maurik *et al.* 2002) and their negative effect on osteoclasts (Zaiss *et al.* 2007) support this assumption. On the one hand, a positive effect was shown in calvarial defect healing, which was stimulated by enhancing autologous bone graft with non-activated Treg substitution 2 days before defect induction (Liu *et al.* 2011). On the other hand, the role of endogenous Treg in the early inflammatory process is yet to be determined.

With regard to innate immune cells, the early inflammatory phase after trauma is associated with the release of interleukins and TNF-α produced by pro-inflammatory M1 macrophages (Nourissat *et al.* 2015). Potentially, innate immune cells such as M1 macrophages were compensating for accordingly, the loss of T cells and CD8+ cells in knockout or depletion experiments described above. On the contrary, the secondary inflammatory response involves anti-inflammatory M2 macrophages, which produce not only anti-inflammatory cytokines, such as IL-10, TGF-β, but additionally growth factors involved in neovascularization, such as VEGF, fibroblast growth factor (FGF) and platelet-derived growth factor (PDGF), and pro-fibrotic factors, such as connective tissue growth factor (CTGF) (Nourissat *et al.* 2015; Chernykh *et al.* 2016). Recently, we could show in a mouse osteotomy model that initial local enforcement of M2 macrophage polarization by immediate burst-like release of IL-4/IL-13 within the osteotomy gap enhances bone fracture healing (Schlundt *et al.* 2015).

Hence, a further immunomodulatory approach targeting time-independent stimulation of innate immune cells during the regeneration process constitutes the addition of G-CSF (granulocyte colony stimulating factor). G-CSF stimulates granulocytes, macrophages and neutrophils. Interestingly, G-CSF induces doubling of all T cell populations when given to patients (Hartung *et al.* 1999). However, *ex vivo,* this growth factor decreased the proliferation of lymphocytes and their secretion of pro-inflammatory cytokines. Furthermore, improved bone formation was observed after G-CSF treatment in rat and rabbit, via intravenous and local application, respectively (Ishida *et al.* 2010; Herrmann *et al.* 2018). Therefore, another crucial innate immune cell type, which early stimulation could potentially positively correlate to fracture regeneration outcome are neutrophils. The depletion of this important cell type led to a reduction of mesenchymal repair tissue within the injured growth plate cartilage in rat (Chung *et al.* 2006a). Moreover, depletion of neutrophils by anti-Ly6G resulted in impairment of fracture healing, potentially due to disruption of downstream events of the inflammatory cascade, including recruitment of monocytes (Chan *et al.* 2015).

Taken together, time-independent strategies for immune modulation to support bone healing are those, which can be administered at any time of the regenerative cascade, in particular, at the onset of the fracture, however, still allow for a considerable pro-inflammation for process induction.

1.4.2 Time dependent modulation

Potent immunosuppressive interventions in bone healing appear to be dependent on the time point at which they are administered to the process. In particular, the use of anti-inflammatory or cytotoxic medications, directly at the onset of the regeneration process, including corticosteroids, non-steroidal anti-inflammatory drugs (NSAIDs), or chemotherapeutic agents, have been shown to be deleterious (Altman *et al.* 1995; Gerstenfeld *et al.* 2003c; Simon & O'Connor 2007; Dimmen *et al.* 2008; Pountos *et al.* 2008; Sandberg & Aspenberg 2015).

Fascinatingly, a sharply circumscribed amplification of the first inflammatory response can even be beneficial to the regenerative process. Chan et al. showed that local treatment with the pro-inflammatory cytokine TNF-α was effective in augmenting fracture healing when administered at the fracture site during the first 24 h after surgery (Chan *et al.* 2015). In contrast, early administration of inflammation suppressing IL-10 into the fracture site, i.e. on days 0 and 1, lead to reduced bone formation. Subsequent chronically high levels of TNF in the process are known to impair fracture healing (Alblowi *et al.* 2009). However, early anti-TNF treatment also delayed healing for at least 4 weeks. In line with this fact, TNFR-deficient mice (TNFR1-/-/TNFR2-/-) show delayed fracture healing (Gerstenfeld *et al.* 2003a). Hence, this is indicating the dual role of TNF-α in the process, which is dependent on the time point of administration.

Crucially, the early inflammatory phase represents a key rate-controlling step in fracture healing for pro-inflammatory signaling. However, broad anti-inflammatory factors such as IL-10 should be administered after the first 24 h in the regeneration process. Hence, delayed administration of strong secretors of this immunosuppressive molecule, such as activated Treg, should be considered as well. A very potent anti-inflammatory pharmacological compound constitutes Iloprost, which is a prostacyclin (PGI_2) analog (see below). Hence, a similar inhibitory effect compared to initial application of for instance IL-10 in fracture healing was found with Iloprost (Dogan *et al.* 2014). This indicates that PGI_2 related molecules should be administered after the early pro-inflammatory phase in bone healing.

1.5 Prostacyclin

Prostacyclin (PGI_2) is a small signaling molecule (Fig. 1.4 A), which is derived from the sequential metabolism of arachidonic acid by cyclooxygenase-2 (COX-2) and prostacyclin synthase (PGIS) (Needleman *et al.* 1976). COX-2 expression is triggered via specific stimulants such as cytokines,

growth factors, bacterial endotoxins, tumor promoters, and hormones by macrophages, neutrophils, and activated MSCs (Jaffar *et al.* 2002; Camacho *et al.* 2008; Gurgul-Convey & Lenzen 2010). Typically, COX-2 is associated during pro-inflammatory conditions like atherosclerotic lesions, aortic aneurysms, or vascular damage (Egan *et al.* 2004). Though COX-2's products mostly provide protective effects in certain chronic inflammatory diseases such as RA, COX-2 can be inhibited by NSAIDs and specific COX-2 inhibitors. PGI_2 is mainly produced in mammalian vasculature with highest levels in pulmonary arterial segments (El-Haroun *et al.* 2008). Additionally, PGI_2 plays an important role in cardiovascular health specifically inhibiting platelet aggregation during bleeding and having powerful vasodilatory effects via relaxation of smooth muscles (Camacho *et al.* 2011; Mohite *et al.* 2011). Since endogenous PGI_2 is chemically stable for only 42 seconds in aqueous solution, Iloprost was developed (Fig. 1.4 A). Iloprost is a stable drug, both chemically and biologically, with a biological half-life of 25 minutes (Dorris & Peebles 2012).

1.5.1 Therapeutic use

Iloprost is used in the clinical setting to treat autoimmune and cardiovascular diseases. Important effects are a widening of blood vessels (vasodilation) via relaxation of smooth muscles, a reduction of vessel permeability and anti-coagulation. Iloprost is approved for treatment of peripheral arterial occlusive disease (Petje *et al.* 2004; Herink *et al.* 2010; Canciglia *et al.* 2011; Riemekasten *et al.* 2012) and pulmonary arterial hypertension (PAH) (Roman *et al.* 2012). At the orthopedic department of the Charité Berlin it was shown that it can be used as a medication in bone to treat bone marrow edema and avascular necrosis (Disch *et al.* 2005), which are even more severe medical conditions. This observation was further confirmed in other clinical studies (Aigner *et al.* 2005; Elder 2006; Tillmann *et al.* 2007; Jager *et al.* 2008; Pabinger *et al.* 2012).

As pharmacologic immune modulators PGI_2 analogs are already in use for pulmonary vascular disease and atherosclerosis (Stitham *et al.* 2011). As typical for natural powerful signaling molecules, also PGI_2 has a second face. Endogenous PGI_2 is functioning as pathophysiological mediator in RA, at which COX-2 inhibitors are used to "cut-off" all endogenous prostaglandin formation as mentioned above. However, this chronic disease is far from being completely understood.

1.5.2 Signaling pathway

Prostaglandin I_2 receptor (IP) is the cell surface receptor designated for PGI_2 and constitutes a seven transmembrane G-protein-coupled receptor (Matsuoka & Narumiya 2008), i.e. it is coupled to a guanosine nucleotide-binding α-stimulatory protein (Gαs). When PGI_2 is binding IP, it stimulates adenyl cyclase, which leads to increased intracellular cyclic adenosine monophosphate (cAMP) (Fig. 1.4 B). The signaling cascade subsequently activates protein kinase A (PKA), which phosphorylates key

proteins (Mohite *et al.* 2011). Downstream events comprise relaxation of muscle cells, such as in smooth muscles or heart muscles (Grobetal *et al.* 2014), as well as reduction of cell proliferation, and other mainly inhibitory mechanisms such as suppression of inflammation (Dorris & Peebles 2012).

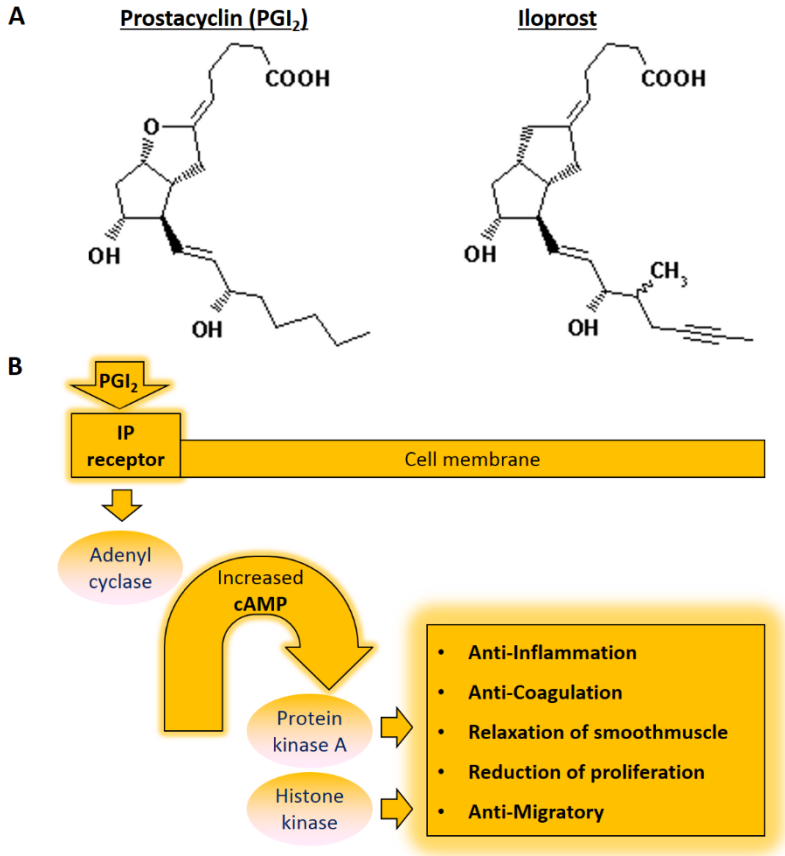

Figure 1.4: Prostacyclin (PGI_2) is a small signaling molecule able to trigger a strong signaling cascade. (A) The molecular structures of PGI_2 and its chemically stable synthetic analog Iloprost. (B) When PGI_2 binds its IP receptor in the cellular membrane a signaling cascade triggers, which is mainly characterized by an increase in intracellular cAMP. Further down-stream, depending on the cell type, this leads to functions such as reduction of inflammation, relaxation of smooth muscles and inhibitory effects. Modified from Dorris & Peebles 2012.

Besides the known membrane IP receptor, a peroxisome proliferator-activated nuclear receptor (PPAR) functions as a transcription factor after activation by binding of PGI_2 to IP (Gurgul-Convey & Lenzen 2010; Mohite et al. 2011). Among the three PPAR isoforms, α, δ (also designated as β), and γ, the latter is potentially involved downstream of the activated IP membrane receptor and thus, can be stimulated via PGI_2 analogs. Besides PGI_2, a broad range of ligands can trigger PPARs responsiveness, such as metabolites of the COX and lipoxygenase pathway and hypolipidemic agents. However, PPARγ is the only PPAR that can be activated through the IP using stable PGI_2 analogs.

Iloprost is further able to bind all of the four receptors of PGE_2, i.e. EP1, EP2, EP3 and EP4 (Moreno 2017). Besides vasodilation of blood vessels, PGE_2 has similar anti-inflammatory effects to PGI_2, in particular to T cells (Wiemer *et al.* 2011), and additionally inhibits proliferation (Huang *et al.* 2007).

Adding to the generally inhibitory function of PGI_2 signaling, it decelerates cellular migration. PGI_2 inhibited eosinophilic migration through the endothelial barrier by affecting chemotaxis, adhesion, and transmigration and by strengthening the endothelial barrier (Konya *et al.* 2010). Chemotaxis was limited by direct stimulation of the IP receptor on eosinophils, due to up-regulation of cAMP despite the use of chemoattractants such as eotaxin and complement component 5a (C5a). Furthermore, rapid up-regulation of eotaxin-induced CD11b adhesion molecule was diminished by PGI_2 leading to decreased adhesion to fibronectin.

Towards the differentiation of MSCs into osteoblasts and to chondrocytes it was claimed that cAMP signaling is involved (Carroll & Ravid 2013). In addition, *in vivo* therapy of myocardial infarction with MSCs modified with prostaglandin I synthase gene improved cardiac performance in mice (Lian *et al.* 2011). Furthermore, PGI_2 induces persistent angiogenic effects in hind limb ischemia through adhesion of endothelial progenitor cells (EPCs) to perivascular sites of neovessels via integrins in addition to paracrine effects (Aburakawa *et al.* 2013). Furthermore, PGs and COX have been reported to play a role in integrin-mediated endothelial migration and angiogenesis. These findings suggest that PGI_2 signaling is essential for EPCs to accomplish their function and plays a critical role in the regulation of vascular remodeling (Kawabe *et al.* 2010). Moreover, in another study COX-1 was inactivated, which led to impaired tube formation and cell proliferation (He *et al.* 2008). Interestingly, this impairment could be rescued by treatment with Iloprost or the selective PPARδ agonist GW501516. However, this was not the case for the selective IP receptor agonist Cicaprost.

1.5.3 PGI_2 as immune modulator

1.5.3.1 PGI_2 and the adaptive immune system

IP receptors are located on a variety of different cell types, such as neurons, smooth muscle cells of the aorta, pulmonary and coronary arteries, as well as on megakaryocytes. Moreover, IP receptors are present on platelets, medullary thymocytes, neutrophils, dendritic cells, eosinophils, T regulatory cells, and activated T cells (Jaffar *et al.* 2002; Lovgren *et al.* 2006). Hence, the PGI_2 analog Beraprost could reduce T cell proliferation, which was stimulated by anti-CD3 (Lee *et al.* 2005). Also the here investigated analog Iloprost shows anti-inflammatory effects. For instance, it reduced IFN-γ and IL-6 induced monocyte chemoattractant protein 1 (MCP-1), IL-8, RANTES, and TNF-α production in human monocytes (Strassheim *et al.* 2009). Moreover, further downstream of this signaling cascade, cAMP responsive element modulator (CREM)α was reported to trans-repress the transmembrane glycoprotein CD8 and is contributing with this mechanism to a shift from CD8+ T cell populations to CD3+CD4-

CD8- T cells (Hedrich *et al.* 2013). Furthermore, cAMP indirectly suppresses CD8+ T cell immunity via dendritic cell differentiation towards a tolerogenic phenotype that may contributes to peripheral tolerance as well as to the establishment of immunosuppressive microenvironments, i.e. defective capacity to prime CD8+ T cells (Challier *et al.* 2013).

Up-regulation of endogenous cAMP is further required for the suppressor function of CD3/CD28-activated murine and human Treg (Bopp *et al.* 2007; Klein *et al.* 2012). It was also claimed that IFN-α deactivates the suppressive function of human CD3/CD28-activated Treg by downregulating their intracellular cAMP level (Bacher *et al.* 2013). However, administered to naïve CD4+ T cells Iloprost favors Th17 differentiation and reduces Treg differentiation upon CD3/CD28 activation (Liu *et al.* 2013b). Another study investigated the effect of 5 days intravenous administered Iloprost on immune response in systemic sclerosis (SSc) patients. There, Iloprost reduced T cell, Treg and TNF-*α* levels both *in vivo* and *in vitro* within PBMCs, but increased TGF-β secretion (D'Amelio *et al.* 2010). Also in another clinical study, pro-inflammatory Th17 and Th22 cells were more abundant in PBMCs of patients with SSc than in healthy donors (Truchetet *et al.* 2012). PGI_2 analogs (Iloprost, Treprostinil and Beraprost) significantly increased IL-17A and IL-22 in those PBMCs while decreasing IFN-γ production. These effects relied on specific expansion of Th17 and Th22 cells and inhibition of Th1 cells. In particular, the enhanced Th17 cell responses depended on increased IL-23 production by monocytes.

Moreover, the general immunosuppressive properties of PGI_2 signaling is to a large extent derived from the inhibition of Th1 and Th2 cytokine production from classic CD4 helper T cells (Nagao *et al.* 2003; Zhou *et al.* 2007b). In a mouse study investigating Cicaprost and Iloprost, IFN-*γ* from Th1 cells and IL-4, L-10, and IL-13 from Th2 cells were diminished in a dose dependent manner (Zhou *et al.* 2007a). The inhibition of these cytokines correlated well with the downregulation of master regulator NF-*κ*B, whilst cAMP levels were rising. PGI_2 further regulates other adaptive cell types, such as B cells. For instance, Beraprost increased the costimulatory molecule CD86 via the IP receptor with following cAMP elevation in activated B cells (Kim *et al.* 2011).

1.5.3.2 PGI_2 and the innate immune system

The IP receptor is also found on macrophages (Lovgren *et al.* 2006). Surprisingly, the responds of macrophages towards PGI_2 analogs is tissue dependent. In peritoneal macrophages activation of the IP receptor inhibited phagocytosis of IgG-opsonized targets more intensively compared to alveolar macrophages in the lungs, suggesting variations in immunomodulatory effects (Aronoff *et al.* 2007). Furthermore, after activation with lipopolysaccharide (LPS) peritoneal macrophages increased production of IL-6 in combination with Iloprost or Carbaprostacyclin. However, alveolar macrophages

showed less increased IL-6 secretion. In addition, these two PGI_2 analogs only suppressed bacterial killing of peritoneal macrophage.

In another study, utilizing LPS stimulated NR8383 alveolar rat macrophages, found that Iloprost reduced secretion of the pro-inflammatory chemokine MCP-1. Moreover, the expression of the anti-inflammatory M2-type macrophage surface markers CD163 and CD206 were increased (Alkhatib *et al.* 2018). *In vivo*, subcutaneously applied Iloprost elevated the number of CD163+ cells at this site. Also in LPS-induced peripheral blood-derived monocytes, PGI_2 analogs reduced pro-inflammatory MIP-1α levels (Tsai *et al.* 2014).

Furthermore, PGI_2 also has important anti-inflammatory effects on dendritic cells. Whilst increasing IL-10 expression, Iloprost inhibited toll-like receptor-mediated expression of TNF-*α* and IFN-*α* in human plasmacytoid dendritic cells (Hung *et al.* 2009). Hence, Iloprost might increase tolerogenic abilities of plasmacytoid dendritic cells. Moreover, PGI_2 analogs decrease maturation of BM derived dendritic cells (BM-DC), function, and pro-inflammatory cytokine production after activation with LPS. In parallel, PGI_2s enhanced secretion of IL-10 in BM-DC and reduced chemokine production in mice. In particular, *in vitro* PGI_2 analogs lowered secretion of TNF-*α*, IL-1*α*, IL-6, and IL-12 in a clear dose-dependent manner (Zhou et al. 2007b).

1.6 Local drug delivery

Local application of drugs in the case of musculoskeletal injury is a promising approach, because the region of injury is in most cases clearly circumscribed and exposed during classical treatment, e.g. during internal fracture stabilization. Hence, the region to place for instance an immune modulator is easily accessible. Local drug delivery comes with a number of benefits compared to systemic administration, such as:

- decreased required dosage
- reduced possible risk of negative effects of the drug
- minimized stress for patients compared to intravenous application
- lowered cost for the drug and treatment

If a biodegradable drug carrier is used a second surgical intervention for its removal is not required, which further decreases risks, costs and stress for the patient.

1.6.1 Core-shell systems

Towards the tuneability of local drug release systems, chemical alterations, for instance, can have tremendous clinical potentials, however they are rather challenging with respect to regulations. On the contrary, a straightforward approach is the design of core-shell systems.

Core-shell structures have two discrete parts, which are an inner core and an enclosing outer shell (Fig. 1.5 A). Each of them can perform independent functions, such as incorporating two different molecules. However, core and shell are both interfaced and molecular interactions between them can affect the other. The obvious shape is a spherical form, but the core-shell system can also be constructed in a continuous fibrous manner (Fig. 1.5 B). For medical purposes, signaling molecules can be incorporated into the core size, and can be loaded in the shell as well. However, in most cases the role of the core is to load therapeutic molecules for delayed release or to hold tissue cells and provide them with 3D culture environments. The shell in turn, protects the inner biological ingredients, controls the release kinetics of the core-contained molecules or harbors viable cells.

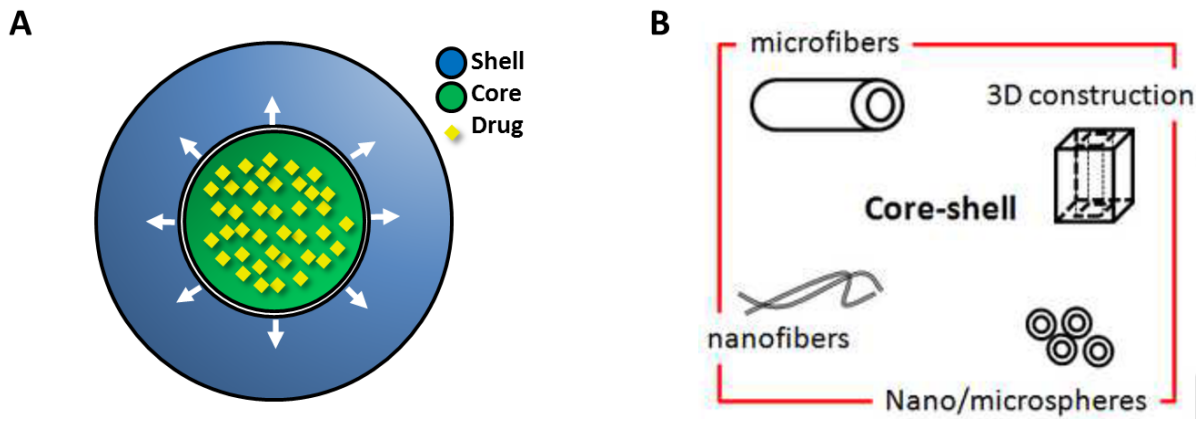

Figure 1.5: Core-shell method for delayed release of therapeutics from biomaterials. (A) Two-dimensional scheme of a drug-loaded core-shell system. The inner core (green) is completely surrounded by the outer shell (blue). Therefore, the drug (yellow) first requires to diffuse out of the core (direction indicated with white arrows) and into the shell material for traveling further. Subsequently, the drug can leave the delivery system to function locally at the desired tissue environment. In these means, the shell controls the release kinetics of the core-contained molecules. (B) The core-shell method comes in various shapes and forms to suit different purposes. Besides the spherical form on micro and nano-scale, the core-shell system can also be constructed in a continuous fibrous manner in the micro or nano-scale. Larger macro-scale designs are also common, e.g. to hold tissue cells and provide them with 3D culture environments. In this case, the shell can protect viable cells. Scheme in (B) adapted from Perez & Kim 2015.

1.6.1.1 Drug loading and delivery

Core-shell designs are required for the delivery of drugs and molecules that have different functionalities, which need to be protected from processing conditions or for a desired time-programmed release.

Modifying parameters of the core-shell system, such as composition, chemical properties, and injection speed, can alter release profiles of delivered molecules (Yang *et al.* 2008; Tiwari *et al.* 2010).

In particular, hydrophilic drugs can be encapsulated in a hydrophilic core material and subsequently shelled with hydrophobic materials, which are only soluble in organic solvents. In this way, a phase separation is achieved similar to the "lotus effect" in nature (Lafuma & Quere 2003). In analogy, a hydrophobic drug could be loaded into a hydrophobic core polymer with a hydrophilic shell layer to strongly delay its release (Ji *et al.* 2010). For instance, a shell of water soluble polyethylene glycol (PEG) was used to entrap BMP-2 within the core of a hydrophobic polycaprolactone (PCL) nanofibrous structure blocking the release for over 24 days (Zhu *et al.* 2013). However, besides the used material, the thickness of the shell has also significant effects on the drug release (Kong *et al.* 2013).

For longterm release, microspheres constructed with synthetic polymers are available. Core-shell systems based on PHBV (Poly(3-hydroxybutyrate-co-3-hydroxyvalerate)) and PLGA (poly-D, L-lactic-co-glycolic acid) show sustained release of hepatocyte growth factor over a month (Zhu *et al.* 2009). Furthermore, tailorability of release kinetics could be achieved with PLGA and the synthetic PGI_2 ONO-1301 (Obata *et al.* 2008). The time point of release can also be chemically programmed to be activated by a specific trigger. For the core-shell systems at the nano-scale, the encapsulation of drug molecules is possible in the course of or after shell formation, and drug release can be triggered by the rupture of the shell composition or simple diffusion through the shell for burst-like or slow sustained release, respectively. In particular, the rupture mechanism is often designed to be stimuli-dependent, in such a way that it is responsive to temperature, pH, or enzymes (Lee *et al.* 2013; Wang *et al.* 2014). Similarly, certain polymers that are protease-sensitive, such as PEG-diacrylate, can be coated on the surface of nanoparticles. This ensures that the incorporated cargo molecules are released only when placed in contact with the protease present in cells *in vitro* or *in vivo* (Singh *et al.* 2011). Targeting hydrophobic properties, this system could again be enhanced. When a hydrophilic polymer was used for the core and layered with a thin hydrophobic shell, the inner matrix held drug molecules more selectively and sometimes more tightly, releasing them in a more controllable and sustained manner (Cao *et al.* 2014). Of course, core-shell designs can be further extended to the delivery of multiple different drugs.

1.6.1.2 Scales and shapes

Depending on shape and size, core-shell constructs can be categorized into microfibers, nanofibers, micro/nanospheres, and, as conducted in this thesis, larger 3D constructs (see above, Fig. 1.5 B) (Perez & Kim 2015). 3D constructs are prepared on the macro-scale, and can be scaled-up further for drug or cell delivery (Matsunaga *et al.* 2011).

Microfibers assembled into core-shell structures can deliver living cells via the core in contrast to more dense material configurations (Lagadic-Gossmann *et al.* 2004; Nicodemus & Bryant 2008). Alginate is

a commonly used polymer for the shell as it can crosslink easily in divalent solutions (Onoe *et al.* 2013; Perez *et al.* 2014). For the core, many other cell compatible hydrogels can be used including collagen, hyaluronic acid, and fibrin (Khademhosseini *et al.* 2006; Liu *et al.* 2013a; Perez *et al.* 2014). The release profiles of signaling molecules can be controlled through diffusion mechanisms through the shell. Additionally, several molecules can be loaded in the core and the shell or further layers for sequential release patterns (Biondi *et al.* 2008).

Nanofibers generated by electrospinning are suitable for incorporating drug molecules instead of cells, due to the nanoscale. However, the nanofibrous network can be used as a scaffolding matrix. Hydrophilic natural polymers favor biological interactions and cellular responses. Therefore, they are generally more suitable as shell materials (Ravichandran *et al.* 2011; Merkle *et al.* 2014). On the contrary, hydrophobic synthetic polymers can provide mechanical robustness, if desired for the core. For instance, inorganic silica xerogels provide relatively hard, but flexible nanofibers as shells for biomaterials in bone tissue regeneration (Toskas *et al.* 2013).

Nanospheres are rather used for drug delivery, whereas microspheres are additionally suitable as cell culture matrix. Hollowed nanospheres that can deliver drug molecules by diffusion, e.g. via the water-in-oil-in-water double emulsion method (Ha *et al.* 2011). There, water-soluble drugs are loaded into hollowed hydrophobic nanospheres such as PLA, PEG or methacrylate. However, to retain the hydrophilic drug the core can also be filled with water-soluble polymers, such as chitosan, alginate or poly(N-isopropylacrylamide) (PNIPAAm) (Narayanan *et al.* 2014).

1.6.2 Fibrin

In recent years, biodegradable and biocompatible polymers have emerged further from tissue engineering research to also promising drug delivery systems. These comprise proteins, such as fibrin, gelatin, collagen, albumin and silk fibroin. Further investigated are currently polysaccharides (alginate, hyaluronic acid, cellulose, chitosan and dextran) and synthetic polymers, such as poly-D, L-lactide (PDLLA). In this group, polymerized fibrin is being used as post-surgery sealant for over a century. Moreover, fibrin currently receives spotlight attention for its potential in the controlled delivery of various pharmaceuticals.

Hence, in the here described thesis project I selected human derived fibrin as a hydrogel-based carrier for the drug delivery in a pre-clinical fracture model, due to the major facts that fibrin:

- is already an abundant endogenous protein in the initial hematoma and granulation tissue
- is approved for biocompatibility, e.g. by the FDA
- is capable of retaining hydrophobic drugs, such as the here investigated drug Iloprost

Furthermore, fibrin gels are still the most extensively studied hydrogels in tissue engineering, regenerative medicine and therapeutic delivery (Spicer & Mikos 2010; Ahmad *et al.* 2015). The already excellent biocompatibility can be further backed up when using autologous precursors in the preparation. Moreover, fibrin matrices have further general advantages compared to other materials. These are ease of therapeutic and cell entrapment, but also the regulation and fine-tuning of the gel porosity. On the one hand, limitations are relatively poor mechanical strength and rapid *in vivo* degradability. On the other hand, this can be overcome by chemical modifications and composites of fibrin with other hydrogels. For instance, during studies with BMP-2 on chondrogenesis, conjugation of fibrin with heparin improved its performance and enhanced bone density as compared to collagen support (Yang *et al.* 2012). Additionally supportive for bone healing is the fact that fibrin matrices offer the advantage over collagen in promoting angiogenesis through modulation of integrin receptor expression.

Important to point out is that clotting of blood flow constitutes a great risk of medical grade fibrin application in highly vascularized regions. However, clinical studies of the fibrin-based drug Tissucol also known as Tisseel (Baxter) in bone tissue did not report adverse effects (Cortellini *et al.* 1995; Wagner *et al.* 2012; Anders *et al.* 2013; Volz *et al.* 2017). Similarly, no reported adverse effects occurred with the similar medical product Evicel (by Ethicon, Johnson and Johnson Medical Ltd.) (Skovgaard *et al.* 2013), nor with Biologx (Biostat) in spine (Yin *et al.* 2014).

The precursor fibrinogen is the key player in blood clotting in higher animals. Its polymerization starts with removal of the C-terminal fibrino-peptide from fibrinogen by the enzyme thrombin, which unmasks the self-aggregation potential of resulting fibrin (Fig. 1.6 A). This further transforms the protein complex into an insoluble three-dimensional network that can entrap molecules and even cells (Fig. 1.6 B) (Ahmad *et al.* 2015). In this process, thrombin's second role comes into play, i.e. conversion of the pro-transglutaminase FXIII (factor XIII) into the active enzyme FXIIIa. For that, thrombin requires the co-factor calcium ions (Ca^{2+}). Subsequently, FXIIIa introduces covalent crosslinking between the fibrin monomers, which reinforces stability (Lorand 2007). Further stabilization is achieved by anti-fibrinolytic agents like aprotinin (Pipan *et al.* 1992). Fibrinogen used in clinical sealants is usually purified from pooled human plasma, either by cryo-precipitation or ethanol fractionation (Sierra 1993). Whereas human recombinant thrombin is produced from the precursor recombinant prethrombin-1, derived from Chinese hamster ovary cell cultures (Chapman *et al.* 2006).

1.6.2.1 Fibrin as drug deliverer

A variety of strategies are available for entrapment of pharmaceuticals in fibrin matrices and their sustained release. Simple alterations of the matrix mechanical properties are possible with adjustments in the concentrations of the polymerization compounds, pH and ionic strength (Kjaergard & Weis-Fogh 1994). In particular, high fibrinogen concentrations cause a decrease in thickness of the fiber bundles

whilst increase their numbers (Herbert *et al.* 1998). In the same way does low concentration of Ca^{2+} lead to a decrease in diameter of the fiber bundles, but an increase in their total numbers. However, reducing the concentration of thrombin results in more compact gels with thicker fibers, which offer more mechanic stability (Rowe *et al.* 2007). On the contrary, preparing gels with high concentrations of thrombin produces thin fibrils and smaller pore size (Breen *et al.* 2006). Thus, the binding surface is increased for drug loading, and furthermore, the fibronectin-binding capacity of fibrin is enhanced, which also can provide improvements in microenvironment for osteoblast differentiation (Oh *et al.* 2012).

1.6.2.2 Entrapment of therapeutics

The most efficient way of loading fibrin with therapeutics is physical entrapment during polymerization. This is applicable to a broad spectrum of molecules independent of polarity or size. Therefore, drugs are added to fibrinogen or thrombin before clot formation (Fig. 1.6 B). Fibrin gels are porous and even macromolecules that are water soluble can diffuse out. However, hydrophobic molecules or those that bind to the hydrogels components by strong electrostatic interactions or affinity are initially retained and subsequently released gradually. In cases of strong interactions, drugs are only released after proteolytic degradation of the matrix. Therefore, a strategy can be to chemically modify therapeutics to increase their hydrophobicity for enhanced retention in the biomaterial (Schmoekel *et al.* 2005). Thus, as a protein fibrin has remarkable innate affinity for several growth factors (Sahni *et al.* 1998), growth factor binding proteins (Campbell *et al.* 1999) and certain drugs (Ait-Daoud & Johnson 2000).

In even more complex approaches, drugs can be anchored to the matrix via covalent linkages and affinity binding. These linkages can be achieved by transglutaminase or other factors, which crosslink with fibrin naturally during clot formation (Arrighi *et al.* 2009; Morton *et al.* 2009). Afterwards, the release of the therapeutic can be controlled by several parameters, including either the degradation of the matrix, the linkage, the affinity between the drug and the link or the relative amount of sites for interaction between gel and drug. In principle, the release of entrapped substances from the material is governed by the rate of diffusion or enzymatic degradation of the fibrin matrix (Sakiyama-Elbert & Hubbell 2000). Furthermore, combinations with other release approaches are possible for more tailored and elongated kinetics, i.e. the drug could be pre-entrapped in liposomes (Frucht-Perry *et al.* 1992; Chung *et al.* 2006c) or synthetic microspheres (Royce *et al.* 2004; Wang *et al.* 2008). Bifunctional reagents like glutaraldehyde can be crosslinked with fibrin matrices to improve mechanical strength, lower pore size or reduce susceptibility to proteolysis (Grassl *et al.* 2003; Capretto *et al.* 2010). Moreover, bifunctional reagents constitute a strategy to covalently link various therapeutics to fibrin. For instance, alkaline phosphatase (ALP) was covalently linked to fibrin with the help of EDC (1-ethyl-3-

(dimethylaminopropyl)carbodiimide hydrochloride), which improved bone formation, (Osathanon *et al.* 2009).

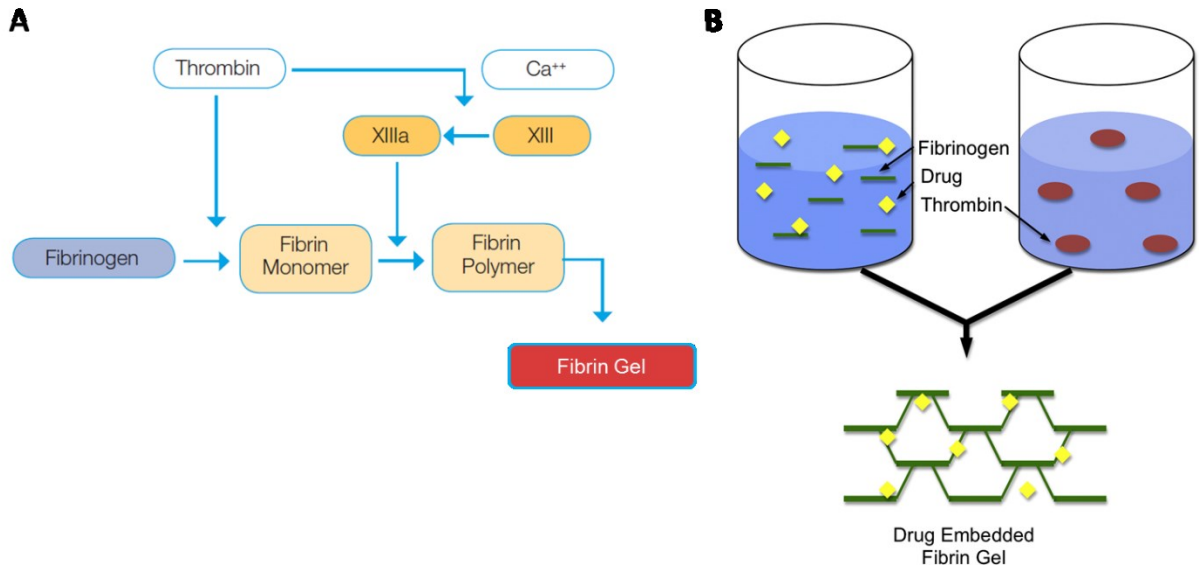

Figure 1.6: Fibrin gel polymerization for drug embedment. (A) Physiological principle of fibrin clotting is that fibrinogen is converted by the enzyme thrombin into fibrin monomers, which become gelatinous via aggregation. In parallel, in presence of calcium ions (Ca^{2+}) thrombin activates factor XIII into faxtor XIIIa for crosslinking and polymerization of the monomers. (B) During the process drugs can be embedded into the solutions of the two-component tissue glue, e.g. into fibrinogen as depicted. For (A) adapted from Tissucol Brochure (Baxter), and for (B) adapted from Spicer & Mikos 2010.

1.6.2.3 Spectrum of deliverable therapeutics

Antibiotics are investigated most intensively for sustained release from fibrin to combat infections with the sealant in post-surgery wound healing at which fibrin is used as gold standard (Ahmad *et al.* 2015). Furthermore, sustained delivery of anti-cancer drugs has also been attempted with the help of fibrin matrices. Doxorubicin incorporated into fibrin with sodium alginate composite and applied on the surface of hepatocellular AH60C tumors at the back of rats resulted in high concentration of the drug in the tumor extracellular fluid than in the plasma (Kitazawa *et al.* 1997). A robust and regulatory-wise favorable way is to select the protein fibrin for sustained release of hydrophobic drugs, which are more retained than hydrophilic ones. For instance, release kinetics of the chemotherapeutic agents Fluorouracil, Mitomycin C and Enocitabine were compared with each other (Yoshida *et al.* 2000). Fluorouracil and Mitomycin C were released rapidly independent of aprotinin addition, while Enocitabine – the most hydrophobic drug – was stronger retained in the presence of aprotinin. Compared to parameters such as protein binding and molecular weight only the hydrophobicity of the drugs correlated with retention.

In this regard, pre-encapsulation in liposomes is one promising strategy used to lower the release of water-soluble therapeutics that otherwise would easily diffuse out from fibrin gels. In particular, surface properties of the liposomes have a crucial role in their retention in the fibrin matrix. For instance neutral surfaces of liposomes are retained for longer durations compared to liposomes coated with water soluble polyethylene glycol (PEG) (Chung *et al.* 2006c). Crosslinking of the fibrin-liposome mixture with glutaraldehyde further decelerated the release of the water-soluble model drug Quinacrine. Similar results were achieved with water-soluble Tirofiban (Wang *et al.* 2008).

Several growth factors strongly bind to both fibrin and its heparin binding domain, such as PDGF/VEGF, FGF, TGF-β and neurotrophin families (Martino *et al.* 2013). Heparin is a negatively charged and highly sulphated glycosaminoglucan. It binds to fibrin with high affinity (Linhardt *et al.* 1991) and moreover interacts electrostatically with positively charged growth factors (Capila & Linhardt 2002). Furthermore, the recombinant fusion protein TG-pl-BMP-2 was generated, which has a trans-glutaminase sensitive binding domain. Hence, it was released from fibrin in a sustained manner and could induce a stronger healing response in rats and dogs as compared to that by bone autograft containing BMP-2 (Schmoekel *et al.* 2005).

Tissue engineering combines cell and molecular biology with materials and mechanical engineering to replace damaged or diseased tissues and organs (Ahmed *et al.* 2008). Towards the entrapment of living cells, fibrin possess several features essential for an ideal regenerative matrix. These include the ability to recruit cell types and deliver signaling components in addition to its biocompatibility (Rice *et al.* 2013). Moreover, receptors like integrins on the surface of several cell types including platelets and leukocytes bind to fibrin and promote cellular adhesion (Mosesson 1999). Subsequently, proteolysis by plasmin and other proteinases facilitates the migration of cells entrapped in the fibrin network.

1.7 Hypothesis and aims

Based on the preliminary work and the literature data, the hypothesis of this doctoral thesis is that the delayed local application of a PGI_2 analog shortens the inflammatory phases of bone healing and therefore accelerates the regenerative process.

To test the hypothesis specific aims were set to investigate the underlying mechanisms involved:

- *In vitro* efficacy testing of varying concentrations of a PGI_2 analog on cultured primary pro- and anti-inflammatory immune cells, such as CD8+ cells, Treg and polarized macrophages.
- Concentration testing of this PGI_2 analog on endochondral differentiation process of cultured MSCs, such as osteo- and chondrogenesis.
- Design and characterization of a local drug delivery system for delayed release of the PGI_2 analog.
- Investigation of the effects of delayed release of the PGI_2 analog on bone healing in an osteotomy model.

2. Materials

All utilized reagents, drugs, antibodies, devices and software are listed in tables 2.1 – 5.

2.1 Reagents and materials

Reagent	Order number	Supplier
2-Naphthoic acid	180246	Sigma-Aldrich
3-Isobutyl-1-methylxanthine (IBMX)	I7018	Sigma-Aldrich
Acetic acid 3 %	KK62	Carl Roth
Acetone	32201	Sigma-Aldrich
Acetonitrile	271004	Sigma-Aldrich
Acid fuchsin	7629	Merck
ACK Lysing Buffer	A1049201	Gibco
Alcian Blue	1A288	Chroma
Alizarin Red S	A5533	Sigma-Aldrich
β-glycerol phosphate (disodium salt pentahydrate)	50020	Sigma-Aldrich
Blade Microm SEC 35	10890701	Microm International
BMP-2 recombinant Human	120-02	Peprotech
Brillant Crocein R	1B109	Chroma
BSA, suitable for cell culture	A9418	Sigma-Aldrich
BSA, protease free	B8894	Sigma-Aldrich
Caspase-Glo® 3/7 assay	G8091	Promega
$CD4^+CD25^+$ Regulatory T Cell Isolation Kit, mouse	130-091-041	Miltenyi Biotec
CD8 S-pluriBead® anti-ms	29-00800-10	pluriSelect
Cetylpyridinium chloride	C0732	Sigma-Aldrich
Chloroform	288306	Sigma-Aldrich
Cryofilm 2C(10) 45mm in width	C-FS106	Section-Lab Co.LTD.
CyQUANT® Cell Proliferation Assay	C7026	Life Technologies

DAPI	32670	Sigma-Aldrich
Dexamethasone	D2915	Sigma-Aldrich
DMEM High Glucose	D6429	Sigma-Aldrich
DMEM Low Glucose	D5546	Sigma-Aldrich
DMSO, for cell culture	A3672,0100	AppliChem
Drill bit 0.45 mm	RIS.590.201	RISystem AG
EDTA	8043	Carl Roth
Embedding Medium SCEM	C-EM001	Section-Lab Co.LTD.
Eosin	2C 140	Waldeck
EtOH 100 %	K928	Carl Roth
FBS Superior	S 0615	Biochrom
Fixator MouseExFix	RIS.611.200	RISystem AG
Fix-Perm-buffer	88-8824-00	ebioscience
Fluorescence mounting medium	S3023	Dako
Formaldehyd, 37 %	BAKR7040.2500	VWR
Gigli saw wire (0.66mm)	RIS.590	RISystem AG
Glutamax	35050-038	Life Technologies
Iloprost, pure substance	18215	Cayman chemical
ImmEdge Hydrophobic Barrier PAP Pen	H-4000	Vector Laboratories
Indomethacin	I7378-5G	Sigma-Aldrich
Insuline from bovine pancreas	I6634	Sigma-Aldrich
Insulin-transferrin-sodium selenite media supplement	I1884 -1VL	Sigma-Aldrich
Iron hematoxilin	2E 032/052	Chroma
L-Ascorbic acid 2-phosphate sesquimagnesium salt hydrate	A8960	Sigma-Aldrich
Linoleic Acid	L1012-1G	Sigma-Aldrich
LIVE/DEAD® Cell Imaging Kit (488/570)	R37601	Life Technologies

LIVE/DEAD™ Fixable Aqua Dead Cell Stain Kit	L34957	Life Technologies
L-Proline	P5607-25G	Sigma-Aldrich
Methanol	HN41.1	Carl Roth
Mouse IFN gamma ELISA Ready-SET-Go!	88-7314-86	ebioscience
Mouse IL-10 ELISA Ready-SET-Go!	88-7105-86	ebioscience
Mouse TNFalpha ELISA Ready-SET-Go!	88-7324-86	ebioscience
MouseExFix MountingPin 0.45 mm	RIS.411.100	RISystem AG
n-Hexane	3907.2	Roth
Nile Red	N3013	Sigma-Aldrich
Nuclear Fast Red	7728	Carl Roth
Object slide	1000200	Marienfeld
Ortho-phosphoric acid	2608	Carl Roth
PBS (Dulbecco's PBS)	14190094	Gibco
PBS 10x	1610780	Biorad
Penicillin-Streptomycin (P/S)	P0781	Sigma-Aldrich
Paraformaldehyde (PFA), 20 %	15713S	Electron Microscopy Sciences
Phosphotungstic acid	3D092	Chroma
Presto Blue™	A13262	Life Technologies
Proteinase K, ≥500 units/mL	P5568	Sigma-Aldrich
rh IL-13	200-13	Peprotech
rh IL-4	200-04	Peprotech
rm IFN-γ	315-05	Peprotech
rm IL-2	P04351	R&D Systems
rm M-CSF	12343115	Immuno Tools
rm TNF-α	315-01A	Peprotech
RPMI media	FG 1215	Biochrome
Saffron du Gâtinais	5A394	Chroma

Saponin	47036-50G-F	Sigma-Aldrich
Sodium Azide, extra pure	822335	Merck
Sodiumpyruvate	A4859,0050	AppliChem
S-pluriBead® Mini Reagent Kit	70-50010-11	pluriSelect
Square box wrench 0.70 mm	RIS.590.111	RISystem AG
Suture material, Prolene 5.0	EH7404H	Ethicon
Tesafilm®	57206-00001	Tesa
rh TGF-βeta1 (mammalian derived)	100-21	Peprotech
Tissue freezing medium	14020108926	Leica
Trizma Base	T1503	Sigma-Aldrich
Trizma Hydrochloride	857645	Sigma-Aldrich
Trypan Blue Stain	15250061	Gibco
TrypLE	12604021	Life Technologies
Tween-20	P1379	Sigma-Aldrich
Vitro-Clud®	04-0001	R. Langenbrink GmbH
White 96 Well plates	136101	Nunclon
Xylol	UN 1307	J. T. Baker
β-Glycerophosphate disodium salt hydrate	G9422	Sigma-Aldrich
β-mercaptoethanol	M6250	Sigma-Aldrich

Table 2.1: Reagents and materials used with order numbers and supplier names.

2.2 Drugs

Drug	Supplier
Bepanthen	Bayer Vital GmbH
Temgesic	RB Pharmaceuticals Ltd
Ilomedine	Bayer AG
Inject®-F Tuberkulin-syringe	B. Braun Melsungen AG

Isoflurane	FORENE, Abott GmbH & Co. KG
Ketamin	Actavis Switzerland AG
Medetomidine	Janssen-Cilag GmbH
Sterican® cannula (size 18; 0.45 x 25 mm)	B. Braun Melsungen AG
Tissucol-kit 2.0 Immuno	Baxter
Tramadol	Gruenenthal

Table 2.2: Drugs used with supplier names. Ordered at Charité inhouse pharmacy.

2.3 Antibodies

Antibodies	Order number	Supplier
anti-CathepsinK	ab19027	Abcam
anti-CD206-PE	141706	BioLegend
anti-CD4	GK1.5	Deutsches Rheumaforschungzentrum
anti-CD68-AF488	MCA1957FT	AbD Serotec
anti-CD80-AF647	104718	BioLegend
anti-CD8-PE	ab25498	Abcam
anti-IFN-γ	559065	BD Pharmingen
anti-Laminin	L9393	Sigma-Aldrich
anti-mouse CD16/CD32 purified	14-0161-82	eBioscience
anti-mouse CD25-APC	102012	BioLegend
anti-mouse CD25-APC/Cy7	102026	BioLegend
anti-mouse CD28	16-0281-82	eBioscience
anti-mouse CD3ε	16-0031-82	eBioscience
anti-mouse CD3ε-PerCP	100326	BioLegend
anti-mouse CD4-Alexa Fluor®700	56-0042	eBioscience
anti-mouse CD62L-APC	104412	BioLegend
anti-mouse CD8a-eFluor®450	48-0081	eBioscience

anti-mouse NK-1.1-FITC	108706	BioLegend
anti-mouse TCRβ-PE	109208	BioLegend
anti-mouse FoxP3-FITC	11-5773-82	eBioscience
anti-rabbit AF647	A31573	Thermo Fisher Scientific
anti-rat AF954	A21207	Thermo Fisher Scientific
anti-TNF-α	559064	BD Pharmingen

Table 2.3: All antibodies used with order numbers and supplier names.

2.4 Devices

Device	Company
µCT Viva 40	SCANCO Medical AG
Axio Observer	Carl Zeiss
Cryotome CM3050S	Leica Biosystems
Electro Force LM1 Test Bench	Bose Corporation
Flow cytometer LSR II	Becton Dickinson Bioscience
Ultimate 3000 UHPLC with DAD	Thermo Fisher Scientific
Infinite M200 PRO	Tecan
Light microscope	Carl Zeiss
LSM 710	Carl Zeiss
Microtome RM2235	Leica Biosystems

Table 2.4: List of devices used.

2.5. Software

Software	Provider
i-control 1.9	Tecan
Axiovision 4.8	Carl Zeiss
Elisaanalysis.com	ELISAkit.com

FACS DIVA 6.1.3	Becton Dickinson Bioscience
FlowJo 9.6.4	FlowJo LLC
ImageJ 1.51J8	open-source
Matlab 7.7	MathWorks
MicroCT systems 6.5-3	SCANCO Medical AG
Office 2016	Microsoft
SPSS 22	IBM
Thermo xcalibur qual browser	Thermo Fisher Scientific
Zen 2011	Carl Zeiss

Table 2.5: Software used.

3. Methods

3.1 *In vitro* studies

Cell culture experiments were carried out under sterile S1 conditions on plastic tissue culture treated well plates or flasks. For all cell cultures a standard incubation chamber was used and kept constantly at 37 °C and 5 % CO_2. *In vitro* cell counts were performed with hemocytometers, trypan blue and light microscopy. If not indicated otherwise all centrifugation steps for the *in vitro* studies were carried out with 300 rcf at 4 °C for 10 min. Dulbecco's PBS without magnesium or calcium was used for *in vitro* work.

3.1.1 Organ harvest for primary cell culture experiments

C57BL/6N female mice were the source for all herein described *in vitro* experiments with primary mouse cells. Animal studies were performed with ethical permission according to the policies and principles established by the Animal Welfare Act, the National Institutes of Health Guide for the Care and Use of Laboratory Animals, and the National Animal Welfare Guidelines. Furthermore, approval was given by the local legal representative animal rights protection authorities (*Landesamt für Gesundheit und Soziales Berlin*: G0008/12; T0119/14; T0249/11).

Mice were kept purposely under semi-sterile conditions, which are described in detail below (see 3.3.1) to moderately activate the immune system. Prior euthanization, animals were deep narcotized with intraperitoneal injection of a mixture of 0.3 mg/kg b.w. Medetomidine and 60 mg/kg b.w. Ketamin for sedation and relaxation, respectively. After pedal withdrawal reflex test confirmed deep narcosis, cervical dislocation was performed. The skin of the abdomen was opened by a longitudinal cut and humeri, femura and tibiae were dissected and cleaned from skin and muscle tissue. Spleens were also harvested and, in particular, for CD8+/Treg isolation abdominal, axillary and brachial lymph nodes were collected. All organs were placed into individual tubes with ice-cooled RPMI media supplemented with 1 % v/v Penicillin-Streptomycin (P/S) antibiotics against bacterial contamination.

Subsequently, under a clean bench, bones were placed into RPMI media in a petri dish and residual flesh was removed. Epiphyses of the bones were cut away and bone marrow flushed out with RPMI media from a syringe into a 40 µm cell strainer located on a new sterile petri dish. Spleens and lymph nodes were also placed accordingly on strainers in RPMI media and cut into smaller pieces. Cells were carefully pushed out of their respective tissue matrix with a plunger. Afterwards, cell suspensions were transferred into 50 ml tubes. Residual cells were washed with respective media from strainer and dish and added into the 50 ml tubes. Cell suspensions derived from bone marrow were used for MSC cultivation and drug testing on macrophages and activated T cells from this organ. Whereas cell suspensions from spleen were allocated to experiments on activated T cells within splenocytes. For

CD8+/Treg isolation cell suspensions from bone marrow, spleen and lymph knots were combined for each individual animal.

Table 3.1 summarizes the performed *in vitro* experiments. Contained are cell types, organ sources, cell numbers, treatments, conducted assays and replicates.

Cell type	Organ source	Cell numbers /well	Treatment	Assays	Replicates
BM suspension	BM	5×10^5	2 days, CD3/CD28 activation, PBS, Iloprost (300 nM, 3 µM)	ELISA (IFN- γ, TNF- α, IL-10), metabolic activity, **conditioned media** harvest	6 biologic, 3 technical each
Splenocytes	Spleen				
CD8+ cells	BM, spleen, lymph knots	1.5×10^5	2 days, CD3/CD28 activation, PBS, Iloprost (3 µM)	ELISA (IFN-γ, TNF-α, IL-10), metabolic activity, **conditioned media** harvest	
Treg		1×10^5		ELISA (IL-10), metabolic activity, **conditioned media** harvest	
CD8+ cells	BM, spleen, lymph knots	5×10^4	5 days, CD3/CD28 activation, PBS, Iloprost (3 µM)	Proliferation, flow cytometry	
Treg					
Macrophages	BM	1×10^6	3 days cultivation, wash, 3 days, M1, M2 polarization, PBS, Iloprost (3 µM)	Immunofluorescence, ELISA (TNF-α, IL-10), metabolic activity	
Mesenchymal stromal cells (MSCs)	BM	1.5×10^4	14 days, osteogenic induction, PBS, Iloprost (300 nM, 3 µM)	Mineralization, metabolic activity, triglyceride formation	
MSCs	BM	2×10^4	5 days, adipogenic induction, PBS, Iloprost (300 nM, 3 µM)	Triglyceride formation	
MSCs	BM	3×10^5 each pellet	21 days, chondrogenic induction, PBS, Iloprost (300 nM, 3 µM)	Proteoglycan formation	
MSCs	BM	1×10^4	14 days, expansion media, PBS, Iloprost (300 nM, 3 µM)	Toxicology (Live/Dead immunofluorescence)	
MSCs	BM	5×10^2	7 days, expansion media, PBS, Iloprost (300 nM, 3 µM)	Proliferation	
MSCs	BM	1.5×10^4	14 days, osteogenic induction, **BM/CD8+/Treg conditioned media**	Mineralization, metabolic activity	
MSCs	BM		14 days, osteogenic induction, IFN-γ (50, 120 ng/ml), TNF-α (40, 60 pg/ml)	Mineralization, metabolic activity	
MSCs	BM	1×10^4	7 days, expansion media, IFN-γ (50, 120 ng/ml), TNF-α (40, 60 pg/ml)	Apoptosis	

Table 3.1: Summary of performed *in vitro* experiments. Conditioned media of immune cells, which were used in subsequent osteoinductive experiments are highlighted in bold. Experiments were performed in 96-well cell culture plates.

3.1.2 Drug concentration tests on activated T cells

For activation of T cells, each respective well was coated overnight at 4 °C with 100 µl PBS containing anti-CD3 (1:100) and anti-CD28 (1:500) prior loading with cell suspension. Accordingly, after centrifugation of cells suspensions from bone marrow and spleens for drug tests on bone marrow cells and splenocytes, cell pellets were resuspended in 2 ml erythrocyte lysis buffer and incubated 4 min at RT. Reaction was stopped via dilution with 20 ml PBS. After centrifugation, cell pellets were resuspended in 10 ml RPMI. Cells were counted and cell concentrations adjusted to plate 5 x 10^5 cells in 225 µl media into 96 well plates in respective experimental media. Experimental RPMI media for bone marrow derived cells and splenocytes contained 10 ng/ml IL-2, 1 % v/v P/S, 10 % v/v FCS, 50 µM β-mercaptoethanol, and a similar volume slot of either PBS, 300 nM Iloprost, or 3 µM Iloprost. After 2 days of incubation at 37 °C and 5 % CO_2 in a cell culture chamber, viability assays were performed with Presto Blue™ (see 3.1.9) and conditioned media (CM) were stored at -80 °C.

3.1.3 Drug concentration tests on polarizing macrophages

For polarization of macrophages 1 x 10^6 bone marrow derived cells per well were plated into 96 well plates and incubated three days with RPMI media supplemented with 50 ng/ml macrophage colony-stimulating factor (M-CSF), 1 % v/v P/S, 10 % v/v FCS, 50 µM β-mercaptoethanol. Macrophage maturation from monocytes was indicated via formation of spindle-shaped cells. Subsequently, media were replaced with the respective media for either M1 or M2 or M0 polarization and incubated for another 3 days. Polarization media all consisted of RPMI media supplemented with 1 % v/v P/S, 10 % v/v FCS, 50 µM β-mercaptoethanol and either 3 µM Ilomedine or equivalent volume of PBS. M1, M2 or M0 polarizations were induced via addition to the media of the same volume of either 20 ng/ml IFN-γ, 20 ng/ml IL-4/IL-13 or PBS, respectively (Sun *et al.* 2016). After 3 days of incubation, culture images were acquired, CM harvested and stored at -80 °C, and viability assays performed (see 3.1.9). Macrophage monolayers were washed twice with 200 µl PBS and fixed with 50 µl 4 % PFA/PBS for 10 min. Storage was done in 200 µl PBS at 4 °C for subsequent confirmation of polarization via immunofluorescence.

3.1.4 Immunofluorescence on macrophage monolayers

Polarization of macrophages (see 3.1.3) was confirmed with immunofluorescence staining of monolayers. After briefly washing with PBS, monolayers were permeabilized in 100 µl 0.1 % PBSTW

for 30 min and then blocked with 5 % FBS in PBS for 30 min. Subsequently, anti-CD68-FITC (1:200), anti-CD206-PE (1:200) and anti-CD80-AF647 (1:100) were applied in 30 µl blocking solution for 1h in dark at RT. Afterwards, wells were washed with PBS for 8 min and stained with 1 µg/ml DAPI in 30 µl PBS for 10 min to reveal nuclei.

Finally, monolayers were washed twice with PBS and 20 µl mounting media for fluorescence was added to preserve fluorescent dyes and well plates placed at 4 °C in dark until imaging. With a standard fluorescence microscope (Axio Observer, Carl Zeiss) images were acquired accordingly in the blue, green, yellow and far-red fluorescence channel.

3.1.5 CD8+ cell isolation and subsequent Treg enrichment

Isolation of CD8+ cells and enrichment of Treg cells were performed in two subsequent steps from cells derived from bone marrow, spleen and lymph nodes of mice housed in semi-sterile conditions (see 3.1.1). For each individual mouse, all three cell suspensions (bone marrow, spleen and lymph nodes) were mixed into one solution. During procedures cells were kept on ice, but all incubations were performed at RT. After centrifugation cell pellets in 15 ml tubes were resuspended in 1 ml erythrocyte lysis buffer and incubated 4 min at RT. Lysis was stopped by diluting with 20 ml MACS buffer. Cells were centrifuged and further processed for CD8+ cell isolation.

3.1.5.1 CD8+ cell isolation

CD8+ cell isolation was performed after manufacture's protocol with anti-CD8 coated beads (pluriSelect). For each sample, 5 ml incubation buffer was added to 5 ml wash buffer. Cell pellets were resuspended in 1 ml before adding 9 ml of this solution. (At this step, 300 µl from suspension of each animal were pooled and separated into 8 x 100 µl in FACS tubes for compensation and titration of FACS measurement.) Cells were counted and adjusted to 5 x 10^6 cells/ml with the buffer solution.

Anti-CD8-Pluri-Bead suspension was vortexed and 250 µl added to each sample to isolate CD8+ cells. The 15 ml tubes carrying the samples were place onto a roller mixer for incubation for 30 min at RT. Afterwards, cells from each mouse were washed through the S-pluriStrainer provided in the isolation kit, which was equilibrated with 1 ml wash buffer into a new 50 ml tube via a provided funnel. The funnel of the strainer was washed in 2 ml steps and discarded. Strainer was then washed circular and the cells in the flowthrough (depleted of CD8+ cells) were counted and placed on ice for subsequent Treg enrichment, see below.

Cells attached to the specific Pluri-Beads were detached with 12 ml detachment buffer. After detachment, obtained cells were counted and samples for FACS analysis were stored on ice to measure purity of isolated cells and their differential state at beginning of the experiment. Cell concentrations were

adjusted and then plated at 1.5 x 10^5 cells per well in 220 µl experimental media into 96 well plates for cytokine secretion experiment and placed into the incubation chamber. For FACS analysis at the end of the experiment and proliferation assay 5 x 10^4 per well were plated in 220 µl and incubated in the same way. Experimental RPMI media for CD8+ cells contained 10 ng/ml IL-2, 1 % v/v P/S, 10 % v/v FCS, 50 µM β-mercaptoethanol, and a similar volume slot of either PBS, 300 nM Iloprost, or 3 µM Iloprost. For proliferation assays, 0 days plates for starting cell numbers were centrifuged, aspirated and stored at -80 °C.

3.1.5.2 Treg enrichment

Flowthrough suspensions from the CD8+ isolation were further processed for Treg cell enrichment with MACS after manufacture's protocol (Miltenyi). With the provided kit all CD4+CD25+ cells of a cell suspension can be enriched. For magnetic labeling of the non-CD4+ cells, suspensions were resuspended each in 40 µl buffer per 1 x 10^7 cells and 10 µl of Biotin-antibody cocktail per 1 x 10^7 cells added. Samples were mixed well and incubated 15 min on ice. Subsequently, 30 µl of MACS-buffer, 20 µl of anti-biotin micro-beads and 10 µl of CD25-PE antibody per 1 x 10^7 cells were added. This mix was vortexed well and incubated 20 min in dark on ice. Subsequently, 40 ml MACS-buffer was added and cells centrifuged. Pellet was resuspended in 1 ml MACS-buffer and applied on pre-equilibrated LD columns in magnetic field for depletion of non-CD4+ T cells.

Afterwards, the column was washed twice with 1 ml MACS-buffer. CD4+ cells were pressed mechanically out of the column and centrifuged. Pellet was resuspended in 90 µl of buffer per 1 x 10^7 cells and 10 µl per 1 x 10^7 cells of anti-PE microbeads were added for incubation for 20 min in dark on ice. This step is included in the manufacture's protocol for terminal analysis of CD25+ cells via FACS without requirement of additional CD25-specific antibodies. However, for final analysis, staining with anti-CD25-APC was performed after complete Treg isolation. Afterwards, cells were washed by adding 20 ml of MACS-buffer and centrifugation. Resulting pellets were then resuspended in 1 ml of MACS-buffer. For magnetic selection of CD4+CD25+ T cells, cell suspension was applied onto a pre-equilibrated MS column in a magnetic field respectively for samples of each animal. Column was washed three times with 500 µl of MACS-buffer.

1 ml MACS-buffer was pipetted onto the column and magnetically labeled cells were pushed out with a plunger. This cell fraction was separated in the same way again with a new column. CD4+CD25+ cells were counted and concentrations adjusted to place 1 x 10^5 cells per well in 110 µl experimental media into 96 well plates for analysis of cytokine secretion in response to Iloprost treatment and cell activation. 5 x 10^4 cells per well in 110 µl experimental media were plated for FACS analysis and proliferation assays. Experimental RPMI media for Tregs contained 400 ng/ml IL-2, 10 ng/ml TGF-β, 100 µg/ml sodium pyruvate, 1 % v/v P/S, 10 % v/v FCS, 50 µM β-mercaptoethanol, and a similar volume slot of

either PBS, 300 nM Iloprost, or 3 µM Iloprost. Remaining cells were stored on ice for subsequent FACS staining and analysis of Treg suspension purity and initial differential status of cells at beginning of the experiment. For later staining for proliferation analysis, plates for 0 days time point were centrifuged, aspirated and stored at -80 °C.

3.1.6 FACS analysis of isolated CD8+ and enriched Treg

Samples from CD8+ T cell and CD4+CD25+ Treg cell enrichments were analyzed for their purity and initial differential state via FACS analysis. Additionally, after 5 days of the experiment FACS analysis was performed to investigate if culture conditions or the drug Iloprost had an influence on the differentiation state of the cells. Centrifugation steps were performed for FACS staining at 350 rcf for 8 min at 4 °C. Supernatants were removed via decantation and blotting onto absorbent paper. Incubation steps were performed in dark and on ice.

Prior collected cells in FACS tubes (see 3.1.5) were washed twice with PBS including a centrifugation step each. 2 µl Live/Dead stain was added to pellets, which were then resuspended and incubated for 30 min. Afterwards, samples were washed and the following antibodies with respective volumes were mixed with cell pellets and incubated for 20 min: 5 µl anti- CD3ε-PerCP, 1 µl anti-CD25-APC, 0.5 µl anti-CD4-AF700 and 1 µl anti-CD8a-eF450. Subsequently, cells were washed and pellets resuspended. 250 µl Fix-Perm-buffer was added and incubated for 1 h. Afterwards, the suspension was washed twice with 1 ml Perm-buffer and 2 µl anti-FoxP3-FITC antibodies added with 30 min incubation. Finally, cells were washed with 2 ml FACS-buffer and pellets kept in dark at 4 °C until measurement with the flow cytometer LSR II (Beckman Coulter). As technical control, titration of antibodies, isotype controls and compensations with single stains and fluorescence minus one (FMO) staining panels were carried out.

3.1.7 Cytokine secretion analysis

CM of immune cells (see 3.1.2, 3.1.3, 3.1.5 and table 3.1) were analyzed towards their secreted concentrations of up to three marker cytokines: IFN-γ, TNF-α and IL-10. Therefore, CM were thawed from -80 °C and respective mouse ELISA kits were carried out after manufacturer's recommendations (ebioscience). For IFN-γ detection samples of activated T cells had to be diluted 1:200. Samples were incubated overnight at 4 °C, final staining reactions were stopped with 1 M H_3PO_4 and absorbance was read at 450 nm with 570 nm reference wavelength via the plate reader. Standard curves were acquired in duplicates and curve fit approached with polynomial quadratic regression using a dedicated webtool (elisaanalysis.com).

3.1.8 MSC cultivation

Bone marrow cells were obtained as described above (see 3.1.1). At least 3 x 10^7 cells were seeded into each T25 flask (25 cm^2 area). 4 ml expansion media (EM) were added consisting of low glucose DMEM media with 10 % v/v FCS, 1 % v/v P/S, and 1 % v/v glutamax. Cells were cultured in an incubator at 37 °C and 5 % CO_2. 48 h later media were changed and with that, non-adherent cells removed. Subsequently, medium was changed twice per week until cultures were confluent. Due to the lag phase of primary mouse MSC cultures (Phinney *et al.* 1999) cells were passaged in a small T25 flask size twice and afterwards twice in T75 flasks (75 cm^2 area). Cultures were then expanded within T150 or T175 flasks and finally in T300 flasks (150, 175 and 300 cm^2 area). For detachments of MSCs, monolayers were washed once with PBS and TrypLE was applied with 5 min into the incubator. TrypLE is not affecting viability of the cells drastically, such as enzymatic methods, e.g. Trypsinization. For cryo-storage, cell concentrations were adjusted to 0.5 – 1 x 10^6 per 500 µl EM supplemented with 10 % v/v DMSO and 10 % v/v FCS. Cell solutions were transferred into standard cryo-vials and frozen to -80 °C at approximately 1 K/min with Mr. Frosty™ freezing containers, filled with isopropanol, and stored in liquid nitrogen afterwards. For experiments, cells were thawed for 1 min in 37 °C waterbath, resuspended in EM and placed into flasks of required culture size. After overnight culture incubation media was changed and cultures expanded until confluence.

3.1.9 Viability assay

Viability of cell culture experiments in 96 well plates was assessed in each well via Presto Blue™ reagent, after manufacture's protocol. In particular, with this assay metabolic activity is measured. Therefore, reagent was diluted 1:10 with EM based on RPMI for immune cell cultures or low glucose DMEM for MSC cultures. 100 µl of respective solutions replaced the media in each well. Accordingly, macrophages, MSCs, whole bone marrow cells, splenocytes or CD8+ cells were incubated with the reagent solution for 1 h in the incubation chamber, while Treg cultures were incubated for 2 h, due to their low cell numbers. Afterwards, 50 µl of the solution were carefully transferred into a new 96 well plate and fluorescence top reading was performed at 560 nm excitation and 590 nm emission with the plate reader. For background correction, fluorescence values of no-cell control wells, which contained only reagent solution were averaged and subtracted from values of experimental wells.

3.1.10 Toxicology assay

For toxicological assessment of Iloprost, MSC monolayers were analyzed for fractions of living and dead cells. Therefore, a Live/Dead imaging kit (Life Technologies) was performed after manufacture's protocol on MSCs cultivated for 2 weeks in EM supplemented with different Iloprost doses (300 nM and 3 µM) and PBS as control. 1 x 10^4 cells were plated per well. With this assay, living cells are

detected by calcein-AM (calcein acetoxymethyl ester) cleavage to green fluorescent calcein, and dead cells are revealed by stainability of their nuclei by red fluorescent propidium iodide (PI). Therefore, the content of one vial of calcein-AM of the staining kit was transferred into one vial of PI and the solution mixed. This staining solution was diluted 1:2 with PBS and 20 µl of this solution transferred into each analyzed well. After incubation in the dark for 15 min at RT plates were read at 488/515 nm (ex/em) and 570/602 nm (ex/em) for living and dead cells, respectively. Afterwards, cells were imaged with a standard fluorescence microscope for visualization.

3.1.11 Proliferation assays

Proliferation was investigated via CyQUANT® cell proliferation assay kit of adherent MSCs and cells with low adherence like CD8+ and Tregs. MSCs were plated into 96 well plates at initial cell numbers of 5 x 10^2 per well and incubated for 7 days. Whereas CD8+ and Treg cells were plated at 5 x 10^4 cells per well and incubated for 5 days. Before freezing of plates media were carefully removed. In particular, low adherent immune cells and all 0 days controls were centrifuged in respective 96 well plates prior to removal of media. Afterwards, plates were frozen at -80 °C and for staining manufacture's protocol was followed and fluorescence read with plate reader at 480/520 nm (ex/em). Plates were thawed and 200 µl of CyQUANT GR dye (1:400) and lysis buffer (1:20) in ddH_2O was added to each well. Based on standard curves fluorescence values were related to cell numbers to calculate population doublings.

3.1.12 Apoptosis

Apoptosis was investigated with measurement of activities of caspase-3 and -7, which are apoptosis specific enzymes. Caspase-Glo® 3/7 assay was conducted according to manufacturer's recommendations. MSCs were seeded in white-walled 96 well plates, required for luminescence detection, with a cell density of 1 x 10^4 per well in 100 µl media. Experimental media consisted of EM supplemented with either 50 or 120 ng/ml of IFN-γ, 40 or 60 pg/ml of TNF-α. These cytokine supplemented media further contained 3 µM Iloprost or an adequate volume of PBS as no drug control. For apoptosis control EM contained 100 µM H_2O_2 (Teramoto et al. 1998). After 2 days of incubation apoptosis was detected by adding Caspase-Glo® buffer and substrate in relation 1:2 into the wells. Plates were covered to protect from light and placed onto a plate shaker at 300 rpm for 30 seconds. Afterwards, plates were incubated at RT for 30 minutes. Subsequently, luminescence values were detected by the plate reader. Measurements were normalized to cell numbers determined by CyQUANT® assay.

3.1.13 Osteogenic differentiation induction

MSCs were seeded in a density of 1.5 x 10^4 cells per well into 96 well plates in EM and allowed to settle and expand for two days. Subsequently, standard osteogenic induction media (OM) was applied, i.e. low glucose DMEM media with 10 % v/v FCS, 100 nM dexamethasone, 10 mM β-glycerol phosphate and 50 µM L-ascorbic acid 2-phosphate in a total volume of 100 µl per well and further supplemented with 1 % v/v P/S, and 1 % v/v glutamax (Zhu *et al.* 2010). Media was changed every 3 to 4 days for 14 days and finally viability assessment and fixation done (see 3.1.10 and 3.1.15). For experiments varying compounds were added to the OM in different combinations: 40 and 60 pg/ml of TNF-α, 50 and 120 ng/ml of IFN-γ, and 300 nM or 3 µM Iloprost or PBS as control.

3.1.14 Osteogenic differentiation induction with conditioned media

The osteoimmunologic link between immune cells and osteogenic cells was further investigated *in vitro* with the impact of CM of immune cells onto osteogenic differentiation as described previously (Reinke *et al.* 2013). CM was derived from incubated activated T cells contained in whole bone marrow cultures. Furthermore, CM was obtained from incubations of isolated T cells, such as CD8+ and Treg cells. For each well of MSC monolayer, a combination of 50 µl of one respective investigated CM and 50 µl of double-concentrated osteoinductive media (2x OM) was applied. The double-concentrated part of 2x OM consisted of low glucose DMEM media with 20 % v/v FCS, 200 nM dexamethasone, 20 mM β-glycerol phosphate and 100 µM L-ascorbic acid 2-phosphate. 2x OM was further supplemented with 1 % v/v P/S, and 1 % v/v glutamax, which was also already contained in this concentration in the CM. Incubation was done in the incubation chamber and media changed accordingly with CM and 2x OM every 3 to 4 days. Differentiation and viability of cells were investigated after 14 days as described (see 3.1.09 and 3.1.15).

3.1.15 Alizarin Red staining

For all experiments containing osteogenic differentiation of MSCs, calcification level of extracellular matrix was visualized and quantified by Alizarin Red staining. After viability assays wells were washed twice carefully with 200 µl PBS. Monolayers were fixed with 50 µl of 4 % PFA/PBS for 10 min and stored in 200 µl PBS at 4 °C. After washing once with 200 µl PBS, nuclei staining was performed with 50 µl of 1 µg/ml DAPI for 10 min at RT in dark. After washing twice with 200 µl PBS DAPI measurement was done in 100 µl PBS with the plate reader with ex/em at 355/460 nm. Based on standard curves fluorescence values were related to cell numbers.

Subsequently, wells were washed twice with 200 µl ddH_2O and wells were incubated with 50 µl 0.5 % Alizarin Red in ddH_2O for 10 min at RT. Wells were washed intensively four times for 5 min with 200

µl ddH_2O and brightfield microscopy was done on dry stained monolayers with 10 x objective. For quantification of mineralization ECM bound Alizarin Red was detached for optical density measurement with 120 µl of 10 % cetylpyridinium chloride for 30 min at RT. Afterwards, 100 µl were transferred into a new well plate and optical density read at 562 nm light absorbance.

3.1.16 Adipogenic differentiation induction

For differentiation of MSCs into adipogenic lineage, cells were seeded in a density of 2 x 10^4 cells per well into 96 well plates in EM and allowed to settle and expand for two days. Adipogenic induction media (AM) was in a first step prepared with high glucose DMEM media containing 1 µM dexamethasone, 2 µM insulin, 500 µM IBMX and 100 µM indomethacin. This solution was then warmed up to 37 °C and sterile filtered, and further supplemented with 1 % v/v P/S, 1 % v/v glutamax and 10 % v/v FCS. With 100 µl per well this complete AM differentiation was performed in incubation chamber for 5 days without media change. For experiments 3 µM Iloprost were added or a dilution of 1:10 in PBS for 300 nM Iloprost or the same volume of PBS as control.

3.1.17 Nile red staining on monolayers

MSC cultures that had received AM displayed strong occurrence of vesicles, which were prone to dislocate. Hence, no stressful viability assessment was performed, but monolayers were directly fixed with carefully pipetting regime as described above (see 3.1.15). First the blank values were read with the plate reader in 100 µl PBS per well for fluorescent DAPI and Nile Red measurements with ex/em at 355/460 nm and 485/540 nm, respectively. Each well received 50 µl of staining solution consisting of 1 x PBS with 0.2 % saponin, 1 µg/ml DAPI and 1 µg/ml Nile Red. Incubation was done for 30 min in dark at RT, and wells were carefully washed with three times 200 µl PBS and measurement was done with the plate reader in 100 µl PBS. Additionally, fluorescence images were acquired with 10 x objective in blue and green channel for DAPI and Nile Red, respectively.

In case of parallel adipogenic differentiation events, which were detected during brightfield microscopic culture controls during incubation with OM, Nile Red staining and data acquisition were performed prior to Alizarin Red staining procedures (see 3.1.15).

3.1.18 Chondrogenic differentiation induction

For each pellet formation, 3 x 10^5 MSCs were transferred into a 15 ml tube. After centrifugation at 500 rcf for 5 min 1 ml PBS was added to the pellet and centrifuged again. Chondrogenic induction media consisted of high glucose DMEM media supplemented with 100 nM dexamethasone, 50 µg/ml L-ascorbic acid 2-phosphate, 350 µM L-proline, 2 mM sodium pyruvate, 6.25 µg/ml Insulin-transferrin-

sodium selenite media supplement (ITS), 1.25 mg/ml BSA, 5.35 µg/ml linoleic acid, 10 ng/ml TGF-β1, 10 ng/ml BMP-2, 1 % v/v P/S, and 1 % v/v glutamax. Carefully 500 µl induction media was applied onto the pellet without stirring it up. Control groups in EM were cultured overnight and processed for fixation, see below. For differentiation pellets were cultivated for 21 days at 37 °C and 5 % CO_2. Media change was done twice a week. The cultivation in pellets as well as the closed 15 ml tubes during differentiation enabled hypoxic conditions.

3.1.19 Histomorphometric quantification of chondrogenic differentiation

Differentiated pellets and EM controls were fixed in 500 µl 4 % PFA/PBS for 2 h after 21 and 1 d of incubation, respectively. Afterwards, pellets were washed twice with 500 µl PBS for 5 min. Subsequently, the pellets were further processed for dehydration with 2 x 500 µl of 70 % EtOH for 30 sec and then with 80 % EtOH for 20 min. For pre-visualization pellets were stained with 300 µl 0.2 % eosin solution in 80 % EtOH for 30 sec, and washed twice with 500 µl of 96 % EtOH and then twice with 100 % EtOH for 20 min each. Subsequently, pellets were incubated for 15 min in Xylol and transferred into 60 °C warm paraffin in metal forms and incubated overnight.

Afterwards, paraffin was cooled on a -7 °C cold plate and a plastic grid with holder was squeezed onto it and filled with hot paraffin. After sample blocks were hardened the metal blocks were removed and the samples stored at 4 °C. Sections with a thickness of 4 µm were produced with a microtome and two subsequent tap water baths at RT and 40 °C, respectively. Sections from three different areas of each pellet were placed on a glass slide, which was dried overnight at 37 °C and stored at RT.

Chondrogenic differentiation was assessed via staining of proteoglycans with Alcian Blue. Sections were deparaffinized with submerging twice into Xylol for 10 min and processed through a descending ethanol series. Therefore, slides were placed for 2 min into pure, 96 %, 80 % and 70 % EtOH. After 2 min wash with ddH_2O slides were equilibrated with 3 % acetic acid for 3 min, stained 45 min in 1 % Alcian Blue, washed in 3 % acetic acid, washed in ddH_2O and stained with Nuclear Fast Red for 2 min. Staining was washed away shortly in ddH_2O and 70 % EtOH. Ascending EtOH series was conducted with a short step in 80 % EtOH followed by 1 min in 96 % EtOH and twice 1 min in pure EtOH. Finally, slides were dehydrated twice in Xylol for 5 min before sealing with coverslip and Vitro-Clud®. Specimens were stored in dark at RT. Imaging was carried out with 10 x magnification in brightfield. Finally, quantitative histomorphometry was performed on blue pixel values of brightfield images via ImageJ.

3.2 Release system characterization *in vitro*

For a delayed release of Iloprost locally at the regenerating site, a core-shell approach was chosen. In principal, the drug is first placed inside the core gel and then traveling via diffusion forces outwards towards the adjacent tissue. Thereby the drug is decelerated in its movement by hydrophobic interactions with the protein-based biomaterial. The biomaterial used here was fibrin of clinical application grade with the Tissucol-kit Immuno (Baxter).

3.2.1 Preparation of fibrin precursors

Preparation of the release system, weight measurement and sample harvest was carried out under sterile S1 conditions. The core gel precursor was prepared with high density fibrinogen, i.e. 240 mg in 1 ml aprotinin solution, which was supplemented with either 54 µl Ilomedine (for 3 µM final Iloprost concentration) or 54 µl PBS for treatment or control group, respectively. For the shell gel precursor, standard density fibrinogen was prepared after manufacture's recommendations, i.e. 160 mg in 1 ml aprotinin. Thrombin solution was prepared with 65 mg lyophilized thrombin (Th-S, Baxter) in 1 ml calcium chloride solution.

3.2.2 Construction of the core-shell system

The core-shell system was prepared stepwise (Fig. 3.1). For release system preparation fibrinogen and thrombin solutions where heated to 37 °C. 30 µl shell-fibrinogen were added to 10 µl thrombin and polymerized for 2 min to prepare the shell. Thrombin was utilized in reduced volume to the manufacture's recommended application of 1:2, to minimize the risk of drug loss during gel preparations. In parallel, the core gel was generated with 30 µl core-fibrinogen, which were added to 10 µl thrombin and polymerized for 2 min. This core gel contained either Iloprost or PBS for treatment and control, respectively. Afterwards this core gel was placed into the shell gel, which was subsequently completed with another addition of 30 µl shell-fibrinogen and 10 µl thrombin were added on top. After 2 min of polymerization, the release system was carefully placed into plastic test tubes, which weight was measured individually with a micro scales before for later subtraction from the sample weights. The release kinetics and degradation properties of the core-shell system were compared to core-only and shell-only drug or PBS loaded systems of same overall size of 90 µl applied fibrinogen volume. All three different compared release system types carried 324 ng Iloprost. Furthermore, for each release system composition 4 samples were prepared and analyzed.

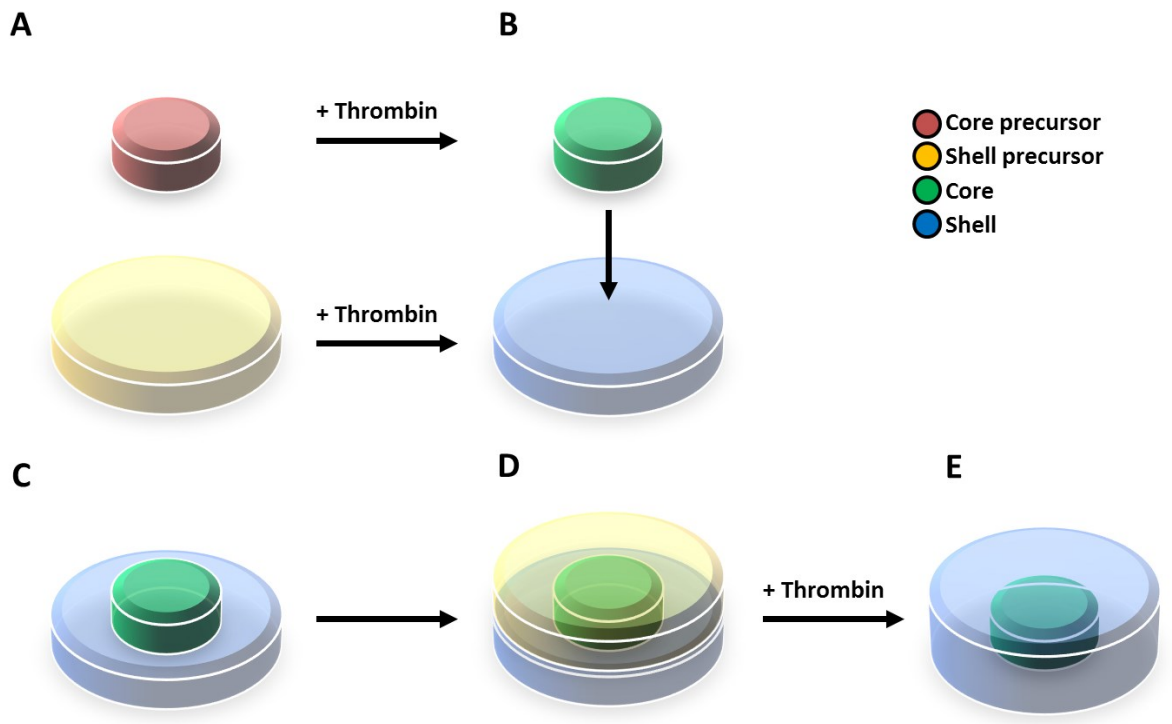

Figure 3.1: Scheme of stepwise preparation of the fibrin-based core-shell drug release system. All solutions were heated to 37 °C as well as the petri dish on which the procedure was performed. (A) Ground base of the shell was prepared in parallel to the core. High and mid density fibrinogen for core and shell were pipetted carefully next to each other. Surface tension contained size of the droplets. Subsequently, thrombin solution was added to each precursor to allow polymerization. (B) Readily polymerized core was placed onto the lower part of the shell. (C) Onto this construct, another layer of shell precursor was very slowly pipetted. (D) Another volume of thrombin was administered carefully on top to seal the shell. (E) Final incubation at 37 °C resulted in the complete core-shell construct, in which the drug-containing core is completely surrounded by the shell fibrin.

3.2.3 Degradation analysis and collection of released drug

Drug release systems were weight measured directly after preparation and placed into reaction tubes of known weight for subtraction from sample weights. Subsequently, samples were submerged in PBS supplemented with 200 µl of 1 µg/ml proteinase K. After 1 h media were harvested and replaced and same procedure performed after 12 h and additionally weights measured of the release system samples. Harvest of media, replacement of media and weight measurements were then performed every 24 h until day 5 and 8 for media and weighting, respectively. For degradation analysis, weights were further measured until day 10, when the last samples had dissolved. The harvested media were frozen at -20 °C for later analysis of released drug quantities.

3.2.4 High performance liquid chromatography

The amount of Iloprost released from the fibrin compositions at different time points was quantified via reversed phase high performance liquid chromatography with UV-detector (RP-HPLC/UV). Sample

preparation and detection was oriented on a method previously described (Scypinski *et al.* 1990). However, procedure was adjusted to smaller sample volumes. Internal standard solution was 15 µg/ml 2-Naphthoic acid dissolved in methanol and was added 1:100 to each sample for a final concentration of 150 ng/ml. Pure Iloprost substance (Cayman chemical) was used to prepare a standard curve and to verify the Iloprost signal of the UV detector. Therefore, 500 µg substance was dissolved in 100 µl methylacetate to prepare the stock solution.

3.2.4.1 Processing of samples

Samples were thawed and 2 µl 2-Naphtoeic acid added. Subsequently, 100 µl chloroform were added to samples, which were then vortexed for 1 min. Phase separation was enforced with centrifugation for 1 min with 2000 rcf. Lower phase of chloroform was collected for each sample separately into glass inlays, which were placed into standard glass vials for HPLC auto samplers. Remaining aqueous phase underwent the same extraction method two more times. Collected chloroform was evaporated under fume hood and hydrophobic compounds like Iloprost were supposed to be then extracted from hydrophilic compounds, e.g. salts. Mobile phase was added, glass vials closed with rubber lid and samples transported to the auto sampler of the HPLC apparatus.

3.2.4.2 Measurement and data acquisition

The analysis via HPLC of released Iloprost was carried out in cooperation with and at the Helmholtz Centre for Environmental Research (Leipzig). The mobile phase consisted of monobasic potassium phosphate:methanol:acetonitrile (v/v 456:144:400). The flow rate was set to 1.8 ml/min and the UV detector to 207 nm. 80 µl sample volume was injected. Each sample was run for 8 min through the system. Finally, Xcalibur software was used for peak analysis and integration. Iloprost exists as two diastereoisomers with distinct hydrophobicities resulting in a double-peak with the UV detector. The areas of both peaks were added to derive the drug concentrations from the prior generated standard curve with pure Iloprost (Cayman chemical).

3.2.5 Histologic analysis of release system *in vitro*

The correct formation of polymerized fibrin during modulation of the core-shell system was analyzed histologically. The fibrin-based release system was prepared similar to the procedure for *in vivo* application (see below, 3.3.4). Directly after preparation, images of the constructs were made by a standard digital camera and further fixed in 4 % PFA/PBS for 2 h at 4 °C, which was prepared by diluting 1:5 20 % PFA in 1 x PBS (10 x PBS diluted in ddH_2O). Fibrin constructs were processed for 7 µm cryo-sectioning of the center of the constructs on adhesive film strips similar to processing of bone tissues

(see below, 3.3.8). Cryo-sections were stored at -80 °C. For staining of fibrin protein with eosin, slides were dried and warmed up at RT for 30 min. After rehydration in ddH_2O for 10 min, slides were stained with 0.2 % eosin in 80 % EtOH for 2 min. Subsequently, slides were shortly rinsed in 96 % EtOH and submerged twice for 2 min in 100 % EtOH for complete dehydration for permanent binding of the stain to the proteins. Finally, slides were submerged in Xylol twice for 2 min before sealing with coverslip and Vitro-Clud®. Stained sections of core-shell samples were stored in dark at RT and images were acquired with 10 x magnification in brightfield.

3.2.6 Biomechanical characterization

The potential impact of the drug solution Ilomedine onto material integrity of fibrin was investigated via resulting material stiffness. This compressive stiffness, also called Young's modulus, of an analyzed material is the relation of applied stress and resulting strain (Formula 1). The stress of the analyzed material is derived from the compressive force divided by the compression area (Formula 2), whereas the strain is the deformation length during compression relative to initial length (Formula 3).

$$Stiffness\ [Pa] = \frac{Stress\ [Pa]}{Strain\ [\%]} \qquad \text{Formula 1}$$

$$Stress\ [Pa] = \frac{Compressive\ force\ [N]}{Compression\ area\ [m^2]} \qquad \text{Formula 2}$$

$$Strain\ [\%] = \frac{Deformation\ length\ [N]}{Initial\ length\ [m^2]} \qquad \text{Formula 3}$$

10 µl core-fibrinogen carrying Ilomedine or PBS were completely polymerized with 10 µl thrombin at 37 °C for 3 min each and kept in PBS prior measurement to protect from dehydration. For both sample types, 4 samples were analyzed. Subsequently, sample stress values were determined via unconfined compression testing. Therefore, samples were mounted to a dedicated custom-made test device, which was connected to an electro force test bench (Bose). Load channel was tared and individual sample heights measured with the device. Samples were compressed once by 15 % strain, i.e. 15 % of their individual initial height. For each sample, compressive force was determined, and compression area was measured with ImageJ on digital images of the gels to calculate the stiffness.

3.3 *In vivo* study

The efficacy of delayed administration of the anti-inflammatory drug Iloprost onto fracture healing was investigated in a mouse osteotomy model, which is especially characterized by an activated immune system. Therefore, an Iloprost loaded release system was placed into the osteotomy gap and the healing process was compared to a vehicle control, which was only loaded with PBS. The precursors of the carrier material fibrin were prepared under sterile conditions and stored at -20 °C. During the setting of the osteotomy, the thawed precursors fibrinogen and thrombin were used to build the release system in parallel.

3.3.1 Mice experiments

In this thesis, female mice of the strain C57BL/6N were used (Charles River Laboratories). This strain was selected, due to its strong regenerative capacity and robust immune competence (Roch & Bach 1991; Manigrasso & O'Connor 2008). Mice were ordered at the age of 8 weeks and were kept for 4 weeks prior study start in the animal facility on the Virchow campus of the Charité Berlin (*Forschungseinrichtung für experimentelle Medizin*). In particular, mice were kept these 4 weeks prior to experiments under semi-sterile conditions, i.e. an area in the facility without an additional barrier and without filtered air supply for the mice cages. This was done intentionally to mimic a naturally experienced immune system. With increasing age, fracture patients show the risk of reduced healing capacity, which could also be shown with this mouse model and was described previously for the same strain and facility (Reinke *et al.* 2013). Other conditions were kept at standard parameters, such as room temperature of 20 °C, 12 h light/dark cycle and food and water availability ad libitum.

3.3.2 Study design

The mice were allocated to one of four distinct groups, which differed in drug treatment and duration of regeneration (Table 3.2). The Iloprost treatment group was compared to a vehicle group, which release system was only loaded with PBS. Furthermore, the healing outcome of each of these two treatment types was investigated at 3 days and 21 days of regeneration via histomorphometry. Accordingly, for 3 days post osteotomy (dpo) and 21 dpo groups, immunohistology and µCT analysis was performed. FACS analysis of bone marrow in contralateral, uninjured femur investigated potential systemic effects of the local drug application.

			Femurs with osteotomy			Contralateral femurs
GROUP	**Time points**	**Sample size**	**µCT analysis**	**Histo-morphometry**	**Immuno-histology**	**FACS analysis**
PBS	3 dpo	6	-	x	x	x
	21 dpo	6	x	x	-	x
ILOPROST	3 dpo	6	-	x	x	x
	21 dpo	6	x	x	-	x

Table 3.2: Study design of the *in vivo* proof of concept study for delayed local drug delivery of Iloprost in a mouse osteotomy model. dpo = days post osteotomy.

3.3.3 Preparation of fibrin precursor materials

To control the release of the drug, a core consisting of high-density fibrin was prepared, which carries the drug. Additionally, a shell of less dense fibrin was produced for the delay of the drug release. These two components of the core-shell release system were made as follows.

The core gel precursor was prepared with high density fibrinogen, i.e. 24 mg in 100 µl aprotinin solution, which was supplemented with 5.4 µl Ilomedine for the treatment group (3 µM final Iloprost concentration) or with the same volume of 5.4 µl PBS for the control group. For the shell gel, standard density fibrinogen was prepared after manufacture's recommendations, i.e. 16 mg in 100 µl aprotinin. 100 µl thrombin solution was prepared with 6.5 mg lyophilized enzyme in 100 µl calcium chloride solution. Fibrinogen compositions and thrombin were stored at -20 °C before application in the osteotomy model (see 3.3.4).

3.3.4 Osteotomy model

Osteotomies were performed on the left femur of the mice by Dr. Katharina Schmidt-Bleek. In parallel the drug release system was prepared fresh for every individual animal by myself (see 3.3.5). After weighting, mice were narcotized by the inhalation of the anesthetic Isoflurane. Subsequently, mice were injected intraperitoneally with 0.03 mg/kg b.w. of the analgesic Temgesic and with 45 mg/kg b.w. of the antibiotics Clindamycin. Eyes of the narcotized animals were covered with Bepanthene to protect them from drying. After shaving and disinfecting the respective skin area of isoflurane-anesthetized animals, a lateral longitudinal incision of the skin from knee to hip was performed. The femur was exposed by blunt preparation of *Musculus vastus lateralis* and *Muscculus biceps femoris*, carefully sparing the sciatic nerve. Serial drilling for pin placement was performed of 0.45 mm diameter through

the connector bar of the external fixator (MouseExFix, RISystem, Davos, Switzerland). The external fixator was positioned laterally to the femur. An osteotomy of 0.7 mm was introduced between the middle pins using a Gigli wire saw (0.66 mm, RISystem, Davos, Switzerland).

Subsequently, the local drug release system was applied, see below. After skin closure mice were placed back into their cages and received additional postoperative analgesia with 25 mg/l Tramadol hydrochloride supplemented to their drinking water for 3 days. Animals were examined daily and after a healing period of 21 days euthanized, as described above (see 3.1.1). Subsequently, the skin of the abdomen was opened by a longitudinal cut and regenerating bones and contra lateral bones were obtained, and further processed and analyzed, as described below in 3.3.6f. and 3.3.15, respectively.

3.3.5 Application of the local drug release system

In the surgery room the core-shell system was prepared stepwise (see above, Fig. 3.1). Fibrinogen and thrombin solutions (both Tissucol-kit Immuno, Baxter) where heated to 37 °C. 3 µl fibrinogen (16 mg per 100 µl) were added to 1 µl thrombin (after manufactures protocol) and polymerized for 2 min to prepare the shell gel. In parallel, the core gel was generated with 3 µl fibrinogen (24 mg per 100 µl) which were added to 1µl thrombin and polymerized for 2 min. 100 µl core gel solution contained either 3 µM Iloprost (5.4 µl of 20 µg/ml Ilomedine in 100 µl fibrinogen) or 5.4 µl PBS for treatment and control, respectively. Hence, 3.24 ng Iloprost were applied to each animal of the treatment group. Afterwards this core gel was placed into the shell gel, which was subsequently completed with another slow addition of 3 µl fibrinogen (16 mg per 100µl). 1 µl thrombin was added on top and after 2 min of polymerization, the release system was carefully placed into the osteotomy gap with a sterile pincette. Finally, the hydrogel composition was glued to the bone tissue using 6 µl fibrinogen (16 mg/100µl) and 2 µl thrombin. The surrounding tissues, such as muscles, were protected from unspecific gluing by a small strip of sterile foil. After 2 min of polymerization, the region was controlled for unspecific glued connections, the strip removed and the wound closed via stitching.

3.3.6 µCT analysis

The newly formed mineralized bone tissues were analyzed using high-resolution micro computed tomography (µCT). Therefore, regenerating femurs were obtained as described above (organ harvest) and were directly fixed in 4 % PFA/PBS for 4 h at 4 °C, which was prepared by diluting 1:5 20 % PFA in 1 x PBS (10 x PBS diluted in ddH_2O). Afterwards, tissues were step-wise dehydrated in 10, 20 and 30 % sucrose gradient in ddH_2O for 24 h each at 4 °C. The osteotomy areas were scanned with a fixed isotropic voxel size of 10.5µm, 55 keVp and 145 µA. The scan axis coincided with the diaphyseal axis of the femurs. A minimum of 190 slices of 10.5 µm was chosen such that the osteotomy callus was completely included.

The cortical bone was semi-automatically excluded from the volume of interest (VOI) in further post-processing. Hence, newly formed bone volume (BV) could be distinguished from total volume of mineralized area (TV). The ratio BV/TV is especially used in closed fracture models to normalize the strong callus variations. A fixed global threshold of 242 was selected that allowed the rendering of mineralized tissue and corresponds to 369.9 mg HA/cm^2. All analyses were performed on the digitally extracted tissue using 3D distance techniques (Scanco® software, Switzerland). Grey value parameters were adjusted based on previous work with similar tissues and mathematical evaluation (Muller *et al.* 1996; Bouxsein *et al.* 2010).

3.3.7 Cryo-embedding of regenerating bones

Cryo-embedding was performed accordingly as previously described for bone tissue, which is not decalcified (Kawamoto 2003). 300 ml acetone were filled into a dewar thermo tank and cooled down with dry-ice. 200 ml n-hexane were filled into a glass beaker, which was then put into the ice-cold acetone. The tissues were placed into self-constructed metal forms, which were filled half full with embedding medium. The forms were placed into the cooled n-hexane until the embedding medium was frozen and external fixators removed from the bones. Subsequently, the tissues were completely covered with additional embedding medium and deep-frozen. Finally, the forms were removed from embedded tissues, which were then stored at -80 °C to be further processed for histology.

3.3.8 Preparations of cryo-sections of regenerating bones

Bone tissues were cryo-sectioned after Kawamoto's method (Kawamoto 2003). Temperature of the cryotome was set to -25 °C and tissue blocks placed from -80 °C into the sectioning chamber to adapt to the set temperature. The adhesive film strips 2C(10) were cut into necessary size and placed onto the appropriate tissue area to prepare 7 µm sections. 10 to 20 consecutive sections were prepared from each sample tissue and each fixed onto a glass slide with standard tesafilm®, which can withstand freezing and staining procedures. After 1 h of drying at RT, the slides were stored at -80 °C.

3.3.9 Movat's pentachrome staining

Connective tissue types on cryo-sections were stained after Movat's pentachrome method (Movat 1955). Procedure was carried out at RT. Respective cryo-sections were placed out of -80 °C to a dry chamber of 37 °C for 30 min. Subsequently, sections were fixed in 4 % PFA/PBSTW for 10 min, washed twice in PBSTW for 5 min and placed into 3 % acetic acid for 3 min. Subsequently, sections were submersed in 1 % Alcianblue in 3 % acetic acid, pH 2.5 for 30 min and differentiated for 5 min in 3 % acetic acid each and washed in ddH_2O for 5 min. Afterwards, sections were incubated in alcaline ethanol for 1 h,

washed twice in tap water for 5 min and submersed shortly in ddH_2O before being stained with Weigert's iron hematoxylin for 10 min. Staining was washed away with tap water three times for 5 min and sections incubated 15 min in brilliant crocein-acid fuchsine. Subsequently, samples were placed shortly into 0.5 % acetic acid prior 20 min incubation with 5 % phosphotungstic acid and afterwards for 1 min again into 0.5 % acetic acid. After equilibration three times in pure ethanol for 5 min samples were stained with Saffron-du-Gatinais solution for 1 h and washed with 100 % EtOH three times for 2 min. Finally, stained sections were dehydrated twice in xylol for 5 min before sealing with coverslip and Vitro-Clud®. Specimens were stored in dark at RT. Mosaic images were acquired in brightfield with a 2.5 x and 10 x objectives and the software AxioVision (Zeiss).

3.3.10 Histomorphometric analysis of connective tissues

The areas of identified different connective tissue types and, if present, the biomaterial for drug release, were quantified histomorphometrically in the acquired images of Movat's pentachrome staining. Therefore, an ImageJ-based analysis tool was used, which was previously programmed in-house for this regeneration model. The ROI was defined to be twice the width of the osteotomy gap, i.e. 1.4 mm. Following tissue types were quantified based on defined color types and intensities relative to total callus area: bone marrow, cartilage, connective tissue, and mineralized bone.

3.3.11 Nile red staining on cryo-sections

Occurrence of adipogenic differentiation at the site of local Iloprost delivery was investigated on cryo-sections of all 3 dpo and 21 dpo biological replicates. Therefore, sections were taken out of -80 °C storage and placed into a dry chamber of 37 °C for 30 min. Subsequently, sections were fixed in 4 % PFA/PBSTW for 10 min and afterwards washed twice in PBSTW for 5 min. Subsequently, slides were placed into staining solution, which consisted of 1 x PBS with 0.2 % saponin, 1 µg/ml DAPI and 1 µg/ml Nile Red. After incubation for 30 min in dark at RT, slides were washed three times in PBSTW for 5 min and once with PBS. Finally, sections were sealed with coverslip and mounting medium for fluorescence. Images were acquired with a standard fluorescence microscope (Axio Observer, Zeiss) with 5 x objective in blue and green channel for DAPI and Nile Red, respectively. Similarly treated and stained peritoneal adipogenic tissue samples were used as positive staining controls.

3.3.12 Immunohistochemistry

Staining procedures were carried out at RT and with 100 µl volumes of solutions if not indicated otherwise. Cryo-sections were placed out of -80 °C to thaw and dry for 1 h at RT. Meanwhile, tissue sections were circled with PAP pen and a humidified chamber was prepared to protect samples from

dehydration. This humidified chamber was always closed for incubations to protect fluorophores additionally from light. Sections were placed into the prepared chamber and fixed with 4 % PFA/PBTW for 20 min and washed twice with PBTW afterwards. Blocking against unspecific epitopes was done with 7 % FCS in TRIS (1 l ddH_2O with 6.6 g Trizma hydrochloride, 0.9 g Trizma base and 8.78 g NaCl, pH 7.6) with 0.05 % Tween for 1 h.

Specific staining procedures for respective panels:

- Macrophage polarization (CD68, CD206, CD80): Blocking solution was washed away with TRIS and anti-CD68 (1:80), anti-CD206 (1:150) and anti-CD80 (1:50) in 70 µl TRIS were applied O/N at 4 °C.
- Activity of CD8 cells vs osteoblasts (CD8, IFN-γ, OCN): Blocking solution was washed away with TRIS and anti-IFN-γ (1:50) and anti-OCN (1:100) in 70 µl TRIS were applied O/N at 4 °C. After washing twice for 8 min with PBTW and once with TRIS sections were incubated with anti-rat-594 (1:500) and anti-rabbit-647 (1:500) in 3.5 % FCS, 0.025 % Tween in 70 µl TRIS for 2 h. Staining solution was washed away three times with PBTW for 8 min and once with TRIS before anti-CD8 (1:75) in 70 µl TRIS was added for 2 h.
- Activity of resorbing cells (CD68, TNF-α, cathepsin K): Before blocking antigen retrieval was performed with Proteinase K, which was diluted 1:500 in PBTW and applied for 15 min. Afterwards, sections were carefully washed with PBTW and re-fixed in 4 % PFA/PBTW for 20 min. After washing twice in PBTW for 5 min blocking procedure was performed, see above. Blocking solution was washed away with PBS and anti-TNF-α (1:40) in 70 µl PBS was applied O/N at 4 °C. After washing three times for 8 min with PBTW and once with TRIS sections were incubated with anti-rat-AF594 (1:500) and anti-cathepsinK (1:60) in 3.5 % FCS, 0.025 % Tween in 70 µl TRIS for 2 h. Staining solution was washed away three times with PBTW for 8 min and once with TRIS and anti-CD68-FITC (1:75) and anti-rabbit-AF647 (1:500) in 3.5 % FCS, 0.025 % Tween in 70 µl TRIS for 2 h.
- T cell subsets and osteoblasts (CD8, CD4, OCN): Blocking solution was washed away with TRIS and sections were incubated with rat-anti-CD4 (1:50) and rabbit-anti-OCN (1:100) in 70 µl TRIS O/N at 4 °C. After washing three times with PBTW for 8 min and once with TRIS anti-rat-594 (1:750) and anti-rabbit-647 (1:500) in 3.5 % FCS, 0.025 % Tween in 70 µl TRIS were applied for 2 h. Staining solution was washed away three times with PBTW for 8 min and once with TRIS and 70 µl of anti-CD8 (1:75) in TRIS were added for 2 h.
- Blood vessel formation: Blocking solution was washed away with PBS and rabbit-anti-laminin (1:400) in 70 µl PBS were applied O/N at 4 °C. After washing three times for 8 min with PBTW sections were incubated with anti-rabbit-AF555 (1:1000) in 3.5 % FCS, 0.025 % Tween in 70µl PBS for 2 h.

Final nuclei stain was performed with 5 µg/ml DAPI solution in PBTW for 10 min. After washing twice with PBTW for 5 min and once with PBS sections were sealed with coverslip and mounting medium for fluorescence.

3.3.13 Laser scanning microscopy

Immunohistochemically stained cryo-sections of 3 dpo were digitalized with the confocal laser scanning microscope LSM 710, which was operated by the software ZEN 2011. Mosaic images could be obtained, which span the tissue area adjacent to the release system in the osteotomy gap. Each cell in this area could be analyzed on marker expression in four regions of the fluorescence spectrum. The defined region of interest (ROI) consisted of 5 x 4 single tiles scans with a frame size of 1024 x 1024 pixels each, and adjacent tiles were set to 10 % overlap. Scans were acquired with a 20 x objective and a pinhole setting for 4.5 µm optical sectioning. A z-stack of up to three images was acquired with distances of 4.5 µm towards each other. Minimum laser power was adjusted to negative stain and/or secondary antibody only controls. The raw images were processed directly in ZEN software, i.e. z-stacks were projected into 2D tile images, which were subsequently stitched to a total mosaic image. Images were further processed with ImageJ for final display.

3.3.14 Quantification of cell subsets in fluorescence images

For quantification of distinguished cell subsets the open-source image analysis software ImageJ was used. Whole mosaic images of the investigated region, containing all acquired fluorescence channels, were converted to 8-bit to conduct the function “Analyze Particles”. This function identified cells according to size, shape and pixel distribution. Subsequently, the mask of identified and numbered cells received from the “ROI Manager” panel was applied onto single fluorescence channels to receive respective pixel values for each cell (Appendix Fig. 8.5). Hence, the fraction of cells according to stained markers could be quantified.

3.3.15 FACS measurement of *in vivo* samples

Systemic effects of the local application of Iloprost were investigated via FACS of T cells from bone marrow of femurs contralateral to the regenerating femur. Single cell suspensions from bone marrow were prepared as described above (see 3.1.1), except for sterile conditions. FACS staining procedures were carried out in parallel for two different staining panels.

Therefore, cells were washed and counted and their concentrations adjusted to 1 x 10^6 per 100 µl. 1 x 10^6 cells were used for panel 1 and 2 x 10^6 for panel 2 in individual FACS tubes. One negative control for each animal was pooled from bone marrow cells and splenocytes. 2 µl Live/Dead stain was mixed

with pellets and incubated for 30 min. After washing with PBS all following washing and staining steps were done in FACS-buffer (1 x PBS with 1 % BSA and 0.1 % sodium azide) and in dark.

- Panel 1 for quantifying: NK1.1+ natural killer cells, NK1.1+CD3+ natural killer T cells, T cells, T cell subpopulations (CD4+, CD8+ and CD8+CD4+), CD8+ and CD4+ memory T cells with CD62L- effector and CD62L+ central memory subsets, and activated (CD25+) CD8+ and CD4+ T cells.

  Cells were washed and stained for 20 min on ice with following antibodies and respective concentrations: anti-CD3ε-PerCP (1:20), anti-CD4-AF700 (1:100), anti-CD8a-eF450 (1:100), anti-CD25-APC-Cy7 (1:25), anti-CD44-PE-Cy7 (1:200), anti-CD62L-APC (1:100), anti-NK1.1-FITC (1:50), and anti-TCRβ-PE (1:50). Subsequently, cells were washed and then fixed in 2 % formaldehyde for 20 min at RT. After final washing step, cells were analyzed with the flow cytometer LSR II.

- Panel 2 for quantifying: specific CD3+CD4+CD25+FoxP3+ Treg cells.

  After washing of cells antibodies were added and incubated for 20 min on ice: anti- CD3ε-PerCP (1:20), anti-CD4-AF700 (1:100), anti-CD8a-eF450 (1:100), and anti-CD25-APC (1:100). Cells were washed, resuspended and incubated with 250 µl Fix-Perm-buffer for 1 h on ice. Afterwards, cells were washed twice with 2 ml Fix-Perm-buffer, resuspended, and stained for 30 min on ice with anti-FoxP3-FITC (1:50). Cells were washed, resuspended and filtered through a 30 µm CellTrics strainer. Finally, cells were washed, resuspended and measured with the flow cytometer LSR II.

Isotype controls, unstained controls and compensations with single stains and fluorescence minus one (FMO) staining panels (Appendix Fig. 8.3) were done as controls.

3.3.16 FACS data analysis

FlowJo software was used to analyze the FACS data. After gating the lymphocyte cell population for size and granularity, singlets were gated to exclude clotted cells from analysis (Appendix Fig. 8.2). Furthermore, only living cells were analyzed and fractioned towards respective markers.

3.3.17 Statistical analysis

All statistically analyzed data are presented in box-plots or line charts. Values of line charts are shown as median with standard deviations. Box-plots contain quartiles and whiskers to visualize value distributions. Outliers and extreme outliers are indicated by circles and grey asterisks, respectively. Statistical calculations and graphs were prepared with the software SPSS. For cell culture and *in vivo*

data, only biological replicates were statistically evaluated. If two study groups were analyzed, the Mann-Whitney U test was applied. For more than two study groups the Bonferroni's post-hoc test was used. P-values < 0.05 were considered to be statistically significant.

4. Results

Endochondral fracture healing is initiated by a brief pro-inflammatory phase. However, a prolonged inflammation can lead to clinical cases of delayed healing or non-unions. The results presented here were analyzed to test the hypothesis that a delayed local release of synthetic PGI_2 from a biodegradable carrier can shorten the pro-inflammatory phase whilst stimulating the early anti-inflammatory phase and therefore accelerate the healing cascade. PGI_2 is a signaling molecule, which receptor is located on a variety of different cell types. The result of its pathway is an elevation in intracellular cAMP, which leads to unique responses, e.g. reduction of inflammation or smooth muscle relaxation. The synthetic analog of endogenous PGI_2 investigated here was Iloprost. This active compound has reportedly diverse anti-inflammatory properties, which were tested here *in vitro* on different immune cell types of mouse C57BL/6N origin to find an optimal dose to load the drug release system. Furthermore, potential effects of the drug on MSCs and their capacity to differentiate into endochondral lineages was investigated. The findings of these experiments were shaping the design of the local drug release system, which is targeting the late pro-inflammatory and early anti-inflammatory phase in bone healing. Ultimately, the concept was proven in an osteotomy model in the same mouse strain at a time point during the inflammatory phases and at a further advanced stage of endochondral regeneration.

4.1. Cell culture studies

4.1.1 Anti-inflammatory effects of Iloprost

Although the anti-inflammatory properties of Iloprost are well described in literature, its clinically approved composition as Ilomedine was tested first *in vitro* on key player cell types in bone healing to find a particular concentration for the subsequent design of the local drug release system. In this scenario, also cells derived from bone marrow were included to mimic endogenous conditions at the fracture site. Analyzed cells were T cells within bone marrow or splenocyte suspensions, isolated CD8+ and Treg cells, and BM-macrophages. From the T cell cultures, conditioned media (CM) were further collected for subsequent indirect co-culture experiments of osteogenic differentiating MSCs.

4.1.1.1 Drug concentration tests on T cells and T cell subsets

In this study, the anti-inflammatory properties of Iloprost were initially tested on CD3/CD28-activated T cells in suspensions of whole bone marrow cells (Fig. 4.1). The bone marrow is the major origin of immune cells during the early healing phase besides the circulation. After two days of incubation of whole bone marrow cells with media supplemented with 300 nM and 3 µM Iloprost, the concentrations of secreted cytokines were significantly reduced for IFN-γ (~130 to ~55 ng/ml) and further for TNF-α (~65 to ~40 pg/ml) and IL-10 (~190 to ~70 pg/ml) in a dose-dependent manner compared to controls

with PBS supplement. In response to the immunosuppressive drug, the values for metabolic cell activity, measured by fluorescence of Presto Blue conversion, were reduced in a dose-dependent manner as well in the activated groups. However, the metabolic activity of non-activated BM cells was not significantly affected by the drug. Similar results were found for CD3/CD28-activated T cells in splenocytes (Appendix Fig. 8.1). Concentration values for IFN-γ and TNF-α for non-activated cells were detected on very low basal levels. The highest applied dose of 3 µM Iloprost was investigated further in the following experiments with immune cells.

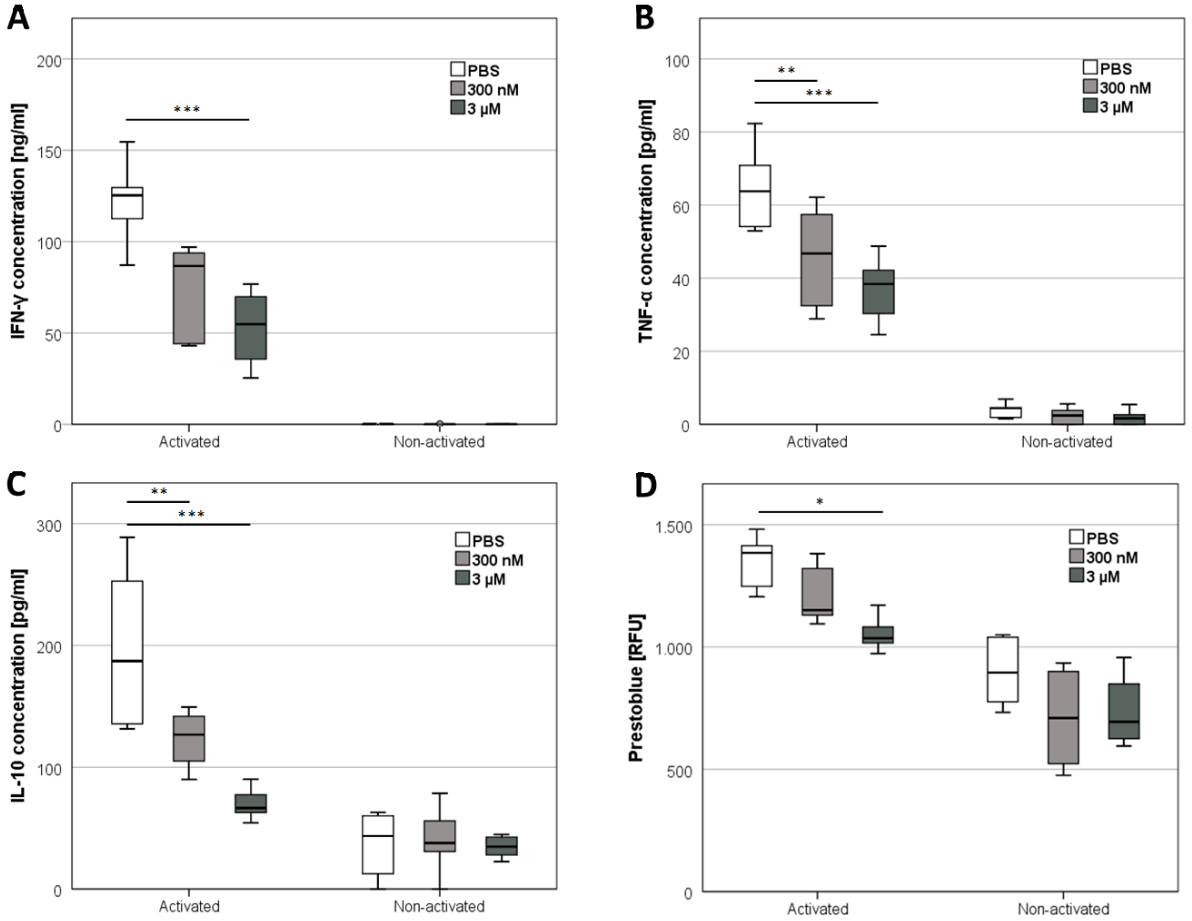

Figure 4.1: Anti-inflammatory effects of Iloprost on CD3/CD28-activated cells in whole BM cells. Concentrations of secreted cytokines were significantly reduced after 2 days in a dose-dependent manner for (A) IFN-γ, (B) TNF-α and (C) IL-10. (D) Metabolic cell activity was reduced by Iloprost in the activated groups. Values for non-activated cells are significantly lower in A and B compared to activated cells. Multiple comparison, n = 6, ***: $p \leq 0.0005$; **: $p \leq 0.005$; *: $p \leq 0.05$.

A major source of pro-inflammatory factors in initial phases of bone healing are the CD8+ T cells. Hence, this cell type was investigated next for its response to Iloprost. CD8+ cells were isolated from spleen and bone marrow of individual mice and cultivated for 5 days in presence of Iloprost (Fig. 4.2). The successful isolation was confirmed with FACS at 0 days as well as the status of the cells after 5

days of activation with anti-CD3/CD28 and Iloprost treatment. An effect onto viability by Iloprost was not observed (Fig. 4.2 A, A'). During cultivation, the frequency of CD3+ cells increased (Fig. 4.2 B, B'). Furthermore, the purity of the culture stayed above 95 % for CD3+CD8+ cells (Fig. 4.2 C, C'). Interestingly, less cells showed high CD8 expression with Iloprost tendency-wise. Almost all cells became CD25+, which marked activation (from ~10 to >95 %). However, Iloprost treated cells tended to be less activated (Fig. 4.2 D, D').

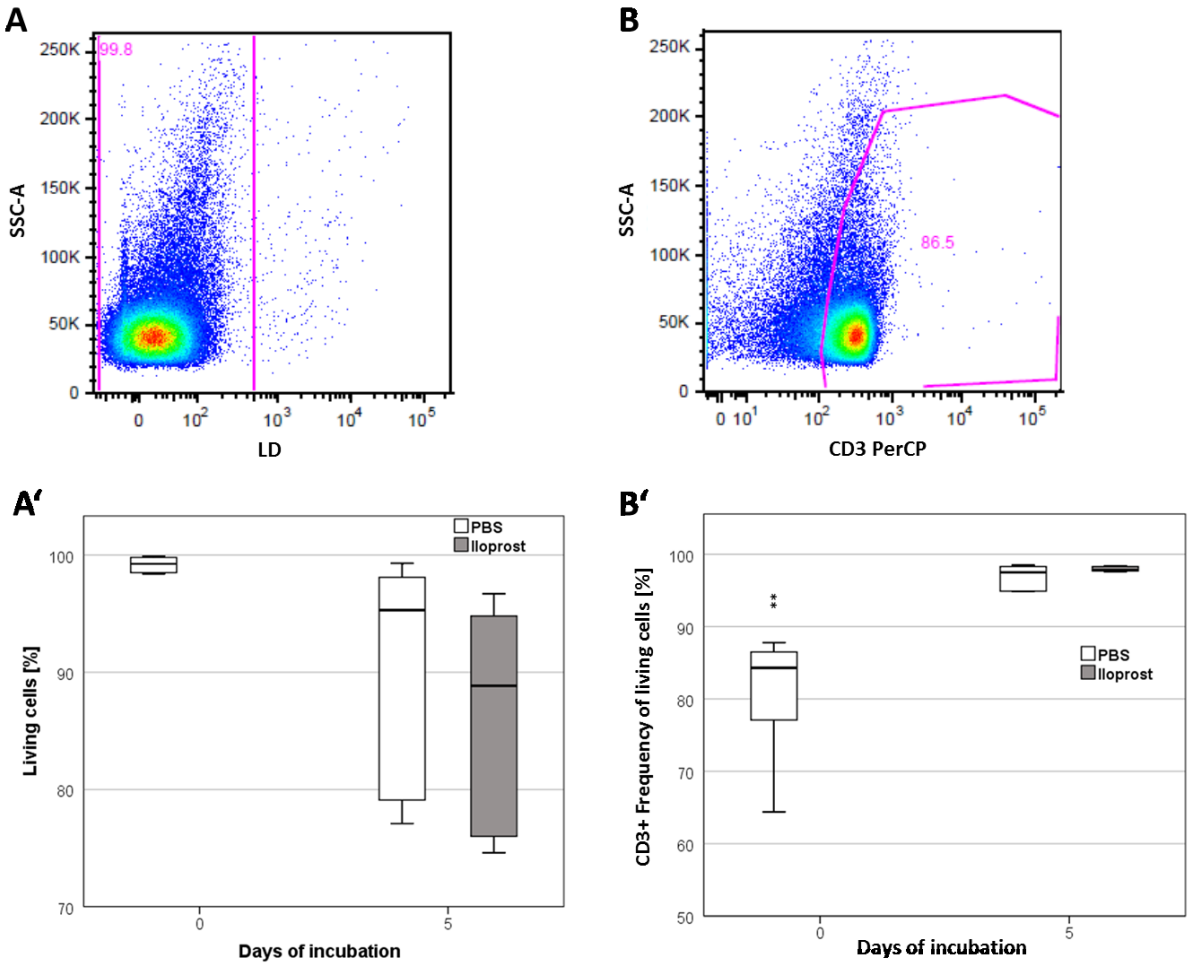

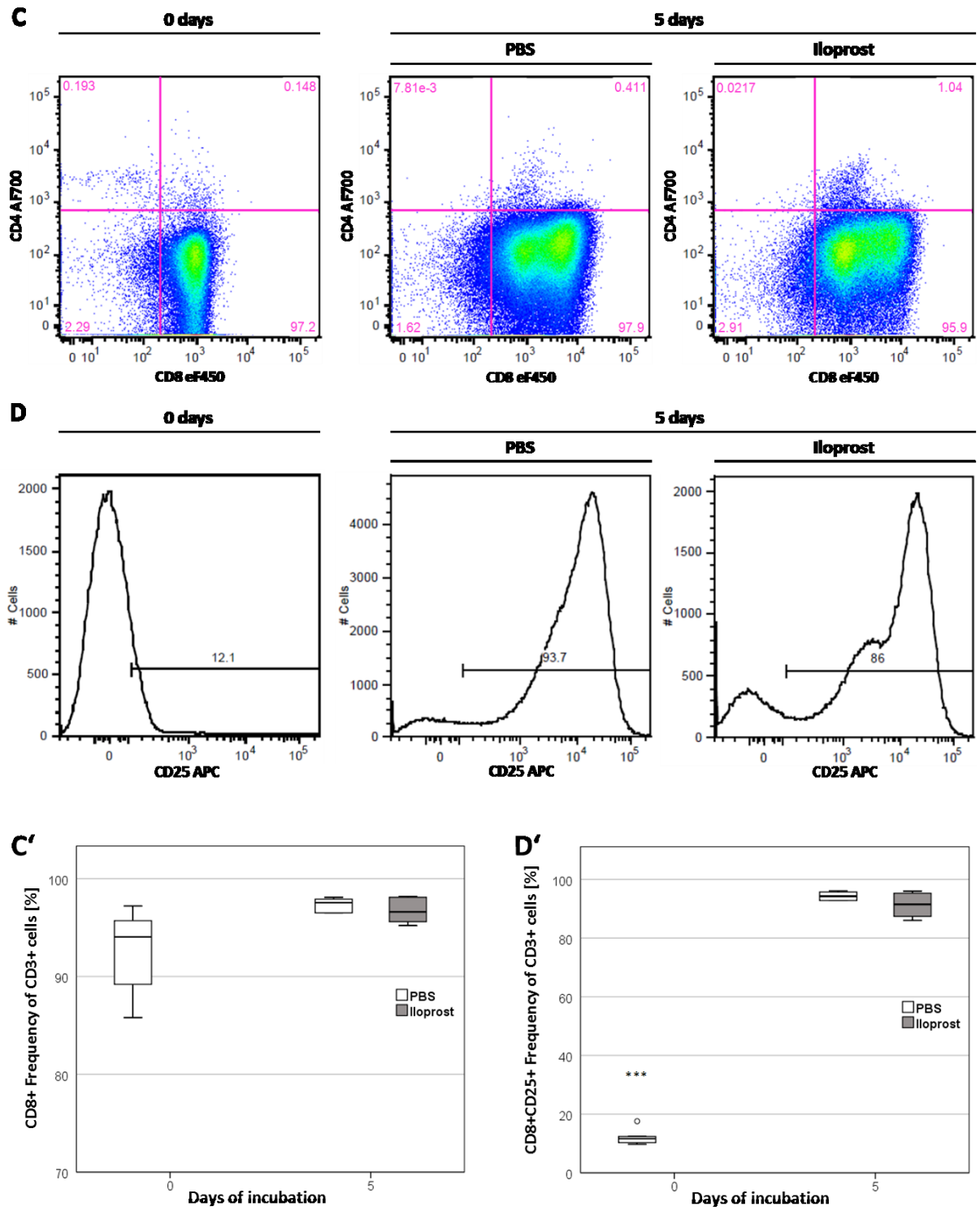

Figure 4.2: Identity confirmation via FACS of CD3/CD28-activated CD8+ isolated T cells during cultivation with Iloprost (3 µM). (A) Pseudo color dot plot of Live/Dead (LD) staining. SSC-A: Area values of sideward scatters. (A') Relative number of living cells showed no significant impact of the drug. (B) Gating for the CD3+ cells within the living cell fraction. (B') During cultivation, the relative numbers of CD3+ cells increased significantly in both treatment groups. (C) Pseudo color plots of CD3+ cells for CD4 and CD8 expression at 0 and 5 days of incubation. (C') CD3+CD8+CD4- T cell frequencies during cultivation. (D) Histograms of CD25+ cells in CD3+CD8+CD4- T cell populations. (D') CD3+CD8+CD4- T cells significantly acquired more CD25 during stimulation with anti-CD3/CD28. However, culture conditions tended to affect the viability. Multiple comparison, n = 6, ***: $p \leq 0.0005$; **: $p \leq 0.005$.

Furthermore, CD8+ secreted cytokine concentrations were measured via ELISA (Fig. 4.3). Cells showed a similar secretion pattern as the activated T cells from bone marrow or spleen. After 2 days of incubation with Iloprost high concentrations of IFN-γ (~410 to ~250 ng/ml) and TNF-α (~275 to ~180 pg/ml) were significantly diminished. In case of the anti-inflammatory cytokine IL-10 concentrations were also significantly diminished in activated CD8+ cells, from ~290 pg/ml down to ~150 pg/ml, which was close to the basal level of the non-activated CD8+ cells of ~120 pg/ml. In presence of Iloprost CD8+ cells ceased almost completely any secretion of IL-10.

The metabolic cell activity via Presto Blue conversion was relatively strong for the CD8+ cells with median ~2200 RFU and even reached levels up to 3000 RFU, which was in range of the much more densely seeded splenocytes (Appendix Fig. 8.1). A tendency was observed for reduction by Iloprost, whereas the non-activated CD8+ cells showed an order of magnitude less activity.

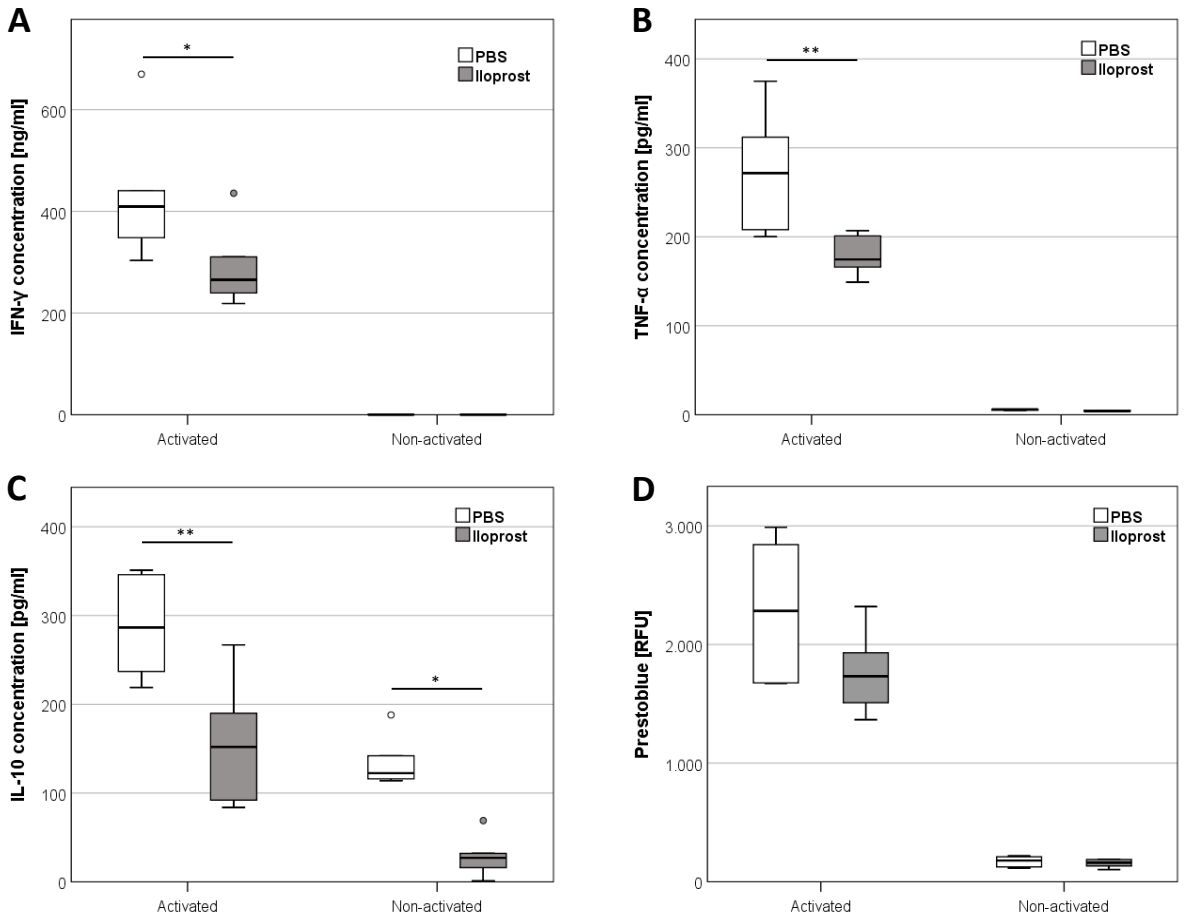

Figure 4.3: Anti-inflammatory effects of Iloprost on CD3/CD28-activated CD8+ T cells. Concentrations of secreted cytokines were significantly reduced after 2 days of incubation with 3 µM Iloprost for (A) IFN-γ and (B) TNF-α. (C) IL-10 concentrations were significantly diminished in activated and non-activated CD8+ T cells. (D) Presto Blue conversion was tendency-wise reduced by Iloprost. Values for non-activated cells are significantly lowest in A, B and D. Multiple comparison, n = 6, **: $p \leq 0.005$; *: $p \leq 0.05$.

During inflammation, pro-inflammatory cells like CD8+ T cells increase their numbers rapidly. On the contrary, the depletion of CD8+ T cells results in faster bone formation (Reinke *et al.* 2013). Here, a strong effect of Iloprost onto proliferation of CD8+ T cells was observed (Fig. 4.4). After 5 days of incubation CD3/CD28-activated CD8+ T cells increased in size and proliferated even in a three-dimensional manner. Iloprost treated cells showed less growth. Instead of almost 3 population doublings in the control group cells achieved only one doubling in response to Iloprost. In case of non-activation with anti-CD3/CD28 CD8+ T cells did neither swell nor proliferate and were rather reduced in numbers.

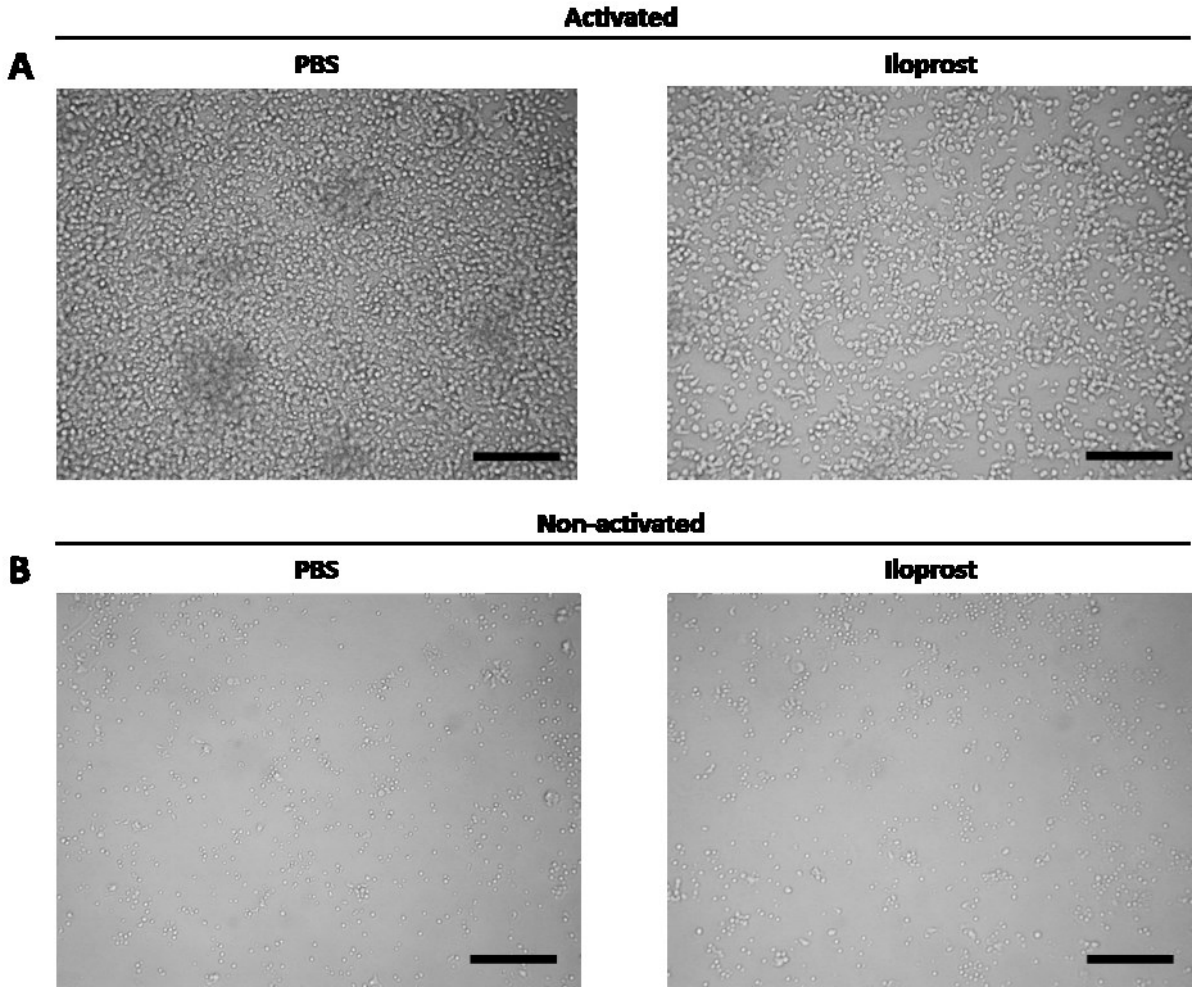

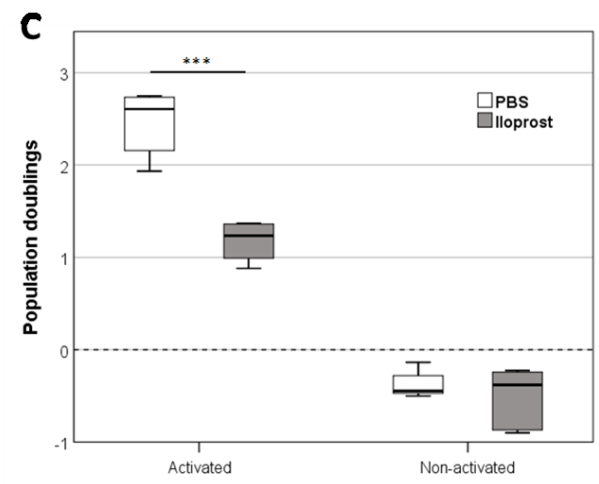

Figure 4.4: Proliferation inhibition of Iloprost treated CD8+ T cells. (A) Brightfield images of activated CD8+ T cells after 5 days of incubation with 3 µM Iloprost. Cells are increased in size and Iloprost treated cells show less three-dimensional proliferation. (B) Brightfield images of non-activated CD8+ T cells did not show any size increase for most cells. (C) Population doublings were significantly reduced in activated CD8+ T cells by Iloprost. No proliferation was detected in non-activated CD8+ T cells. Multiple comparison, n = 6, ***: $p \leq 0.0005$. Scale bars equal 200 µm.

T regulatory cells (Treg) are anti-inflammatory cells that are the most potent in suppression of pro-inflammatory cells and are expressing the IP receptor. Treg were isolated from a pool of spleen, bone marrow and lymph nodes for each individual biological replicate. The isolation and the marker expression after 5 days of Iloprost treatment was analyzed via FACS. Additionally, the response to Iloprost was tested at different stages of CD3/CD28 receptor stimulation.

At first, CD3+ T cells were gated within the living cell population (Fig. 4.5 A, B). After 5 days, the relative number of living cells showed a tendency of reduced viability by Iloprost. However, the fraction of CD3+ T cells stayed stable. To quantify the Treg population, the CD3+ T cells were first gated for CD4+CD8- and subsequently for CD25+FoxP3+ (Fig. C, D). The initial median purity of the parent CD3+CD4+ and in particular the Treg culture (CD3+CD4+CD25+FoxP3+) was > 95 % and > 90 %, respectively (Fig. 4.5 C' and D'). During cultivation, CD3+CD4+CD8- median population numbers dropped to median ~49 % to ~42 % for PBS and Iloprost treated groups, respectively. The CD3+CD4-CD8- fractions increased accordingly (Fig. 4.5 C). However, the relative Treg numbers within the CD3+CD4+CD8- populations stayed stable (Fig. 4.5 D') with an occurrence of a minor CD3+CD4+CD25-FoxP3- T cell fraction after 5 days of incubation (Fig. 4.5 D). Any significant effects of Iloprost on marker expression or viability was not observed.

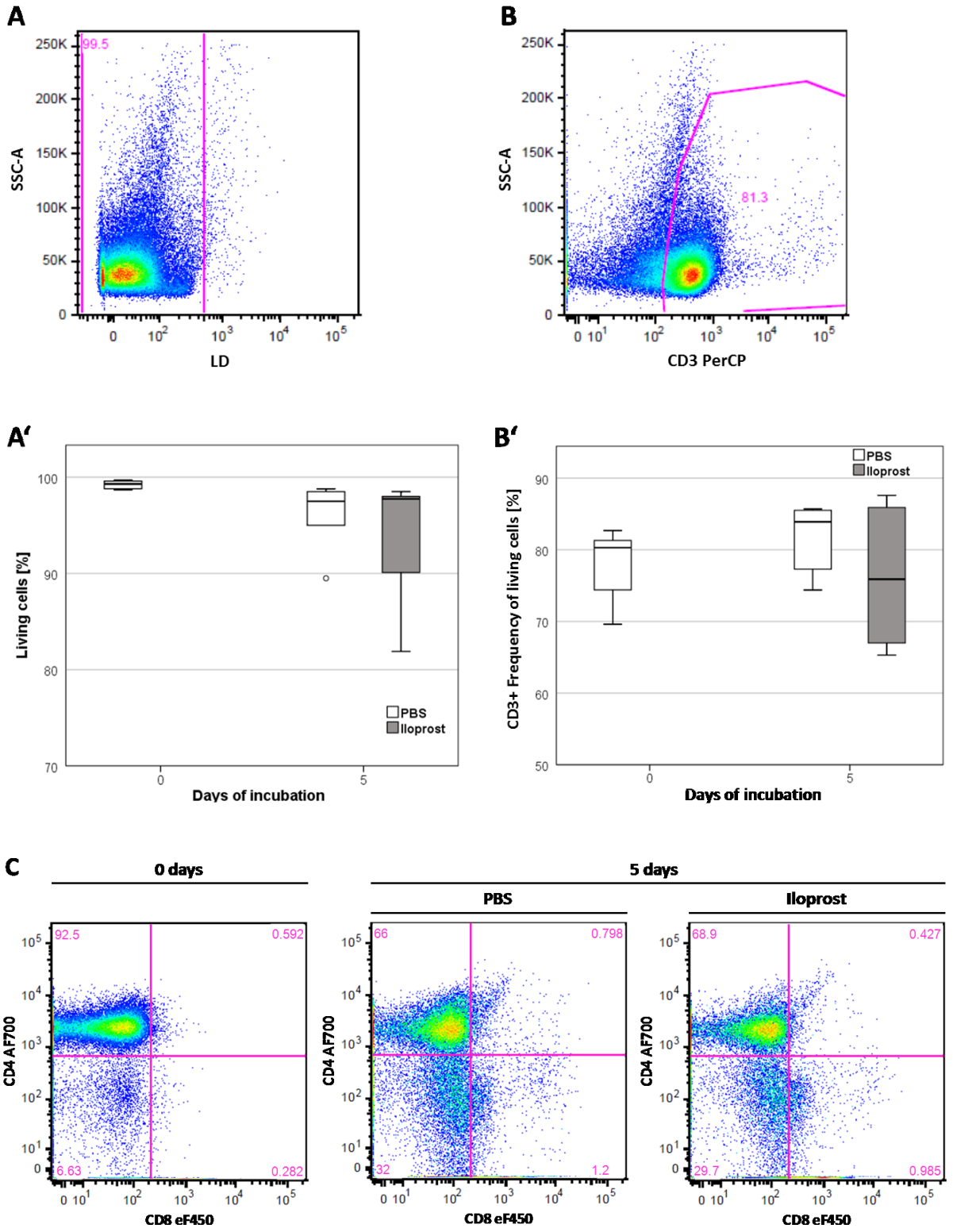
A
SSC-A
LD
99.5
B
SSC-A
CD3 PerCP
81.3
A'
Living cells [%]
Days of incubation
PBS
Iloprost
B'
CD3+ Frequency of living cells [%]
Days of incubation
PBS
Iloprost
C
0 days
5 days
PBS
Iloprost
CD4 AF700
CD8 eF450
92.5
0.592
6.63
0.282
66
0.798
32
1.2
68.9
0.427
29.7
0.985

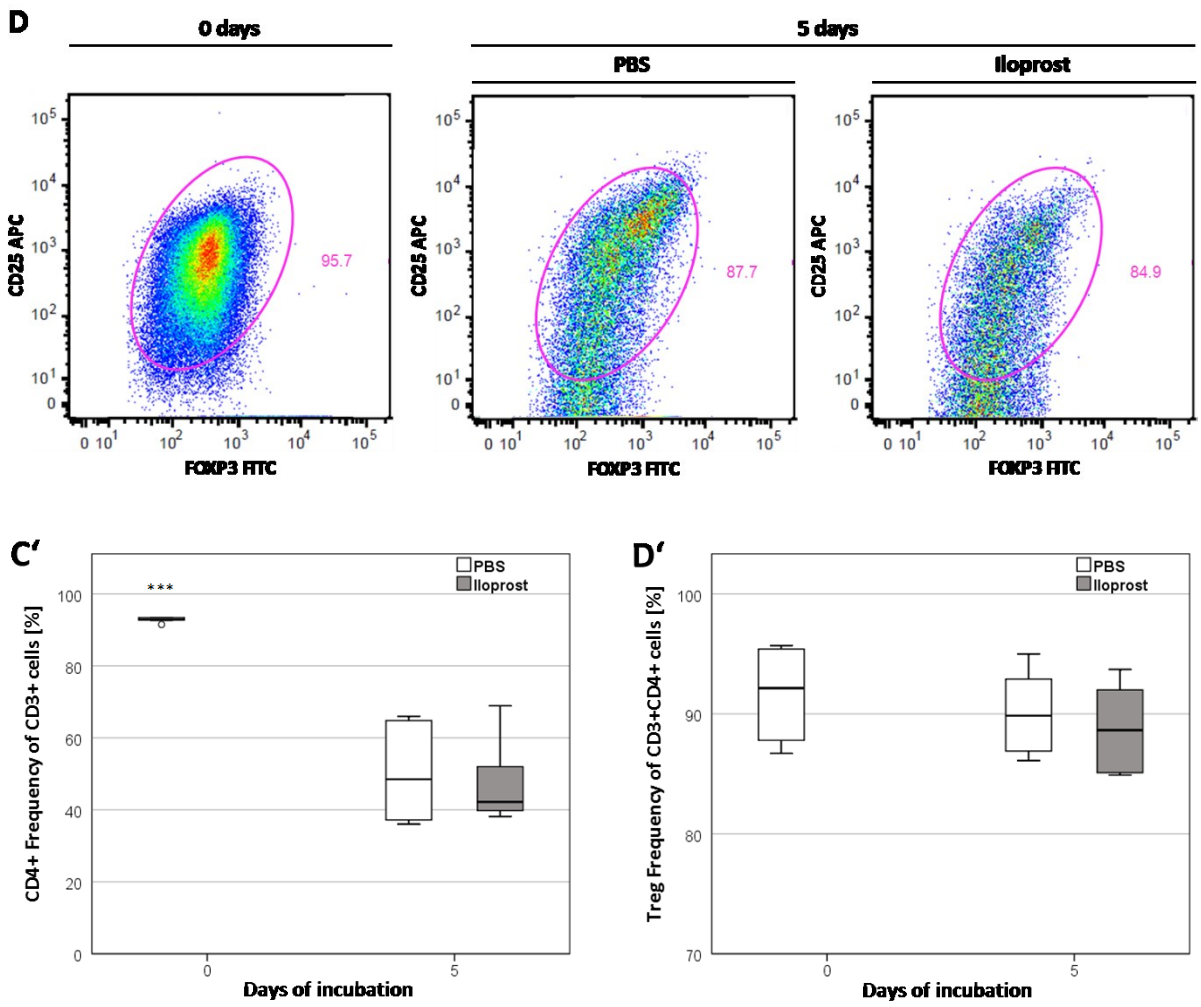

Figure 4.5: Identity confirmation via marker expression with FACS of CD4+CD25+ isolated Treg cells. Treg were activated with anti-CD3/CD28 and treated with 3 µM Iloprost for 5 days. (A) Displayed is the pseudo color dot plot of Live/Dead (LD) staining of singlet cells. SSC-A: Area values of sideward scatters. (A') Overall relative number of living cells showed no significant impact of the drug or cultivation. (B) Within the living cell fraction, CD3+ T cells were gated. (B') The relative numbers of CD3+ T cells stayed stable for the enriched Treg culture. (C) Pseudo color plots of CD3+ T cells for CD4 and CD8 expression. During culture, the CD4- fraction within the CD3+ population increased. (C') CD3+CD4+ frequency reduction during cultivation in PBS and Iloprost groups. (D) Pseudo color plots of CD25+FoxP3+ Treg cells in CD3+CD4+CD8- populations. After 5 days of incubation, minor fractions of CD3+CD4+CD25-FoxP3- cells occurred. (D') However, CD25+FoxP3+ Treg cells frequencies of CD3+CD4+ fraction were not affected by cultivation nor Iloprost. Multiple comparison, n = 6, ***: $p \leq 0.0005$.

Il-10 is the master regulator of anti-inflammatory signaling. It is secreted intensively by CD3/CD28-activated Treg and on a basal level by non-activated Treg. Here, the activation dependent response to Iloprost by Tregs was investigated with secreted IL-10 concentrations as readout. Non-activated Treg showed increased IL-10 levels with Iloprost treatment (Fig. 4.6 A). The cell metabolic activity was assessed by Presto Blue, which in turn rather decreased tendency-wise in response to Iloprost (Fig. 4.6 B). Regarding CD3/CD28-activated Treg a tendency of lowered Il-10 secretion with Iloprost was

observed and the Presto Blue conversion was significantly reduced by Iloprost treated activated Treg (Fig. 4.6 C, D).

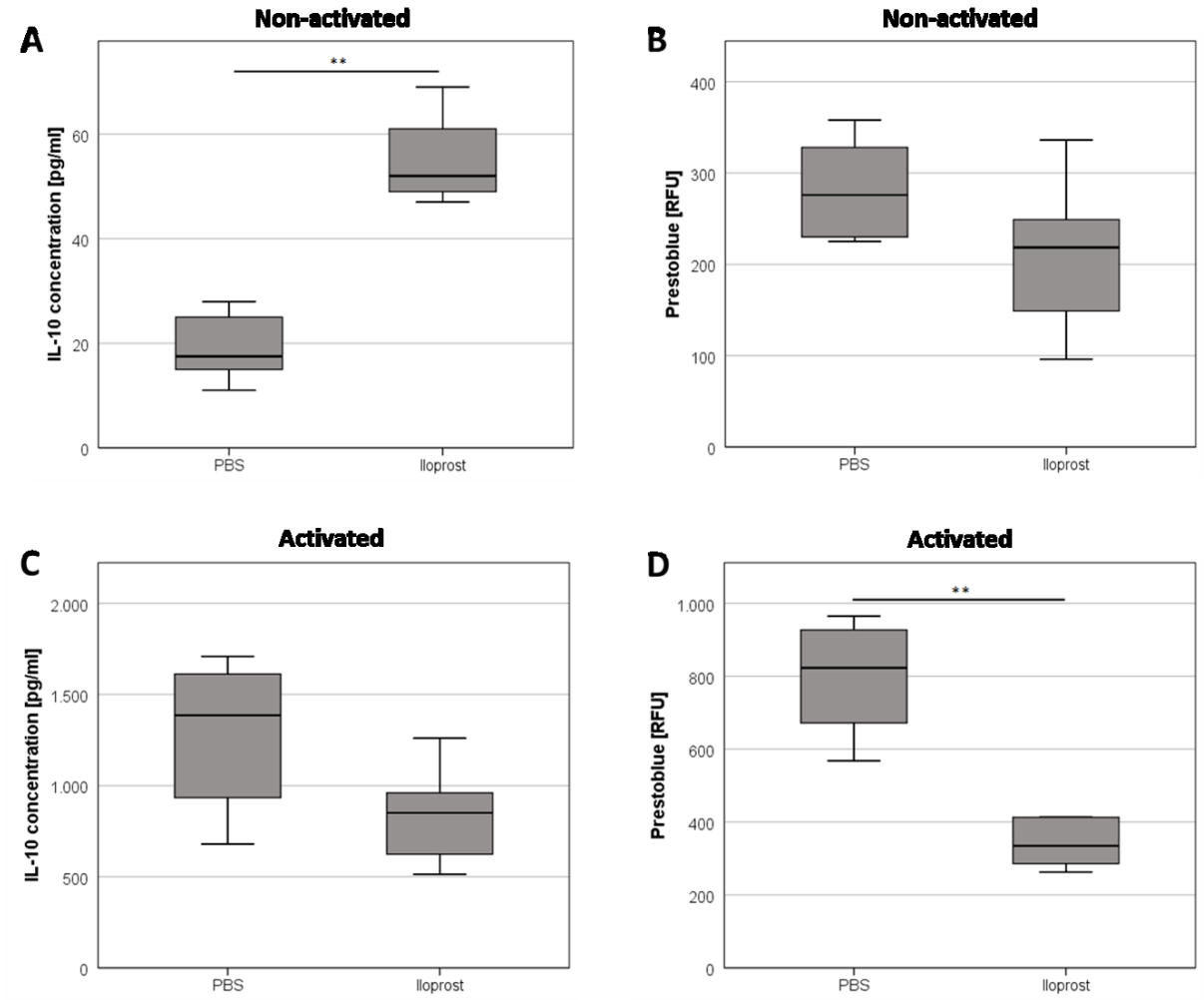

Figure 4.6: CD3/CD28-activation dependent response to Iloprost by Tregs towards IL-10 secretion and metabolic activity. (A) Non-activated Treg show increased IL-10 with 3 µM Iloprost treatment after 2 days of incubation and (B) Presto Blue fluorescence values were not significantly altered. (C) CD3/CD28-activated Treg show a tendency of reduced Il-10 secretion with Iloprost. (D) Presto Blue conversion was significantly lowered by Iloprost treated activated Treg. Pairwise comparison, n = 6, **: $p \leq 0.005$.

The culture for activated Treg secreted high amounts of IL-10. However, the size of the activated cells was not increased compared to according non-activated cultures after 5 days of incubation (Fig. 4.7). Furthermore, Treg did not proliferate during culture nor in response to CD3/CD28 activation nor Iloprost treatment.

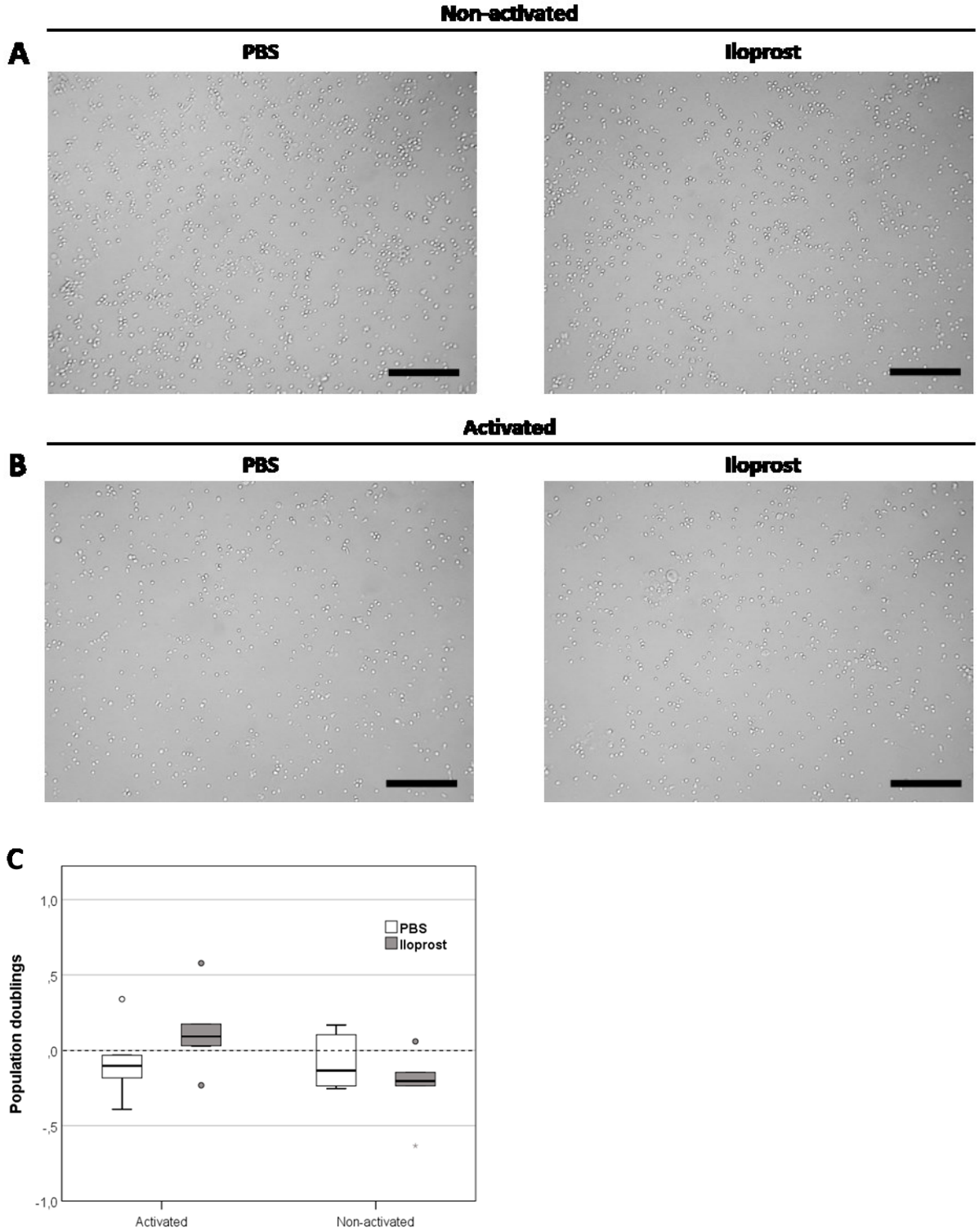

Figure 4.7: Proliferation of Treg cells not induced by Iloprost. Brightfield images of (A) activated and (B) non-activated Treg cells after 5 days of incubation. (C) Proliferation was not induced by culture, CD3/CD28 activation nor 3 µM Iloprost treatment. Scale bars equal 200 µm.

4.1.1.2 Influence of Iloprost onto macrophage polarization

Macrophages are crucial for bone regeneration and fulfill multiple roles at distinct phases of the process. In particular, upon respective signaling input, they can polarize into different phenotypes, e.g. pro-inflammatory M1-type or anti-inflammatory M2-type. The polarization is characterized by several markers. Here, a simplified characterization was conducted with CD68 to identify mononuclear cells as macrophages and further CD80 and CD206 to reveal M1-types and M2-types, respectively. CD68+CD80+ M1-type macrophages respond in a pro-inflammatory manner after pathogen invasion or tissue injuries. However, during bone healing, CD68+CD206+ M2-type macrophages are emerging in the anti-inflammatory phase and are especially capable of secreting extracellular matrix modulating enzymes, which becomes increasingly necessary towards the endochondral phases of fracture healing. Otherwise, macrophages are residing at various sites in the organism in their dormant state as M0-tpye at which they are CD68 positive but CD80 and CD206 negative, regarding the here used markers.

Similar to other immune cells, macrophages are also responsive to PGI_2 signaling. Hence, potential effects of Iloprost during macrophage polarization were investigated *in vitro* as well. Therefore, whole bone marrow cells were incubated for three days and subsequently polarized for another three days towards pro-inflammatory M1 and anti-inflammatory M2-type with 20 ng/ml IFN-γ and 20 ng/ml IL-4/IL-13, respectively. Immune fluorescence could confirm the successful initiation of polarization events (Fig. 4.8 A, B, C). Utilization of ELISA further quantified the presence of TNF-α and IL-10 in conditioned media (Fig. 4.8 D, E). 3 µM Iloprost had a significant effect onto lowering secreted concentrations of TNF-α (~50 to ~20 pg/ml) of M1 macrophages and for basal levels of M0-type macrophages. On the contrary, elevated IL-10 concentrations of ~410 pg/ml were detected only for the Iloprost group of the M2-type macrophages compared to ~290 pg/ml of the control. Interestingly, Presto Blue values are significantly reduced for M2 macrophages with Iloprost compared to control (~1600 to ~1300 RFU). The CD68+CD80-CD206- M0-type macrophages showed lowest metabolic activity compared to the other macrophage types.

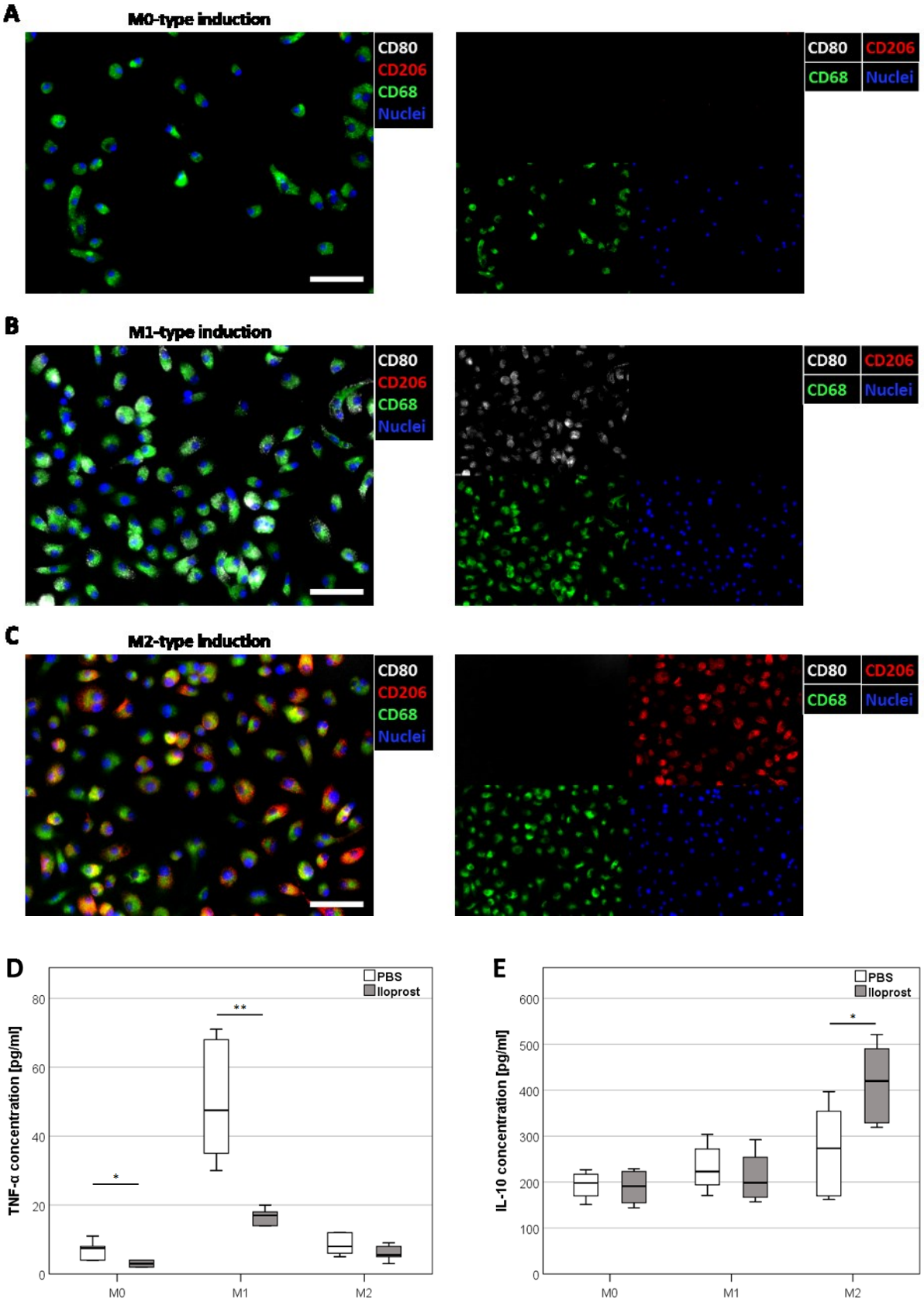
A
M0-type induction
CD80
CD206
CD68
Nuclei
B
M1-type induction
C
M2-type induction
D
PBS
Iloprost
TNF-α concentration [pg/ml]
M0
M1
M2
E
IL-10 concentration [pg/ml]

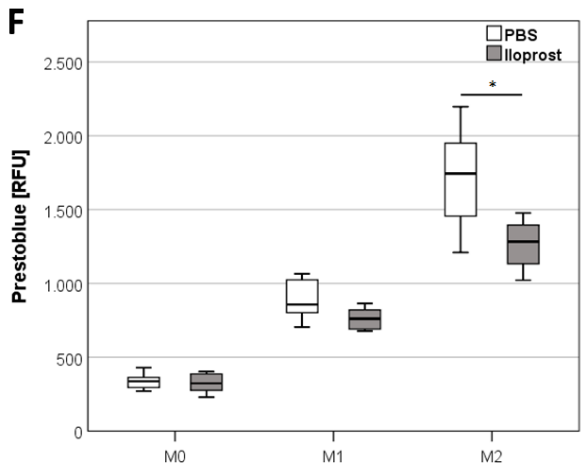

Figure 4.8: Anti-inflammatory effects of Iloprost during macrophage polarization. Bone marrow cells were incubated for three days and subsequently polarized three days towards pro-inflammatory M1- and anti-inflammatory M2-type. (A) Immune fluorescence image of un-polarized M0-type CD68+ macrophages. (B) After M1-type induction with 20 ng/ml IFN-γ, CD80+CD68+ double positive cells could be detected. (C) M2-type induction with 20 ng/ml IL-4/IL-13 lead to CD206+CD68+ double positive cells. (D) Secreted concentrations of TNF-α were significantly smaller for M0 and M1 in response to 3 µM Iloprost compared to PBS supplementation. (E) M2-type macrophages had elevated IL-10 concentrations with Iloprost treatment, but (F) lower Presto Blue signals. M0-type macrophages showed lowest Presto Blue conversion. Multiple comparison, n = 6, **: $p \leq 0.005$; *: $p \leq 0.05$. Scale bars equal 100 µm.

4.1.2 Effects of Iloprost onto MSC differentiation

Effects of different doses of Iloprost (Ilomedine) onto osteogenic, adipogenic and chondrogenic differentiation of primary MSCs cultures were investigated as well. These insights were clarifying if the time-window of local drug application during the regenerative cascades could be extended from the inflammatory phases to the endochondral phases. Furthermore, response of MSCs towards the drug in viability and proliferation was tested.

4.1.2.1 Osteogenic differentiation

Mesenchymal stroma cells (MSCs) express the IP-receptor and differentiate into the matrix producing cell lineages of the endochondral phases. Hence, their response towards Iloprost was investigated during induction of osteogenic differentiation into osteoblasts *in vitro*. After 14 days of incubation, monolayers were stained with Alizarin Red to reveal calcification of the differentiated osteoblasts. The osteoinductive media (OM) were supplemented with different doses of Iloprost, which had no significant effect onto the osteogenic differentiation process (Fig. 4.9 A, B). However, the highest applied dose of 3 µM lead to the parallel sporadic occurrence of adipogenic vesicles. Nile Red staining, which was carried out prior Alizarin Red staining, confirmed triglyceride formation (Appendix Fig. 8.4).

Cell activity and cell numbers were not affected by any drug dose (Fig. 4.9 C, D). Cells of expansion media (EM) control showed significantly highest Presto Blue values of median ~4500 RFU.

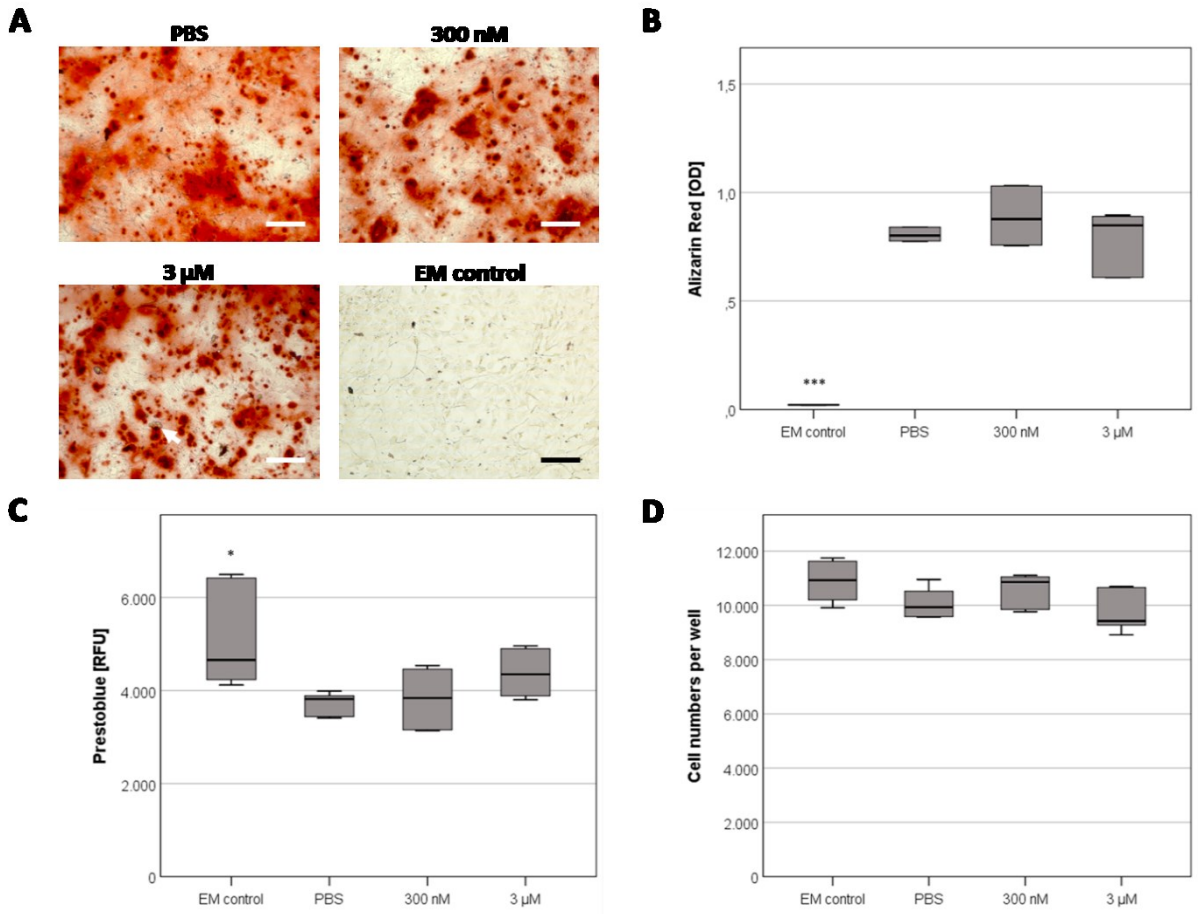

Figure 4.9: Absent effect of Iloprost onto osteogenic differentiation determined by quantification of mineralized matrix deposits. (A) Alizarin Red stained monolayers of MSCs after incubation for two weeks with osteoinductive media (OM) supplemented with PBS, 300 nM and 3 µM of Iloprost. White arrow marks an adipogenic vesicle, which occurred in the highest dose. (B) Optical density values of chemically detached Alizarin Red. (C) Expansion media (EM) control showed highest Presto Blue conversion. (D) Cell numbers derived from quantification of DAPI fluorescence. Multiple comparison, n = 6, ***: $p \leq 0.0005$, *: $p \leq 0.05$. Scale bars equal 200 µm.

4.1.2.2 Adipogenic differentiation

PGI_2 is known for its stimulatory effect onto adipogenic differentiation (Fujimori 2012). This fact was confirmed by application of the same Iloprost doses as before during differentiation with adipoinductive media (Fig. 4.10). Fluorescence reading of Nile Red stain increased in a dose-dependent manner, from ~420 to ~600 RFU for control and 3 µM Iloprost, respectively.

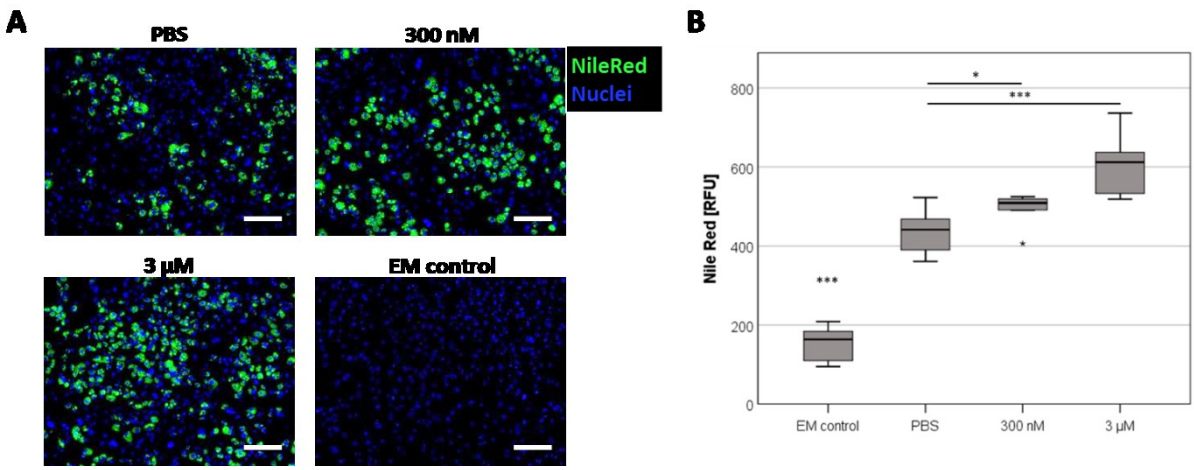

Figure 4.10: Iloprost effect onto adipogenic differentiation. (A) Fluorescence images of Nile Red and DAPI stained monolayers of MSCs after incubation for 5 days with adipoinductive media supplemented with PBS, 300 nM or 3 µM of Iloprost. (B) Fluorescence values of Nile Red increased significantly in a dose-dependent manner. Multiple comparison, n = 6, ***: $p \leq 0.0005$; *: $p \leq 0.05$. Scale bars equal 200 µm.

4.1.2.3 Chondrogenic differentiation

During the phases of bone regeneration the peak of the endochondral soft callus phases ensues the inflammatory phases. Initially the soft callus is formed by cartilage formation consisting of chondrocytes. A potential influence by Iloprost onto chondrogenic differentiation of MSCs was investigated via pellet formation and chondroinductive media supplemented with varying doses of the drug. Paraffin sections of the pellets were stained with Alcian Blue to reveal proteoglycans and counterstained with nuclear fast red (Fig. 4.11). All chondroinduced groups differentiated and images of three different areas of each pellet were recorded. Quantitative image analysis of the pixel intensities of Alcian Blue staining was carried out and data show no effect of Iloprost.

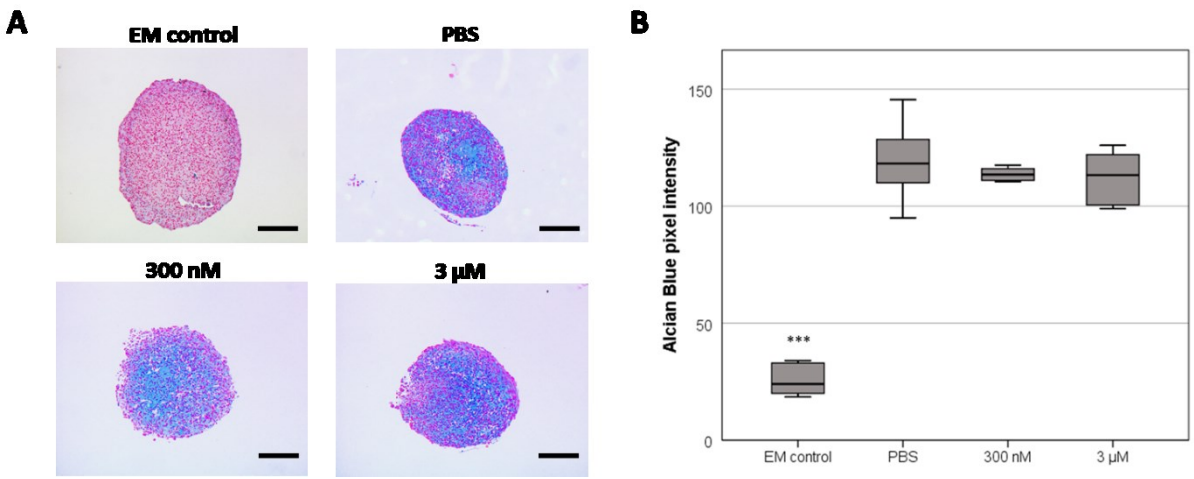

Figure 4.11: Absent Iloprost effect onto chondrogenic differentiation of MSCs. (A) Alcian Blue stained sections of pellets after incubation for three weeks with chondroinductive media supplemented with PBS, 300 nM or 3 µM of Iloprost. (B) Image analysis of Alcian Blue pixel intensities revealed no significant impact of Iloprost. Multiple comparison, n = 6, ***: $p \leq 0.0005$. Scale bars equal 200 µm.

4.1.2.4 Viability of MSCs

Potential negative effects onto viability of MSCs by Iloprost, or the components of its composition as Ilomedine for intravenous application, were tested with Live/Dead staining of MSC monolayers (Fig. 4.12 A, B, C). Values for living and dead cells were not significantly affected, respectively. However, the highest dose of 3 µM Iloprost reduced proliferation significantly to 2.18 population doublings after 7 days in comparison to control, which had reached 2.40 doublings (Fig. 4.12 D).

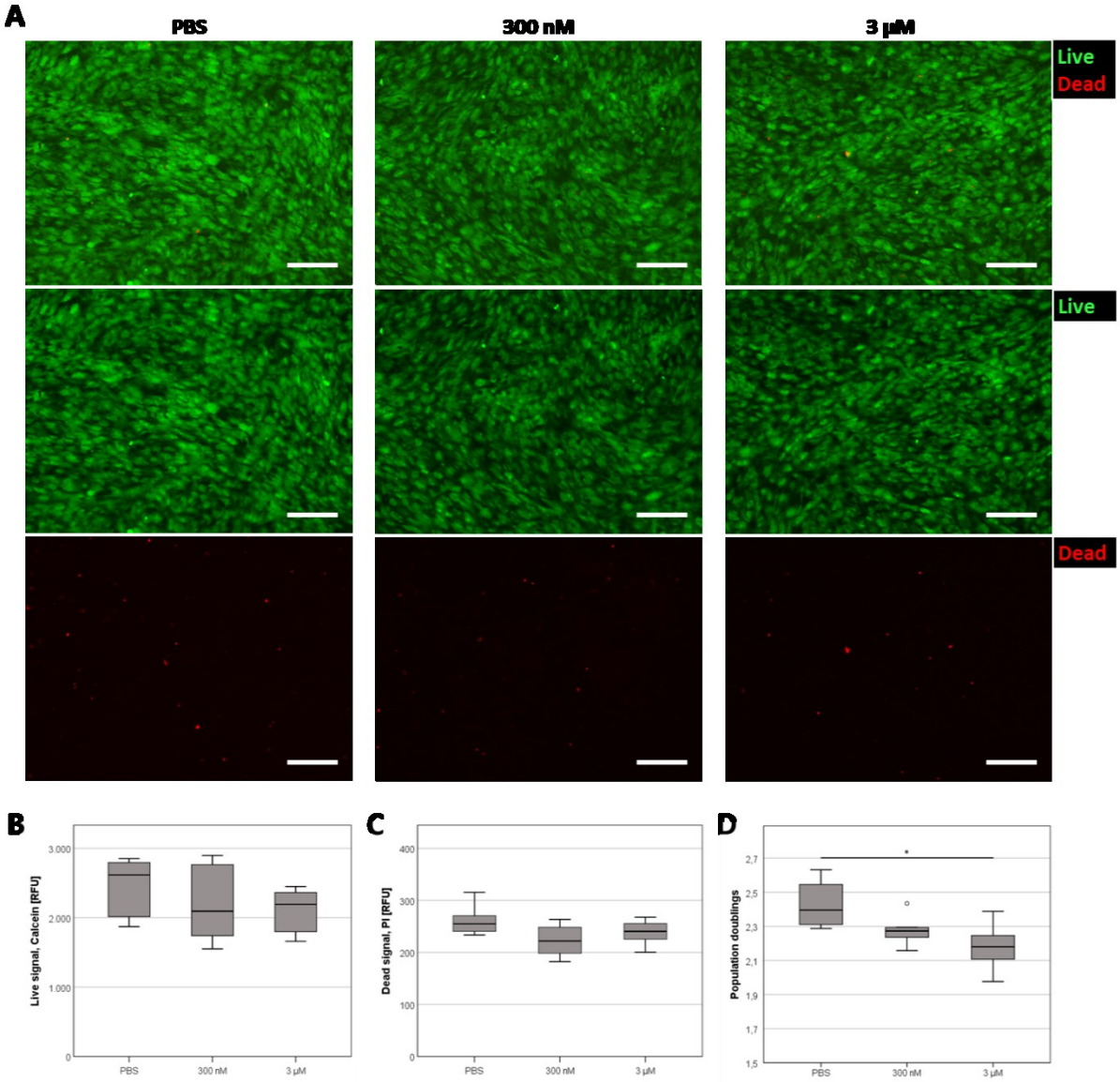

Figure 4.12: No effect on MSC viability but on proliferation after 7 days of Iloprost treatment in expansion media. (A) Fluorescence images (merged and single channel) after Live/Dead staining of MSCs monolayers. Green stained cells converted incorporated calcein-AM (calcein acetoxymethyl ester) to fluorescent calcein and were alive, whereas DNA in nuclei of dead cells could be revealed by red fluorescence of propidium iodide (PI) stain. Quantification of fluorescence signals of (B) live and (C) dead cells revealed no significant impact of Iloprost. (D) Proliferation was significantly reduced with highest dose of Iloprost of 3 µM. Multiple comparison, n = 6, *: $p \leq 0.05$. Scale bars equal 200 µm.

4.1.3 Osteoimmunological impact of Iloprost

The immune system constitutes diverse roles in the organism. Its primary function is the defense against invading pathogens. Fascinatingly, immune cells are additionally crucial for regenerative processes. However, there their roles are of a bivalent nature, e.g. the secreted cytokines can be beneficial but also inhibitive for osteogenic differentiation depending on type and concentration. The results found above confirmed that Iloprost is a strong and wide targeting anti-inflammatory agent, and no negative impact by the drug onto viability and osteogenic differentiation of MSCs were observed. Hence, the consequences for osteogenic differentiation of Iloprost's anti-inflammatory implications were investigated further by indirect co-cultures utilizing conditioned media (CM).

4.1.3.1 Conditioned media of Iloprost treated T cells onto osteogenic differentiation

Therefore, conditioned media, which were loaded with cytokines by CD3/CD28-activated and 3 µM Iloprost treated bone marrow cells were mixed 1:2 with double-concentrated osteoinductive media (OM) and applied onto MSC monolayers for 2 weeks. CM were collected in parallel during the experiment described above in which Iloprost was suppressing the secretion of TNF-α, IFN-γ and IL-10 significantly (see above Fig. 4.1). Hence, CM from Iloprost treated immune cells contained reduced cytokine concentrations compared to control treatment with PBS supplemented media.

Alizarin Red staining of calcified extracellular matrices and its subsequent quantification revealed a strong suppressive function of cytokine-loaded CM derived from CD3/CD28-activated BM T cells, i.e. from ~0.7 OD in the control group and down to ~0.4 OD (Fig. 4.13). However, the CM of Iloprost treated activated cells showed a significant reversal of this effect to ~0.6 OD in median. Effects of CM derived from non-activated whole BM cell culture were not significant. Monitoring of metabolic cell activity indicated a similar pattern to the calcification results. Presto Blue conversion was reduced significantly down to approximately half RFU with CM of activated cells. On the contrary, cell activity was less affected when CM of Iloprost treated cells was applied.

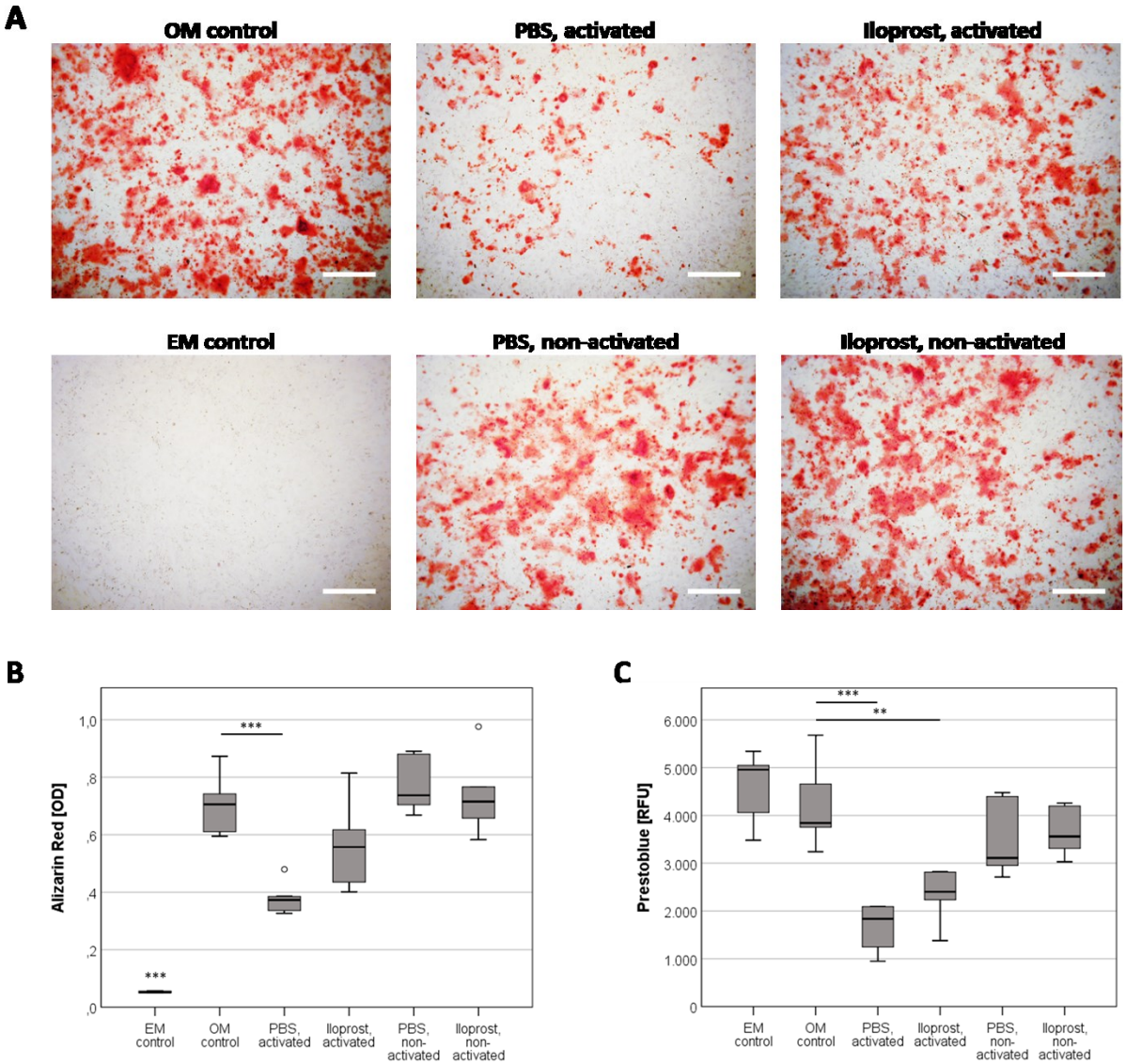

Figure 4.13: Reduced osteoimmunological impact of CM from CD3/CD28-activated and -non-activated bone marrow cells by Iloprost (3 µM). Double-concentrated osteoinductive media (OM) were mixed 1:2 with respective CMs. (A) Alizarin Red stained monolayers of MSCs after osteoinduction for two weeks with respective media. (B) Optical density values of chemically detached Alizarin Red from monolayers. Without Iloprost CM of CD3/CD28, activated T cells in BM cells suppressed osteogenic differentiation. (C) Presto Blue conversion was lowered significantly, when CM of activated cells were applied. CM of Iloprost treated cells reduced the negative effect of the highly cytokine enriched CMs. Multiple comparison, n = 6, ***: $p \leq 0.0005$; **: $p \leq 0.005$. Scale bars equal 200 µm.

Repeating this osteoimmunological cell culture experiment in a similar way with CM derived from CD8+ and Treg cells, respectively, analog results were achieved as compared to the CM of whole bone marrow cells. CM of CD3/CD28-activated CD8+ cells were reducing matrix calcification and cell activity (0.27 OD and ~2700 RFU), whereas Iloprost (0.52 OD and ~3300 RFU) could significantly diminish these suppressive effects (Fig. 4.14).

Interestingly, CM of activated Treg also reduced osteogenic differentiation, though in a less intensive manner, i.e. down to 0.53 OD in comparison to control of 0.87 OD (Fig. 4.15). When activated Tregs were treated with Iloprost, their CM subsequently could rescue the osteogenic differentiation process significantly up to 0.75 OD. CM of non-activated Treg did not impact the differentiation process. Furthermore, cell activity was not affected among samples of Treg-derived CM from any condition.

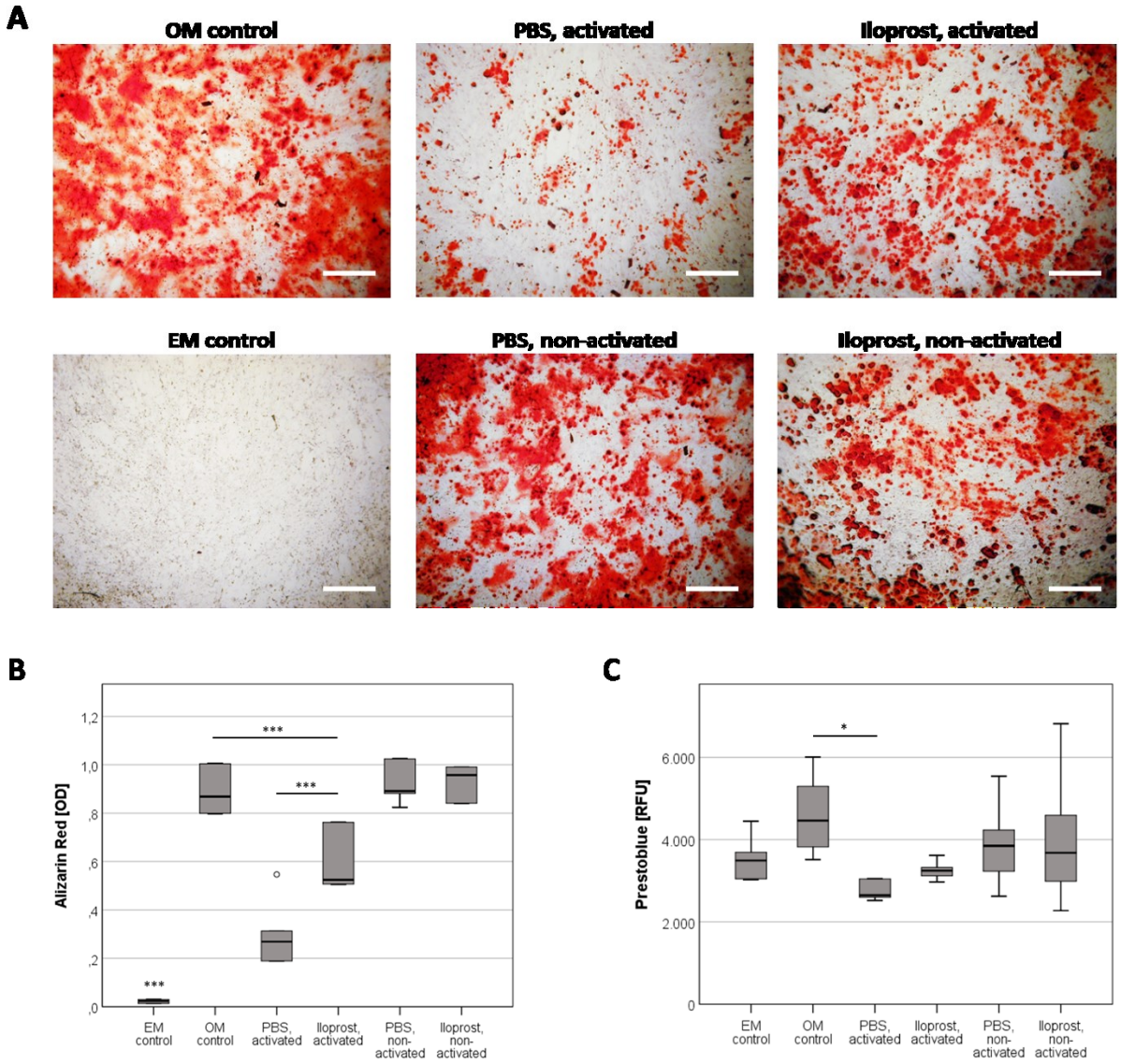

Figure 4.14: Reduced osteoimmunology by Iloprost towards CD3/CD28-activated CD8+ cells. OM were mixed 1:2 with CM of activated or non-activated cells, which were additionally treated with 3 µM Iloprost or PBS. (A) Alizarin Red stained monolayers of MSCs after osteoinduction for two weeks with respective media. (B) Optical density values of chemically detached Alizarin Red. Iloprost could significantly diminish the suppressive effects of CM derived from CD3/CD28-activated CD8+ cells onto osteogenic differentiation. (C) Presto Blue conversion was significantly reduced by CM of activated CD8+ cells without Iloprost. Multiple comparison, n = 6, ***: $p \leq 0.0005$; *: $p \leq 0.05$. Scale bars equal 200 µm.

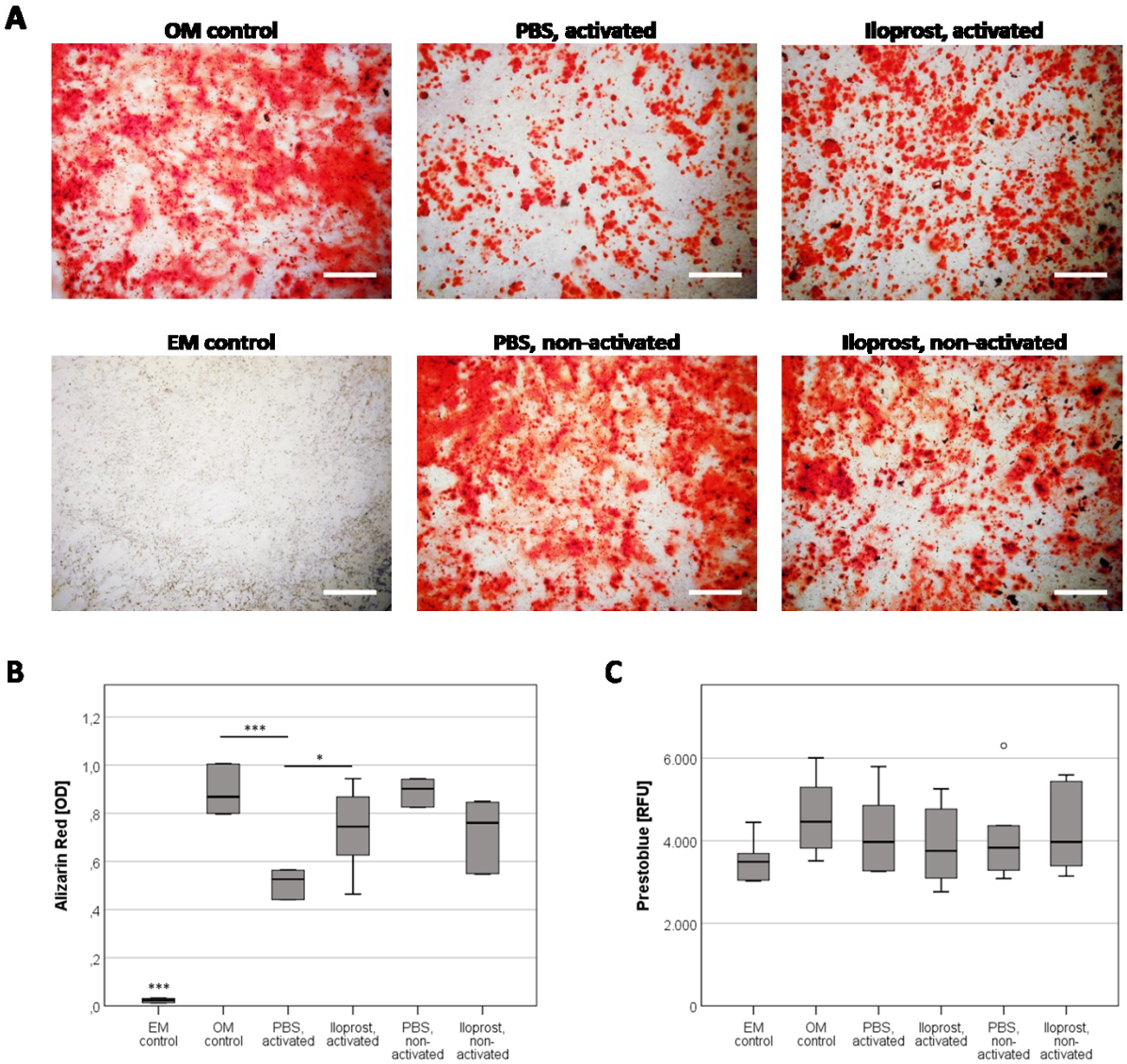

Figure 4.15: Reduced osteoimmunology of Iloprost treated Tregs. CM of activated or non-activated Treg cells with 3 µM Iloprost treatment were mixed 1:2 with OM. (A) Alizarin Red stained monolayers of MSCs after osteoinduction for two weeks with respective media. (B) Optical density values of chemically detached Alizarin Red. Iloprost could significantly counteract the suppressive effects of CM of CD3/CD28-activated Treg cells. (C) Presto Blue conversion was not affected by CM of Tregs. Multiple comparison, n = 6, ***: $p \leq 0.0005$; *: $p \leq 0.05$. Scale bars equal 200 µm.

4.1.3.2 Cytokine effects onto osteogenic differentiation

In addition to cytokine enriched CM from immune cells, the particular influence of TNF-α and IFN-γ onto osteogenic differentiation and further onto apoptosis was investigated (Fig. 4.16). According to values for Iloprost treated activated T cells in bone marrow, OM were supplemented with high or low concentrations of IFN-γ (120 or 50 ng/ml) or TNF-α (60 and 40 pg/ml) (see above Fig. 4.1).

Quantification of Alizarin Red staining in this experiment found the OM control to be at median 0.71 OD. The high TNF-α concentration resulted in a significant reduction in differentiation to ~0.4 OD.

Strikingly, especially strong suppression of matrix mineralization was revealed for all applied IFN-γ concentrations down to one order of magnitude. The OD values among the groups, which received IFN-γ were not significantly different from each other. Furthermore, cell metabolic activity values were significantly lowered for combinations with high IFN-γ concentrations from ~3800 RFU of the OM control down to ~1000 RFU for IFN-γ alone and ~900 RFU in combination with TNF-α.

The low IFN-γ concentration reduced cell activity only tendency-wise but were significantly higher compared to IFN-γ treatment in high doses with ~2700 RFU and ~2900 RFU for IFN-γ alone and with additional low concentrated TNF-α, respectively.

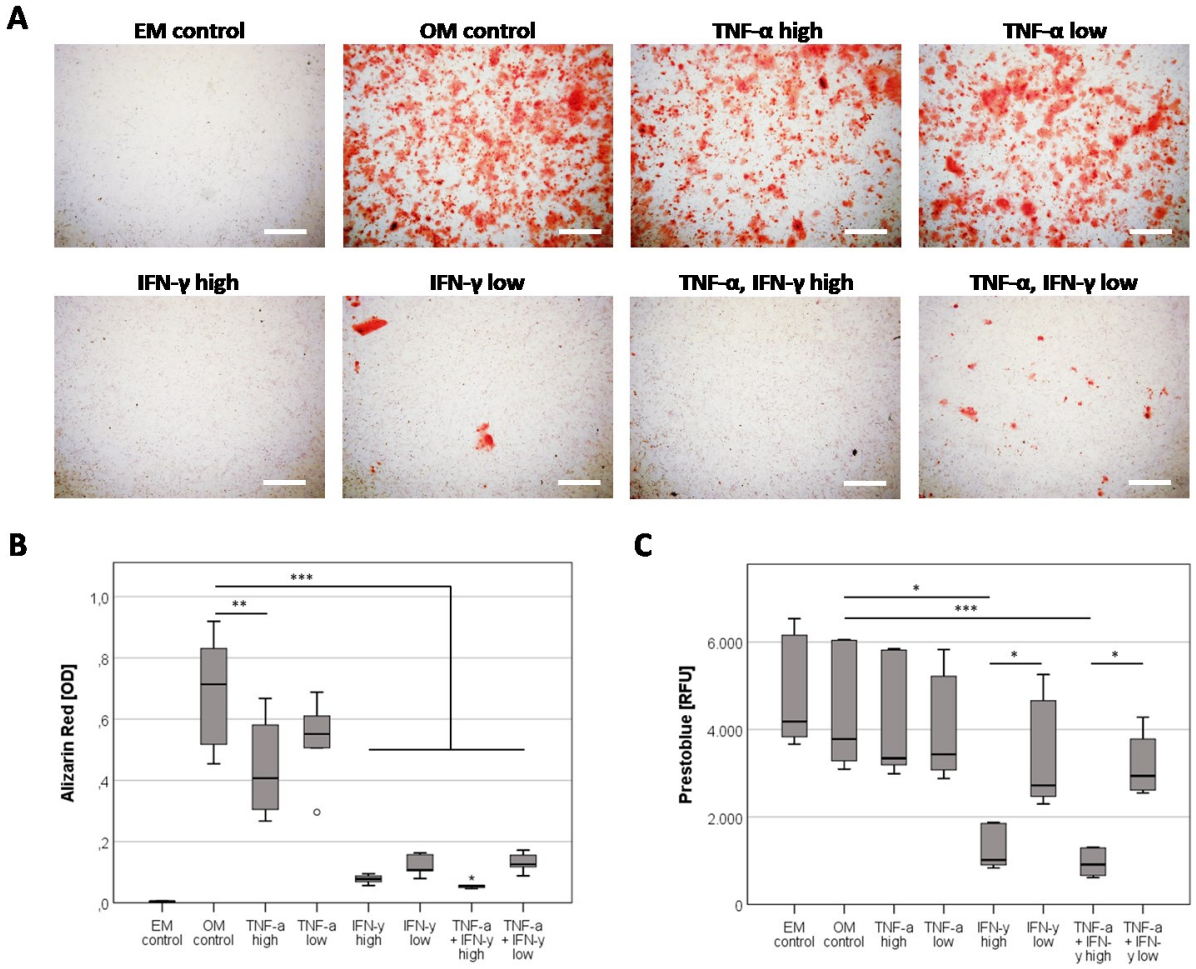

Figure 4.16: Varying negative effect of cytokines and doses onto osteogenic differentiation and viability of MSCs. OM were supplemented with high or low concentrations of IFN-γ (120 or 50 ng/ml) or TNF-α (60 and 40 pg/ml) or both pro-inflammatory cytokines in high or low concentrations, according to values for 3 µM Iloprost or PBS treated activated T cells within bone marrow cultures, which had resulted in relative low or high cytokine secretion levels, respectively (see above Fig. 4.1). (A) Alizarin Red stained monolayers of MSCs to reveal osteogenic differentiation for the respective cytokine types and doses. EM=expansion media, OM=osteoinductive media. (B) OD values of Alizarin Red showed significant reduction in differentiation for high TNF-α concentration and strong reduction for all IFN-γ applications. Small grey asterisk marks extreme outlier. (C) Presto Blue values indicate a significant impact of cytokine combinations onto cell metabolic activity with high IFN-γ concentrations. Cells that

received lower doses of IFN-γ showed significant higher activity. Multiple comparison, n = 6, ***: $p \leq 0.0005$; **: $p \leq 0.005$; *: $p \leq 0.05$. Scale bars equal 200 µm.

4.1.3.3 Apoptotic effect of cytokines in MSCs

To investigate in-depth the impact of the cytokines and Iloprost onto viability, apoptosis levels of MSCs were measured by caspase activity analysis relative to cell numbers (Fig. 4.17). Apoptosis was detectable for all applied cytokine doses (TNF-α: 60 and 40 pg/ml; IFN-γ: 120 and 50 ng/ml) compared to H_2O_2 positive control and was the most active for the highest IFN-γ concentration of 120 ng/ml. Iloprost could diminish this effect slightly and also on the basal levels in EM only. Applied TNF-α induced apoptosis values were not significantly different to positive control with and without addition of Iloprost.

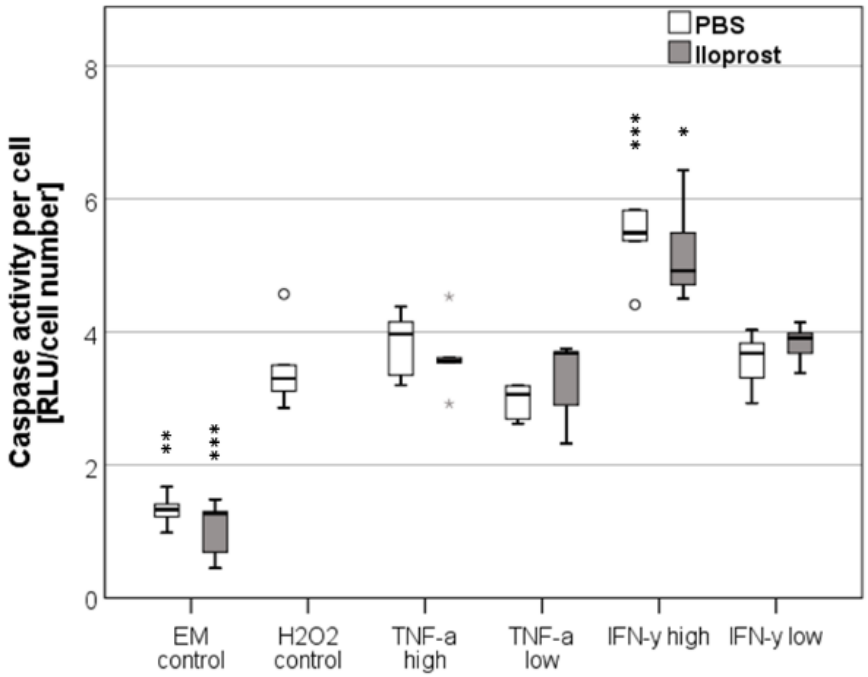

Figure 4.17: High apoptosis induction of IFN- γ reduced by Iloprost in MSCs. Displayed are caspase activities per cells in response to high or low concentrations of TNF-α (60 and 40 pg/ml) or IFN-γ (120 and 50 ng/ml) and 3 µM Iloprost in EM. All cytokine doses induced caspase activity and the high IFN-γ concentration increased the values significantly. Iloprost reduced this effect slightly also in the base line activity with only EM. 100 µM H_2O_2 were supplemented in the positive control for apoptosis induction. Multiple comparison, n = 6, ***: $p \leq 0.0005$; **: $p \leq 0.005$; *: $p \leq 0.05$. Black asterisks indicate significance towards all other sample groups; grey asterisks mark extreme outliers.

4.2. Local drug delivery system

The cell culture data indicate clearly that the anti-inflammatory characteristics of Iloprost could potentially be the most efficient properties of the drug towards an improvement of bone regeneration. Hence, the time window directly succeeding the process-initiating pro-inflammatory phase after about 24 hours appears to be the most promising target for the application of the drug. Crucially, Iloprost entails additionally anti-hypertensive effects when administered intravenously, which is not beneficial in bone healing and could lead to negative side effects in fracture patients with normal blood pressure. Due to this fact, a local drug release was chosen to proof the hypothesis of this thesis. This can be accomplished by either direct injection into the callus or the release of the drug from a carrier material at the fracture site. Latter approach was selected for the proof of concept study, due to its reduced stress for the animals and its superior spatial control directly after inflicting the osteotomy before closing the wound. Local injections into the hematoma through the skin for instance at 24 h post osteotomy would be a risk for the integrity of the hematoma. Furthermore, the local drug delivery of the drug Ilomedine from a carrier material, which is additionally of medial grade, such as the here used fibrin glue, could facilitate the potential translation of this approach into the clinics.

4.2.1 Material characterization of applied fibrin compositions

Considering the biodegradable material, human derived fibrin was selected as a hydrogel-based carrier for the drug delivery, due to three reasons. First, fibrin is a protein that is abundant in the endogenous initial hematoma during fracture healing, and introduction of additional fibrin has the lowest risk of non-beneficial consequences. Second, fibrin is approved for biocompatibility even by the Food and Drug Administration. Third, fibrin is capable of retaining hydrophobic drugs, such as the here investigated drug Iloprost.

The challenge of designing an appropriate drug release system was the desired property of delaying the release of Iloprost to target the peak pro-inflammatory phase and the beginning of the anti-inflammatory phase at approximately 24 hours of bone regeneration. A variety of approaches is discussed in the literature for delaying the release of drugs from a carrier material. These include, e.g. chemical alterations or microspheres. However, these complex approaches are accompanied by the risk of negative side effects or too prolonged retention, respectively. Therefore, a simple approach was investigated here first by designing a core-shell system (Fig. 4.18 A).

By modulating a shell of fibrin around a drug-loaded core of fibrin, the drug is required to diffuse through the empty shell before leaving the carrier. During its path through the hydrophobic material, the hydrophobic drug is impeded by nonpolar interactions. This results theoretically in a delayed release of Iloprost from the core-shell system consisting of fibrin, which was desired. The correct formation of polymerized fibrin during modulation of the core-shell system was further investigated histologically

(Fig. 4.18 C). Eosin staining of cryosections revealed typical pore and fiber formation of fibrin. Interestingly, a dense periphery of fibrin formed between the core and the shell, which was accompanied by areas of either large or rather small pores. Note that, during this hydrophobic staining, ruptures of areas at the core hydrogel occurred.

Furthermore, degradation analysis of the carrier material fibrin was performed in the presence of proteinase K at 37 °C to mimic the enzymatic stress in the early fracture. Therefore, the weights of fibrin in the different compositions of shell, core (high concentrated fibrinogen) and core-shell were measured at several time points until complete degradation (Fig. 4.18 D). All investigated compositions were loaded with 324 ng Iloprost for collection of samples for drug release analysis during weight measurements (see below Fig. 4.20). After 5 days, the shell fibrin started to collapse at 80 % initial weight. However, the core and the core-shell lasted a day longer at 90 % and 75 % of initial weight, respectively. From day 7 to day 9, the core fibrin with highest protein density kept significantly higher weight than shell and core-shell compositions.

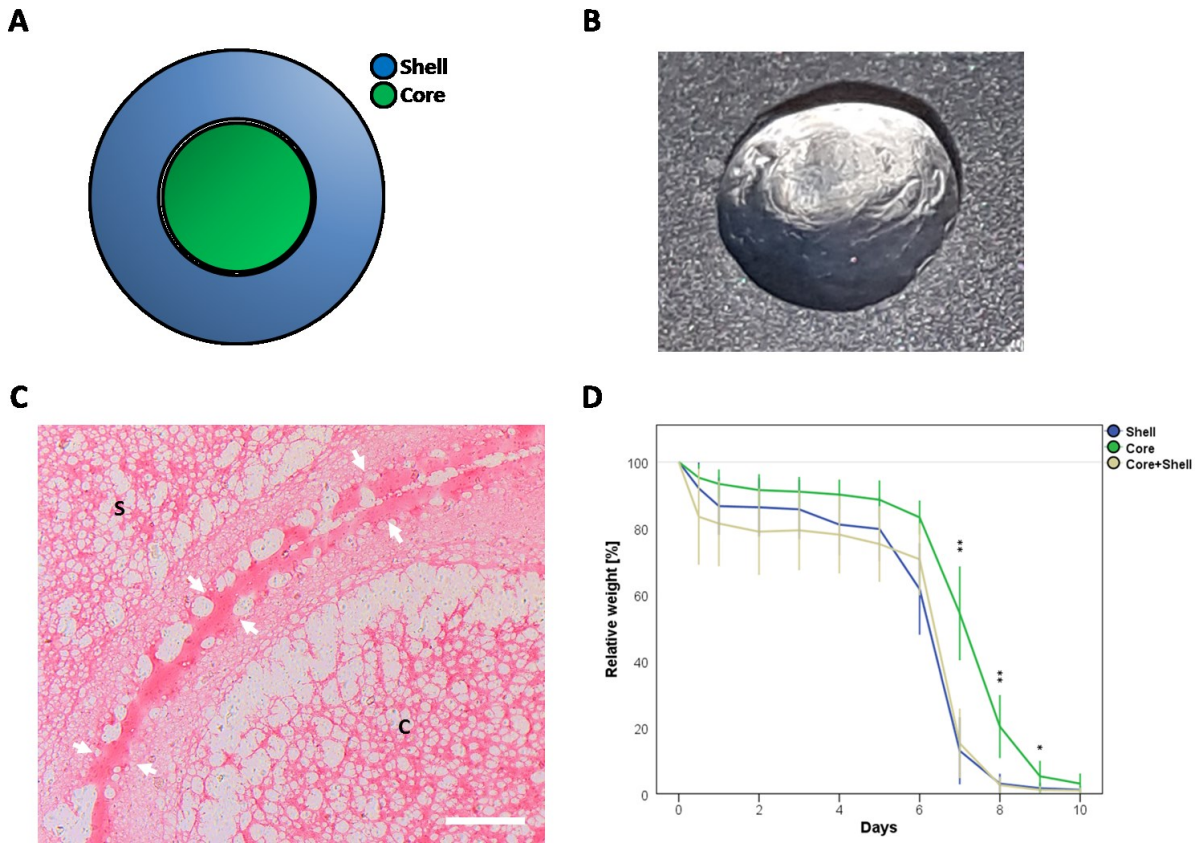

Figure 4.18: Characteristics of the core-shell system modulated with fibrin. (A) Two-dimensional schematics of the core-shell composition. Core (green), which consists of high-density fibrin, is surrounded by shell fibrin with standard density. (B) Image of the release system composition during the final polymerization phase at which the shell is still transparent and therefore the core hydrogel visible. The composition is lying in a petri dish, which is placed on a heating plate at 37 °C. Image made by a standard digital camera. Width of the displayed fibrin composition is approximately 4.5 mm and this is the dimension, which was applied in the *in vivo* experiments. (C)

Histology of the core-shell system with eosin staining of a 7 µm cryo-section. Core (c), shell (s), white arrows mark periphery, scale bar equals 100 µm. (D) Degradation analysis of the carrier material fibrin in the different compositions of shell, core (high concentrated fibrinogen) and core-shell. Displayed are weights relative to the starting weight of the *in vitro* release experiment. The shell fibrin started to collapse at day 5, whereas the core and the core-shell followed in bulge degradation at day 6. The core material with highest protein density degraded significantly slower than shell and core-shell from day 7 to 9. Multiple comparison for each time point, n = 4, **: $p \leq 0.005$; *: $p \leq 0.05$.

The drug Ilomedine consists of the biologically active molecule Iloprost and its excipient solution of water, NaCl, HCl, Tris buffer and ethanol. These substances could potentially alter the molecular composition of the biomaterial fibrin of the release system during or after the polymerization. Hence, compression testing of freshly polymerized fibrin was carried out. Therefore, precursor fibrinogen was supplemented with either PBS or Ilomedine. The drug had no significant impact onto material stiffness (Fig. 4.19). Only a tendency of higher median stiffness values was found for fibrin prepared with Iloprost-supplemented fibrinogen in comparison to PBS control of 203 kPa and 155 kPa, respectively.

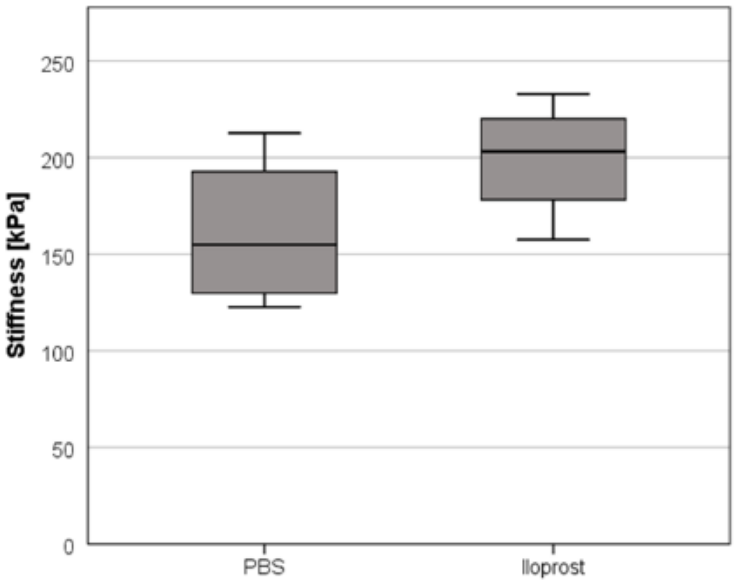

Figure 4.19: Compression testing of fibrin supplemented with PBS and with Ilomedine. The drug had no significant impact onto material stiffness measured. Pairwise comparison, n=4.

4.2.2 Release kinetics of Iloprost from core-shell system

To proof the delayed Iloprost release by the core-shell system *in vitro*, an HPLC/UV-based quantification method for detection of the low molecular weight compound Iloprost was carried out similarly as to previously described (Scypinski *et al.* 1990). In this method, the released drug is separated from degraded fibrin via liquid-liquid extraction based on relative solubility to chloroform. Subsequently, the chloroform is evaporated and the samples are resolved in mobile phase solution of

the HPLC setting. The drug is then purified even down to the diastereoisomers level by its interaction with a reversed-phase matrix in the separation column of the HPLC apparatus. Hence, based on their hydrophobic properties, compounds are eluted after another with reproducible retention times and quantified by transmission measurement via an UV-detector.

The figure below depicts the chromatogram of Iloprost with its characteristic double-peak detected at the retention times of 6.18 and 6.70 min (Fig. 4.20 A). The area under this double-peak was related to Iloprost concentrations of a standard solution with pure Iloprost. The internal standard 2-Naphtoic acid (2-NA), which was added to each harvested sample during release, was detected at a retention time of 3.58 min (Fig. 4.20 A). The measured concentration of 2-NA was stable for each fibrin composition and time point (see Appendix Fig. 8.7 B).

Resulting kinetics showed that the core fibrin alone released 87 % (282 of 324 ng/ml) of the drug into the media after 24 hours (Fig. 4.20 B). On the contrary, a burst like release of already 99 % (320 of 324 ng/ml) Iloprost was detected within 24 hours when released from only the low-density shell fibrin material. Strikingly, the modification of the system with a shell of empty fibrin could delay the release of Iloprost significantly from the start up to day 3. After 24 h, only ~62 % (202 of 324 ng/ml) of Iloprost had been released into the media by the core-shell system. Crucially, 88 % (284 of 324 ng/ml) release was reached after an additional day had passed. Taken together, the core-shell system could delay the drug for approximately 24 h compared to core fibrin alone. All fibrin compositions had fully released their loaded Iloprost molecules at day 4, which is before collapse initiation of the fibrin clots at day 5 and 6 (see above Fig. 4.18). Note that the initial retention at the washing step at 0 days of Iloprost with the core-shell system was also improved. Only 78 ng/ml were retrieved in the media, which is substantial less than the 177 and 144 ng/ml of shell and core alone, respectively.

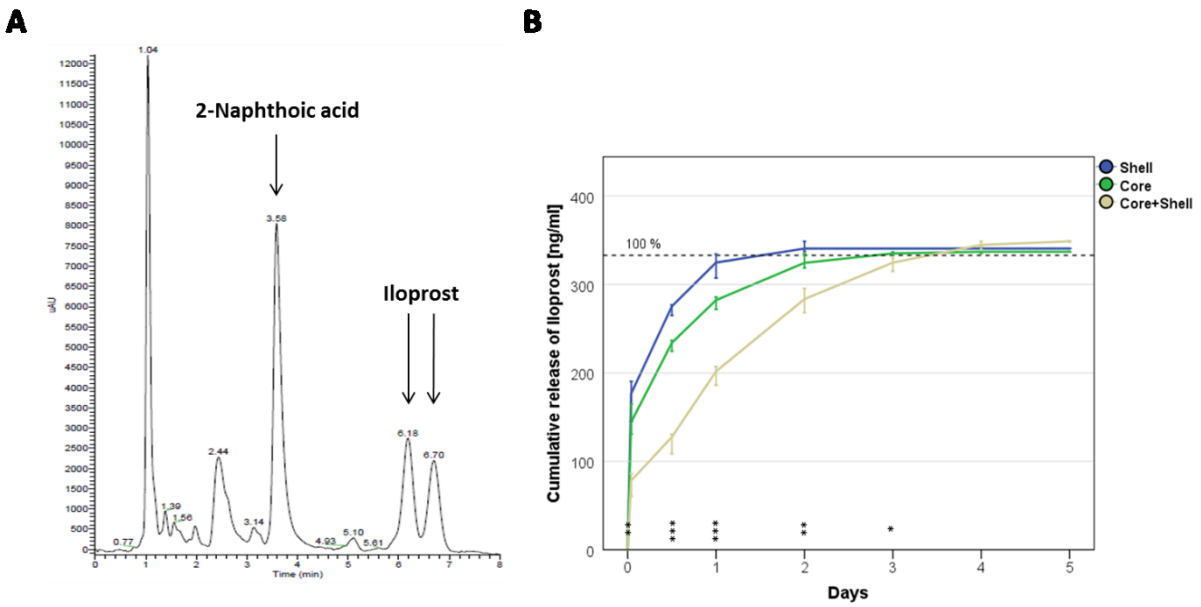

Figure 4.20: Delayed release of Iloprost with a core-shell system consisting of fibrin. (A) Representative chromatogram of Iloprost measured by HPLC-UV with micro absorbance unit (µAU) of the UV detector at 207 nm. The double-peak of Iloprost was detected at the retention times of 6.18 and 6.70 min. Area under the double-peak quantified Iloprost concentrations according to standard substance. The internal standard of 2-Naphtoic acid (2-NA) had a retention time of 3.58 min. Other peaks in the chromatogram derived from the injection process and less hydrophobic molecules contained in the extracts. (B) Cumulative release of Iloprost from shell, core and core/shell system. The core-shell system could significantly decelerate the release of the drug into the media. Dotted line: indicates theoretical value of 100 % recovery of Iloprost (324 ng/100 µl) for the *in vitro* experiment. Multiple comparison for each time point, n=4, ***: $p \leq 0.0005$; **: $p \leq 0.005$; *: $p \leq 0.05$.

4.3 *In vivo* studies

4.3.1 Application of the drug release system in an osteotomy model

The *in vitro* data confirmed the anti-inflammatory phase of the bone regeneration cascade as optimal target for the application of Iloprost with its immune suppressive functions to potentially supporting the healing process. For this purpose, the biodegradable drug release system with a core-shell approach was designed to decelerate the full release of Iloprost to allow the first pro-inflammatory phase to initiate the healing process. To proof the hypothesis of improving bone regeneration with the suppression of the late pro-inflammatory phase a mouse osteotomy model was chosen. Osteotomy models utilize external fixateurs or directly laterally attached plates and benefit from low variations compared to three point bending fracture models, which are merely stabilized with an internal lateral nail. Furthermore, the smaller callus area of this rigidly fixed osteotomy accelerated complete analysis of this region with for instance immunohistological methods, compared to internal nail fixation. Figure 4.21 exhibits a specimen of a mouse osteotomy (indicated by white arrow) of the left femur bone, which is fixed with four connected pins of the utilized externally fixator (Fig. 4.21 A). The osteotomy gap had a size of 0.7 mm and the core-shell release system loaded with 3.24 ng Iloprost (3 µM in core gel volume) or PBS as

control could be placed into this space and was subsequently glued to the bone tissue with extra shell fibrin (Fig. 4.21 B).

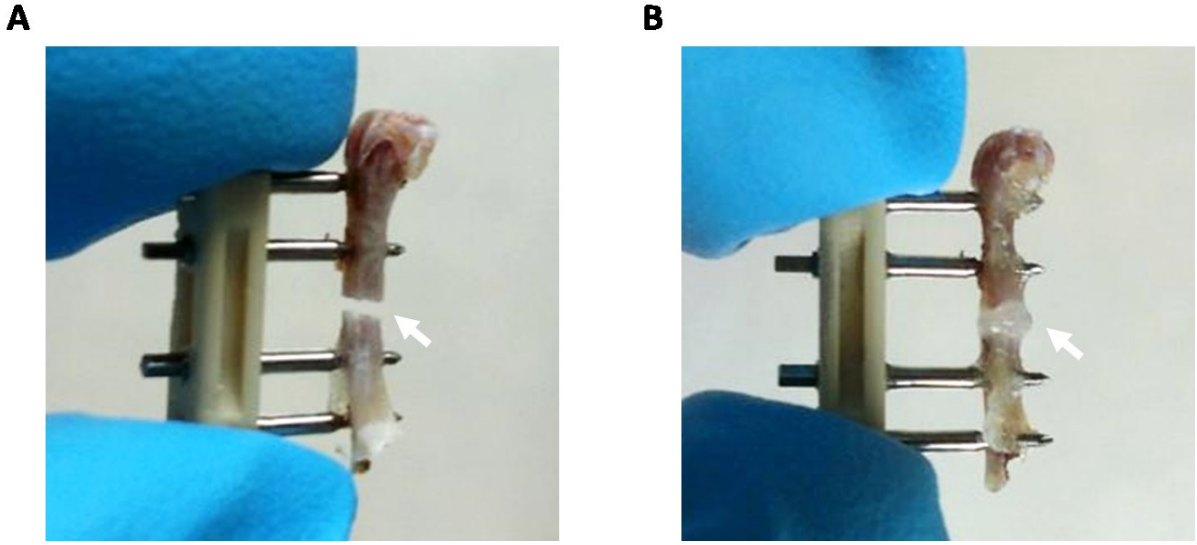

Figure 4.21: Application of the drug release system into the gap of an osteotomy model. (A) Depicted is a specimen of a mouse femur bone, which was fixed with four connected pins of an external fixator bar. This allowed the introduction of a fracture gap in the middle of the bone indicated by white arrow. (B) Into this gap, the release system was placed (white arrow) and further glued to the bone tissue by additional shell fibrin.

4.3.1.1 Investigation of endochondral healing phases

After 21 days post osteotomy (dpo), the regenerating femurs were harvested and processed for µCT analysis of newly formed mineralized bone tissue. Afterwards, these fracture samples were cryo-stored for further histological analysis. Additionally, bone marrow from uninjured bones of regenerating animals was analyzed by flow cytometry to account for potential systemic effects onto T cell subpopulations by the local drug delivery (see below 4.3.2).

Indeed, Iloprost application showed advanced bone formation after 21 days of regeneration in comparison to the PBS-loaded control (Fig. 4.22 A). Mineralized bone was bridging the osteotomy gap in the Iloprost groups in contrast to the control. Quantification revealed that the Iloprost group had reached significantly more median bone volume (BV) of 1.24 mm^3 compared to only 0.46 mm^3 in the control group (Fig. 4.22 B). Furthermore, a median total volume of 1.01 mm^3 of the callus (TV) was measured in the control group and double the volume of 2.01 mm^3 was found after Iloprost treatment. This resulted in a significant larger ratio of BT/TV of 0.62 compared to 0.46 after the local application of Iloprost compared to control.

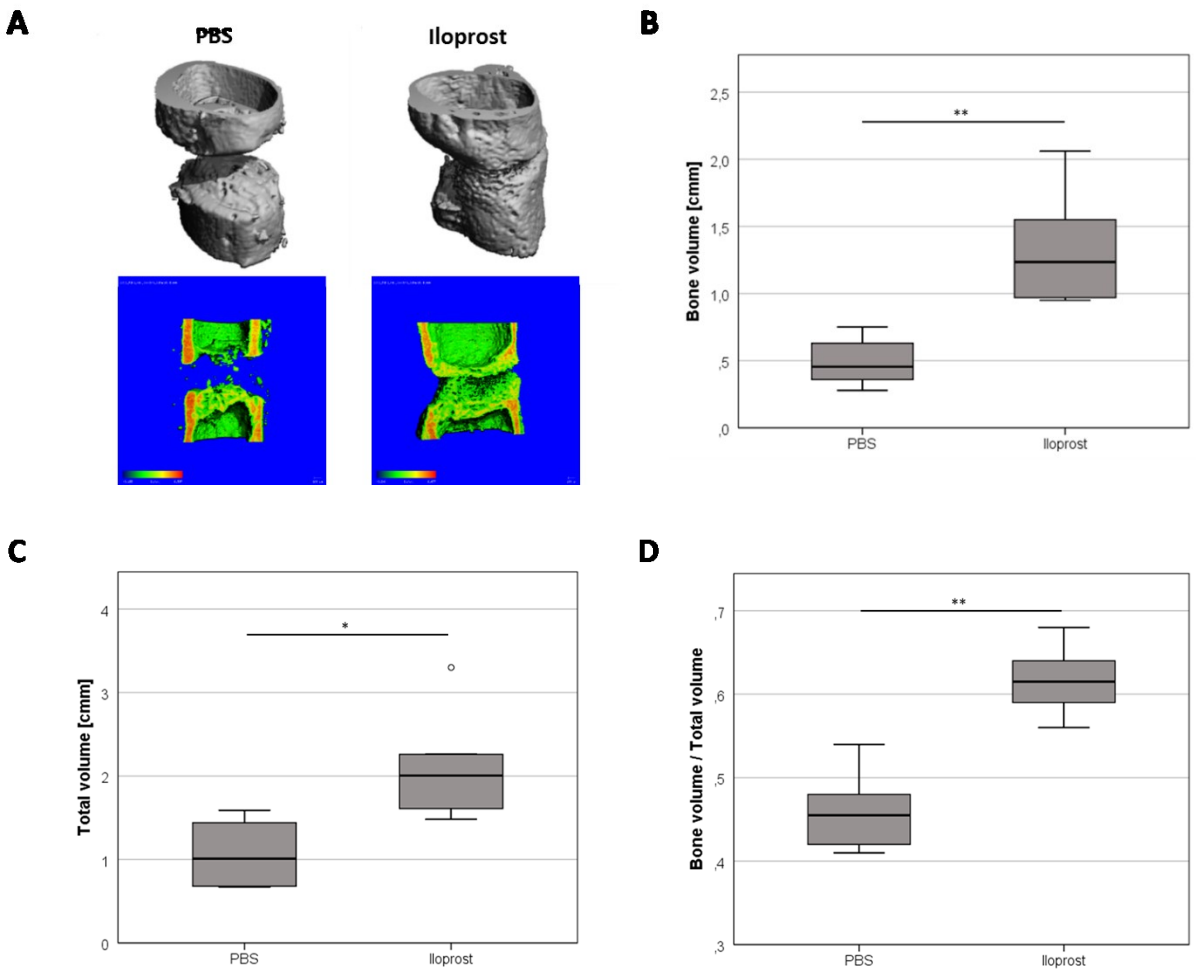

Figure 4.22: Proof of concept with *in vivo* experiments in mouse osteotomies. Core-shell system was loaded with either PBS or 3.24 ng Iloprost and was placed into the 0.7 mm gap of the left femur bone. After 21 days, volumes of regrowing calcified bone tissue was measured with µCT ex vivo. (A) Three-dimensional image reconstruction of the regenerating bone with longitudinal split image with false colors indicating mineral density from low density in green to high density in red. Iloprost application lead to significantly increased formation of new (B) Bone volume and (C) Total volume of calcified area and their relation (D) Bone volume / Total volume. Cmm: cubic millimeters. Pairwise comparison, n = 6, **: $p \leq 0.005$; *: $p \leq 0.05$.

To understand the causes of these effects in more detail an additional earlier time point of three days after osteotomy was examined. This allowed to further investigating histologically the immediate crucial impact of the drug and the carrier onto the regenerating tissues and key player cells during early inflammation. The examination of tissues participating in the healing process was carried out with Movat's pentachrome staining, which utilizes five different staining dyes. Figure 4.23 A' shows an overview image of the left femur of a mouse with osteotomy in the center. There, the region of interest (ROI) for histomorphometry is indicated with a black rectangle. This staining disclosed that the fibrin-based carrier was degraded after 21 days of regeneration, but showed no sign of degradation at 3 days yet (Fig. 4.23 A). At the early time point of 3 dpo, no significant differences between treatment and control group were detected by histomorphometry (Fig. 4.23 B-E).

Furthermore, after 21 days the fractures in the mouse model that received the drug were already in the transition phase from the cartilage phase towards the calcification phase of the callus. In contrast, the fractures without drug had not reached the endochondral phases at that time point. In particular, these control fractures showed partial ingrowth of connective tissue. Histomorphometry confirmed these findings statistically after 21 days of regeneration. In comparison to the control, the Iloprost treated group showed significantly larger areas of mineralized bone after 21 days of regeneration (Fig. 4.23 B). In median, 10.0 % of the callus area were mineralized in the Iloprost group after 21 days and only 2.3 % in the control group. This is also the case for the relative area occupied by newly formed cartilage in the soft callus phase (Fig. 4.23 C). In particular, the control group displayed mere 0.68 % median relative cartilage area whereas Iloprost application had led to corresponding 3.35 %. However, the Iloprost treated groups showed strong variations at 21 days of regeneration. The size of areas that were positively stained in the Iloprost groups for mineralized bone and cartilage was ranging from 4.68 % to 14.39 % and from 1.18 % to 8.99 %, respectively. The PBS treated groups showed a tendency of larger relative areas of connective tissue and lower areas filled with bone marrow compared to the Iloprost group at 21 dpo (Fig. 4.23 D, E).

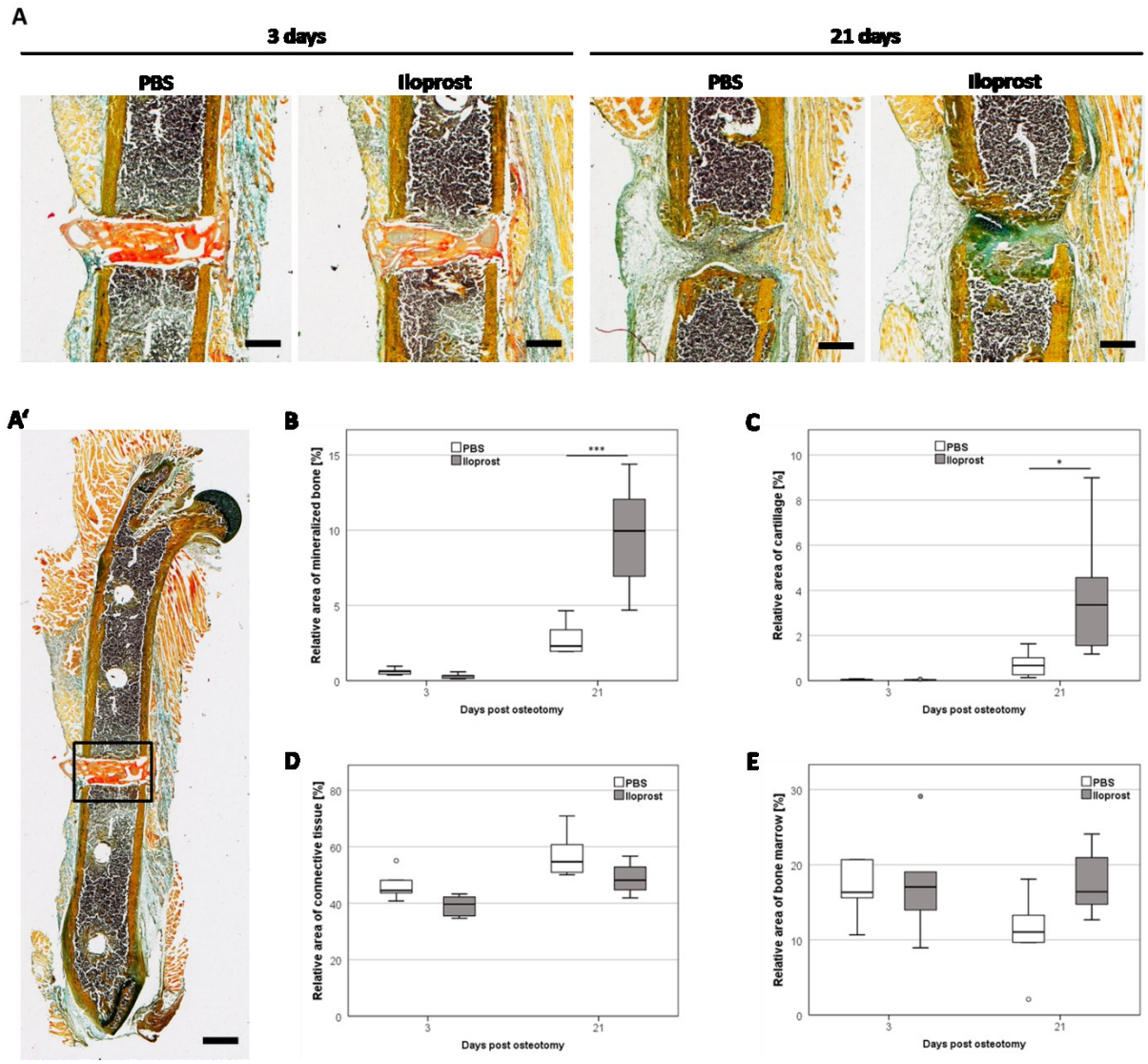

Figure 4.23: Histological analysis of *in vivo* experiments in mouse osteotomies at days 3 and 21 shows advanced endochondral healing progression with 3.24 ng Iloprost treatment compared to control. (A) Movat's pentachrome staining on 7 µm cryo-sections revealed the fibrin-based release system intact in the bone gap at 3 days post osteotomy (dpo). After 21 days, the Iloprost loaded release system resulted in advanced healing progression indicated by hypertrophic cartilage and mineralization in contrast to connective tissue of the soft callus and early mineralization at the periphery of bone marrow and callus. Fibrin is red/orange; muscle fibers: light orange; mineralized bone collagen: yellow; nuclei: dark purple; cartilage: dark blue-green; connective tissue: light blue-green. (A') Representative overview of a left mouse femur with osteotomy in the center with Movat's Pentachrome stain. Black rectangle: region of interest (ROI) for histomorphometry. Note the four boreholes of the removed pins of the fixator. Histomorphometry confirms for Iloprost treated groups significantly higher detection of (B) mineralized bone and (C) cartilage after 21 days of regeneration. (D) Connective tissue area and (E) bone marrow size were not affected significantly by Iloprost application. Multiple comparison, n = 6, ***: $p \leq 0.0005$; *: $p \leq 0.05$. Scale bars: (A) equal 500 µm. (A') equals 1 mm.

4.3.1.2 Analysis of the inflammatory phase

Considering the *in vitro* release kinetics of Iloprost from the core-shell system at which after 3 days the drug had left the carrier material almost completely, an impact of anti-inflammatory nature should be

detectable in proximity of the fracture gap. Furthermore, this is also the time point at which the anti-inflammatory phase is taking place in this osteotomy model as we had described previously for occurrences of immune cell markers via fluorescence immunohistochemistry (Schlundt *et al.* 2015). The here conducted approach was to quantify the presence of distinct cell markers in the bone marrow area, which was supposed to be mainly affected by the released drug. In this way, an assessment of the immune modulation *in vivo* was attempted. Analyzed were immune cells, such as CD8+, CD4+ and polarized macrophages. Furthermore, the cytokines IFN-γ and TNF-α were co-localized to identify and quantify active immune cells. To investigate any early endochondral activities, OCN+ osteoblast were counted in the ROI as well as cathepsin K (CTSK) positive macrophages, which can remodel extra cellular matrices. Therefore, cells in acquired images were identified with computational image analysis and respective mean pixel intensities of every fluorescence channel for each singular cell were assessed (comparable to FACS analysis). Hence, cells could be counted for expression of investigated markers, the possession of a nucleus and even for double-staining of distinct markers. Finally, cell numbers were normalized to numbers of all detected nuclei in the region of interest.

Results of the analysis of CD8+, CD4+ and OCN+ cells at 3 days post osteotomy at the fracture gap is shown in figure 4.24. Figure 4.24 A'' represents a left mouse femur bone with osteotomy, harboring the fibrin-based release system, revealed by Movat's Pentachrome staining. There, the region of interest (ROI) for cell counting is highlighted by a black rectangle. The detected CD8+ and CD4+ cells appear to be evenly distributed in the observed region of the bone marrow (Fig. 4.24 A). Note that the release system in the fracture gap, which was visible in staining with transmission light before (Fig. 4.24 A''), is not visible in the detected fluorescence range. The OCN+ cells are rather condensed along the cortices and in proximity to the fracture gap. Furthermore, OCN+ cells are less dense distributed over the rest of the bone marrow with more abundant occurrence in the distal site.

The numbers of CD8+ cell populations were strongly reduced with Iloprost from 4.18% down to 2.30 % (Fig. 4.24 B). Additionally, the CD4+ fraction was reduced significantly as well. Only 1.78 % CD4+ cells were counted in the Iloprost treated group in contrast to 2.56 % for the control group. Regarding the CD8+ to CD4+ ratios of these T cell fractions, the vehicle control group showed 1.6:1 and the drug treatment group 1.3:1. Furthermore, an insignificant fraction of CD8+CD4+ cells was detected in every sample. OCN+ relative cell numbers showed no significant change with Iloprost.

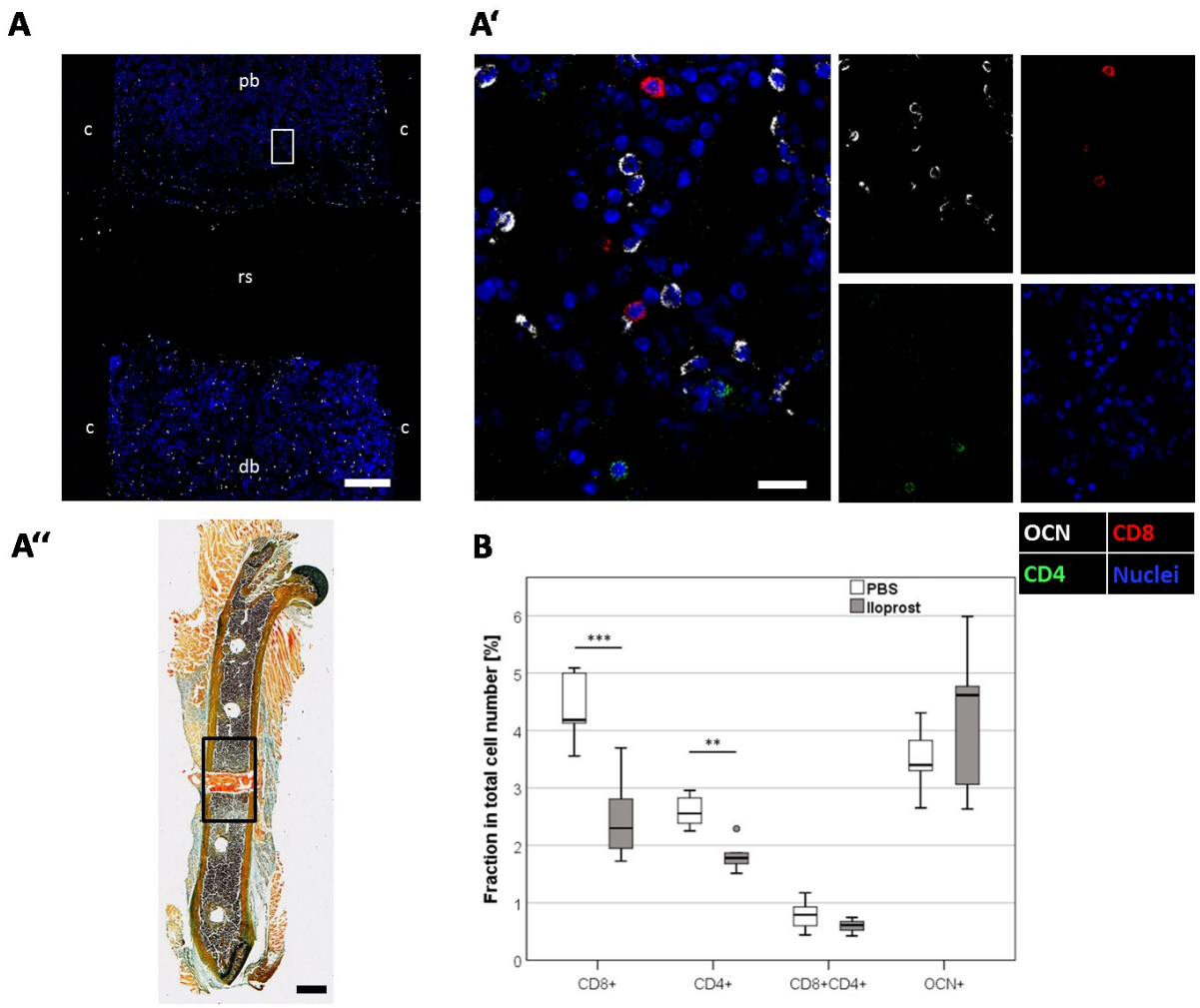

Figure 4.24: Immunosuppression of CD8+ and CD4+ cells at 3 dpo at the fracture gap, which is filled by the drug release system. (A) Mosaic immunohistochemical image with indicated cortices (c), proximal bone marrow (pb), distal bone marrow (db), and release system (rs). White square indicates crop-out area for A'. (A') Representative area close to the release system containing CD8+ (red), CD4+ (green) and OCN+ cells (white) additionally with individual fluorescence channels. (A'') Representative overview of a left femur with central osteotomy with Movat's Pentachrome stain. The proximal site is clearly identifiable by the femoral head of the hip joint. Black rectangle depicts the ROI for the cell counting. Note the four boreholes of the removed pins for fixation. (B) Quantification of detected cell types relative to number of nuclei. The values for CD8+ and CD4+ cell reduction with 3.24 ng Iloprost are significant and a small fraction of CD8+CD4+ cells was detected in every sample. OCN+ cell numbers showed no significant change in numbers with Iloprost. Pairwise comparison, n = 6, ***: $p \leq 0.0005$; **: $p \leq 0.005$. Scale bars: A equals 200 µm. A' equals 20 µm. A'' equals 1 mm.

A strong reduction in cell numbers of pro-inflammatory activated CD8+ in response to Iloprost treatment was also seen before *in vitro* (see above Fig. 4.4). Furthermore, a significant decrease in IFN-γ+ cells with Iloprost was detected here in the mouse fracture model, which is also in line with the strong reduction of the secreted IFN-γ from activated T cells and CD8+ cells in particular *in vitro* (see above Fig. 4.1, 4.3). In addition, isolated activated CD8+ cells that were incubated with Iloprost showed a tendency-wise reduced expression of CD25, which is a marker for T cell activity (see above Fig. 4.2). Here, immunohistochemistry of IFN-γ, CD8 and OCN at the fracture sites at day 3 revealed an even

distribution of cells positive for the cytokine (Fig. 4.25). This is similar to the CD8+ and CD4+ pattern observed above (Fig. 4.24).

Quantification confirmed the strong reduction in CD8+ cells at the fracture after 3 days of regeneration (Fig. 4.25 B). Additionally, IFN-γ+ cells were suppressed as well by Iloprost (5.86 %) in comparison to control (8.47 %). Furthermore, CD8+IFN-γ+ double positive cells indicate highly active pro-inflammatory CD8+ cells (yellow arrows Fig. 4.25 A'). These highly active CD8+ cells responded again to Iloprost with a significant reduction in numbers from 2.91 % down to 1.19 %. OCN+ cell numbers showed again no significant response to Iloprost release.

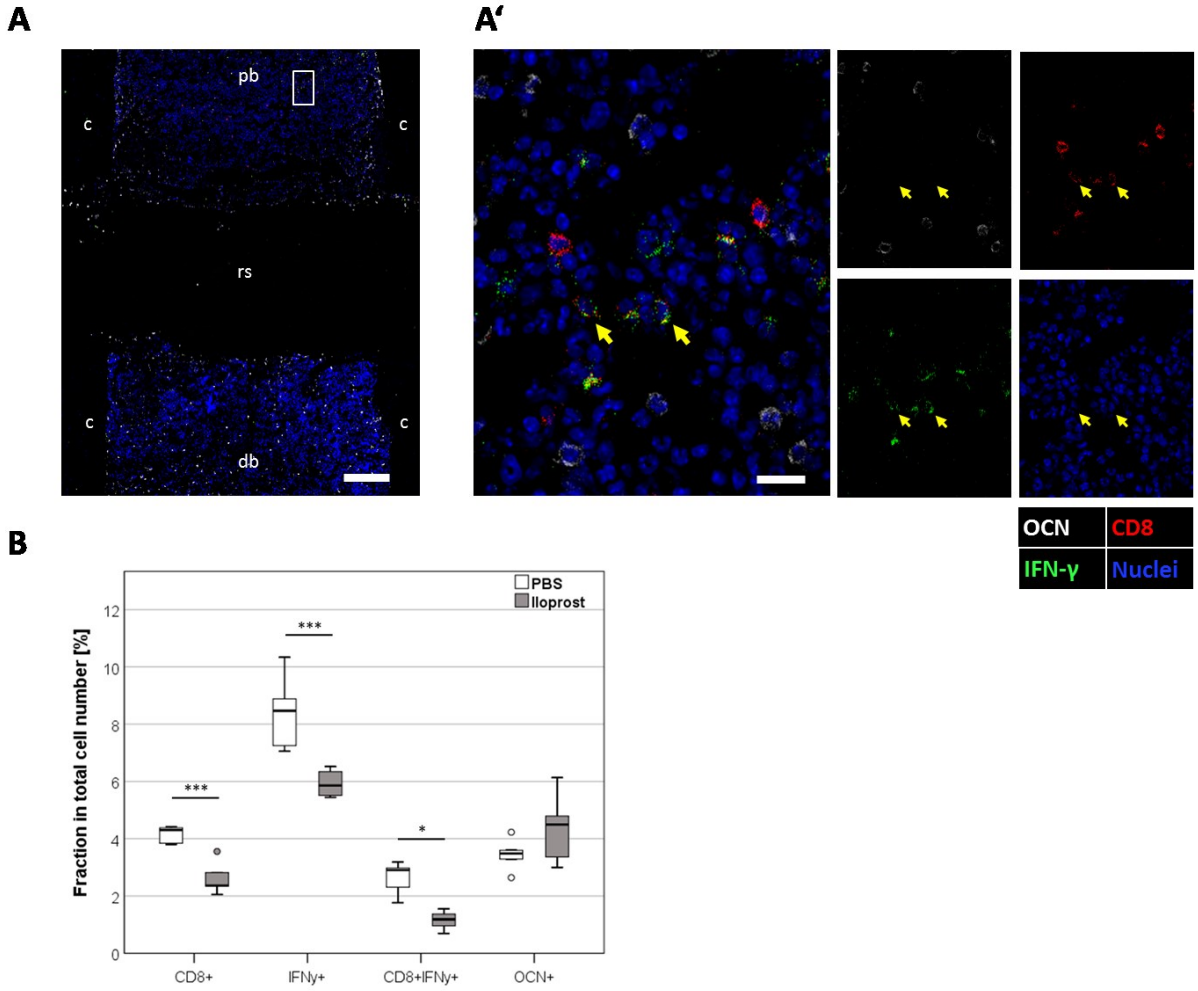

Figure 4.25: Immunosuppression of CD8+ and IFN-γ+ cells at 3 dpo at the drug release system in the fracture gap. (A) Mosaic immunohistochemical image with marked cortices (c), proximal bone marrow (pb), distal bone marrow (db), and release system (rs). White square indicates crop-out area for A'. (A') Representative area close to the release system containing CD8+ (red), IFN-γ+ (green) and OCN+ cells (white) with individual fluorescence channels. CD8+IFN-γ+ double positive cells (yellow arrows) indicate highly active pro-inflammatory CD8+ cells. (B) Quantification of detected cell types relative to number of nuclei revealed significantly less CD8+ and IFN-γ+ cells with 3.24 ng Iloprost application. Values for CD8+IFN-γ+ cells in response to Iloprost are lowered. Pairwise comparison, n = 6, ***: $p \leq 0.0005$. Scale bars: A equals 200 µm. A' equals 20 µm.

Macrophage polarization was analyzed as well at the early fracture gap by the markers CD80, CD206 and CD68 (Fig. 4.26 A). CD68+ cells were present in the entire bone marrow, however, occurred condensed at the proximal site of the fracture. The markers CD80 and CD206 were rather evenly distributed in the bone marrow on either site of the fracture gap. Figure 4.26 A' depicts a representative area close to the release system containing CD80+, CD206+ and CD68+ cells. In particular, white arrows indicate CD80+CD68+ double positive M1-type macrophages and CD206+CD68+ M2-type macrophages are pointed out by yellow arrows. Interestingly, CD68+ cell numbers were less prominent in the fractures that received an Iloprost-loaded release system (Fig. 4.26 B). Only a median fraction of 19 % was detected in comparison to control with 24 %. Furthermore, within the CD68+ fraction, Iloprost treatment reduced significantly M1 macrophages from 14 % down to 10 %. On the contrary, the presence of M2 macrophages was significantly elevated with Iloprost from 6 % up to 10 %.

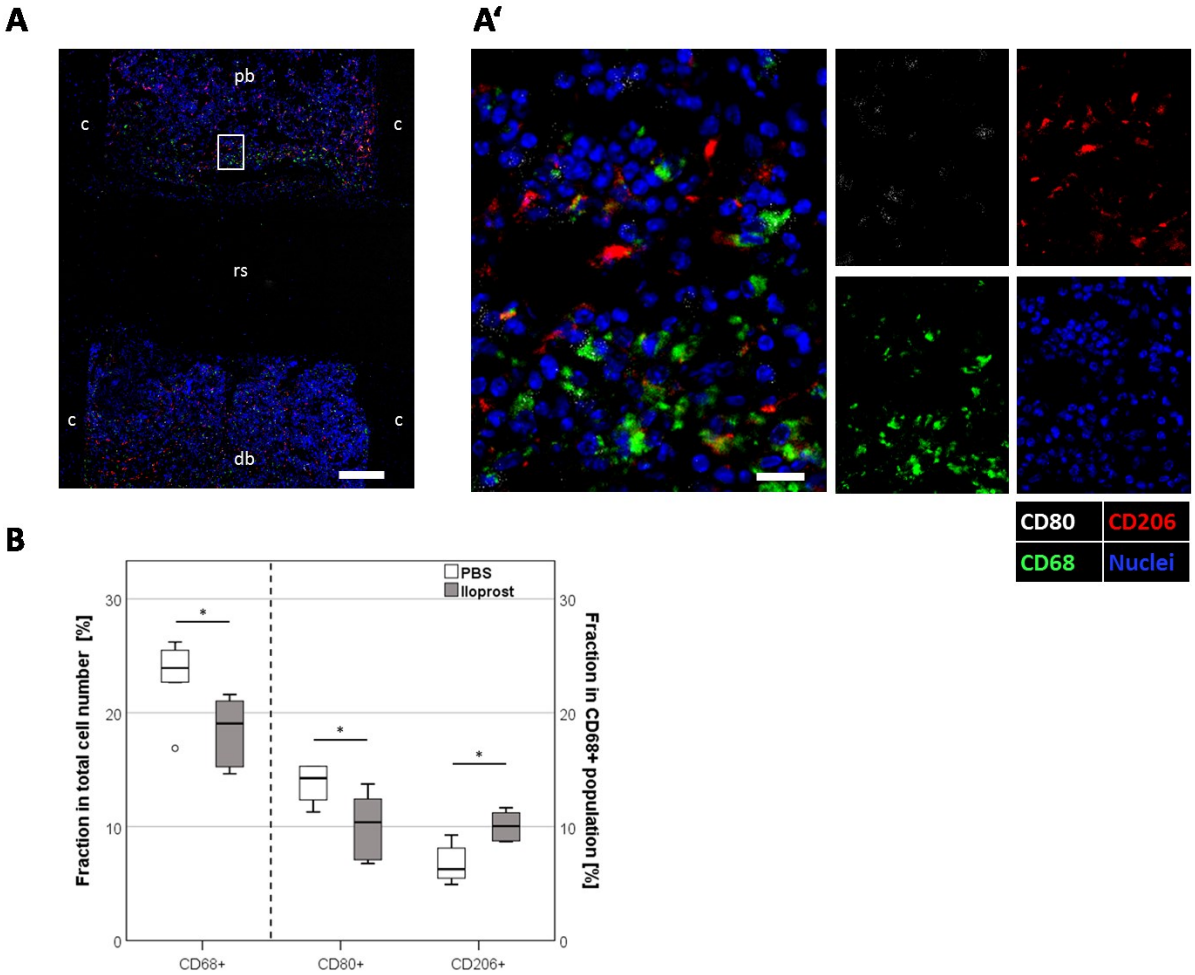

Figure 4.26: Anti-inflammatory macrophage polarization revealed by detection and quantification of CD80+, CD206+ and CD68+ cells at the fracture gap at 3 dpo. (A) Mosaic immunohistochemical image with labeled cortices (c), proximal bone marrow (pb), distal bone marrow (db), and release system (rs). White square indicates crop-out area for A'. (A') Representative area close to the release system containing CD80+ (white), CD206+ (red) and CD68+ cells (green) with individual fluorescence channels. Double positive cells identify polarization of

macrophages, i.e. CD80+CD68+ for M1-type (white arrows) and CD206+CD68+ for M2-type (yellow arrows). (B) Cell numbers revealed significant impact of 3.24 ng Iloprost treatment on macrophage numbers and polarization, i.e. reduced overall CD68+ counts, inhibition of M1 macrophages and higher numbers of M2 macrophages. Pairwise comparison, n = 6, *: $p \leq 0.05$. Scale bars: A equals 200 µm. A' equals 20 µm.

Furthermore, the impact of delayed Iloprost application onto the factors TNF-α and cathepsin K (CTSK) was analyzed, which can be secreted by CD68+ cells during fracture healing. CD68 is a marker for not only macrophages but also multinuclear osteoclasts. However, latter cell type is not dominantly present at this early phase. On the contrary, pro-inflammatory M1 macrophages are indeed active in high numbers at this stage and secrete TNF-α. This cytokine in turn is involved in mediating osteoclastogenesis (Ritchlin *et al.* 2003). Another investigated factor is the enzyme CTSK, which purpose is remodeling and resorption of bone matrix and is secreted by osteoclasts and M2 macrophages. Immunohistochemistry disclosed CTSK expression condensed at the fracture sites and the cortices, in particular, with more abundance in general in the proximal bone marrow (pb) region (Fig. 4.27 A). TNF-α appeared to be rather evenly distributed in both parts of the bone marrow at the fracture site. Figure 4.27 A' shows a representative area in proximity to the release system with CTSK+ (white), TNF-α (red) and CD68+ cells. Furthermore, white arrows indicate CD68+CTSK+ double positive mononuclear cells and CD68+TNF-α+ macrophages are pointed out by yellow arrows. CD68+ cell quantification confirmed again their reduction in response to Iloprost (Fig. 4.27 B). Furthermore, the drug treatment group had significantly reduced CD68+TNF-α+ M1 macrophages from 12.6 % down to 8.9 %. On the contrary, numbers for CD68+CTSK+ double positive M2 macrophages show a trend to be higher in response to Iloprost from 10.0 % up to 14.5 %.

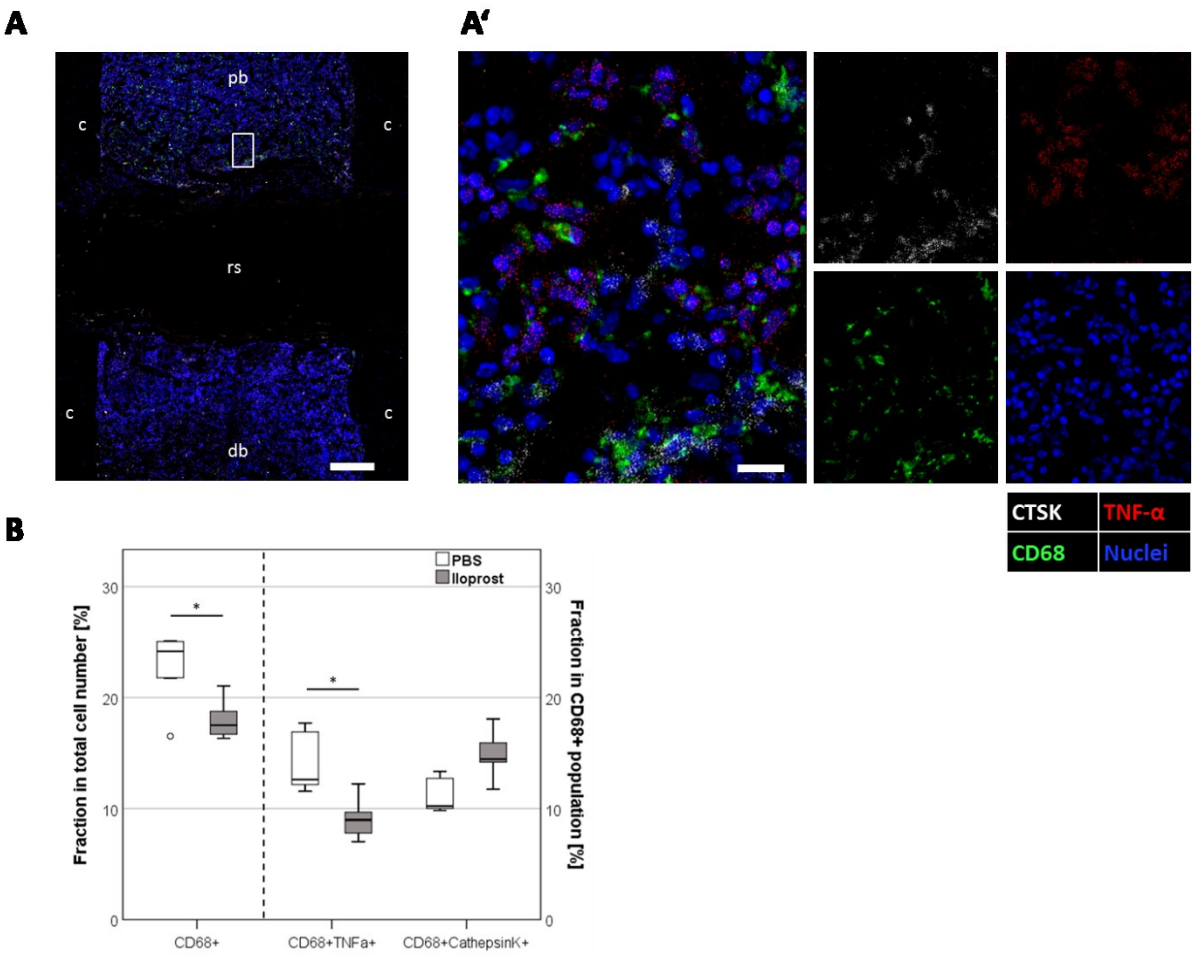

Figure 4.27: Impact onto secreted factors of CD68+ cells by delayed Iloprost application at 3 dpo. CD68+ cells were quantified for double staining with pro-inflammatory cytokine TNF-α or remodeling enzyme CTSK in proximity to the fracture gap at 3 days post osteotomy. (A) Mosaic immunohistochemical image with indicated cortices (c), proximal bone marrow (pb), distal bone marrow (db), and release system (rs). White square indicates representative enlargement shown in A'. (A') Area close to the release system containing CTSK+ (white), TNF-α (red) and CD68+ cells (green) and individual fluorescence channels. Double positive cells indicate CD68+TNF-α+ (yellow arrows) and mononuclear CD68+CTSK+ (white arrows) cells, i.e. pro-inflammatory M1 macrophages and remodulatory M2 macrophages. (B) Quantification showed significant reduction in CD68+ and CD68+TNF-α+ cells. CD68+CTSK+ cells tended to be more abundant in 3.24 ng Iloprost treated fractures. Pairwise comparison, n = 6, *: $p \leq 0.05$. Scale bars: A equals 200 µm. A' equals 20 µm.

4.3.1.3 Quantification of blood vessel formation

Trauma regeneration of any kind is always dependent on the reconstruction of the blood supply. Hence, angiogenesis and vascularization are highly important in fracture healing. PGI_2 is involved in these processes as well, and an addition of synthetic PGI_2 potentially exerts beneficial effects on blood vessel growth in fracture healing. Hence, regrowth of blood vessels was investigated here at 3 days of regeneration with marker expression of laminin. This marker of angiogenesis and vascularization is for instance used in tumor diagnostics (Holler 2005). The staining revealed a stronger expression at the proximal site of the osteotomy (Fig. 4.28 A). Quantification of relative occupied area by laminin

revealed only a tendency of up-regulation with medians of 14.7 % for the Iloprost treated group and 9.1 % for the control group (Fig. 4.28 B).

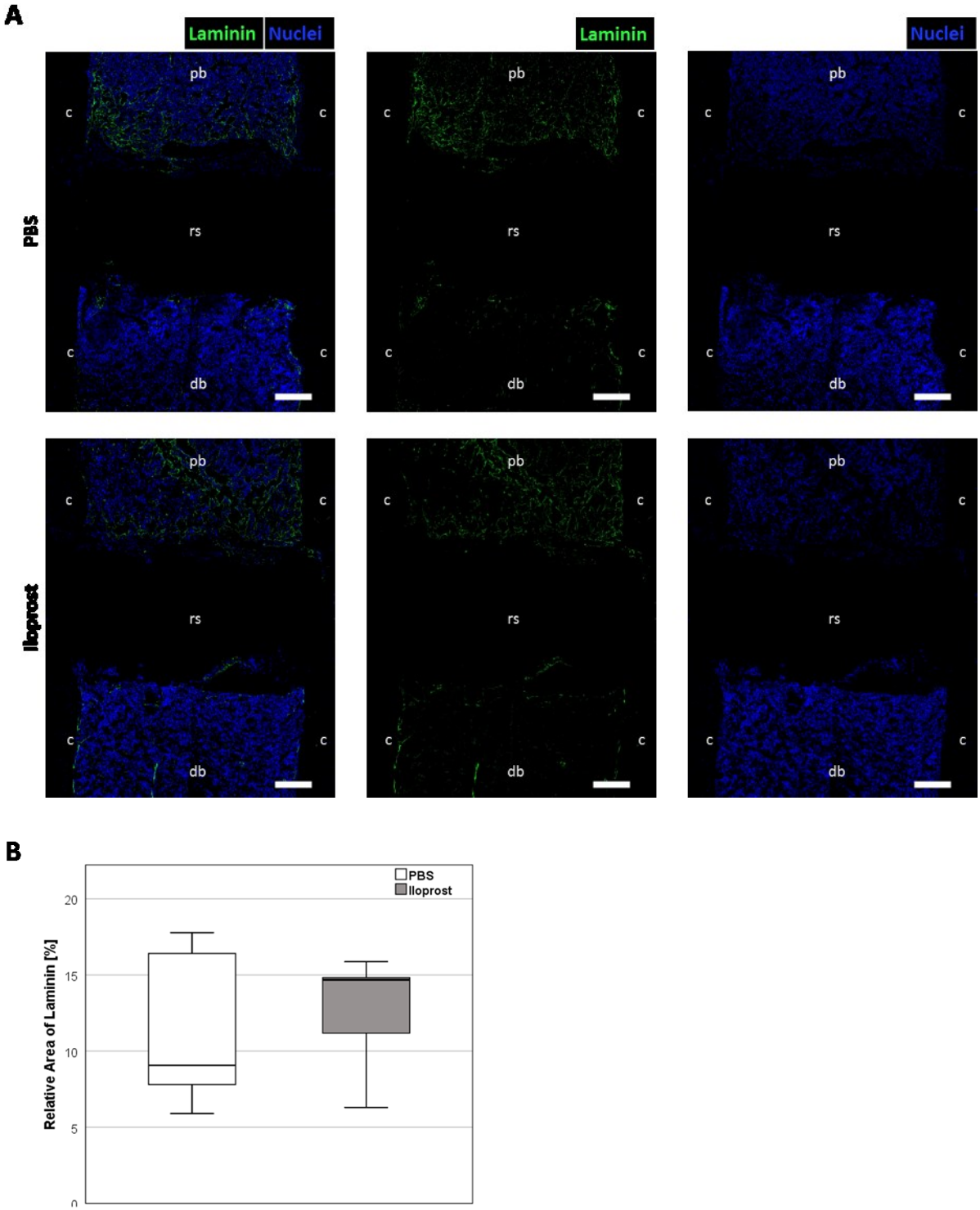

Figure 4.28: Immunohistochemical analysis of blood vessel presence at 3 dpo. (A) Representative mosaic images of laminin stained vasculature at fracture sites for PBS and 3.24 ng Iloprost treated groups. Indicated are cortices (c), proximal bone marrow (pb), distal bone marrow (db), and release system (rs). In both groups, laminin (green)

was more abundant at the proximal site of the osteotomy. (B) Quantification of laminin occupied area relative to area occupied by nuclei with tendency-wise up-regulation. Pairwise comparison, n = 6. Scale bars equal 200 µm.

4.3.2 Control of systemic effects of local drug release

Iloprost was released locally from a biodegradable delivery system in the osteotomy model. One of the major benefits of this application type is the minimal systemic impact of the drug, as pointed out before. Negative side effects of a strong systemic application of Iloprost are possible as for instance in the standard intravenous administration of this drug against hypertension. These unwanted effects could be a too low blood pressure or a system wide suppression of the immune system. The ladder has the risk of leaving the organism vulnerable for invading pathogens. Hence, the systemic effect of the local delivery of Iloprost in the osteotomy model was investigated with flow cytometry analysis of T cell subpopulations in the bone marrow of uninjured bone tissue (humeri, tibia and contralateral femur).

First, for each sample, cells were identified for parameters, such as size, granularity and viability (see Appendix Fig. 8.2). Subsequently, NK1.1+ natural killer cells were analyzed, as well as, various T cell subpopulations, which were NK1.1+CD3+ natural killer T cells, CD8+, CD4+ and CD8+CD4+ (Fig. 4.29). Further in-depth, activated CD8+CD25+ and CD4+CD25+ cells were analyzed. Additionally, for CD8+ and CD4+ T cells, their respective CD62L- effector and CD62L+ central memory T cells subsets (CD44+) were quantified. Conclusively, Iloprost application had no significant effect onto the investigated immune cell types. Only an impact of the regeneration process itself could be identified, i.e. NK1.1+CD3- cells were reduced, but NK1.1+CD3+ cells increased in numbers (Fig. 4.29 A’ and A’’). An additional staining panel detected, in particular, the CD3+CD4+CD25+FoxP3+ Treg cells (Fig. 4.30). In addition, this population was not affected in its numbers in bone marrow of uninjured bones by the anti-inflammatory agent after 3 or 21 days of regeneration. Fluorescence minus one (FMO) controls are shown in appendix for every used fluorescence marker (see Appendix Fig. 8.3).

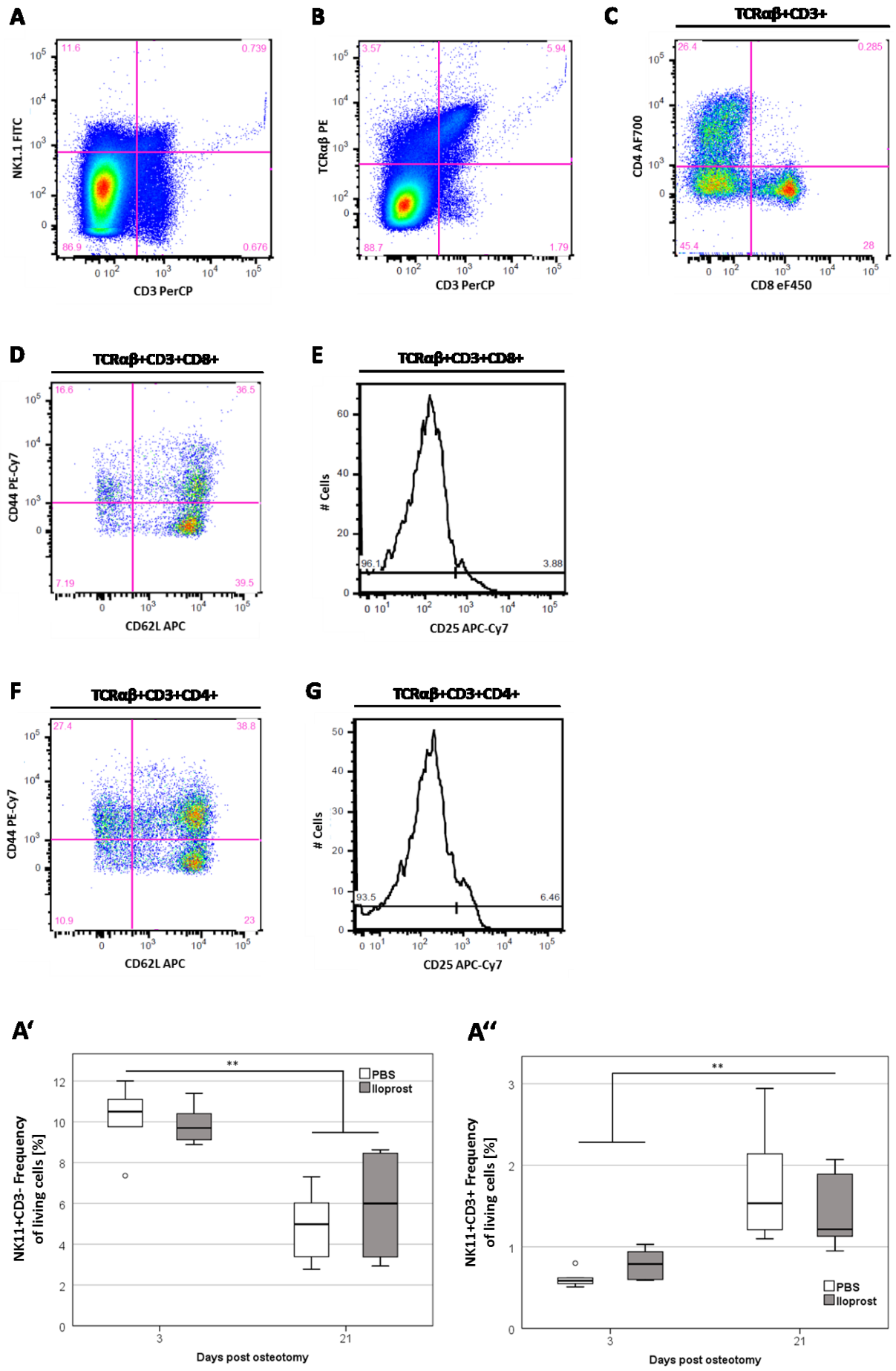
A
NK1.1 FITC
CD3 PerCP
11.6
0.739
86.9
0.676
B
TCRαβ PE
CD3 PerCP
3.57
5.94
88.7
1.79
C
TCRαβ+CD3+
CD4 AF700
CD8 eF450
26.4
0.285
45.4
28
D
TCRαβ+CD3+CD8+
CD44 PE-Cy7
CD62L APC
16.6
36.5
7.19
39.5
E
TCRαβ+CD3+CD8+
Cells
CD25 APC-Cy7
96.1
3.88
F
TCRαβ+CD3+CD4+
CD44 PE-Cy7
CD62L APC
27.4
38.8
10.9
23
G
TCRαβ+CD3+CD4+
Cells
CD25 APC-Cy7
93.5
6.46
A'
NK11+CD3- Frequency of living cells [%]
Days post osteotomy
PBS
Iloprost
**
A''
NK11+CD3+ Frequency of living cells [%]
Days post osteotomy
PBS
Iloprost
**

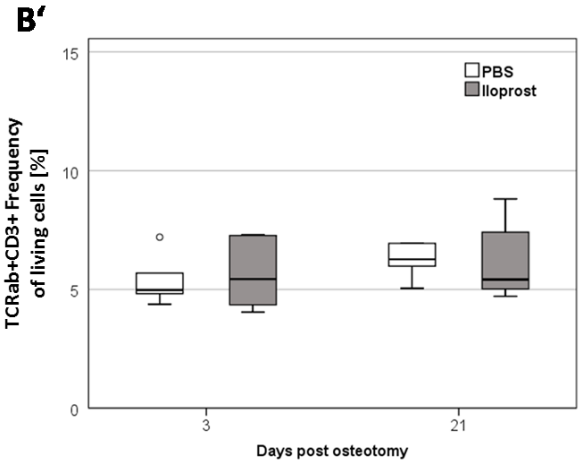
B'
TCRab+CD3+ Frequency of living cells [%]
PBS
Iloprost
Days post osteotomy
3
21

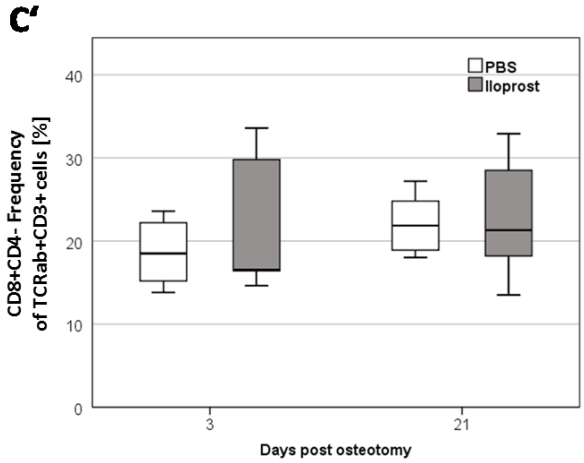
C'
CD8+CD4- Frequency of TCRab+CD3+ cells [%]
PBS
Iloprost
Days post osteotomy
3
21

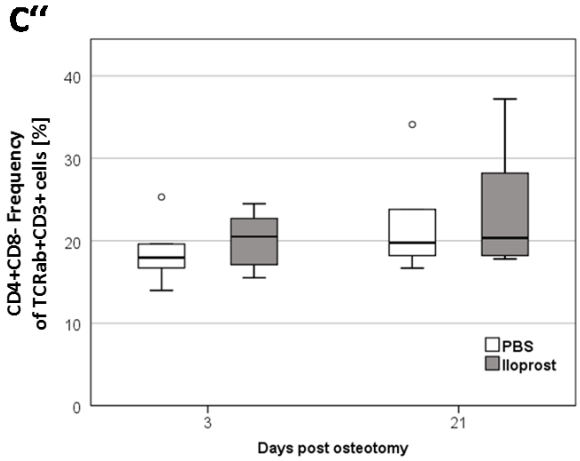
C''
CD4+CD8- Frequency of TCRab+CD3+ cells [%]
PBS
Iloprost
Days post osteotomy
3
21

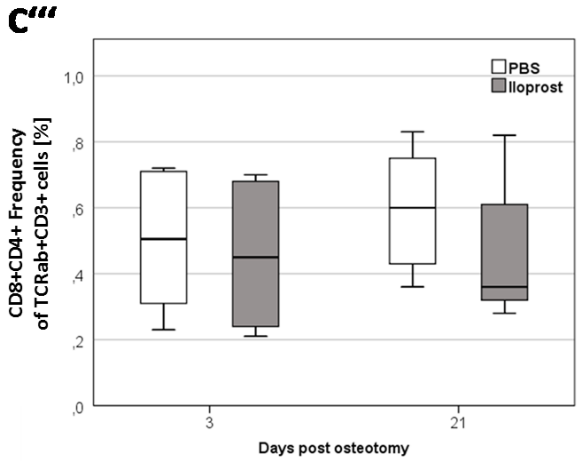
C'''
CD8+CD4+ Frequency of TCRab+CD3+ cells [%]
PBS
Iloprost
Days post osteotomy
3
21

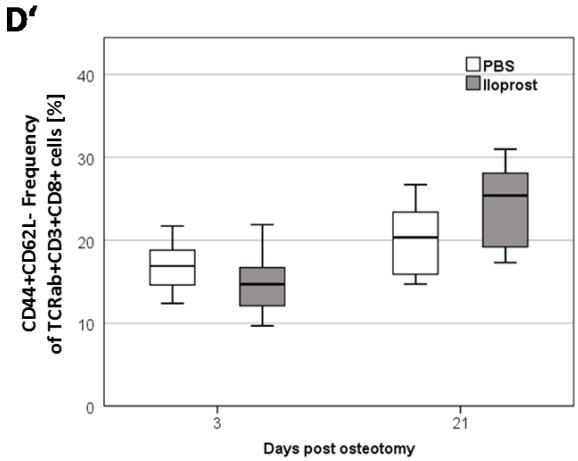
D'
CD44+CD62L- Frequency of TCRab+CD3+CD8+ cells [%]
PBS
Iloprost
Days post osteotomy
3
21

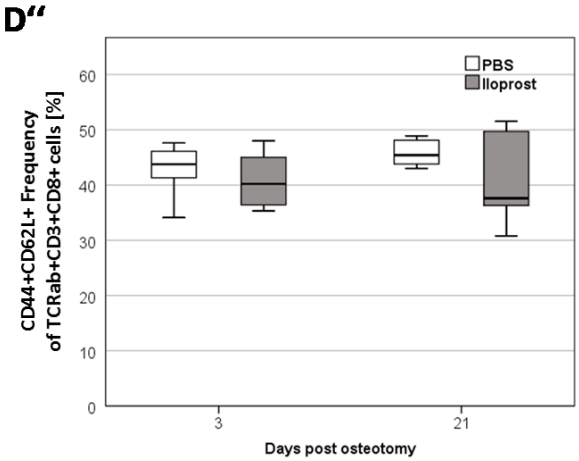
D''
CD44+CD62L+ Frequency of TCRab+CD3+CD8+ cells [%]
PBS
Iloprost
Days post osteotomy
3
21

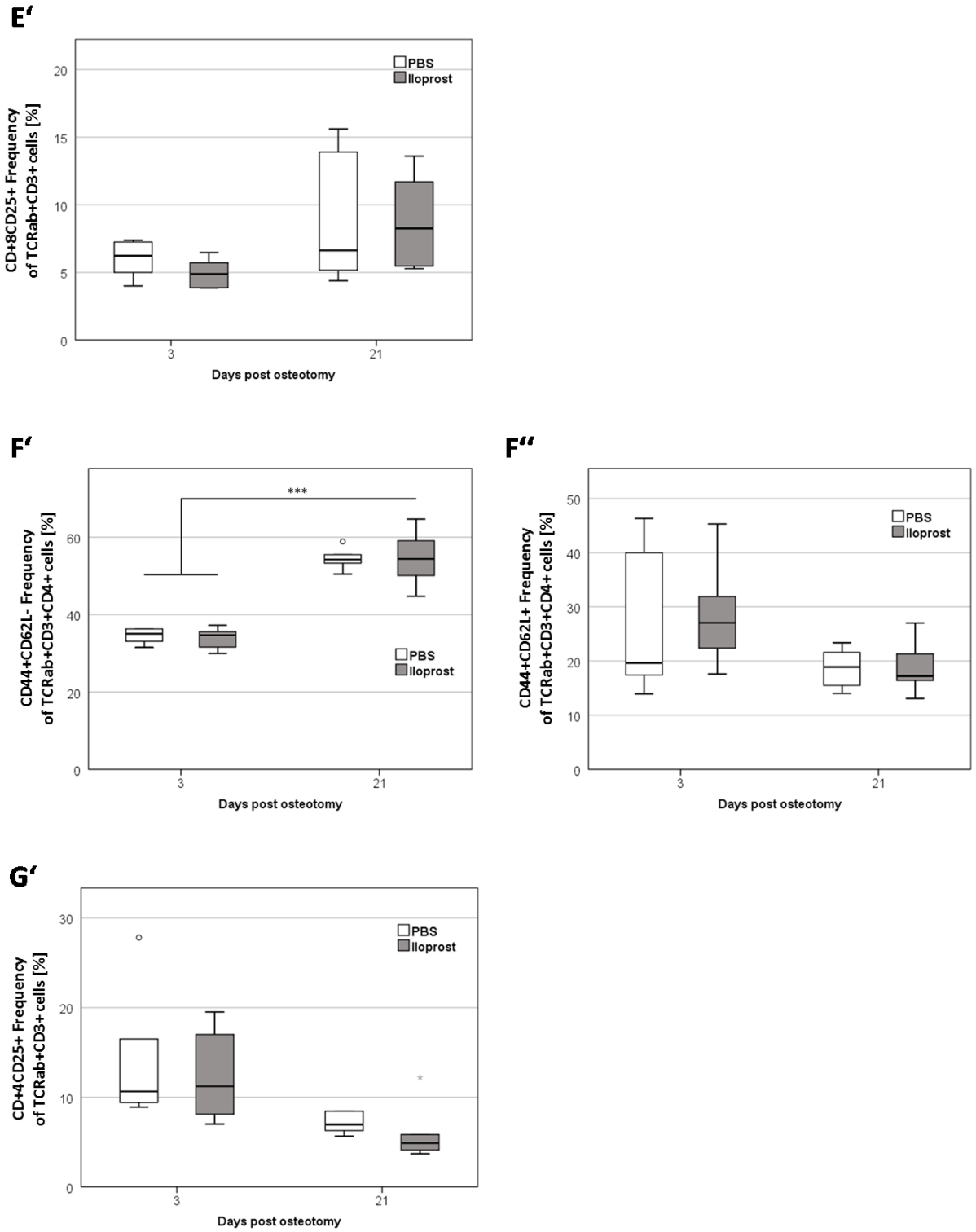

Figure 4.29: FACS analyses of immune cells subsets from bone marrow of uninjured bones at 3 days and 21 days of regeneration in the osteotomy model. Local Iloprost release (3.24 ng) had no significant systemic effect. Pseudo color plot for identification of (A) NK1.1+ natural killer cells and NK1.1+CD3+ natural killer T cells, (B) TCRαβ+CD3+ T cells, (C) CD4+, CD8+ and CD8+CD4+ subpopulations, (D) and (F) respective CD8+ and CD4+ CD44+ memory T cells with CD62L- effector and CD62L+ central memory subsets, (E) and (G) respective CD8+ and CD4+ CD25+ activated T cells. ', '', ''' mark statistics graphs for the respective pseudo color plots. Multiple comparison, n = 6, ***: $p \leq 0.0005$; **: $p \leq 0.005$.

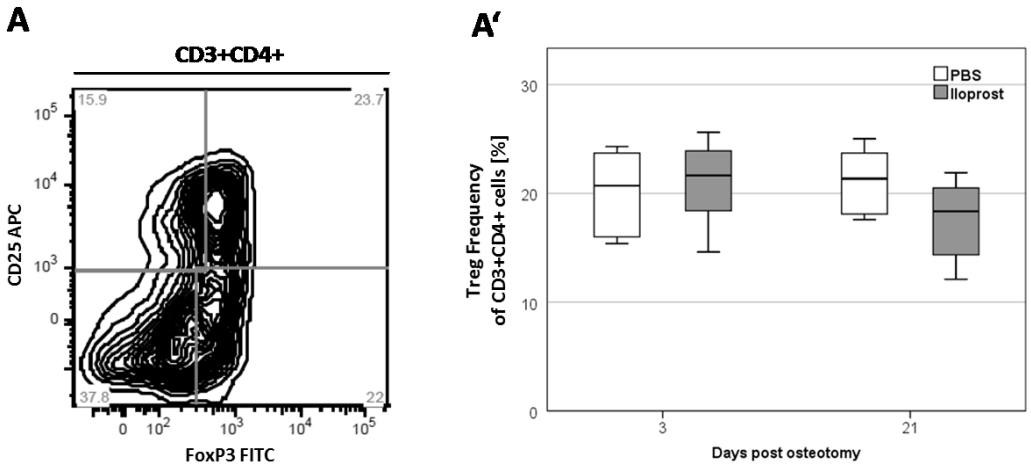

Figure 4.30: FACS analyses of CD3+CD4+CD25+FoxP3+ Treg cells derived from bone marrow of uninjured bones at 3 days and 21 days of bone healing in the osteotomy model. Local release of 3.24 ng Iloprost had no significant effect on Treg numbers. (A) Representative contour plot and (A‘) corresponding statistics graph. Multiple comparison, n = 6.

5. Discussion

In this thesis, the potential of the inflammatory phase of bone healing as therapeutic target was demonstrated. We could confirm our hypothesis that the delayed local application of a PGI_2 analog shortens the inflammatory phases of bone healing and therefore accelerates the regenerative process. In particular, the anti-inflammatory PGI_2 analog Iloprost reduced cytokine secretion of isolated CD8+ T cells, as well as their population doublings. Enriched Tregs secreted more anti-inflammatory IL-10 in response to Iloprost, however only on low levels. Furthermore, macrophage polarization was shifted by the synthetic PGI_2 to an anti-inflammatory pattern. The reduction in pro-inflammatory signals in conditioned media correlated with improved osteogenic differentiation of MSCs and diminished apoptosis. To allow the early pro-inflammatory phase to initiate the regenerative cascade a local drug delivery system was successfully designed and characterized, which could release Iloprost in a delayed manner. Subsequently, this concept of a fibrin-based core-shell design loaded with Iloprost was proven in a mouse osteotomy model. The early fracture site showed a shift towards a less inflammatory cell composition. Finally, later stages of the bone healing model were advanced in the Iloprost treated groups demonstrating the therapeutic potential of interfering with the anti-inflammatory phase of bone healing.

5.1 PGI_2 effects on key cells in bone healing

5.1.1 PGI_2 as anti-inflammatory agent

Since 1977 PGI_2 is known to be involved in anti-inflammatory pathways (Kuehl *et al.* 1977). These properties were also found for its chemically stable analogs, such as Iloprost (Archer *et al.* 1984). In particular, immune-suppression of Iloprost was shown, e.g. that this compound regulates TNF-α synthesis at both transcriptional and post-transcriptional levels (Jorres *et al.* 1997). Additionally, Iloprost's anti-inflammatory properties comprise decreasing of IFN-γ production both in PBMCs of healthy donors and patients with systemic sclerosis (Truchetet *et al.* 2012). Not investigated yet were responses of immune cells in or derived from BM suspensions towards additional supplementation with PGI_2 or its analogs. Furthermore, not reported is the potential of delayed administration of this anti-inflammatory agent during fracture regeneration.

5.1.1.1 Adaptive immune cells

In this thesis, Iloprost was investigated for its use as anti-inflammatory agent to support fracture healing. These insights could be used to prevent delayed bone healing in patients with an unfavorable immune response as low-risk alternative to growth factor applications. Indeed, I confirmed the dose dependent reduction in secretion of cytokines of CD3/CD28-activated T cells in bone marrow cell suspension of mice (Fig. 4.1). This was the case for the pro-inflammatory cytokines IFN-γ and TNF-α, and for the

anti-inflammatory cytokine IL-10. This response pattern was found with splenocytes as well, though in higher overall secreted cytokine concentrations (Appendix Fig. 8.1). These higher concentrations secreted by splenocytes account most likely for the higher T cell density in the mouse spleen compared to bone marrow. Furthermore, the immunosuppressive action of the PGI_2 analog was also seen, but not in a pronounced manner, in the metabolic cell activity of the activated T cells in whole BM cells and splenocytes. Since the measured metabolic activity was not affected by the drug in the non-activated groups, an effect on cell viability of the drug can be excluded. Hence, the observed effects can be related to the anti-inflammatory function of Iloprost. As expected, the non-activated control groups secreted very low amounts of pro-inflammatory factors. Interestingly, a basal level of IL-10 was secreted by the non-activated BM cells, which was in similar range to the suppressed levels of activated T cells, which had received the highest tested dose of 3 µM of Iloprost.

The reduction of secretion of the anti-inflammatory master-regulator IL-10 in immune cell compositions that contain activated T cells can be explained by several facts. For instance, it was found by Zhou et al. that PGI_2 analogs inhibit not only the production of Th1 cytokines, e.g. IFN-γ, but also Th2 cytokines, such as IL-4, IL-10, and IL-13 in a dose-dependent pattern (Zhou *et al.* 2007a). The inhibitory effect was dependent on dose and partially on IP receptor signaling and was correlated with elevated intracellular cAMP and down-regulated NF-κB activity. Additionally, the CD8+ cells that I isolated showed reduction of their own IL-10 secretion levels when activated and even in non-activated state (Fig. 4.3 C). Furthermore, Iloprost treatment did not stimulate further the strong IL-10 secretion in activated Treg (Fig. 4.6 C). By work of others, a stimulatory effect of Iloprost regarding IL-10 production was only reported for BM-DCs (Zhou *et al.* 2007b). However, BM-DCs pre-treated via Iloprost inhibit IL-13, IFN-γ and IL-10 production by T cells (Kuo *et al.* 2012).

From a broader mechanistic prospective, IL-10 might be not required in the milieu of CD3/CD28-activated BM cell suspensions with Iloprost treatment. Hence, it could be down-regulated in a feedback-loop manner, since the synthetic PGI_2 inhibited the pro-inflammatory cell types already. Therefore, anti-inflammatory cells, such as Treg might not receive sufficient stimuli to secrete IL-10. This is in line with the general characteristic of PGI_2 signaling, that although displaying direct immune-suppressive efficacy on pro-inflammatory cell types, a variety of anti-inflammatory cell types are suppressed as well. Furthermore, administered to human PBMCs or isolated naïve CD4+ T cells, Iloprost favors Th17 differentiation and reduces Treg differentiation (Truchetet *et al.* 2012; Liu *et al.* 2013b). In patients, a reduction of Treg cells after 5 days of Iloprost infusion is in line with this fact (D'Amelio *et al.* 2010). This could additionally explain that the response of isolated activated Treg towards Iloprost was even tendency-wise reduced. Only the non-activated Treg showed an increase in their basal secretion of IL-10.

The highest tested Iloprost dose of 3 µM in BM cell and splenocyte cultures was used to investigate the underlying mechanisms further. In particular, T cell subsets were regarded, which are current scientific

targets to assess their role in the inflammatory phases of bone healing and therapeutic potential. As was shown previously, the depletion of pro-inflammatory CD8+ T cells revealed a positive impact onto fracture healing (Reinke *et al.* 2013). Interestingly, I found that Iloprost did not reduce the expression of the CD8 co-receptor (Fig 4.2 C). This is in contrast to findings of others, whereat cAMP increase in CD8+ cells was correlated to a dedifferentiation process by cAMP responsive element modulator alpha (CREMα) (Hedrich *et al.* 2013). In addition, the fraction of the high-density seeded and activated CD8+ cells was not significantly altered, as was indicated by the CD8+CD25+ cell fractions (Fig 4.2 D'). However, the activated CD8+ cells tended to form a fraction with higher CD8 expression as revealed in the pseudo color dot plots (Fig 4.2 C). Iloprost reduced this effect tendency-wise, as well as, for CD8+CD25+ cells. Importantly, the median number of living cells was not significantly affected by the drug. Only the culture conditions lead to pronounced variations in living cell fractions of the activated CD8+ cells after incubation with a duration of 5 days. Of note is that overall less parent CD3+ T cells were detected in the anti-CD8+ isolated suspension at start of the culture compared to 5 days of incubation. This could account for CD3-CD8+ natural killer cells and dendritic cells in the living cells fraction (Vremec *et al.* 2000; Campbell *et al.* 2008; Shortman & Heath 2010), which have vanished and/or outgrown by CD8+ T cells during the CD3/CD28-activation culture.

The strongest directly observable effect of the drug onto activated CD8+ cells was the inhibition of proliferation by almost three-fold (Fig 4.4 C). This confirmed the fact that PGI_2 reduces cell division of activated T cells (Lee et al. 2005), which is similar to the major inhibitory effect of MSCs on activated T cells (Le Blanc et al. 2003). As shown in smooth muscle cells (SMCs), the anti-mitogenic effect of PGI_2 signaling result from inhibition of G1 phase progression by blocking the degradation of p27 and the activation of cyclin-dependent kinase E-cdk2 (Kothapalli et al. 2005). This fact could explain the trend of reduced metabolic cell activity measured after the initial 2 days of incubation for cytokine secretion analysis (Fig. 4.3 D). Hence, the reduction of IFN-γ, TNF-α and IL-10 of activated CD8+ cells could be the result of two facts. On the one hand, due to the direct anti-inflammatory signaling of Iloprost and on the other hand, due to the slower accumulation of cells in response to the drug.

It is a fascinating phenomenon that pro-inflammatory cells like CD8+ cells are also secreting anti-inflammatory cytokines, such as IL-10. This general principal of feedback loops and self-suppression in biological systems reflects the complexity of micro-management in such systems, which is not only relying on a few key functional units with limited tasks. The reduction of IL-10 by CD8+ cells in response to PGI_2 appears logic, since no further anti-inflammatory signaling is used. This fact might also explain the tendency-wise negative response of activated Treg towards additional Iloprost.

A direct analysis of isolated Treg in cell activity or IL-10 and TGF-β secretion in response to PGI_2 and its analogs was never reported to date. However, Treg were investigated as possible Iloprost target in PBMCs cultures, and Treg numbers diminished in response to the drug (D'Amelio *et al.* 2010). After stimulation with phytohemagglutinin (PHA), Iloprost treatment lead to an increased detection of TGF-

β1 by the PBMC culture, which is, however, secreted by most leukocytes. Moreover, it is known so far that intracellular cAMP is required for the suppressor function of activated Treg in both mouse and human (Bopp *et al.* 2007; Klein *et al.* 2012; Bacher *et al.* 2013). In addition, Tregs express the IP receptor to respond to PGI_2 signaling during differentiation (Liu *et al.* 2013b).

Therefore, also the response of Treg onto the dose of 3 µM Iloprost was investigated onto activated and non-activated cells analog to CD8+ T cells. The drug had no significant impact onto Treg cell markers or number of living cells. As expected, proliferation was not affected since it was shown by others that Tregs hypoproliferate upon antigen stimulation (Sakaguchi *et al.* 2008) or by stimulation with TGF-β (Tran 2012). Interestingly in this regard is that rather activated CD8+ cells died during cultivation compared to activated Treg. This is probably due to the rapid proliferation and metabolic activity to produce cytokines of activated CD8+ cells and the corresponding deprivation of nutrition and oxygen. This high activity of the cells was also indicated by their size increase.

IL-10 secretion was elevated in non-activated Treg by three-fold, whereas overall measured cellular metabolic activity was not affected. On the contrary, activated Treg secreted an order of magnitude more of the anti-inflammatory cytokine. The Iloprost treated group of the activated Treg tended to produce reduced concentrations of IL-10. This hints to the fact that the activation of the Treg with CD3/CD28, achieved already maximal activity of this cell type and stronger IL-10 secretion is not possible, i.e. the boundaries of the pharmacologic efficacy of Iloprost for this cell type were reached. As described before, CD3/CD28 activation is increasing cAMP levels in Treg to high levels already (Bacher *et al.* 2013). On the one hand, elevation of cAMP has been shown to increase IL-10 production in monocytes through phosphorylation of cAMP response element-binding protein (CREB) (Liopeta *et al.* 2009). On the other hand, using normal peripheral T lymphocytes stimulated through CD3/CD28, Liopeta et al. revealed that IL-10 is produced mainly by memory T lymphocytes and is inhibited by cAMP elevating agents. The tendency of reduced IL-10, as found here, could further indicate potential self-regulating feedback loops in the cells or toxicities. Further adding to self-suppression by Tregs could be the release of cytotoxic T-lymphocyte-associated protein 4 (CTLA-4) by activated Treg (Walker & Sansom 2011). CTLA-4 is preventing co-stimulation of T cells through CD28 on effector T cells.

The impact of toxicities can be excluded from the metabolic cell activity values of the incubated Treg, since they were still two-fold higher for the activated Iloprost group compared to the non-activated group by unchanged cell numbers. Furthermore, PGI_2 is reducing activity in a variety of cells, due to the mechanism of its anti-inflammatory property. Since activated Treg cells secrete also high levels of anti-inflammatory TGF-β (Kingsley *et al.* 2002), the levels of this cytokine should be investigated in the future in response to PGI_2 analogs. An interesting target constitutes also secretion levels of IL-35 for the verification that PGI_2 analogs fail to increase further the immunosuppressive characteristics of highly activated Treg (Geem *et al.* 2015).

Of note is that accordingly in median ~49 % to ~42 % for PBS and Iloprost treated groups in the CD3+CD4+ populations were detected in the living fraction of enriched Treg cells after 5 days of activation with CD3/CD28 and stimulation with 400 ng/ml IL-2 (Fig. 4.5 C'). The 5-day assessment point was chosen to compare culture effects to the proliferation assay. Potentially, the emerged ~30 % CD3+CD4- populations derived from dedifferentiated CD3+CD4+ cells (Fig. 4.5 C). This process is dependent on the activation status of the CD4+ populations, their metabolism and the environment. In particular, the dedifferentiation is regulated by mTOR mammalian target of rapamycin (mTOR) (Caza & Landas 2015). Alternatively, the resulting CD3+CD4- cells in the living cell fraction after 5 days of incubation could result from impurities of ~6 % CD3+CD4- in the starting culture at 0 days. Since the CD3+ cells were CD3/CD28-activated, proliferation events would have appeared. However, in this culture the Treg were still the majority of cells, even after 5 days. The resulting CD3+CD4- population should be further identified in the future. In particular at the earlier time point of 2 days of incubation, when IL-10 secretion was measured. Data of my working group also showed a reduction of the CD3+CD4+ population after already 12 hours of incubation of 86.6 %, at 48 h 52.4 % and at 72 h 43.3 % with 360 ng/ml IL-2 stimulation (PhD thesis Claudia Schlundt 2017). However, within the remaining CD3+CD4+ population the relative CD25+FoxP3+ Treg numbers stayed stable as well in the previous study.

At 5 days of incubation, the emerged ~15 % of CD3+CD4+CD25-FoxP3- cells in the remaining CD3+CD4+ cells could have been pro-inflammatory T helper cells, such as Th1, Th2 and Th17 (Fig. 4.5 D). However, they would lack the activation marker CD25. These cells could have proliferated from the starting ~5 % impurity of the starting CD3+CD4+CD25-FoxP3- population that was detected. Furthermore, also the existence of CD4+CD25-FoxP3-CD69+ T cells was reported, which secrete IL-10, TGF-β1, IL-2, and also IFN-γ (Han *et al.* 2009). Therefore, CD69 should be analyzed in potential future studies in this setting. On the contrary, the major observed IL-10 secretion levels and Iloprost responses resulted most likely from enriched Treg. Finally, encountered CD3- cells in the CD4+CD25+ MACS-enriched cell suspension could have accounted for dendritic cells (Vremec *et al.* 2000). Whereas, potential macrophages were eliminated by the enrichment process by lineage markers, such as CD11b.

5.1.1.2 Innate immune cells

Macrophages are essential during the inflammatory and endochondral phases of bone healing as our data have shown (Schlundt *et al.* 2015). Additionally, the impact of Iloprost and other synthetic PGI_2s onto macrophages were reported by others (Aronoff *et al.* 2007). However, the drug's efficacy seemed to depend onto the location in the body at which the macrophages are residing, i.e. alveolar and peritoneal macrophage. A postulated reason for the differences was the differential expression of IP receptors on the two macrophage cell types and different receptor binding properties of PGI_2 analogs.

In the study reported by Aronoff et al., the drugs failed to suppress alveolar macrophage inflammatory capacity to the same degree that it did in peritoneal macrophages.

In this thesis, differentially polarized macrophage types were investigated in their response to Iloprost. The macrophages derived from whole bone marrow cells, where fracture healing actually takes place. This was never investigated before. As we previously reported, during the bone healing process an endogenous switch in macrophage polarization is occurring (Schlundt *et al.* 2015). There, initial pro-inflammatory CD80+ M1 macrophages polarize into anti-inflammatory CD206+ M2 macrophages. Additionally, an enforced M1/M2 switch with the interleukins 4 and 13 had a significant positive impact onto fracture healing. Hence, the possibility of mimicking or support of this switch with the drug was assessed here.

Furthermore, I induced the switch towards M1-type with IFN-γ as previously described (Sun *et al.* 2016). Interestingly, pro-inflammatory M1 macrophages could be suppressed with the drug indicated by reduced levels of secreted TNF-α (Fig. 4.8 D). In contrast, the drug supported the IL-4/IL-13-induced shift further towards the M2-type macrophages shown in elevated secretion of the anti-inflammatory master regulator IL-10 (Fig. 4.8 E). The switch of macrophages towards M2-type by IL-4 or IL-13 is regarded as alternative activation (Gordon & Taylor 2005). These cells are characterized among others by increased parasite killing, endocytic activity, cell growth, and tissue repair. For a stronger anti-inflammatory stimulation, macrophages can also be polarized towards intensified production of IL-10, TGF-β and PGE_2 by induction with IL-4/TGF-β together with IL-10 itself (Mia *et al.* 2014). In this case, macrophages would have to be fully polarized before detection of secreted factors into fresh media. In my thesis, I could show that Iloprost can suppress or amplify the characteristic cytokine secretion of either M1-type or M2-type polarization of macrophages, respectively, which were derived from whole bone marrow cells incubated with M-CSF.

5.1.1.3 Osteoimmunological causalities

The impact of the immune system onto endochondral regeneration is of bivalent nature. Though immune cells are initiating the process, a prolonged inflammatory phase leads to delayed bone healing or even non-unions (Kolar *et al.* 2011; Schmidt-Bleek *et al.* 2012a; Schmidt-Bleek *et al.* 2012b). Additionally, secreted cytokines can be beneficial but also inhibitive for osteogenic differentiation depending on type and concentration (Deshpande *et al.* 2013). Therefore, the subsequent consequences of Iloprost's anti-inflammatory effect on immune cells were investigated further, i.e. its osteoimmunological implications for differentiation of MSCs. Conditioned media (CM) from drug-treated isolated immune cells were mixed with osteoinductive media (OM) to assess possible osteoimmunological linkages of Iloprost use.

The cytokine enriched CM of CD3/CD28-activated T cells within BM cultures had a negative effect onto osteogenic differentiation of MSCs (Fig. 4.13). However, CM of Iloprost-treated activated BM

cells had no such detrimental effects. Hence, the drug could partly rescue the osteogenic differentiation outcome from the suppressive impact of CM of activated BM cells. CM of non-activated BM cells was loaded with low concentrations of IFN-γ and TNF-α by the cells, and IL-10 was secreted only at basal levels. As expected, no significant impact onto osteogenic differentiation of these CM could be detected. Interestingly, metabolic cell activity was affected in a similar pattern and indicates a connection to cell activity in response to cytokine signaling, rather than merely a direct suppression of the osteogenic differentiation pathway.

Compared to the CM of BM cells the CM of isolated CD8+ and Treg cells contained even higher concentrations of the two regarded pro-inflammatory cytokines and IL-10, respectively. Interestingly, CM of both particular T cell types led to a similar result in osteogenic differentiation patterns (Fig. 4.14 and 4.15). Cytokine loaded CM reduced the mineralization of the MSC monolayers. However, CM of Iloprost treated CD8+ and Treg cells showed significantly less detrimental effects on either osteogenic differentiation settings. Since Treg derived CM did not affect measured metabolic cell activity it can be concluded that strong IL-10 signaling suppresses the differentiation events directly, but not the cell activity. CM of non-activated cells of both T cell types did not show significant effects on MSC differentiation.

In particular, suppression of osteogenic differentiation by CM of enriched and CD3/CD28-activated Treg was significantly attenuated when Treg were treated with Iloprost. An obvious interpretation is the tendency-wise less IL-10 secretion in the Iloprost treated group. However, the significant difference in osteogenic mineralization to the treatment control group appear to have further causes. Future studies should investigate for instance potential changes in the secretion pattern of pro-osteogenic factors by Treg, such as TGF-β by Iloprost. Concentration values found for these factors could individually be applied to osteogenic differentiation to understand these osteoimmunologic effects in more detail.

In fracture healing, activated Treg application would already suppress the process-initiating early pro-inflammatory phase, especially when applied locally at the fracture site, e.g. in a blood clot. However, application of non-activated Treg systemically can be carried out early and has beneficial effects on mineralization (Liu *et al.* 2011). In addition, data of my working group showed that under sterile conditions systemic application on non-activated Treg resulted in increased volumes of new formed bone in the mouse osteotomy model after 21 days (PhD thesis Claudia Schlundt 2017). Interestingly, in semi-sterile conditions, the healing groups were divided in ‘good’ and ‘bad’ healers, i.e. compared to untreated osteotomy control, bone formation was higher and lower, respectively. This phenomenon was related to the systemic CD8+ T cell/Treg ratio prior osteotomy and not to direct effects of adoptively transferred Treg onto bone formation.

The impact of immune cells onto osteogenic differentiation is mostly caused by released cytokines. Regulated are cell behavior, apoptosis, adhesion, and cell permeability (Kuhn & Tuan 2010). In

particular, the osteoimmunological effect of Iloprost was investigated at the molecular level of signaling factors. Therefore, high and low concentrations of TNF-α and IFN-γ were applied in OM for differentiation of MSCs into the osteogenic lineage. To mimic the effects of potential *in vivo* application of Iloprost directly onto the BM in a fracture, these concentrations derived from values obtained from the initial experiment with activated T cells in whole bone marrow cell suspensions (see above Fig. 4.1).

Interestingly, TNF-α applied at high concentrations resulted in significant reduction of differentiation, whereas low concentrations of the cytokine did not show any significant effects. On the contrary, all tested concentrations of IFN-γ lead to strong reduction in mineralization. The applied doses of IFN-γ were considerably higher than those of TNF-α, as seen in activated T cells in whole BM cells. Metabolic cell activity measurements indicated a significant impact of cytokine combinations onto cell activity with high applied IFN-γ concentrations. Hence, cells that received lower doses of IFN-γ showed significant higher activities. On the contrary, TNF-α doses were not affecting cell activity significantly. Based on these results, it can be concluded that the suppressive effect on differentiation of IFN-γ occurred especially due to reductions in cell activity. However, the applied TNF-α concentrations lead to dose dependent reductions of mineralization of MSC monolayers, but not to significant effects in cell activity.

Since Presto Blue conversion is reflecting cell activity and only indirectly viability, the effect of those IFN-γ and TNF-α concentrations were further tested regarding apoptotic induction. In this way, it could be clarified if observed reductions in osteogenic differentiation could be due to impaired viability. Furthermore, any possible apoptotic or anti-apoptotic effects of Iloprost were investigated as well. Indeed, caspase activities per cells revealed that all applied cytokine doses induced apoptosis and the high IFN-γ concentration increased the values the strongest. Unexpectedly, Iloprost could slightly reduce these effects for all samples to which it was applied. Since this was also the case for the EM control, which caspase activity levels were below that of the positive H_2O_2 control it could be speculated that PGI_2 might suppress caspase activity. This aspect is controversial discussed in literature. On the one hand, mice that overexpress PGIS in the pulmonary vasculature showed decreased endothelial cell apoptosis in a tobacco smoke model (Nana-Sinkam *et al.* 2007). On the other hand, PGI_2 was reported to induce apoptosis in vascular smooth muscle cells (Li *et al.* 2004).

It has been reported that TNF-α actively directs BM-MSCs away from an osteoblastic fate. However, the effects are dose dependent. For instance, the treatment of human BM-MSCs with a high dose of 50 ng/mL of TNF-α transdifferentiates them into a neural fate (Egea *et al.* 2011). In this thesis, TNF-α concentrations were applied in osteoinductive media on mouse MSC monolayers ranging from 0.04 to 0.06 ng/ml (40-60 pg/ml), as was found in whole BM cells with activated T cells. Others tested a comprising dose range of TNF-α of 0.01-10 ng/mL on murine BMSCs cultured in osteoinductive media as well (Lacey *et al.* 2009). At these concentrations cells showed impaired osteogenesis as demonstrated through reduced mineralization and marker expressions, such as ALP, Runx2, Osx, α1(I) procollagen,

osteonectin, and OPN. Reinke et al. found osteosuppressive effects with TNF-α in a dose-dependent manner beginning with 1 ng/ml upwards (Reinke *et al.* 2013).

On the expression levels, a contradicting study showed that levels of osteogenic differentiation markers, such as RUNX2, OSX, OCN and ALP were up-regulated in cell cultures treated with TNF-α at 0.1 ng/mL, while down-regulated in cell cultures treated with TNF-α at higher concentrations of 10 ng and above (Huang *et al.* 2011). However, all doses were inhibitory to mineralization quantified by Alizarin Red staining. Furthermore, extended treatment with TNF-α at any dose was inhibitory on mineralization as well. Adding to the discussion, 1 ng/ml was claimed to be an optimal concentration of TNF-α to stimulate osteogenic differentiation (Glass *et al.* 2011).

Similar to TNF-α, the effects of IFN-γ on osteogenic differentiation are clearly inhibitory in a dose-dependent manner (Liu *et al.* 2011; Reinke *et al.* 2013). This was found also in this thesis. IFN-γ has reportedly strong effects on MSCs, which can explain the deviation from an osteoblastic fait irrespective of osteoinductive media. For instance, IFN-γ induces immune regulation of MSCs in human (Krampera 2011) and mouse (Ren *et al.* 2008). Furthermore, IFN-γ inhibits proliferation and can alter neural, adipogenic and osteogenic differentiation of MSC by the activation of IDO (Croitoru-Lamoury *et al.* 2011).

Taken aside different reported effective concentrations, published studies concur that TNF-α possesses apoptotic effects. In addition, the combination of IFN-γ and TNF-α has a synergistic effect onto MSCs in inducing apoptosis in mouse MSCs (Liu *et al.* 2011) or in suppressing osteogenic differentiation in human MSCs (Reinke *et al.* 2013). While this was also shown in this thesis, the two mentioned prior studies found no significant impact of application of IFN-γ alone onto the viability of MSCs, derived from either mouse or patients. This was the case even at high concentrations of the cytokine of up to 200 ng/ml. This is in contrast to my findings, which revealed reduced viability and increased apoptosis dose-dependently with 50 and 120 ng/ml.

Explanations for the discrepancy between the findings could potentially be found in technical aspects of the cell handling protocols or the polarization of the used MSCs towards certain lineage commitments. Cryo-preservation of MSCs is a standard method in life sciences, however, it was recently identified as a factor, which increases the susceptibility of MSCs to T cell-mediated apoptosis (Chinnadurai *et al.* 2016). Interestingly, temporary pre-treatment of MSCs before the freeze-thawing cycle with IFN-γ modified the MSCs and mitigated this susceptibility. For instance, Liu and Reinke et al. did not use cryo-preserved MSCs.

Regarding the susceptibility of viability of cells to cytokines at different stages of the osteogenic lineage, it is known that terminally differentiated osteoblasts show negative responses to transient exposure of pro-inflammatory cytokines (Sidney *et al.* 2014). This leads to reducing effects on mineralized nodules and cell numbers. In particular, IL-1β, TNF-α, and IFN-γ cause apoptosis of osteoblasts, which is

intensified when applied in combination (Kuzushima *et al.* 2006). In contrast, mouse ESCs, which were *in vitro* differentiated into osteogenic lineage and treated with this cytokine combination, maintain viability and formation of mineralized nodules remained unaffected (Sidney *et al.* 2014).

Hence, the developmental and aging stage of the bone marrow and in this way of osteoprogenitors and MSCs might influence their responses to cytokines. For instance, it was reported that the bone marrow is transforming with age towards adipose tissue with causes not fully disclosed yet (Griffith *et al.* 2012). This phenomenon occurs also in rodents (Scheller *et al.* 2016). In particular, age-related alterations in MSCs might relate to shifts in differentiation potential from the osteogenic to the adipogenic lineage (Kim *et al.* 2012). Liu et al. 2011 did not specify age and strain of mice for BM-MSC isolation, and Reinke et al. 2013 used BM derived from patients aged 39 to 90 years. Very recently, an *in vivo* study revealed that IFN-γ-ARE-Del mice with increased IFN-γ production specifically lose their BM-MSCs between 3 – 30 weeks of age (Goedhart *et al.* 2018). It was concluded that IFN-γ negatively affects maintenance of BM-MSCs. Furthermore, another example is that during inflammatory conditions, IFN-γ can have a detrimental effect on the maintenance and self-renewal of HSCs (de Bruin *et al.* 2013; Matatall *et al.* 2014).

The anti-inflammatory cytokine IL-10 has reportedly anti-osteogenic effects as well (Deshpande *et al.* 2013). In particular, in mouse BM-MSCs, treatment with IL-10 does not impact cell proliferation, however, inhibits osteogenesis (Van Vlasselaer *et al.* 1993). However, when MSCs progress to stages of differentiation subsequent to peak of ALP expression, this IL-10-induced downregulation is not observed. This indicates that IL-10 only mediates early osteogenic differentiation before ALP expression but not late osteogenesis. The inhibitory effect of IL-10 is thought to be caused by its inhibition of TGF-β, as exogenous administration of IL-10 suppressed TGF-β synthesis, and furthermore, inhibited matrix mineralization, and downregulated ALP, collagen, and OCN expression in murine BM-MSCs (Van Vlasselaer *et al.* 1994).

As described by Toben et al., the rapid healing demonstrated by recombination activation gene 1 (RAG1) knockout mice contained a strong anti-inflammatory component to the cytokine milieu (Toben *et al.* 2011). These mice are characterized by an impaired adaptive immune system, i.e. lack of mature T and B cells. In particular, production of anti-inflammatory cytokines, such as IL-10, was increased during bone regeneration, whereas pro-inflammatory cytokines such as TNF-α, lymphotoxin β, IFN-γ, IL-2, and IL-4 were diminished. Regarding histologic aspects of fracture healing, acceleration of endochondral ossification and elevated mineralization were detected. However, despite increase in volume, the quality of regenerated bones was impaired for RAG1-/- mice, as interpreted by increased stiffness values, i.e. reduced flexibility of the newly formed bone tissue. In light of the consistent IL-10 expression of the RAG1-/- fracture model, it is likely that the endochondral phases were influenced by the osteosuppressive effects of IL-10.

As we have recently shown, this is also the case for uninjured bones for RAG1-/- mice, i.e. the consistently altered inflammatory milieu in the bone tissue impairs also the elasticity of bone in homeostatic state (El Khassawna *et al.* 2017). In particular, during regenerating state, collagen deposition as well as localization of osteoblasts in the callus was dysregulated. However, the reduced bone formation shown by Chan et al. obviously resulted from suppression of process-initiating earliest pro-inflammatory phase by direct injections of IL-10 into the fracture at days 0 and 1 (Chan *et al.* 2015).

The impact of CM of polarized macrophages onto osteogenic differentiation was not investigated in this thesis. This is due to the fact that the outcome when using CM of M1- and M2-type macrophages was expected to show similar tendencies to that of CM from CD8+ and Treg. In particular, the impact on osteogenic differentiation would be expected to be in a reduced manner, due to the lower cytokine levels released by the polarized macrophages compared to the activated T cells. Furthermore, a crucial necessity of M2-type macrophages during fracture healing, in addition to immune modulation, is of indirect nature, i.e. by their ability of matrix remodeling, due to strong secretion of MMPs (Brown *et al.* 2012a; Raggatt *et al.* 2014) and vascular growth factors (Nourissat *et al.* 2015; Chernykh *et al.* 2016). Hence, as we have shown, macrophage depletion leads to an arrest of fracture healing at the first endochondral phase of cartilage formation (Schlundt *et al.* 2015).

5.1.2 PGI_2 as anabolic agent

The IP receptor of the endogenous version of Iloprost is expressed on MSCs (Hoogduijn *et al.* 2010). Hence, also the drug response of this crucial cell type for endochondral fracture healing was investigated. However, even the highest applied concentration of 3 µM Iloprost had no significant negative effect onto osteogenic differentiation of the mouse MSCs. In literature, the response of MSCs onto osteogenic and chondrogenic differentiation towards PGI_2 signaling and increasing intracellular cAMP levels remains a controversy.

On the one hand, when regarding cAMP elevation, phosphodiesterase 4 (PDE4) mediates cAMP degradation. Interestingly, the PDE4 inhibitor cilomilast enhanced the osteoblastic differentiation of MSCs in primary cultured MSCs (Munisso *et al.* 2012). Moreover, cAMP was claimed to be an important signaling component for complete differentiation of MSCs not only into the osteolineage but also for chondrogenic differentiation (Carroll & Ravid 2013). This was also stated by another study, which, in addition, found that cAMP suppresses osteoclast differentiation and function (Mediero & Cronstein 2013; Ramaswamy *et al.* 2017).

On the other hand, prostaglandins directly applied in culture affected osteogenic differentiation differentially. For instance, in human adipose tissue-derived MSCs, PGI_2, but also PGE_2 and $PGF_{2\alpha}$ decreased ALP activity (Knippenberg *et al.* 2007). Whereas, low-dose $PGF_{2\alpha}$ could lead to a detectable increase in activity of this differentiation marker at day 14. However, at day 4, PGI_2 and $PGF_{2\alpha}$

upregulated osteopontin gene expression, and $PGF_{2\alpha}$ upregulated α1(I)procollagen gene expression instead. Mineralization was not investigated in that study. In addition, Iloprost was reported to be partially antagonizing the suppressor effects of indomethacin onto osteogenic differentiation of BM-MSCs (Kemper *et al.* 2014).

In the here described study, a reduction of proliferative capacity of BM-MSCs was observed additionally, which is in line with the anti-mitogenic properties of PGI_2 as discussed above for CD8+ cells (5.1.1.1). Furthermore, chondrogenic differentiation in response to the PGI_2 analog was investigated with the primary mMSCs, which required pellet formation and paraffin sectioning. Also for this differentiation process quantitative image analysis of Alcian Blue staining on these paraffin sections indicated no interference of the drug, although chondrogenic differentiation is dependent on cAMP pathways (Lee & Chuong 1997).

An interesting aspect was that adipogenic differentiation occurred in parallel in a small fraction of MSCs in the monolayer with the highest tested dose of the drug of 3 µM (Appendix Fig. 8.4). The phenomenon that a small fraction in the monolayer of the MSCs differentiated towards the adipogenic lineage even in osteoinductive media can be explained with the heterogeneity of the BM-MSCs (Breitbach *et al.* 2018). Potentially, some MSCs appeared to be rather oriented towards the adipogenic lineage. MSCs have stem cell like characteristics. However, they lack a crucial aspect of stem cells, which is the clear defined niche.

A stem cell niche, e.g. the HSC niche, consists of the stem cells, which are in direct contact to differentiated partner cells, which control their status, i.e. differentiation into specific proliferating progenitor cells or performance of self-renewal (Sieber *et al.* 2018). However, the differentiation potential of MSCs, i.e. the possible lineages the MSC can commit to, varies between cells of this type obtained from different tissues (Keating 2012). Hence, the differentiation potential of MSCs might be defined by the specific tissue milieu, in which they reside. A similar phenomenon can also be observed, for instance, in macrophages of different tissue origins. Diverging responses to different PGI_2 analogs were connected to differential expression of IP receptors on the macrophage cell types (Aronoff *et al.* 2007). In this regard, the density of receptors of the prostaglandin family might differ on the heterogeneous BM-MSCs and results in variations in the conducted differentiation experiments. Of note is that MSCs themselves are thought to be a relevant influencers of the HSC niche, due to their paracrine activity or direct contact with these stem and progenitor cells (Costa *et al.* 2018).

PGI_2 is known to be involved in adipogenesis (Negrel 1999; Jia *et al.* 2012). Thus, as expected, the PGI_2 analog supported clear adipogenic differentiation of the BM-MSCs dose-dependent in respective induction media as well, i.e. large lipid vesicles could be detected (Fig. 4.10). However, in the *in vivo* investigation of the drug release system loaded with Iloprost, which is discussed further below, no hint of adipogenic vesicles was found at 3 nor 21 days after application (Appendix Fig. 8.6). Hence, a high

dose of Iloprost, as applied in MSC monolayer culture, was not immediately released in the *in vivo* model.

Another aspect of adipogenesis of PGI_2 signaling is the activation of PPARγ by PGI_2 analogs (Gurgul-Convey & Lenzen 2010; Mohite *et al.* 2011). The expression pattern of PPARγ comprises localizations in spleen, large intestine and adipose tissue. PPAR activation is initiated through COX and lipoxygenase pathway and furthermore hypolipidemic agents. Hence, PGI_2 can be related to lipid metabolism through the IP/PPARγ receptor. An obvious explanation for the detection of differentiated adipocytes found in response to Iloprost on osteogenic induction medium on MSC monolayers could be the presence of adipogenic stem cells. However, this aspect can rather be excluded, since young mice of the age of 12 weeks were used in this thesis to extract and culture the primary MSCs. Hence, age-related occurrence of adipose tissue in the BM can be ruled out.

Concerning receptor specificity of synthetic PGI_2 analogs, in particular of Iloprost, it is known that, in addition to the IP receptor, Iloprost is able to bind to the receptors of PGE_2, which are EP1, EP2, EP3 and EP4 (Moreno 2017). This fact was not investigated further in this thesis work, since the efficacy towards the regarded cell types and processes is similar. For instance, PGE_2 has immunosuppressive effects onto T cells (Wiemer *et al.* 2011), and is anti-proliferative (Huang *et al.* 2007). In addition to the unclear role of PGI_2/cAMP signaling in osteogenic differentiation, diverging findings for the effects of PGE_2 signaling onto osteogenic differentiation are described in literature as well. On the one hand, PGE_2 application had anabolic effects for cancellous bone formation in aged rats (Keila *et al.*, 2001). Furthermore, PGE_2 increased the number of mineral nodules during osteogenic differentiation with BM-MSCs (Keila *et al.* 2001). On the other hand, PGE_2 inhibited mineralization by BM-MSC derived osteoblasts by cAMP signaling (Mirsaidi *et al.* 2017). In addition, PGE_2 was shown to increase bone marrow mineralized nodule formation when administrated systemically, suggesting that the number of committed progenitors is increased and that PGE_2 has a role in bone homeostasis (Weinreb *et al.* 1997). However, EP1 receptor maintains MSCs in an undifferentiated state, and thus is a negative regulator of osteoblastic differentiation and bone formation (Feigenson *et al.* 2017).

Taken together, the effects of PGI_2 directly onto osteogenic and chondrogenic differentiation appear to be faint and dependent on several cofactors. Hence, this corners the anti-inflammatory phase to be the optimal therapeutic target for PGI_2 application in fracture repair.

5.2 Fibrin as drug carrier

5.2.1 Fibrin properties

Human derived fibrin was selected by me as a hydrogel-based carrier to investigate the local delivery of Iloprost in the fracture model, mainly due to its approved biocompatibility and its capability of retaining

hydrophobic drugs (Yoshida *et al.* 2000). Since endogenous fibrin is also abundant in the early hematoma and the succeeding granulation tissue, this carrier material was expected to minimize the biochemical interference with the early stage of that process. To maximize the carrier surface onto which the drug could bind, the density of the core fibrin was increased by using 150 % fibrinogen concentration of the initial pre-solution of the manufacture's recommendations for wound sealant purposes. The shell around this core was kept at 100 % concentration to reduce the overall material load that the organism would have to degrade and absorb.

A relatively high concentration of the enzyme thrombin (Th-S instead of lower concentrated Th-L of the applied kit) was used for the polymerization of fibrinogen into fibrin. The use of highly concentrated thrombin enhances the fibronectin-binding capacity of fibrin, which in turn provides an improved microenvironment for osteoblast differentiation (Oh *et al.* 2012). Hence, potentially remaining carrier residues could support differentiation processes in the endochondral phases of bone healing. However, dense fibrin residues were not detected with histologic staining at the endochondral phases at 21 dpo (Fig. 4.23).

In particular, high concentrations of thrombin lead to thin fibrils and small pores sizes of fibrin in the process (Breen *et al.* 2006). These characteristics can occur in the endogenous hematoma at the beginning of fracture healing (Wang *et al.* 2017). However, those properties vary in endogenous fibrin clots of the fracture hematoma, and depend on the fibrin polymerization process. In particular, the endogenous fibrin formation process is influenced by protein concentrations and cytokines, growth factor bindings and cellular infiltration. For instance, activated platelets secrete polyphosphates, which increase fibrin pore size and reduce the abundance of fiber branching points (Mutch *et al.* 2010; Feghhi & Sniadecki 2011). Whereas, thrombospondin, secreted also by platelets, promotes the formation of thinner and denser fibers (Nehls & Herrmann 1996). Interestingly, leukocytes, fibroblasts and endothelial cells, are influencing the final fibrin structure as well by secreting factors that modulate thrombin levels (Ovanesov *et al.* 2005; Campbell *et al.* 2009).

Thinner fibers allow for a tight clot conformation, which can retain larger amounts of signaling factors, such as growth factors (Woo *et al.* 2003; Oh *et al.* 2012). However, the downside for fracture healing with densely packed clots is that they retard cellular ingress. Hence, the vehicle control group shown in this thesis reached a less advanced healing stage in the here used mouse osteotomy model at 21 dpo, compared to an empty fracture gap of this model (Reinke *et al.* 2013), i.e. faint bridging compared to complete bridging, respectively. The faint bridging at 21 dpo was also previously shown by us for a collagen scaffold in the fracture gap of this model (Schlundt 2015). Furthermore, a higher rate of protofibril assembly is known to increase the number of thinner fiber generations (Geer et al., 2008). This improves the low mechanical stability of the fracture hematoma, however with a low fiber density, which is beneficial for controlling hemorrhage at the fracture site (Di Stasio et al., 1998; Lord, 2011).

Histology of *in vitro* samples of the release system revealed typical formation of porous fibrin in the core and shell areas of the drug release system (Fig. 4.18 C). The fibrils were relatively thin and pores small, which is expected for the used high concentrations of thrombin (Breen *et al.* 2006). Interestingly, a dense area of thick fibrils formed at the periphery of the core and the shell. Low concentrations of thrombin at this site are the obvious explanation (Rowe *et al.* 2007). Potentially, thrombin was diffusing towards the center of the fibrin clots during polymerization. Evaporation of the water content on the surface would have rather increased the concentration of thrombin. The sporadic occurrences of large pores at that site might be due to gas inclusions during polymerization or shrinking related ruptures during fixation and hydrophobic histological staining of cryosections.

Degradation assays *in vitro* showed a dominant effect of applied fibrinogen density-dependent hydrolysis and susceptibility towards enzymatic proteolysis with proteinase K of the carrier (Fig. 4.18 D). Proteinase K was chosen to mimic the degradation of the proteins of the ECM or exogenous protein-based materials in the fracture callus. The fibrin samples lost initially weight through the digestive degradation process and hydrolysis, however at certain time points the structures collapsed rapidly. This can be explained by the disruption of protein linkages throughout the material. In particular, the low-density shell fibrin started to collapse at day 5, whereas the core and the core-shell composition followed in bulge degradation at day 6. The core material degraded significantly slower than shell and core-shell from day 7 to 9, which is most likely due to the higher protein content. If this lead in particular to an increase in fibril connections or thicker fibrils was not investigated here. The enzymatic proteolysis model applied here appears to be mimicking endogenous remodeling processes well. Also in mouse, rat or rabbit models, the fibrin-rich granulation matrix is replaced by the soft callus at days 7 to 9 post trauma (Einhorn 1998). An acceleration of the degradation model *in vitro* to match endogenous mechanisms could be co-culture experiments with M2-type macrophages. These cells are major key players in matrix remodeling during bone regeneration, due to their release of MMPs (Schlundt *et al.* 2015).

Furthermore, the potential effect of Iloprost or its carrier solution onto structural integrity of fibrin was tested via compression testing. Interestingly, the incorporated drug lead to a tendency of increased stiffness, which compression testing revealed. On the one hand, strong anti-coagulating effects of Iloprost can be ruled out during the fibrin formation *in vitro*, since that mechanism targets platelet cells (Deep *et al.* 2017). On the other hand, the vehicle solution of Ilomedine consists of water, ethanol, NaCl, HCl and Tris buffer. Hence, an explanation could be found again in the performance of thrombin. From the substances in the vehicle solution, ethanol most likely reduced activity of this enzyme, since the inhibitory effects of ethanol onto thrombin activity are reported (Marumo & Wakabayashi 2009).

Hence, the polymerization process of fibrin might have been decelerated for the clots that were loaded with the drug, which would have led to more compact fibrin gels that poses thicker fibers (Rowe *et al.* 2007). This in turn could have provided the observed tendency towards increased mechanical stiffness.

Future studies could investigate this explanation via quantitated histologic analysis or via three-dimensional analysis with means of scanning electron microscopy (SEM).

In literature, the stiffness values (also known as Young's modulus or equilibrium modulus) for blood clots and fibrin sealants vary, due to experimental conditions and different pre-cursor concentrations, respectively. These values are usually lower as have been found here, i.e. ranging from approximately 0.5 kPa for fresh blood clots (Wang et al. 2016) over 30 kPa for fibrin sealants (White et al. 2015). However, the here detected range of approximately 150 – 200 kPa was found to be optimal for high proliferation rates in fibrin matrices (Lucarelli *et al.* 2010). Hence, the here used high density fibrin matrices could have retarded cellular invasion, but were still in range to interact with surrounding cells to eventually be degraded after drug release to make way for new bone tissue.

5.2.2 Release kinetics

Release kinetics were performed to examine the gain of deceleration with the core-shell approach and furthermore with the higher density of the core fibrin. Therefore, the released drug was extracted from the media and analyzed with HPLC/UV. The derived kinetics revealed a burst like release within 24 h of the complete drug load with the shell fibrin, and only a moderate reduction with the high-density core material (Fig. 4.20).

Strikingly, the modification of the system with the protective outer layer of shell fibrin could delay the release of this amount of drug by additional 24 h in this *in vitro* model. This was the crucial desired aspect of the system for the *in vivo* application – the delayed release of anti-inflammatory Iloprost in fracture healing to faster end the pro-inflammatory phase and support the anti-inflammatory phase. 88 % of Iloprost was released until day 2 with the core-shell system, instead of 87 % and 99 % of the compositions without empty shell already after 24 hours. Hence, the drug must have diffused through the shell material before it was released into the surrounding media into which the composition was immersed. A too immediate administration in effective high concentrations at 24 h post fracture would suppress the early pro-inflammatory phase, which is necessary to initiate the healing process. For instance, a too early efficacy of Iloprost locally was interpreted as inhibitive for bone healing in a closed tibia fracture model in rat with daily drug injections beginning at 0 days until 5 days (Dogan *et al.* 2014). The inhibitory mechanism would be comparable to anti-inflammatory IL-10 injections into the callus at 0 and 24 h post fracture (Chan *et al.* 2015).

Of note is that fibrin as drug carrier is not able to withhold this drug completely. This means at the initial washing step 78 ng/ml of the loaded 324 ng/ml were already retrieved in the media from the core-shell system. However, this is substantial less than the 177 and 144 ng/ml Iloprost immediately released from shell and core alone, respectively. Unbound Iloprost can interfere with initial hematoma formation, due to its anti-coagulative properties (Deep *et al.* 2017).

As described above, all fibrin-based drug carrier *in vitro* samples started to collapse not earlier than at day 5 (Fig. 4.18). Importantly, this is after the drug was fully released in every composition, which was latest at day 4. From that fact, it can be concluded that the complete release of the drug was rather dependent on limitations of the capacity of fibrin to retain the hydrophobic drug Iloprost, rather than simply due to the dissolution of this carrier material. Since the resulting release kinetics revealed that after 4 days all fibrin compositions had released their full load of 324 ng Iloprost (Fig. 4.20 B), this in turn shows that Iloprost was detectable for the investigated timeframe and not degraded. In fact, detected quantities exceeded the 100 % mark slightly, which could indicate background noise, which was detectable in the mobile phase only control (Appendix Fig. 8.7 A).

Application in the osteotomy model of a core with a density of fibrinogen precursor as recommended in manufacturer's protocol, i.e. 100% instead of 150% concentrated fibrinogen, appears to be sufficient and could be tested in future studies, as long as a shell is provided. In this way, less protein content would be administered to the fracture, which might be beneficial, since less clearance from the tissue would be necessary. An alternative approach to the core-shell release system investigated here could have been the usage of microspheres. For instance, biodegradable polymer PLGA was shown to be able to release the prostacyclin analog ONO-1301 in a sustained manner (Obata *et al.* 2008). The release of this system is tailorable by size of the microspheres, e.g. with the smallest described sphere diameter of 21.2 µm an *in vitro* release of ~80% of the PGI_2 analog could be detected after 7 days. Hence, if even smaller diameters of these spheres could be achieved, comparable delayed kinetics as described in this thesis could be gained for targeting the pro-inflammatory phase in fracture healing. Any pre-mature releases of unbound drug could also be reduced. However, the microspheres still would have to be immobilized in another carrier matrix, such as fibrin or another hydrogel for the local application.

Further alterations of the here described core-shell system, such as coating with a hydrophilic shell, might have delayed the release too extensively for immune modulation during the pro-inflammatory phase of bone healing. One has to keep in mind that when comparing dosages between *in vivo* and *in vitro* systems, physiological factors such as diffusion in tissue are usually not considered in *in vitro* models. Hence, the *in vitro* release kinetics of the core-shell system were a first proof of concepts of the possible delay of the drug release and an estimate of the release *in vivo*.

5.3 Proof of concept in the osteotomy model

A delayed release of Iloprost was desired in this study to tolerate the early pro-inflammatory phase, which is required to initiate the bone healing process (Schmidt-Bleek *et al.* 2012b; Schmidt-Bleek *et al.* 2014; Chan *et al.* 2015). Hence, the fibrin composition was prepared immediately prior surgery in the way that a core of fibrin was loaded with the drug and subsequently was surrounded by a shell consisting

of pure, non-loaded fibrin. The *in vitro* release kinetics confirmed the delay of the release of Iloprost from the core-shell composition by an additional 24 hours compared to core alone.

The effect of the decelerated release of the PGI_2 analog into the osteotomy model was measured via quantification of newly formed mineralized bone tissue at 21 dpo and via histological analysis of cryo-sections at 3 and 21 dpo. Indeed, *in vivo* results showed significantly increased volumes of newly formed bone matrix after 21 days of regeneration in comparison to the control. The examination of tissues participating in healing and the interaction with the hydrogel of the release system revealed that the fibrin-based carrier was degraded after 21 days of regeneration, but not at 3 days. Furthermore, after 21 days, the fractures in the mouse model that received the drug were already in the transition phase from the cartilage towards the calcification phase of the callus. In contrast, the fractures without Iloprost treatment, did not reach endochondral phases of tissue restauration. Partial signs of ingrowth of connective tissue rather indicated potential emergence of a pseudoarthrosis. Hence, the dense amount of exogenous fibrin that was broad into the initial fracture gap could potentially describe a non-union model. In contrast, reasons for clear signs of endochondral regeneration in the Iloprost treated group could be found in further stimulation of signals, which polarize macrophages into the matrix remodeling anti-inflammatory M2-type as shown *in vitro* (Fig. 4.8 E).

5.3.1 Late stage healing process

The late stage fractures of Iloprost treated animals showed relatively strong variations in the soft and hard callus tissues. This reflects different stages of the early endochondral phases. The fractures of some individual mice were in the process of before, some in between and others after the soft callus phase. Besides general differences in regenerative capacity of the animals, a reason for individual variations in the distinct healing phase could be the response to the anti-inflammatory drug.

The mice of the mouse model used in this study were kept in semi-sterile conditions to enable a certain immune experience for each animal to mimic the immune status of an otherwise young and healthy patient. Studies of my working group on adoptive Treg transfer in the mouse osteotomy model revealed strong variations of the individual immune status of mice under these semi-sterile conditions (PhD thesis Claudia Schlundt 2017). In particular, the healing outcome appeared to correlate negatively to the ratio of CD8+ effector T cells and CD4+ Treg in blood measured before osteotomy. Although an impact of the early inflammatory phases was not investigated in the study of my colleagues, it could be concluded that the individual immune status of mice is correlated to the fracture healing outcome. These findings confirmed other data of colleagues in patients, i.e. that the CD8+ T_{EMRA} titer of fracture patients can predict the quality of the healing outcome (Reinke *et al.* 2013). The clinical relevance is given by the established concepts of immunosenescence and inflamm-aging (Xia *et al.* 2016; Fulop *et al.* 2017; Ventura *et al.* 2017). However, individuals display significant differences and parameters are varying

strongly also among same-aged patients. These individual variations in immunocompetence has various reasons, which can be found in direct genetic traits, but also in neurological and endochrinological phenotypes, and the number of pathogenic encounters.

Hence, in the near future, elderly fracture patients could be stratified according to these parameters of immunosenescence/inflamm-aging for prophylactic, individual immunomodulatory and/or growth factor therapies. As we have shown very recently with aged mice, the experience level of the adaptive immune system influences bone healing and bone homeostasis (Bucher *et al.* 2019). Therefore, in a following preclinical study the individual systemic immune status of mice could be investigated prior osteotomy with the delayed local Iloprost administration and related to respective healing outcome. For instance, effector cells could be tested, such as the ratio of CD8+ effector T cells and CD4+ Treg. In the here described study, contralateral moderate variations in cell subsets measured by FACS and also low variations at local site in subsets at the early time point of 3 dpo identified histologically were apparent.

5.3.2 Early stage healing process

The impact of anti-inflammatory effects of Iloprost was investigated in the osteotomy model at 3 days of regeneration. Therefore, the areas in proximity of the fracture gap were analyzed with fluorescence immunohistochemistry and key target cells quantified, i.e. CD8+, CD4+, macrophages and osteoblasts. Furthermore, at 3 days of bone healing the anti-inflammatory phase is taking place (Schmidt-Bleek *et al.* 2012b; Schlundt *et al.* 2015). Another important aspect is that after 3 days the *in vitro* release kinetics of Iloprost from the core-shell system showed that almost 100 % of the drug had left the carrier material. On the one hand, the drug might be released slower from the carrier material within tissue than in the aqueous media of the *in vitro* release kinetics experiment. On the other hand, mechanical or strong enzymatic stress in the living environment might trigger a faster release.

Additional animal studies, which would investigate the *in vivo* release of Iloprost in the mouse model, e.g. via chromatographic methods, were not considered. That the delayed release commenced *in vivo* as intended can be derived from the positive bone formation outcome after 21 days of regeneration, as well as, from the confirmed anti-inflammatory cellular pattern change at 3 days. Furthermore, an early burst-like release of Iloprost did not show significant changes in bone formation after an experiment in sheep by my colleagues, which data are included in a published patent application (WO/2019/043148), which is based on my thesis.

A similar negative result with early release of Iloprost was found by others in a rat fracture model (Dogan *et al.* 2014). The detrimental effect of suppressing the early pro-inflammatory phase in bone healing was also shown with the anti-inflammatory master regulator cytokine IL-10 (Chan *et al.* 2015). Due to these known reasons a study group with burst-like release was not included in this project to confirm this fact again, e.g. with Iloprost-loaded core-only fibrin in the osteotomy without a shell.

5.3.2.1 Adaptive immune cells

CD8+ cells are known to be unbeneficial for bone healing. At the early fracture side, the number of these cells was found to be strongly diminished with Iloprost (Fig. 4.24). This confirmed the *in vitro* proliferation data for CD8+ cells. The CD4+ fraction contains pro- and anti-inflammatory T cells, such as T helper cells and Treg, respectively. Interestingly, also CD4+ cell numbers were significantly reduced, indicating the broad suppressive effect of Iloprost onto immune cells. Considering the number of cells in distinct T cell populations, ~2.5 % for CD8+ and 1.5 % for CD4+ is typically found in resting bone marrow in mice (Zeng *et al.* 2002; Mazo *et al.* 2005). Here, in the case of the early regeneration phase, after the peak pro-inflammatory response, detected numbers, for instance in vehicle control, almost doubled. Furthermore, in bone marrow CD8+ cells have a ratio of 2:1 towards CD4+ cells usually. This is the opposite for peripheral blood or spleen. During the healing process this ratio, however, was approximately 1.3:1 in the treatment group and 1.6:1 in the control group. Hence, in this osteotomy model, the CD4+ cells are still outnumbered by the CD8+ cells, but the latter are more effected by the PGI_2 treatment.

In vitro data showed a significant reduction in CD8+ cells in direct response to Iloprost, which was confirmed in the delayed drug release in the osteotomy model. Additionally, the activity of this cell type was significantly reduced at the early fracture side after the Iloprost application. Pro-inflammatory CD8+ showed peak activity *in vivo* and their secreted IFN-γ was detectable immunohistochemically (Fig. 4.25). The *in vitro* data had confirmed the detrimental effect of the pro-inflammatory cytokine IFN-γ onto osteogenic differentiation and cell viability. *In vivo*, the overall number of IFN-γ+ cells was significantly diminished in the treatment group at 3 dpo at the fracture site.

The OCN+ relative osteoblast numbers were not changed significantly at this early time point of 3 dpo with Iloprost. Furthermore, this was expected, since direct application of the drug onto osteogenic differentiation did not show efficacy as well *in vitro*.

Treg cells were not investigated further *in vivo*, since they only responded positive to Iloprost on basal levels of non-activated cells. Moreover, the numbers of endogenous Treg are potentially low at the early stage of inflammation in bone healing, considering 0.5 % in homeostatic BM. However, future studies could include histologic analysis of the transcription factor FoxP3, which is a characteristic marker for Treg. Since transcription factors can be challenging in immunohistochemistry and harsh epitope retrieval on the here used adhesive filmstrips is not recommended, alternative markers for Treg could be the combination of the surface markers CD4+CD25++. The histology, as well as, the FACS analysis of bone marrow revealed a marginal fraction of cells that were double-positive for CD8 and CD4. The function of these cells is not completely revealed yet, however they account mainly for immature T cells that can be found in blood and peripheral lymphoid tissues (Coles & Raulet 2000; Overgaard *et al.* 2015).

5.3.2.2 Innate immune cells

Furthermore, the impact onto the polarization of CD68+ macrophages was investigated with the markers CD80 and CD206 to distinguish M1- and M2-types, respectively (Fig. 4.26). Macrophages make up a substantial fraction of 20 – 30 % of mononuclear cells in the BM (Gabrilovich & Nagaraj 2009). In addition, here, CD68+ cells occupied up to 24 % of the regenerating area. However, with the therapeutic approach this number dropped to 19 %. In particular, the treatment reduced pro-inflammatory M1 macrophages. Interestingly, the number of anti-inflammatory M2 macrophages was elevated with Iloprost. This is in contrast to the general observations that Iloprost was suppressing pro- and anti-inflammatory activated cells. However, a stimulation of M2 macrophages with this compound was also seen in cell culture, as described above. Hence, macrophage polarization appears to be affected by Iloprost in the way that pro-inflammatory types are suppressed, whereas anti-inflammatory types are stimulated. These M2-type macrophages can suppress inflammation further to add to the ultimate cease of inflammation in the callus. Furthermore, the lack of additional stimulation of matrix remodeling M2-type macrophages in the vehicle control groups could be an explanation for the signs of emerging pseudoarthrosis in this group after 21 dpo. In particular, the high amount of dense exogenous fibrin of the release system appears to be challenging for the regeneration process itself and requiring additional matrix degrading cells.

Previously, we discussed the role of M2-type macrophages in the endochondral phases of bone healing, in which the tissue is reconstructed via intensive remodulation of weight bearing structural tissue types such as condrogenic and calcified matrices (Schlundt *et al.* 2015). M2 macrophages are essential in these tissue-reorganizing events, due to their resorbing abilities, enabled by secretion of protein digesting enzymes. To investigate the impact of Iloprost treatment onto the remodeling facet of macrophages, cathepsin K (CTSK) was detected and quantified (Fig. 4.27). CTSK is a lysosomal cysteine protease, which is secreted by macrophages and by osteoclasts in bone tissue (Buhling *et al.* 2001). On the one hand, the anti-inflammatory action of Iloprost treatment was confirmed again *in vivo* with reduced number of M1 macrophages, which were highly active and positive for CD68 and TNF-α. The anti-inflammatory CD68+CTSK+ M2 macrophages, on the other hand, were tendency-wise more abundant after the pharmacologic treatment.

Taken together, the effects seen in immune cell numbers at 3 dpo appear to be due to the anti-inflammatory effect of Iloprost and the investigated cellular pattern is typical for a more advanced stage of the anti-inflammatory phase compared to vehicle control.

5.3.2.3 Revascularization

Revascularization is essential for successful bone repair (Keramaris et al. 2008)(Schmidt-Bleek *et al.* 2015). Hence, potential effects of the PGI_2 analog onto angiogenesis at the early time point of 3 dpo

wear analyzed with the blood vessel marker laminin. Laminin staining revealed a positive tendency of up-regulation for the Iloprost treated group. The positive trend with Iloprost is in line with the fact that a shortening of the pro-inflammatory phase is beneficial for blood vessel re-growth during fracture healing (Schmidt-Bleek *et al.* 2015). In particular, only after the peak pro-inflammatory phase, revascularization can commence. As stated above, a clear shift from a pro- to an anti-inflammatory pattern was detected in immune cell numbers at 3 dpo at the fracture site after decelerated release of Iloprost.

Furthermore, the observed tendency for increased laminin detection might be due to other secondary effects, such as the general advancement of the regenerative process in the Iloprost treatment group compared to control. For instance, neo-vascularization is following migrating osteoprogenitors during fracture repair and developing bone (Maes *et al.* 2010). Potentially, the time point was too early to reveal a clear therapeutic effect of Iloprost onto abundance of new blood vessels. In general, the expressions of angiogenic factors such as VEGF, PDGF, HIF1α and HMOX1 are only reaching peak up-regulation levels between 2 to 3 days in the process. Interestingly, a stronger expression at the proximal site of the osteotomy was apparent (Fig. 4.28 A). This could be due to a stronger blood pressure from the proximal site, which might supports revascularization at this site more effectively with nutrition and oxygen.

PGI_2 appears to be required for blood vessel growth. However, the potential of exceeding this process by additional PGI_2 is not reported. In a study utilizing chick embryos chorioallantoic membrane (CAM) assays, treatment with Iloprost did not show any angiogenic effects nor *in vitro* with HUVECs (Doganci *et al.* 2015). However, it was reported that PGI_2 induced persistent angiogenic effects in endothelial progenitor cells and mediated potent circulation recovery in an ischemic hind limb model (Aburakawa et al. 2013). Furthermore, the PGI_2-IP system was found to be essential for endothelial progenitor cells to accomplish their function and critical in negative regulation of vascular remodeling (Kawabe *et al.* 2010). In another study, inactivation of COX-1 impaired tube formation and cell proliferation (He *et al.* 2008). These endogenous processes were rescued by the treatment with Iloprost or the selective peroxisome proliferator–activated receptor-δ (PPARδ) agonist GW501516. It appears that any further positive stimulatory effects of PGI_2 on vessel formation are indirect.

Of note is that blood vessels are already a strong source of the endogenous version of this signaling molecule. For instance, it could be shown that angiogenesis induced by inflammation of the central nervous system promoted neuronal remodeling through capillary endothelial cell-derived PGI_2 (Muramatsu *et al.* 2012). In clinics, the edema-reducing effect of Iloprost, e.g. in avascular necrosis of the proximal femur, is based on a reduction of hydrostatic pressure in the area of the venous branches of the terminal vascular bed and not directly based on stimulation of angiogenesis (Disch *et al.* 2005).

5.3.3 Systemic effects

The systemic effect of the local delivery of Iloprost in the osteotomy model was evaluated in bone marrow of uninjured bone tissue for individual mice. These bone tissues included humeri, tibia and the contralateral femur. As expected, FACS analysis of T cell subpopulations revealed no immunomodulatory systemic effects onto these populations. Hence, the beneficial effect of local drug delivery over systemic application could be achieved in this project. The immune modulation occurred exclusively at the desired site, i.e. the regenerating tissue. This was significantly detectable at 3 dpo by quantitative immunohistochemistry of immune cells and cytokines, such as CD8+, CD4+, macrophage subsets, TNF-α and IFN-γ. Hence, with this local delivery approach the risk of negative systemic side effects is reduced, additionally due to reduced doses of drug that are required. Besides the fact that a long-term systemic suppression of the immune system can be a risk for patients, especially the aged ones, other risks of negative side effects would comprise potentially too low blood pressures of this vasodilator.

Interestingly, the regeneration process itself showed to have an impact on a view regarded subpopulations in uninjured BM. This was the case for NK1.1+ natural killer cells. The NK1.1+CD3- fraction was increased at the early inflammatory time point of 3 dpo compared to the later time point of 21 dpo, whereas the NK1.1+CD3+ cells were reduced in numbers at 3 dpo. This is indicating a potential systemic activation of proliferation of NK1.1+CD3- cells during the pro-inflammatory phase of bone healing, ensued by a differentiation towards NK1.1+CD3+ cells during the course of regeneration. Moreover, the CD62L- effector subset of the CD4+CD44+ memory T cells was increased after 21 days of regeneration in uninjured bone marrow compared to the status at 3 days. This was expected and indicates that the T_{EM}, which are CD62L-, had been activated by the regenerative process to migrate to the inflamed tissue and conduct immediate effector functions. Apparently, T_{EM} still resided in increased numbers in the body of the animals at 21 dpo. In contrast, CD62L+ T_{CM}, which are found in the lymph nodes and peripheral circulation, appeared to be unaffected in their numbers, at least at the observed early and late time points. However, T_{CM} home to secondary lymphoid organs, including the BM, to conduct their functions. Proliferated T_{CM} might have all differentiated into T effector cells. However, these processes were not affected by local application of Iloprost at the fracture site.

6. Summary and conclusion

The work presented in this thesis has shown that delayed local delivery of the PGI_2 analog Iloprost during the initial inflammatory phases can augment bone regeneration, and was published partially this year (Wendler *et al.* 2019).

The pro-inflammatory phase induces the regenerative process of the bone tissue. However, its termination is a prerequisite for the subsequent reconstructive phases and for the final healing outcome. This termination is achieved in the anti-inflammatory phase. In the clinics, patients who suffer from delayed healing or even non-unions often show a too pronounced fracture-induced inflammation. For instance, CD8+ T_{EMRA} titers can be used as diagnostic tool for an impaired healing process in fracture patients. Hence, a shortening – but not prevention – of the pro-inflammatory phase with administration of anti-inflammatory drugs, such as Iloprost, could represent an elegant therapeutic strategy.

Therefore, *in vitro* drug dose testing was performed on activated T cells in BM cell suspension to find optimal cytokine reduction. The most efficacious concentration inhibited pro-inflammatory CD8+ proliferation and suppressed M1-type macrophage polarization. Furthermore, anti-inflammatory M2-type macrophage polarization could be further stimulated with the synthetic PGI_2, which was shown in elevated IL-10 secretion. Furthermore, the stimulation of enriched Treg with the drug could be achieved, which also secreted higher levels of anti-inflammatory cytokine. Cytokines of activated T cells in whole bone marrow, as well as, isolated CD8+ and Treg had inhibitory effects onto osteogenic differentiation, when conditioned media of respective cells were added to osteogenically induced MSCs during indirect co-cultures. Iloprost could significantly reduce these inflammatory effects of cytokine enriched media onto osteolineage differentiation and furthermore on apoptosis induction. Direct application of the PGI_2 analog onto osteogenic or chondrogenic differentiation did not impair the matrix formation of these processes. Therefore, the *in vitro* data confirmed the late pro-inflammatory phase and the anti-inflammatory phase as optimal target for the efficacy of Iloprost

For the *in vivo* proof of concept study, a local drug delivery system was designed with a biocompatible and degradable carrier, i.e. clinical grade fibrin. The two drugs were combined in a way that a desired decelerated release of the PGI_2 analog could be achieved to avoid impairments of hematoma formation of the anti-coagulating synthetic PGI_2 and to allow the first pro-inflammatory phase to commence to initiate the regeneration cascade. Therefore, to allow a delayed drug release, I designed the local delivery as such an empty shell of fibrin was modulated around a core of fibrin, which was loaded with Iloprost at the most efficacious *in vitro* tested dose. The presence of Iloprost and its vehicle solution did not significantly alter material properties of the fibrin carrier and therefore potentially not its stability *in vivo*.

HPLC/UV-derived kinetics of *in vitro* samples of Iloprost revealed a delayed major release of the drug with the fibrin-based core-shell system after 48 hours compared to only 24 hours with core alone. The

fibrin matrix collapsed in presence of proteinase K only after complete release of Iloprost in all test samples. Hence, biodegradability occurred, but was not a cause for the release and remaining material would make way for the reconstruction of endogenous tissue matrices during bone healing.

With delayed local drug delivery of Iloprost, a significantly elevated volume of newly formed calcified matrix was detected in the mouse osteotomy model after 21 dpo compared to the vehicle control. After the peak pro-inflammatory phase at 3 dpo fibrin carriers were clearly identifiable in the osteotomy gap, and did not show signs of degradation yet. However, in the 21 dpo groups the dense fibrin matrix of the drug carrier was dissolved. At this stage of regeneration, the treatment group showed superior endochondral tissue types compared to the control group, such as hypertrophic cartilage and mineralized tissue.

The hypothesis of this doctoral thesis was that the delayed local application of a PGI_2 analog shortens the inflammatory phase of bone healing and therefore accelerates the regenerative process. Confirming this hypothesis is the reduced number of pro-inflammatory CD8+ cells and M1-type macrophages in response to Iloprost treatment at 3 dpo, and the advanced endochondral phases at 21 dpo compared to control. Adding to the beneficial immune cell pattern by Iloprost application was the reduction of CD4+ cells at 3 dpo, whilst an increased abundance of anti-inflammatory M2 macrophages was detected. Furthermore, the TNF-α secreting CD68+ cell fraction, which reflects activated pro-inflammatory macrophages was reduced significantly at 3 dpo in response to the immune modulation. Table 6.1 is summarizing the major new findings gained with this thesis.

Taken together, strong immune modulation in support of fracture healing represents a pharmacologic alternative to growth factor applications, when a suitable phase during inflammation is targeted.

Prior knowledge	Gain of knowledge
In vivo fracture healing: - Early Iloprost administration unbeneficial - Early other pharmacologic immunosuppressor administration unbeneficial - Early macrophage depletion inhibitive - M2 macrophages beneficial - CD8+ cells unbeneficial	*In vivo* fracture healing: - Delayed Iloprost administration (+ 48 h) beneficial Cell numbers at 3 dpo with Iloprost: - Reduced: CD8+ cells, CD4+ cells, M1 macrophages, IFN-γ, TNF-α - Elevated: M2 macrophages
Local drug delivery: - Fibrin and Iloprost are hydrophobic - Core/shell systems modulate drug releases	Local drug delivery: - Core/shell system with fibrin decelerates Iloprost release
- Immunosuppression by (synthetic) PGI_2 in splenocytes, PBMCs, BM-DCs	- Immunosuppression by Iloprost in bone marrow (BM) cell suspension with T cell activation
- Immunosuppression by (synthetic) PGI_2 in alveolar, peritoneal and peripheral blood-derived macrophages - Iloprost increases M2 marker expression of alveolar macrophages	- Iloprost suppresses TNF-α secretion of BM-derived M1 macrophages - Iloprost increases IL-10 secretion of BM-derived M2 macrophages
Conditioned media of enriched Treg cultures: - High IL-10 secretion from activated Treg - High cAMP required by activated Treg - High doses of IL-10 suppress osteogenic differentiation *in vitro* - Early systemic Treg administration in fracture healing can be unbeneficial with experienced host immune system	Conditioned media of enriched Treg cultures: - Elevated IL-10 content with Iloprost by non-activated Treg - Inhibitive for activated Treg in osteogenic mineralization - Less inhibitive if prior Iloprost treatment with activated Treg

Table 6.1: Summary of major gain of knowledge aspects achieved with this thesis compared to prior knowledge.

7. Outlook

7.1 Drugs and cellular targets in osteoimmunology

An important overlooked aspect in research on fracture healing is the necessity of inflammation to initiate the regenerative process. Hence, many studies interpreted the effects of anti-inflammatory drugs as detrimental for fracture healing. This was reported for instance for NSAIDs when the daily administration started already before the induction of the fracture in pre-clinical models (Bergenstock *et al.* 2005; Lu *et al.* 2012; Chen & Dragoo 2013; Sandberg & Aspenberg 2015). As an important outlook of the osteoimmunological work described in this thesis, approved anti-inflammatory medications should be tested with delayed administration for potential off-label use in fracture regeneration. The wide range of immunosuppressive therapeutics that would be feasible for regeneration processes comprise corticosteroids, the mentioned NSAIDs, prostaglandins, antibodies and anti-inflammatory cells. Expected growth rates of 5.9 % from 2015 – 2020 of the market of anti-inflammatory therapeutics indicate spreading variety in established drugs with many patient years and increasing diagnosis rates of elevated states of the immune system (www.alliedmarketresearch.com). Besides the most efficient route of biomaterial based local drug delivery, for proof-of-concept studies, less elaborate techniques can be used such as injections into the system or directly into the callus.

In particular, further investigations of the PGI_2 signaling pathway to support fracture healing or at least osteogenic differentiation should include phosphodiesterase inhibitor IV, dibutyryl cAMP or other factors that augment directly or indirectly the activity of cAMP or the downstream product adenosine. Interesting would be to measure cAMP levels in isolated Treg in response to Iloprost. This could clarify how much further Treg could be stimulated by this drug.

In addition to directly or indirectly elevating cAMP levels the number of pharmacologic tools available for selective targeting of undesired immune responses has increased intensively within the last decades, which could be harnessed for musculoskeletal regeneration processes. In particular, numerous biologicals and antibodies that allow for selective depletion/inactivation of immune cell subsets, or their cytokines, are already available in the clinics or are in the developmental pipeline (Polk & Rosenwasser 2017). For example, monoclonal antibodies are applied in clinics for depleting T cells or their progenitors – the thymocytes. Other antibody-based immunologic therapies comprise blocking of APC/T cell interaction, depletion and inactivation of memory/effector T or B cells, or neutralizing cytokine signaling such as TNF-α. In addition, small molecules constitute strong tools that target T cell activation pathways such as calcineurine inhibitors and inhibitors of mTOR, or IL-2, which support anti-inflammatory Treg. Even direct targeting of gene expression via antisense oligonucleotides to RNA has reached the pharmacological market, such as mipomersen, which binds to the messenger RNA coding for apolipoprotein B-100 in homozygous familial hypercholesterolemia (Waldmann *et al.* 2017). On the one hand, micro RNAs (miRNAs) and small interfering RNAs (siRNAs) have not been developed

further past phase II trials, which target inflammatory factors, such as IL-4 and STAT-6 (Qiu *et al.* 2016). On the other hand, ongoing phase II trials for the siRNA ALN-CC5 targeting complement component C5 of the innate immunity, have shown promising results in myasthenia gravis (Kusner *et al.* 2019).

In animal experiments, non-depleting anti-CD4 monoclonal antibody is a powerful inducer of tolerance in transplant recipients. These antibodies block the activation of effector T cells but support the development of Treg (Sawitzki *et al.* 2004). *In vivo* depletion of CD8+ T cells showed positive results in fracture repair studies in porcine (Lohse *et al.* 2006) and rodent models (Kingsley *et al.* 2007; Reinke *et al.* 2013). Interestingly, adoptive transfer of Treg modulates an effector T cell mediated rejection of transplants or autoimmune reactions (van Maurik *et al.* 2002).

Another consideration for osteoimmunological therapies is that cellular immune modulation, e.g. via Treg, is only time independent if cells are not pre-activated and can be administered at 0 days post fracture, or in preclinical models before fracture induction (Liu *et al.* 2011). Activated Tregs, when administered systemically, would be comparable to early IL-10 administration and hence, would lead in the same way to an impaired healing outcome with high probability, due to the suppression of the early process-inducing pro-inflammatory phase (Chan *et al.* 2015). It appears that adaptive immune cells, especially T cells, fulfill a role of fine tuners in later stages of the endochondral regeneration (Toben *et al.* 2011). The potential positive effect of non-activated immune cells and their secreted cytokines on a basal level should be elucidated further.

Furthermore, quantification of endogenous Tregs during the process of fracture healing is required to be revealed to evaluate their role in this process. This is of particular importance, since differentiated Treg do not proliferate in contrast to their pro-inflammatory CD8+ counterpart in the T cell fraction of immune cells. However, rapid increase in numbers from their initial 0.5 % in bone marrow (Zeng *et al.* 2002; Zou *et al.* 2004), or infiltration from the circulation would be necessary to impact the short time frame of the inflammatory phases of bone healing starting directly after hematoma formation and lasting usually 1 week in young healthy individuals. For instance, the positive effects of TGF-β on fracture healing could be due to the stimulation of Treg, besides the stimulation of endochondral differentiation of MSCs. Of consideration is that systemic administration of Tregs show short-lived efficacy, since cells are cleared out of the system rapidly (Riley *et al.* 2009). This is the case also for MSC-based therapies and have similar efficacy and kinetics to signaling molecules and growth factors, however, with increased risks. Hence, signaling factors of such cell types are investigated as cell-free pharmacologic approach (Phinney & Pittenger 2017).

Further promising cell types in future osteoimmunological studies, especially for time-independent pharmacological intervention, are those of the innate immune system as we have shown with macrophages before (Schlundt *et al.* 2015). Burst-like release of M2-type inducing factors led to increased bone formation. Furthermore, neutrophils are important study objects in this research field

(Chan *et al.* 2015). Neutrophils are the most abundant leukocyte subset in the blood and initiate the inflammatory process in fracture healing. Hence, patients with insufficient neutrophils suffer from inadequate wound healing (Lekstrom-Himes & Gallin 2000). A similar case is observed in patients whose neutrophils are unable to adhere to the endothelium or ECM (van de Vijver *et al.* 2012). Well known is that pharmacologic G-CSF administration is stimulating neutrophils. Interestingly, daily administration of G-CSF starting 5 days prior to fracture induction significantly improved bone formation indicating time-independence of treatment as well (Herrmann *et al.* 2018).

Since the IP receptors are present on further multiple myeloid cell types including platelets, medullary thymocytes, dendritic cells and eosinophils, these cells could add to the mode of action investigated in this thesis (Dorris & Peebles 2012). As discussed, effects of PGI_2 and prostaglandins in general on osteogenic differentiation is not congruent to direct increase of cAMP, e.g. via db-cAMP. This phenomenon should be addressed in future studies to benefit from this alternative pathway to growth factor application for amelioration of chondrogenic and osteogenic differentiation.

Patient groups that could benefit from the here investigated therapeutic approach are basically all fracture patients. However, of particular need for anti-inflammatory treatment are fracture patients, who in particular, are compromised, i.e. with age-related reduced regenerative capacity, osteoporosis and additional co-morbidities, e.g. metabolic disorders such as diabetes and cachexia. These compromised conditions lead to higher incidences of delayed or incomplete posttraumatic musculoskeletal healing. Furthermore, patients could benefit, who have conditions of immune disbalances such as enhanced levels of CD8+ T_{EMRA} cells, e.g. due to their age-related matured immune systems (Reinke *et al.* 2013).

7.2 Transferability to other regenerative mechanisms

Cellular immune modulation, or more elegant drug-mediated immune modulation, in support of fracture healing can outline a blue print for other regenerative processes of the musculoskeletal apparatus, such as muscle injury and tendon rupture. This approach can be considered as an alternative to growth factor applications, which entail high-risk negative side effects. As recently described, the regenerative process of muscle tissue is similarly initiated by inflammatory phases compared to fractures (Sass *et al.* 2018). Moreover, comparing immune cell composition of fracture and muscle hematoma revealed that the compromising $CD8^+$ cytotoxic T cells stayed longer and in higher concentrations at the site of the muscle injury compared to the fracture hematoma (Schmidt-Bleek *et al.* 2009). This indicates that the muscle regeneration process constitutes an important target for immune modulation. In addition, the ratio between unbeneficial $CD8^+$ T cells and potentially beneficial $CD4^+$ T cells was elevated in the muscle in comparison to the fracture hematoma.

Interestingly, bone regeneration triggers central and peripheral neuropeptide Y (NPY) neuronal pathways (Alves *et al.* 2016). Little is known about the interplay of these two mechanisms, however, as

shown in a femoral-defect mouse model, the NPY system activity is increased and encompassing the inflammatory response and ossification phases. In addition, in another murine model for experimental autoimmune encephalomyelitis (EAE) it was shown that inhibition of IP receptor signaling impaired motor recovery, whereas the IP receptor agonist Iloprost promoted axonal remodeling and motor recovery (Muramatsu *et al.* 2012). This implies a need for further understanding of the mode of action of the beneficial effects for bone regeneration with Iloprost described in this thesis.

7.3 Further study of the core-shell system

Regarding the here described project, potential future studies could further explain and confirm the hypothesized mechanism of delayed local immune modulation. For chemical detection of the release of Iloprost from the drug carrier into the surrounding tissue at different time points HPLC analysis of extracted samples could be used, similar to the *in vitro* kinetics experiment. However, due to the smaller scales a more sensitive detector would be required, e.g. a mass spectrometric detector. This would suffice as long as a relatively wide spanning amount of tissue would be harvested around the drug carrier, since the mass spectrometric detector is also specific to the analyzed compound. Alternatively, the release system could be extracted and remaining retained drug quantified. The sensitivity of this detector would also reduce requirements of amounts of material and drug for further *in vitro* studies of drug release kinetics.

During *in vitro* assessments, the core material degraded significantly slower than shell and core-shell, which is most likely due to the higher protein content. If this lead in particular to an increase in fibril connections or thicker fibrils, would be interesting to learn via quantified imaging analysis of large groups of samples or even scanning electron microscope for three-dimensional spatial analysis. However, the effect in delay was not proportional to the higher protein content and the goal should be to reduce the amount of degradable material introduced into the fracture for minimal possible interference with the endogenous regeneration process.

The tendency of increased stiffness in fibrin when combined with Ilomedine could be analyzed in more depth. On the one hand, these changes in material properties are relevant in fracture therapies. On the other hand, for clinical studies it is a pre-requisite to investigate any potential properties of the combination of different drugs. In fact, authorities, such as the local *Bundesinstitut für Arzneimittel und Medizinprodukte* (BfArM), regard drugs that are mixed outside the patient's organism as completely new drugs with new potentially toxic side effects. This entails required pre-clinical investigations, such as ADME (absorption, distribution, metabolism, and excretion) for the combination of material and signaling molecule, which might alter each other chemically in an unwanted way, such as intrinsic physiochemical properties and non-covalent interaction of the carrier. For example, drug conjugation to the cysteine-34 position changes the endocytosis mechanism of serum albumin (Kratz 2008). Another

example is that chemical modification of hyaluronic acid influences the receptor-mediated uptake by cancer cells (Choi *et al.* 2012). Hence, chemical alterations of the drug or the carrier material, such as introduction of anchor molecules for delayed or inducible release, can delay translation of basic scientific findings into clinics for decades.

7.4 Biomaterials as drug carriers

In recent years, progress has been achieved in new technologies for controlled drug release, such as covalent linkage and physical encapsulation. However, biocompatibility of drugs and materials still remains an academic challenge and the recent 40 to 50 years did not change the basic investigated material sets. Improvements of clinical versatility have been incremental, such as higher purities and mass scale production. On the one hand, biocompatibility is a restricted concept and most chemically diverse materials have non-distinguishing immunologic foreign body responses, such as inflammation and encapsulation by macrophages (Brown *et al.* 2012b). On the other hand, biocompatibility is context specific, i.e. the same material can show diverging responses when placed into different host physiological milieus (Aamodt & Grainger 2016).

Natural biological carriers including proteins, such as fibrin and gelatin, and polysaccharides, such as alginate, have the advantage of good compatibility, biodegradability, non-toxicity and non-immunogenicity. Furthermore, the portfolio of deliverable substances is increasing steadily, comprising drugs, proteins, genes, imaging probes or living cells. However, clinicians require more versatile and tailorable properties, e.g. in terms of robustness, elasticity, inducible degradation and drug loading. So far, there is no “one-size-fits-all”-type of biomaterial existent.

Hence, to realize multiple functions an increasing scientific undertaking is existing in the field to develop combined applications of different biomacromolecules and synthetic polymers with the addition of organic nanoparticles in one carrier system. For instance, the synthetic polymer PLGA is well tolerated in fractured bone tissue (Suuronen *et al.* 2004), and in microsphere form, release kinetics of PLGA for synthetic PGI_2 can be tailored (Obata *et al.* 2008). Furthermore, there are still challenges to be solved related to production, quality control, storage, safety and selectivity of natural protein- and polysaccharide-based drug carriers. If enhanced stability towards proteolysis of protein-based carriers is desired, encapsulation methods, cross-linkers and protease inhibitors are investigated. Moreover, polysaccharide-based materials are explored to be altered for selective tissue distribution and cell type-specific targeting (Mo *et al.* 2016).

Taken together, research and development efforts of anti-inflammatory agents released from local delivery systems to target initial inflammation post-fracture is promising, and the modulation of the early phase typically coincides with the timing of surgical treatment. Therefore, a local application can be for instance envisioned by an injection of Iloprost into the site of the injury or by a transplantation of

a pharmacokinetically well-described combination of a hydrogel comprising the drug in proximity to the injured tissue after 24 hours.

8. Appendix

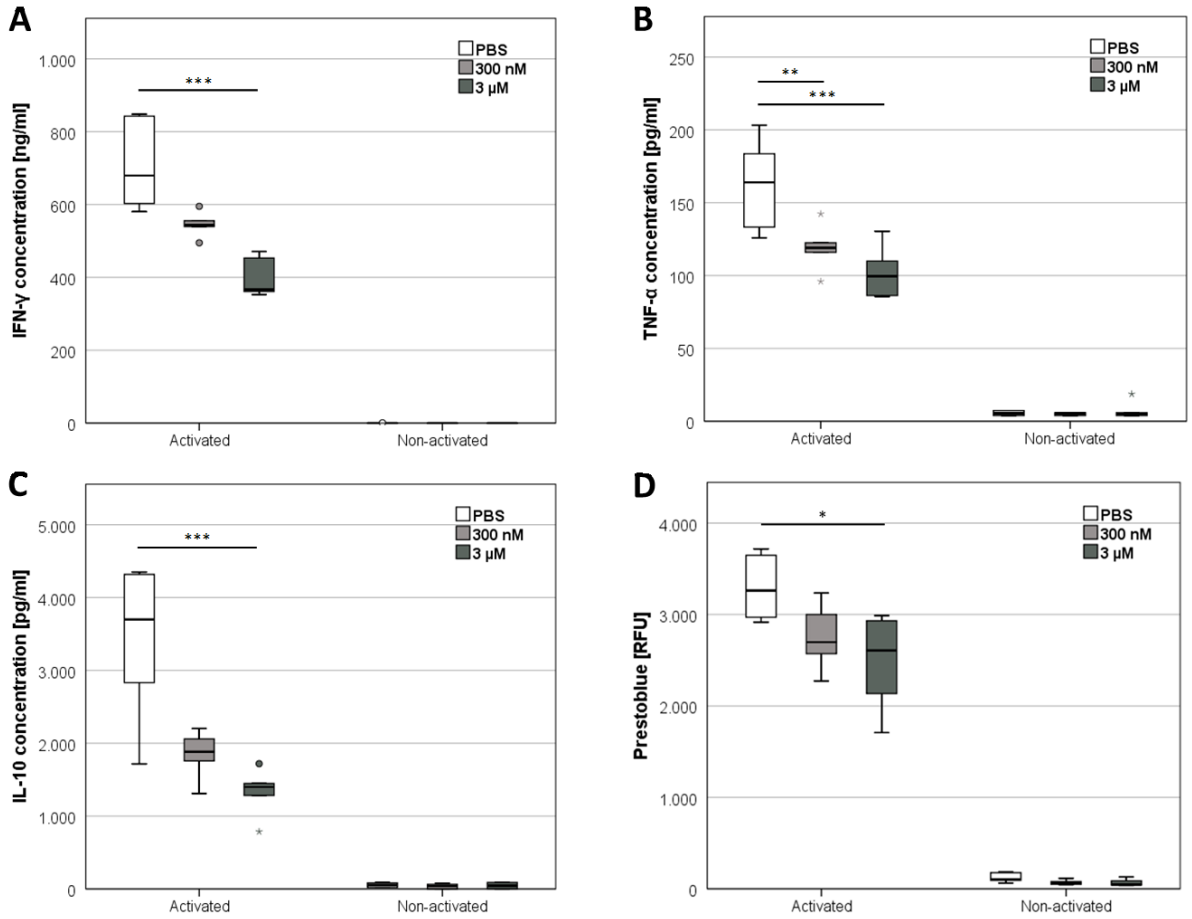

Figure 8.1: Anti-inflammatory effects of Iloprost on CD3/CD28-activated T cells in splenocytes. Confirmed anti-inflammatory property of Iloprost for secretion of (A) IFN-γ, (B) TNF-α and (C) IL-10. (D) Metabolic cell activity was also reduced by Iloprost in the activated T cells. Multiple comparison, n = 6, ***: $p \leq 0.0005$; **: $p \leq 0.005$; *: $p \leq 0.05$.

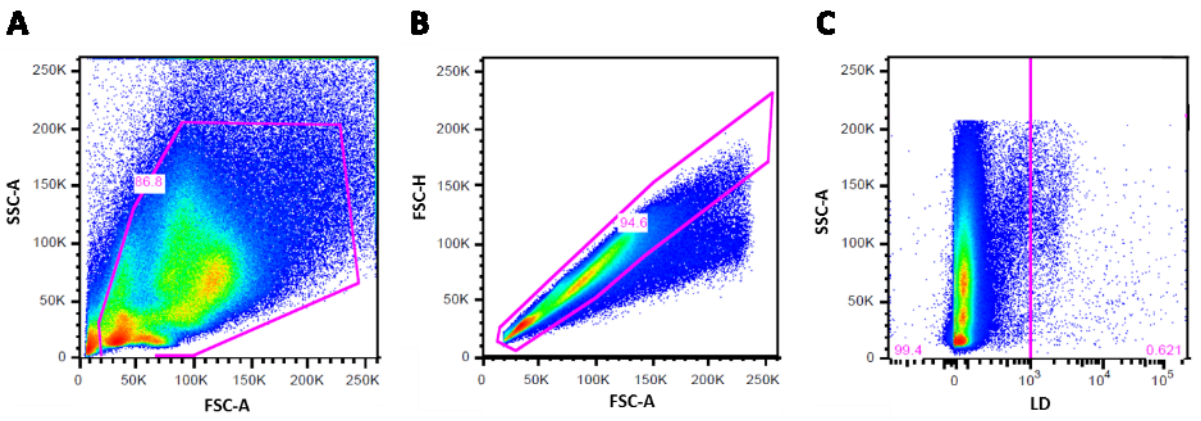

Figure 8.2: General initial gating strategy of FACS analyses depicted with cells collected from bone marrow. (A) Classifying signals towards size and granularity of cells with forward scatter (FSC) and sideward scatter (SSC), respectively. (B) Subsequent gating for single cells with FSC signal height (FSC-H) versus signal area (FSC-A). (C) Out of this population living cells were further analyzed, which were negative for Live/Dead staining (LD).

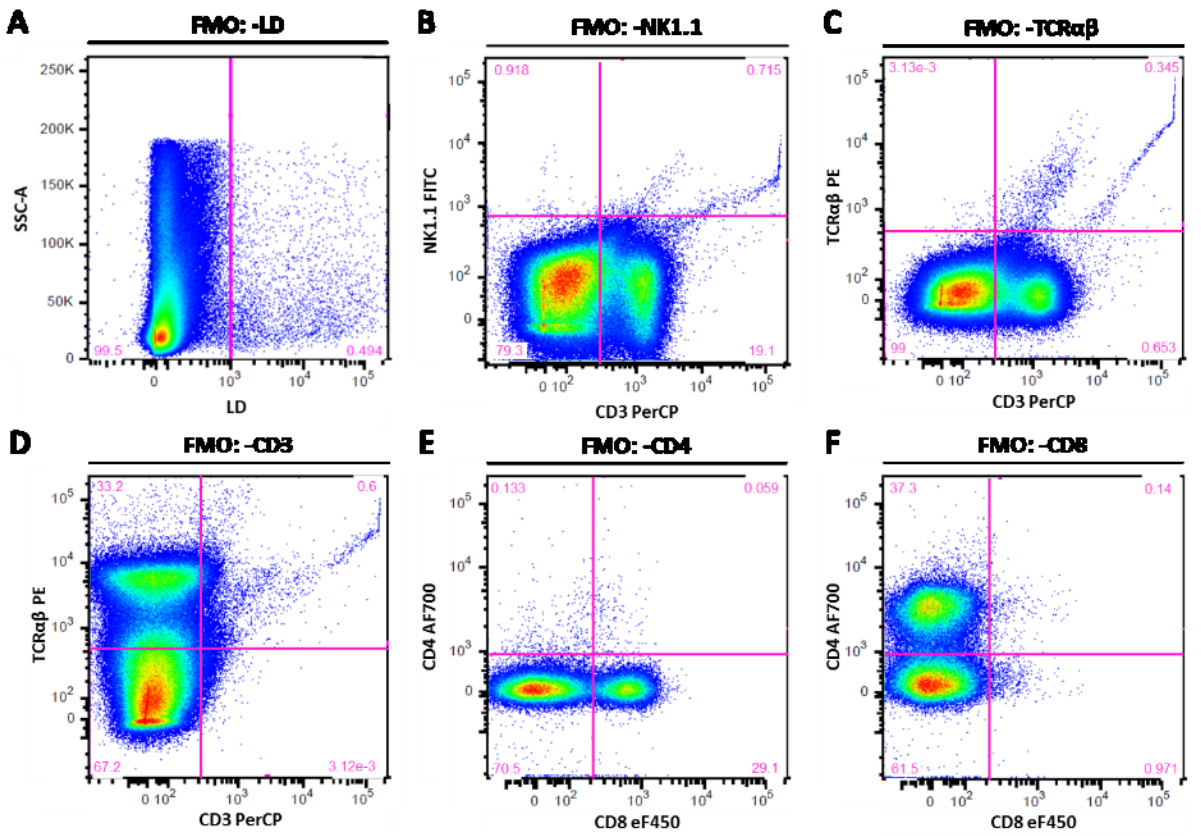

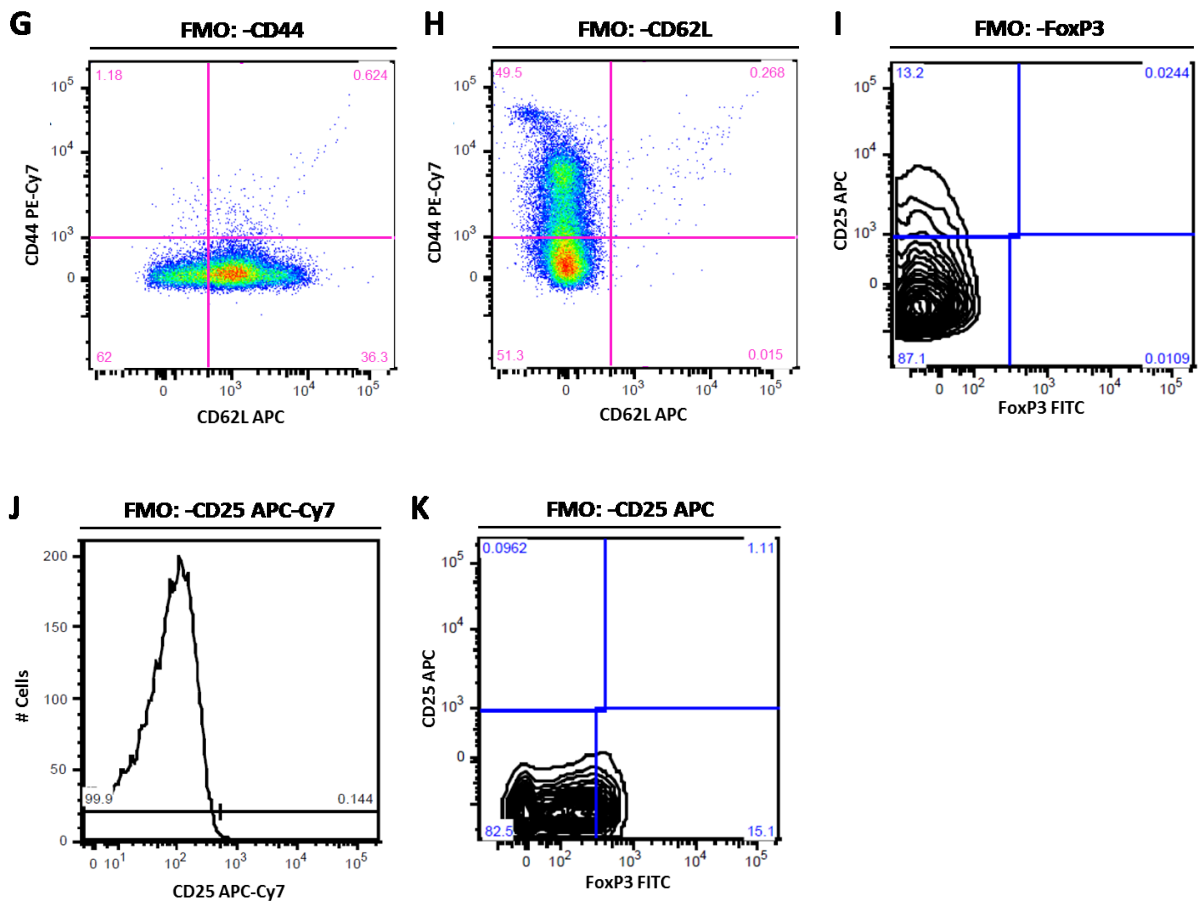

Figure 8.3: Displayed are dot plots, histograms or density plots of fluorescence minus one (FMO) staining control signals with bone marrow cells of all utilized FACS markers. (A) –Live/Dead, (B) –NK1.1, (C) –TCRαβ, (D) –CD3, (E) –CD4, (F) –CD8, (G) –CD44, (H) –CD62L, (I) –FoxP3. FMOs for the both anti-CD25 antibodies (J) –CD25 APC-Cy7 and (K) –CD25 APC.

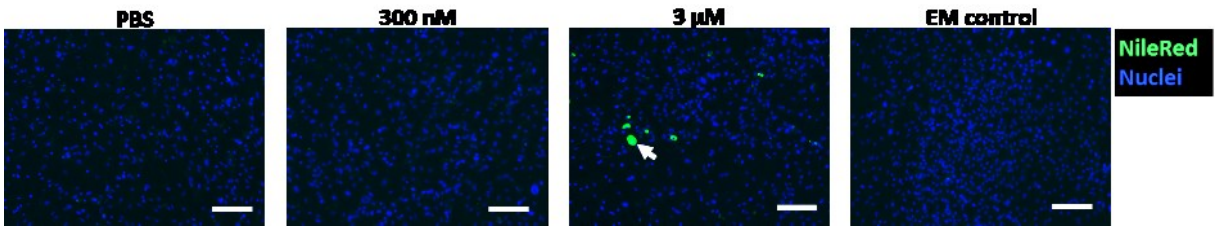

Figure 8.4: Fluorescence images of Nile Red stained MSC monolayers after incubation with osteoinductive media for 14 days. White arrow marks adipogenic vesicle, which occurred sporadically in the highest dose of 3 µM. Scale bars equal 200 µm.

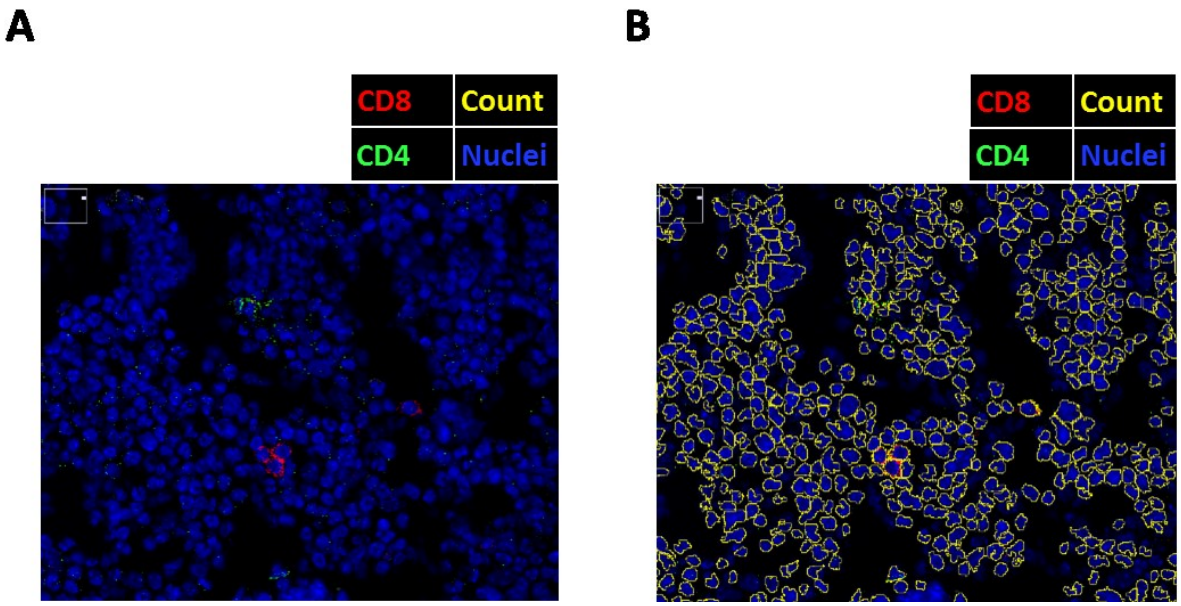

Figure 8.5: Example of cell identification and quantification in fluorescence images. (A) An immunohistochemistry image of a cryosection of BM with stained CD8+ and CD4+ cells and nuclei. (B) Same image with overlayed masks with identified regions of interest via ImageJ. This mask was overlayed onto separate channels to quantify pixel intensity of each marker for each identified cell.

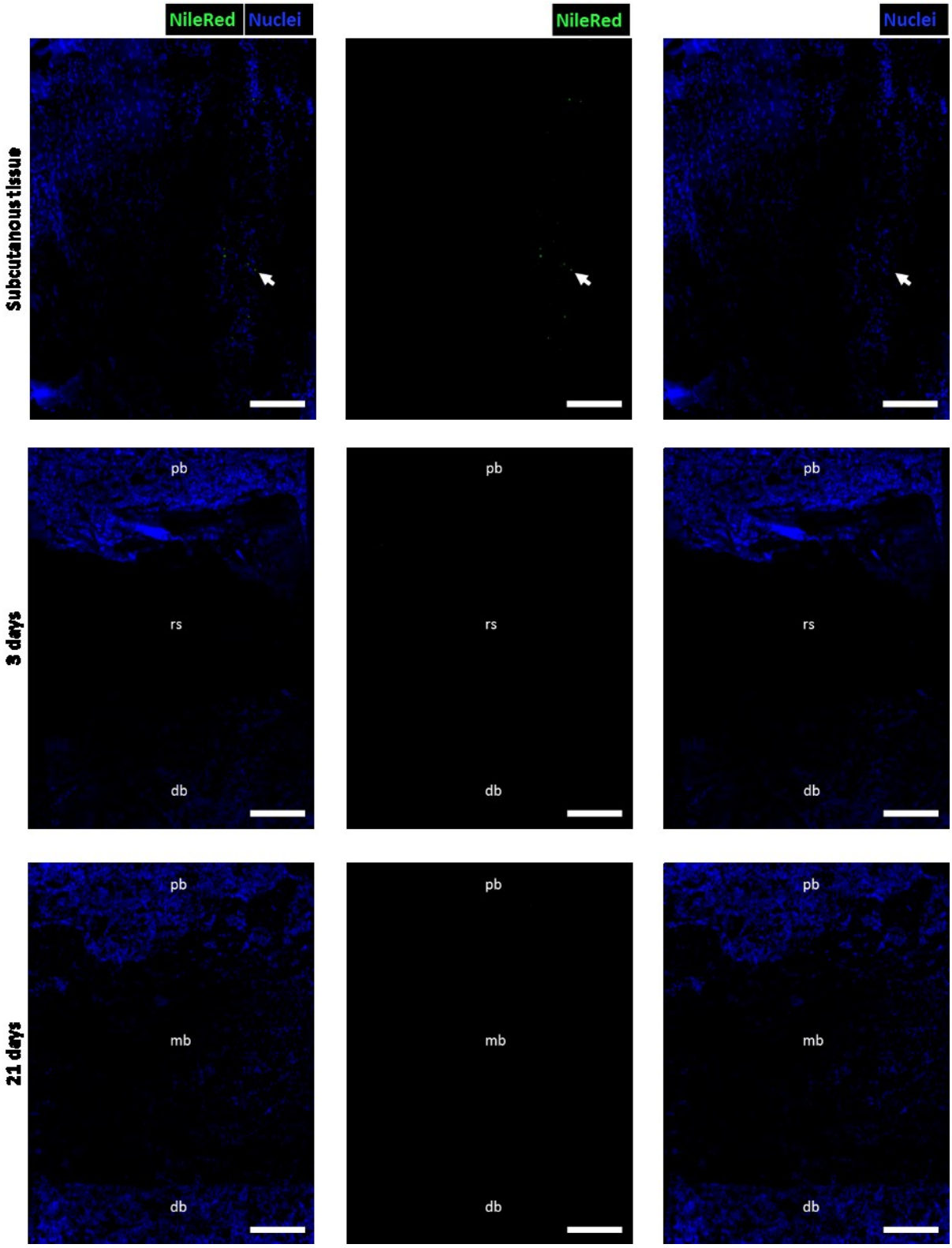

Figure 8.6: Nile Red staining on cryo-sections of fractures after 3 and 21 dpo. Fractures had received local Iloprost delivery. No adipose vesicles could be detected in any sample. Subcutaneous tissue (between muscle and skin tissue) was used as positive staining control. There, white arrow indicates exemplary stained vesicles. Mineralized bone (mb), proximal bone marrow (pb), distal bone marrow (db), scale bars equal 200 µm.

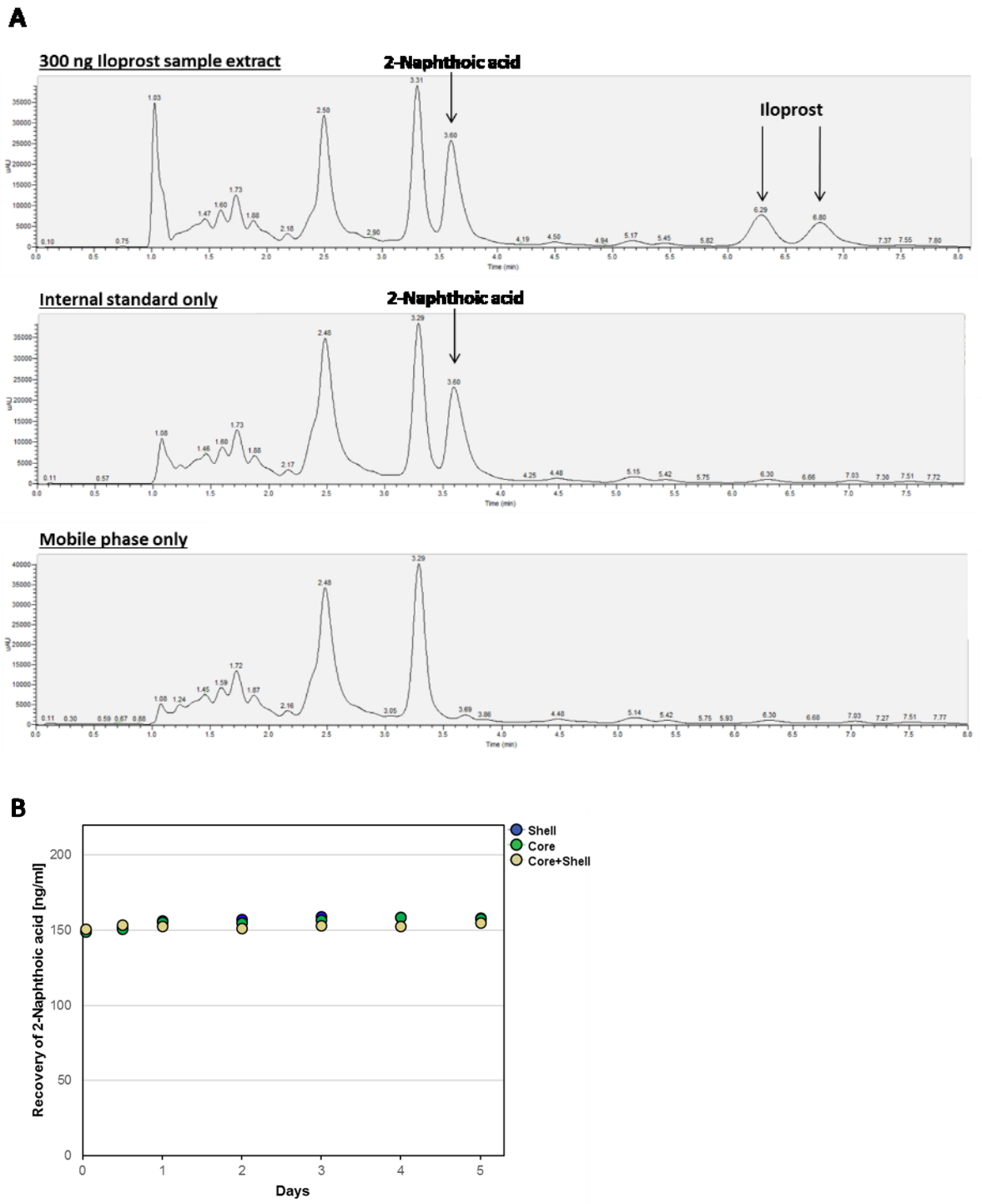

Figure 8.7: Positive and negative controls for the quantification of Iloprost via RP-HPLC/UV. (A) Exemplary chromatograms of 300 ng Iloprost sample detection via RP-HPLC/UV. Iloprost exists as two diastereoisomers, and hence, has a double-peak at retention times ~6.30 and ~6.80 min. 2-NA, which was added to each harvested sample of the release experiment was detected at ~3.60 min. Additionally, chromatograms are displayed of 2-NA alone and with mobile phase only. (B) Internal standard control. Quantification of the area under the 2-NA peak revealed a stable concentration of ~150 ng/ml for each fibrin composition and time point.

9. References

Aamodt JM , Grainger DW (2016). Extracellular matrix-based biomaterial scaffolds and the host response. *Biomaterials*. **86**, 68-82.

Aburakawa Y, Kawabe J, Okada M, Yamauchi A, Asanome A, Kabara M, Matsuki M, Takehara N, Nakagawa N, Okumura S, Minami Y, Mizukami Y, Yuhki K, Ushikubi F , Hasebe N (2013). Prostacyclin stimulated integrin-dependent angiogenic effects of endothelial progenitor cells and mediated potent circulation recovery in ischemic hind limb model. *Circulation Journal: Official Journal of the Japanese Circulation Society*. **77**, 1053-1062.

Aggarwal S , Pittenger MF (2005). Human mesenchymal stem cells modulate allogeneic immune cell responses. *Blood*. **105**, 1815-1822.

Ahmad E, Fatima MT, Hoque M, Owais M , Saleemuddin M (2015). Fibrin matrices: The versatile therapeutic delivery systems. *International Journal of Biological Macromolecules*. **81**, 121-136.

Ahmed TA, Dare EV , Hincke M (2008). Fibrin: a versatile scaffold for tissue engineering applications. *Tissue engineering. Part B, Reviews*. **14**, 199-215.

Ai-Aql ZS, Alagl AS, Graves DT, Gerstenfeld LC , Einhorn TA (2008). Molecular mechanisms controlling bone formation during fracture healing and distraction osteogenesis. *Journal of Dental Research*. **87**, 107-118.

Aigner N, Petje G, Schneider W, Meizer R, Wlk M, Kotsaris S, Knahr K , Landsiedl F (2005). Bone marrow edema syndrome of the femoral head: treatment with the prostacyclin analogue iloprost vs. core decompression: an MRI-controlled study. *Wiener klinische Wochenschrift*. **117**, 130-135.

Ait-Daoud N , Johnson BA (2000). Drugs, the Brain, and Behavior: the Pharmacology of Abuse and Dependence. Edited by John Brick and Carlton Erickson. 186 pp., illustrated. New York: Haworth Medical Press. *International Journal of Neuropsychopharmacology*. **3**, 87.

Alblowi J, Kayal RA, Siqueira M, McKenzie E, Krothapalli N, McLean J, Conn J, Nikolajczyk B, Einhorn TA, Gerstenfeld L , Graves DT (2009). High levels of tumor necrosis factor-alpha contribute to accelerated loss of cartilage in diabetic fracture healing. *The American Journal of Pathology*. **175**, 1574-1585.

Alexander KA, Chang MK, Maylin ER, Kohler T, Muller R, Wu AC, Van Rooijen N, Sweet MJ, Hume DA, Raggatt LJ , Pettit AR (2011). Osteal macrophages promote in vivo intramembranous bone healing in a mouse tibial injury model. *Journal of Bone and Mineral Research: the Official Journal of the American Society for Bone and Mineral Research*. **26**, 1517-1532.

Alkhatib K, Poseno TM, Diaz Perez A, Durdik JM , Stenken JA (2018). Iloprost Affects Macrophage Activation and CCL2 Concentrations in a Microdialysis Model in Rats. *Pharmaceutical Research*. **35**, 20.

Altman RD, Latta LL, Keer R, Renfree K, Hornicek FJ , Banovac K (1995). Effect of nonsteroidal antiinflammatory drugs on fracture healing: a laboratory study in rats. *Journal of Orthopaedic Trauma*. **9**, 392-400.

Alves CJ, Alencastre IS, Neto E, Ribas J, Ferreira S, Vasconcelos DM, Sousa DM, Summavielle T , Lamghari M (2016). Bone Injury and Repair Trigger Central and Peripheral NPY Neuronal Pathways. *PLOS ONE*. **11**, e0165465.

Anders S, Volz M, Frick H , Gellissen J (2013). A Randomized, Controlled Trial Comparing Autologous Matrix-Induced Chondrogenesis (AMIC(R)) to Microfracture: Analysis of 1- and 2-Year Follow-Up Data of 2 Centers. *The Open Orthopaedics Journal*. **7**, 133-143.

Andrew JG, Andrew SM, Freemont AJ , Marsh DR (1994). Inflammatory cells in normal human fracture healing. *Acta Orthopaedica Scandinavica*. **65**, 462-466.

Archer CB, Frohlich W, Page CW, Paul W, Morley J , MacDonald DM (1984). Synergistic interaction between prostaglandins and PAF-acether in experimental animals and man. *Prostaglandins*. **27**, 495-501.

Argintar E, Edwards S , Delahay J (2011). Bone morphogenetic proteins in orthopaedic trauma surgery. *Injury*. **42**, 730-734.

Aronoff DM, Peres CM, Serezani CH, Ballinger MN, Carstens JK, Coleman N, Moore BB, Peebles RS, Faccioli LH , Peters-Golden M (2007). Synthetic prostacyclin analogs differentially regulate macrophage function via distinct analog-receptor binding specificities. *Journal of Immunology*. **178**, 1628-1634.

Arrighi I, Mark S, Alvisi M, von Rechenberg B, Hubbell JA , Schense JC (2009). Bone healing induced by local delivery of an engineered parathyroid hormone prodrug. *Biomaterials*. **30**, 1763-1771.

Bacher N, Raker V, Hofmann C, Graulich E, Schwenk M, Baumgrass R, Bopp T, Zechner U, Merten L, Becker C , Steinbrink K (2013). Interferon-alpha Suppresses cAMP to Disarm Human Regulatory T Cells. *Cancer Research*. **73**, 5647-5656.

Bais MV, Wigner N, Young M, Toholka R, Graves DT, Morgan EF, Gerstenfeld LC , Einhorn TA (2009). BMP2 is essential for post natal osteogenesis but not for recruitment of osteogenic stem cells. *Bone*. **45**, 254-266.

Banchereau J, Briere F, Caux C, Davoust J, Lebecque S, Liu YJ, Pulendran B , Palucka K (2000). Immunobiology of dendritic cells. *Annual Review of Immunology*. **18**, 767-811.

Barbul A, Breslin RJ, Woodyard JP, Wasserkrug HL , Efron G (1989). The effect of in vivo T helper and T suppressor lymphocyte depletion on wound healing. *Annals of Surgery*. **209**, 479-483.

Barnes GL, Kostenuik PJ, Gerstenfeld LC , Einhorn TA (1999). Growth factor regulation of fracture repair. *Journal of Bone and Mineral Research: the Official Journal of the American Society for Bone and Mineral Research*. **14**, 1805-1815.

Baron R , Hesse E (2012). Update on bone anabolics in osteoporosis treatment: rationale, current status, and perspectives. *The Journal of Clinical Endocrinology and Metabolism*. **97**, 311-325.

Barry FP , Murphy JM (2004). Mesenchymal stem cells: clinical applications and biological characterization. *The International Journal of Biochemistry & Cell Biology*. **36**, 568-584.

Becker TC, Coley SM, Wherry EJ , Ahmed R (2005). Bone marrow is a preferred site for homeostatic proliferation of memory CD8 T cells. *Journal of Immunology*. **174**, 1269-1273.

Bergenstock M, Min W, Simon AM, Sabatino C , O'Connor JP (2005). A comparison between the effects of acetaminophen and celecoxib on bone fracture healing in rats. *Journal of Orthopaedic Trauma*. **19**, 717-723.

Bernardo ME , Fibbe WE (2013). Mesenchymal stromal cells: sensors and switchers of inflammation. *Cell Stem Cell*. **13**, 392-402.

Biondi M, Ungaro F, Quaglia F , Netti PA (2008). Controlled drug delivery in tissue engineering. *Advanced Drug Delivery Reviews*. **60**, 229-242.

Bolander ME (1992). Regulation of fracture repair by growth factors. *Proceedings of the Society for Experimental Biology and Medicine. Society for Experimental Biology and Medicine*. **200**, 165-170.

Bonewald LF (2011). The amazing osteocyte. *Journal of Bone and Mineral Research: the Official Journal of the American Society for Bone and Mineral Research*. **26**, 229-238.

Bopp T, Becker C, Klein M, Klein-Hessling S, Palmetshofer A, Serfling E, Heib V, Becker M, Kubach J, Schmitt S, Stoll S, Schild H, Staege MS, Stassen M, Jonuleit H , Schmitt E (2007). Cyclic adenosine monophosphate is a key component of regulatory T cell-mediated suppression. *The Journal of Experimental Medicine*. **204**, 1303-1310.

Boursinos LA, Karachalios T, Poultsides L , Malizos KN (2009). Do steroids, conventional non-steroidal anti-inflammatory drugs and selective Cox-2 inhibitors adversely affect fracture healing? *Journal of Musculoskeletal & Neuronal Interactions*. **9**, 44-52.

Bouxsein ML, Boyd SK, Christiansen BA, Guldberg RE, Jepsen KJ , Muller R (2010). Guidelines for assessment of bone microstructure in rodents using micro-computed tomography. *Journal of Bone and Mineral Research: the Official Journal of the American Society for Bone and Mineral Research*. **25**, 1468-1486.

Brandau S, Jakob M, Hemeda H, Bruderek K, Janeschik S, Bootz F , Lang S (2010). Tissue-resident mesenchymal stem cells attract peripheral blood neutrophils and enhance their inflammatory activity in response to microbial challenge. *Journal of Leukocyte Biology*. **88**, 1005-1015.

Breen A, Strappe P, Kumar A, O'Brien T , Pandit A (2006). Optimization of a fibrin scaffold for sustained release of an adenoviral gene vector. *Journal of Biomedical Materials Research Part A*. **78**, 702-708.

Breitbach M, Kimura K, Luis TC, Fuegemann CJ, Woll PS, Hesse M, Facchini R, Rieck S, Jobin K, Reinhardt J, Ohneda O, Wenzel D, Geisen C, Kurts C, Kastenmuller W, Holzel M, Jacobsen SEW , Fleischmann BK (2018). In Vivo Labeling by CD73 Marks Multipotent Stromal Cells and Highlights Endothelial Heterogeneity in the Bone Marrow Niche. *Cell Stem Cell*. **22**, 262-276 e267.

Brown BN, Londono R, Tottey S, Zhang L, Kukla KA, Wolf MT, Daly KA, Reing JE , Badylak SF (2012a). Macrophage phenotype as a predictor of constructive remodeling following the implantation of biologically derived surgical mesh materials. *Acta Biomaterialia*. **8**, 978-987.

Brown BN, Ratner BD, Goodman SB, Amar S , Badylak SF (2012b). Macrophage polarization: an opportunity for improved outcomes in biomaterials and regenerative medicine. *Biomaterials*. **33**, 3792-3802.

Bucher CH, Schlundt C, Wulsten D, Sass FA, Wendler S, Ellinghaus A, Thiele T, Seemann R, Willie BM, Volk HD, Duda GN , Schmidt-Bleek K (2019). Experience in the Adaptive Immunity Impacts Bone Homeostasis, Remodeling, and Healing. *Frontiers in Immunology*. **10**, 797.

Buhling F, Reisenauer A, Gerber A, Kruger S, Weber E, Bromme D, Roessner A, Ansorge S, Welte T , Rocken C (2001). Cathepsin K--a marker of macrophage differentiation? *The Journal of Pathology*. **195**, 375-382.

Burr SP, Dazzi F , Garden OA (2013). Mesenchymal stromal cells and regulatory T cells: the Yin and Yang of peripheral tolerance? *Immunology and Cell Biology*. **91**, 12-18.

Camacho M, Rodriguez C, Guadall A, Alcolea S, Orriols M, Escudero JR, Martinez-Gonzalez J , Vila L (2011). Hypoxia upregulates PGI-synthase and increases PGI(2) release in human vascular cells exposed to inflammatory stimuli. *Journal of Lipid Research*. **52**, 720-731.

Camacho M, Rodriguez C, Salazar J, Martinez-Gonzalez J, Ribalta J, Escudero JR, Masana L , Vila L (2008). Retinoic acid induces PGI synthase expression in human endothelial cells. *Journal of Lipid Research*. **49**, 1707-1714.

Campbell JP, Guy K, Cosgrove C, Florida-James GD , Simpson RJ (2008). Total lymphocyte CD8 expression is not a reliable marker of cytotoxic T-cell populations in human peripheral blood following an acute bout of high-intensity exercise. *Brain, Behaviour and Immunity*. **22**, 375-380.

Campbell PG, Durham SK, Hayes JD, Suwanichkul A , Powell DR (1999). Insulin-like growth factor-binding protein-3 binds fibrinogen and fibrin. *The Journal of Biological Chemistry*. **274**, 30215-30221.

Campbell RA, Overmyer KA, Selzman CH, Sheridan BC , Wolberg AS (2009). Contributions of extravascular and intravascular cells to fibrin network formation, structure, and stability. *Blood*. **114**, 4886-4896.

Canciglia A, Mandolfino T , D'Alfonso M (2011). The efficacy of Iloprost for the treatment of chronic venous ulcers of the lower limbs. *Il Giornale di chirurgia*. **32**, 434-437.

Cao Y, Wang B, Wang Y , Lou D (2014). Dual drug release from core-shell nanoparticles with distinct release profiles. *Journal of Pharmaceutical Sciences*. **103**, 3205-3216.

Capila I , Linhardt RJ (2002). Heparin-protein interactions. *Angewandte Chemie, International Edition*. **41**, 391-412.

Capretto L, Mazzitelli S, Luca G , Nastruzzi C (2010). Preparation and characterization of polysaccharidic microbeads by a microfluidic technique: application to the encapsulation of Sertoli cells. *Acta Biomaterialia*. **6**, 429-435.

Carragee EJ, Chu G, Rohatgi R, Hurwitz EL, Weiner BK, Yoon ST, Comer G , Kopjar B (2013). Cancer risk after use of recombinant bone morphogenetic protein-2 for spinal arthrodesis. *The Journal of Bone and Joint Surgery. American Volume*. **95**, 1537-1545.

Carroll SH , Ravid K (2013). Differentiation of mesenchymal stem cells to osteoblasts and chondrocytes: a focus on adenosine receptors. *Expert Reviews in Molecular Medicine*. **15**, e1.

Cassatella MA, Mosna F, Micheletti A, Lisi V, Tamassia N, Cont C, Calzetti F, Pelletier M, Pizzolo G , Krampera M (2011). Toll-like receptor-3-activated human mesenchymal stromal cells significantly prolong the survival and function of neutrophils. *Stem Cells*. **29**, 1001-1011.

Caza T , Landas S (2015). Functional and Phenotypic Plasticity of CD4(+) T Cell Subsets. *BioMed Research International*. **2015**, 521957.

Ceradini DJ, Kulkarni AR, Callaghan MJ, Tepper OM, Bastidas N, Kleinman ME, Capla JM, Galiano RD, Levine JP , Gurtner GC (2004). Progenitor cell trafficking is regulated by hypoxic gradients through HIF-1 induction of SDF-1. *Nature Medicine*. **10**, 858-864.

Challier J, Bruniquel D, Sewell AK , Laugel B (2013). Adenosine and cAMP signalling skew human dendritic cell differentiation towards a tolerogenic phenotype with defective CD8(+) T-cell priming capacity. *Immunology*. **138**, 402-410.

Chan JK, Glass GE, Ersek A, Freidin A, Williams GA, Gowers K, Espirito Santo AI, Jeffery R, Otto WR, Poulsom R, Feldmann M, Rankin SM, Horwood NJ , Nanchahal J (2015). Low-dose TNF augments fracture healing in normal and osteoporotic bone by up-regulating the innate immune response. *EMBO Molecular Medicine*. **7**, 547-561.

Chapman WC, Lockstadt H, Singla N, Kafie FE , Lawson JH (2006). Phase 2, randomized, double-blind, placebo-controlled, multicenter clinical evaluation of recombinant human thrombin in multiple surgical indications. *Journal of Thrombosis and Haemostasis*. **4**, 2083-2085.

Chaudhry A , Rudensky AY (2013). Control of inflammation by integration of environmental cues by regulatory T cells. *The Journal of Clinical Investigation*. **123**, 939-944.

Chen MR , Dragoo JL (2013). The effect of nonsteroidal anti-inflammatory drugs on tissue healing. *Knee Surgery, Sports Traumatology, Arthroscopy*. **21**, 540-549.

Chen Y , Alman BA (2009). Wnt pathway, an essential role in bone regeneration. *Journal of Cellular Biochemistry*. **106**, 353-362.

Cheng L, Hammond H, Ye Z, Zhan X , Dravid G (2003). Human adult marrow cells support prolonged expansion of human embryonic stem cells in culture. *Stem Cells*. **21**, 131-142.

Chernykh ER, Shevela EY, Starostina NM, Morozov SA, Davydova MN, Menyaeva EV , Ostanin AA (2016). Safety and Therapeutic Potential of M2 Macrophages in Stroke Treatment. *Cell Transplantation*. **25**, 1461-1471.

Chinnadurai R, Copland IB, Garcia MA, Petersen CT, Lewis CN, Waller EK, Kirk AD , Galipeau J (2016). Cryopreserved Mesenchymal Stromal Cells Are Susceptible to T-Cell Mediated Apoptosis Which Is Partly Rescued by IFNgamma Licensing. *Stem Cells*. **34**, 2429-2442.

Cho TJ, Gerstenfeld LC , Einhorn TA (2002). Differential temporal expression of members of the transforming growth factor beta superfamily during murine fracture healing. *Journal of Bone and Mineral Research: the Official Journal of the American Society for Bone and Mineral Research*. **17**, 513-520.

Choi KY, Saravanakumar G, Park JH , Park K (2012). Hyaluronic acid-based nanocarriers for intracellular targeting: interfacial interactions with proteins in cancer. *Colloids and Surfaces B: Biointerfaces*. **99**, 82-94.

Chung R, Cool JC, Scherer MA, Foster BK , Xian CJ (2006a). Roles of neutrophil-mediated inflammatory response in the bony repair of injured growth plate cartilage in young rats. *Journal of Leukocyte Biology*. **80**, 1272-1280.

Chung SJ, Lee JH, Kim SJ, Kwun BD , Lee MC (2006b). Subdural hematoma in spontaneous CSF hypovolemia. *Neurology*. **67**, 1088-1089.

Chung TW, Yang MC , Tsai WJ (2006c). A fibrin encapsulated liposomes-in-chitosan matrix (FLCM) for delivering water-soluble drugs. Influences of the surface properties of liposomes and the crosslinked fibrin network. *Int J Pharm*. **311**, 122-129.

Cipitria A, Boettcher K, Schoenhals S, Garske DS, Schmidt-Bleek K, Ellinghaus A, Dienelt A, Peters A, Mehta M, Madl CM, Huebsch N, Mooney DJ , Duda GN (2017). In-situ tissue regeneration through SDF-1alpha driven cell recruitment and stiffness-mediated bone regeneration in a critical-sized segmental femoral defect. *Acta Biomaterialia*. **60**, 50-63.

Claes L, Recknagel S , Ignatius A (2012). Fracture healing under healthy and inflammatory conditions. *Nature Reviews. Rheumatology*. **8**, 133-143.

Clements JR, Carpenter BB , Pourciau JK (2008). Treating segmental bone defects: a new technique. *The Journal of Foot and Ankle Surgery: Official Publication of the American College of Foot and Ankle Surgeons*. **47**, 350-356.

Coles MC , Raulet DH (2000). NK1.1+ T cells in the liver arise in the thymus and are selected by interactions with class I molecules on CD4+CD8+ cells. *Journal of Immunology*. **164**, 2412-2418.

Colnot C, Huang S , Helms J (2006). Analyzing the cellular contribution of bone marrow to fracture healing using bone marrow transplantation in mice. *Biochemical and Biophysical Research Communications*. **350**, 557-561.

Cortellini P, Pini Prato GP , Tonetti MS (1995). No detrimental effect of fibrin glue on the regeneration of intrabony defects. A controlled clinical trial. *Journal of Clinical Periodontology*. **22**, 697-702.

Costa MHG, de Soure AM, Cabral JMS, Ferreira FC , da Silva CL (2018). Hematopoietic Niche - Exploring Biomimetic Cues to Improve the Functionality of Hematopoietic Stem/Progenitor Cells. *Biotechnology Journal*. **13**.

Couper KN, Blount DG , Riley EM (2008). IL-10: the master regulator of immunity to infection. *Journal of Immunology*. **180**, 5771-5777.

Cramer T, Yamanishi Y, Clausen BE, Forster I, Pawlinski R, Mackman N, Haase VH, Jaenisch R, Corr M, Nizet V, Firestein GS, Gerber HP, Ferrara N , Johnson RS (2003). HIF-1alpha is essential for myeloid cell-mediated inflammation. *Cell*. **112**, 645-657.

Croitoru-Lamoury J, Lamoury FM, Caristo M, Suzuki K, Walker D, Takikawa O, Taylor R , Brew BJ (2011). Interferon-gamma regulates the proliferation and differentiation of mesenchymal stem cells via activation of indoleamine 2,3 dioxygenase (IDO). *PLOS ONE*. **6**, e14698.

Cutler AJ, Limbani V, Girdlestone J , Navarrete CV (2010). Umbilical cord-derived mesenchymal stromal cells modulate monocyte function to suppress T cell proliferation. *Journal of Immunology*. **185**, 6617-6623.

D'Amelio P, Cristofaro MA, D'Amico L, Veneziano L, Roato I, Sassi F, Bisignano G, Saracco M, Pellerito R, Patane S, Ferracini R, Pescarmona GP , Isaia GC (2010). Iloprost modulates the immune response in systemic sclerosis. *BMC Immunology*. **11**, 62.

Daley JM, Thomay AA, Connolly MD, Reichner JS , Albina JE (2008). Use of Ly6G-specific monoclonal antibody to deplete neutrophils in mice. *Journal of Leukocyte Biology*. **83**, 64-70.

de Bruin AM, Demirel O, Hooibrink B, Brandts CH , Nolte MA (2013). Interferon-gamma impairs proliferation of hematopoietic stem cells in mice. *Blood*. **121**, 3578-3585.

Deep A, Zoha M , Dutta Kukreja P (2017). Prostacyclin as an Anticoagulant for Continuous Renal Replacement Therapy in Children. *Blood Purification*. **43**, 279-289.

Dejbakhsh-Jones S, Jerabek L, Weissman IL , Strober S (1995). Extrathymic maturation of alpha beta T cells from hemopoietic stem cells. *Journal of Immunology*. **155**, 3338-3344.

Deshpande S, James AW, Blough J, Donneys A, Wang SC, Cederna PS, Buchman SR , Levi B (2013). Reconciling the effects of inflammatory cytokines on mesenchymal cell osteogenic differentiation. *The Journal of Surgical Research*. **185**, 278-285.

Devine L, Sun J, Barr MR , Kavathas PB (1999). Orientation of the Ig domains of CD8 alpha beta relative to MHC class I. *Journal of Immunology*. **162**, 846-851.

Di Nicola M, Carlo-Stella C, Magni M, Milanesi M, Longoni PD, Matteucci P, Grisanti S , Gianni AM (2002). Human bone marrow stromal cells suppress T-lymphocyte proliferation induced by cellular or nonspecific mitogenic stimuli. *Blood*. **99**, 3838-3843.

Dimitriou R, Tsiridis E , Giannoudis PV (2005). Current concepts of molecular aspects of bone healing. *Injury*. **36**, 1392-1404.

Dimmen S, Nordsletten L, Engebretsen L, Steen H , Madsen JE (2008). Negative effect of parecoxib on bone mineral during fracture healing in rats. *Acta Orthopaedica*. **79**, 438-444.

Disch AC, Matziolis G , Perka C (2005). The management of necrosis-associated and idiopathic bone-marrow oedema of the proximal femur by intravenous iloprost. *The Journal of Bone and Joint Surgery. British Volume*. **87**, 560-564.

Dogan A, Duygun F, Kalender AM, Bayram I , Sungur I (2014). Iloprost inhibits fracture repair in rats. *Chinese Medical Journal, English*. **127**, 2960-2965.

Doganci S, Yildirim V, Yesildal F, Erol G, Kadan M, Ozkan G, Avcu F , Ozgurtas T (2015). Comparison of angiogenic and proliferative effects of three commonly used agents for pulmonary artery hypertension (sildenafil, iloprost, bosentan): is angiogenesis always beneficial? *European Review for Medical and Pharmacological Sciences*. **19**, 1900-1906.

Dorris SL , Peebles RS, Jr. (2012). PGI2 as a regulator of inflammatory diseases. *Mediators of Inflammation*. **2012**, 926968.

Egan KM, Lawson JA, Fries S, Koller B, Rader DJ, Smyth EM , Fitzgerald GA (2004). COX-2-derived prostacyclin confers atheroprotection on female mice. *Science*. **306**, 1954-1957.

Egea V, von Baumgarten L, Schichor C, Berninger B, Popp T, Neth P, Goldbrunner R, Kienast Y, Winkler F, Jochum M , Ries C (2011). TNF-alpha respecifies human mesenchymal stem cells to a neural fate and promotes migration toward experimental glioma. *Cell Death & Differentiation*. **18**, 853-863.

Eggenhofer E , Hoogduijn MJ (2012). Mesenchymal stem cell-educated macrophages. *Transplantation Research*. **1**, 12.

Einhorn TA (1998). The cell and molecular biology of fracture healing. *Clinical Orthopaedics and Related Research*, S7-21.

Einhorn TA , Lane JM (1998). Significant advances have been made in the way surgeons treat fractures. *Clinical Orthopaedics and Related Research*. S2-3.

Einhorn TA, Majeska RJ, Rush EB, Levine PM , Horowitz MC (1995). The expression of cytokine activity by fracture callus. *Journal of Bone and Mineral Research: the Official Journal of the American Society for Bone and Mineral Research*. **10**, 1272-1281.

Eisman JA, Bogoch ER, Dell R, Harrington JT, McKinney RE, Jr., McLellan A, Mitchell PJ, Silverman S, Singleton R , Siris E (2012). Making the first fracture the last fracture: ASBMR task force report on secondary fracture prevention. *Journal of Bone and Mineral Research: the Official Journal of the American Society for Bone and Mineral Research*. **27**, 2039-2046.

El-Haroun H, Clarke DL, Deacon K, Bradbury D, Clayton A, Sutcliffe A , Knox AJ (2008). IL-1beta, BK, and TGF-beta1 attenuate PGI2-mediated cAMP formation in human pulmonary artery smooth muscle cells by multiple mechanisms involving p38 MAP kinase and PKA. *American Journal of Physiology. Lung Cellular and Molecular Physiology*. **294**, L553-562.

El Khassawna T, Serra A, Bucher CH, Petersen A, Schlundt C, Konnecke I, Malhan D, Wendler S, Schell H, Volk HD, Schmidt-Bleek K , Duda GN (2017). T Lymphocytes Influence the Mineralization Process of Bone. *Frontiers in Immunology*. **8**, 562.

Elder GJ (2006). From marrow oedema to osteonecrosis: common paths in the development of post-transplant bone pain. *Nephrology (Carlton)*. **11**, 560-567.

Fassbender M, Strobel C, Rauhe JS, Bergmann C, Schmidmaier G , Wildemann B (2011). Local inhibition of angiogenesis results in an atrophic non-union in a rat osteotomy model. *European Cells & Materials*. **22**, 1-11.

Feehan J, Nurgali K, Apostolopoulos V, Al Saedi A , Duque G (2019). Circulating osteogenic precursor cells: Building bone from blood. *EBioMedicine*. **39**, 603-611.

Feghhi S , Sniadecki NJ (2011). Mechanobiology of platelets: techniques to study the role of fluid flow and platelet retraction forces at the micro- and nano-scale. *International Journal of Molecular Sciences*. **12**, 9009-9030.

Feigenson M, Eliseev RA, Jonason JH, Mills BN , O'Keefe RJ (2017). PGE2 Receptor Subtype 1 (EP1) Regulates Mesenchymal Stromal Cell Osteogenic Differentiation by Modulating Cellular Energy Metabolism. *Journal of Cellular Biochemistry*. **118**, 4383-4393.

Feuerer M, Beckhove P, Mahnke Y, Hommel M, Kyewski B, Hamann A, Umansky V , Schirrmacher V (2004). Bone marrow microenvironment facilitating dendritic cell: CD4 T cell interactions and maintenance of CD4 memory. *International Journal of Oncology*. **25**, 867-876.

Fontenot JD, Gavin MA , Rudensky AY (2003). Foxp3 programs the development and function of CD4+CD25+ regulatory T cells. *Nature Immunology*. **4**, 330-336.

Francois M, Romieu-Mourez R, Li M , Galipeau J (2012). Human MSC suppression correlates with cytokine induction of indoleamine 2,3-dioxygenase and bystander M2 macrophage differentiation. *Molecular Therapy*. **20**, 187-195.

Friedenstein AJ, Deriglasova UF, Kulagina NN, Panasuk AF, Rudakowa SF, Luria EA , Ruadkow IA (1974). Precursors for fibroblasts in different populations of hematopoietic cells as detected by the in vitro colony assay method. *Experimental Hematology*. **2**, 83-92.

Frucht-Perry J, Assil KK, Ziegler E, Douglas H, Brown SI, Schanzlin DJ , Weinreb RN (1992). Fibrin-enmeshed tobramycin liposomes: single application topical therapy of Pseudomonas keratitis. *Cornea*. **11**, 393-397.

Fujimori K (2012). Prostaglandins as PPARgamma Modulators in Adipogenesis. *PPAR Res*. **2012**, 527607.

Fulop T, Larbi A, Dupuis G, Le Page A, Frost EH, Cohen AA, Witkowski JM , Franceschi C (2017). Immunosenescence and Inflamm-Aging As Two Sides of the Same Coin: Friends or Foes? *Frontiers in Immunology*. **8**, 1960.

Gabrilovich DI , Nagaraj S (2009). Myeloid-derived suppressor cells as regulators of the immune system. *Nature Reviews Immunology*. **9**, 162-174.

Geem D, Harusato A, Flannigan K , Denning TL (2015). Harnessing regulatory T cells for the treatment of inflammatory bowel disease. *Inflammatory Bowel Diseases*. **21**, 1409-1418.

Gerstenfeld LC, Alkhiary YM, Krall EA, Nicholls FH, Stapleton SN, Fitch JL, Bauer M, Kayal R, Graves DT, Jepsen KJ , Einhorn TA (2006). Three-dimensional reconstruction of fracture callus morphogenesis. *The Journal of Histochemistry and Cytochemistry: Official Journal of the Histochemistry Society*. **54**, 1215-1228.

Gerstenfeld LC, Cho TJ, Kon T, Aizawa T, Tsay A, Fitch J, Barnes GL, Graves DT , Einhorn TA (2003a). Impaired fracture healing in the absence of TNF-alpha signaling: the role of TNF-alpha in endochondral cartilage resorption. *Journal of Bone and Mineral Research: the Official Journal of the American Society for Bone and Mineral Research*. **18**, 1584-1592.

Gerstenfeld LC, Cullinane DM, Barnes GL, Graves DT , Einhorn TA (2003b). Fracture healing as a post-natal developmental process: molecular, spatial, and temporal aspects of its regulation. *Journal of Cellular Biochemistry*. **88**, 873-884.

Gerstenfeld LC, Thiede M, Seibert K, Mielke C, Phippard D, Svagr B, Cullinane D , Einhorn TA (2003c). Differential inhibition of fracture healing by non-selective and cyclooxygenase-2 selective non-steroidal anti-inflammatory drugs. *Journal of Orthopaedic Research: Official Publication of the Orthopaedic Research Society*. **21**, 670-675.

Ghannam S, Bouffi C, Djouad F, Jorgensen C , Noel D (2010). Immunosuppression by mesenchymal stem cells: mechanisms and clinical applications. *Stem Cell Research & Therapy*. **1**, 2.

Glass GE, Chan JK, Freidin A, Feldmann M, Horwood NJ , Nanchahal J (2011). TNF-alpha promotes fracture repair by augmenting the recruitment and differentiation of muscle-derived stromal cells. *Proceedings of the National Academy of Sciences of the United States of America*. **108**, 1585-1590.

Glennie S, Soeiro I, Dyson PJ, Lam EW , Dazzi F (2005). Bone marrow mesenchymal stem cells induce division arrest anergy of activated T cells. *Blood*. **105**, 2821-2827.

Goedhart M, Cornelissen AS, Kuijk C, Geerman S, Kleijer M, van Buul JD, Huveneers S, Raaijmakers M, Young HA, Wolkers MC, Voermans C , Nolte MA (2018). Interferon-Gamma Impairs Maintenance and Alters Hematopoietic Support of Bone Marrow Mesenchymal Stromal Cells. *Stem Cells and Development*. **27**, 579-589.

Gordon S , Mantovani A (2011). Diversity and plasticity of mononuclear phagocytes. *European Journal of Immunology*. **41**, 2470-2472.

Gordon S , Martinez FO (2010). Alternative activation of macrophages: mechanism and functions. *Immunity*. **32**, 593-604.

Gordon S , Taylor PR (2005). Monocyte and macrophage heterogeneity. *Nature Reviews Immunology*. **5**, 953-964.

Granero-Molto F, Weis JA, Miga MI, Landis B, Myers TJ, O'Rear L, Longobardi L, Jansen ED, Mortlock DP , Spagnoli A (2009). Regenerative effects of transplanted mesenchymal stem cells in fracture healing. *Stem Cells*. **27**, 1887-1898.

Grassl ED, Oegema TR , Tranquillo RT (2003). A fibrin-based arterial media equivalent. *Journal of Biomedical Materials Research Part A*. **66**, 550-561.

Griffith JF, Yeung DK, Ma HT, Leung JC, Kwok TC , Leung PC (2012). Bone marrow fat content in the elderly: a reversal of sex difference seen in younger subjects. *Journal of Magnetic Resonance Imaging*. **36**, 225-230.

Grobetal T, Hammer E, Bien-Moller S, Geisler A, Pinkert S, Roger C, Poller W, Kurreck J, Volker U, Vetter R , Fechner H (2014). A novel artificial microRNA expressing AAV vector for phospholamban silencing in cardiomyocytes improves Ca2+ uptake into the sarcoplasmic reticulum. *PLOS ONE*. **9**, e92188.

Gruber R, Koch H, Doll BA, Tegtmeier F, Einhorn TA , Hollinger JO (2006). Fracture healing in the elderly patient. *Experimental Gerontology*. **41**, 1080-1093.

Grundnes O , Reikeras O (1993). The importance of the hematoma for fracture healing in rats. *Acta Orthopaedica Scandinavica*. **64**, 340-342.

Guihard P, Danger Y, Brounais B, David E, Brion R, Delecrin J, Richards CD, Chevalier S, Redini F, Heymann D, Gascan H , Blanchard F (2012). Induction of osteogenesis in mesenchymal stem cells by activated monocytes/macrophages depends on oncostatin M signaling. *Stem Cells*. **30**, 762-772.

Gurgul-Convey E , Lenzen S (2010). Protection against cytokine toxicity through endoplasmic reticulum and mitochondrial stress prevention by prostacyclin synthase overexpression in insulin-producing cells. *The Journal of Biological Chemistry*. **285**, 11121-11128.

Ha W, Fan MM, Zhang S , Li BJ (2011). Self-assembly of chitosan-g-PEG and alpha-cyclodextrin into hollow spheres in aqueous solution. *Journal of Controlled Release: Official Journal of the Controlled Release Society*. **152 Suppl 1**, e204-205.

Haas NP (2000). [Callus modulation--fiction or reality?]. *Der Chirurg; Zeitschrift fur alle Gebiete der operativen Medizin*. **71**, 987-988.

Han Y, Guo Q, Zhang M, Chen Z , Cao X (2009). CD69+ CD4+ CD25- T cells, a new subset of regulatory T cells, suppress T cell proliferation through membrane-bound TGF-beta 1. *Journal of Immunology*. **182**, 111-120.

Hartung T, Doecke WD, Bundschuh D, Foote MA, Gantner F, Hermann C, Lenz A, Milwee S, Rich B, Simon B, Volk HD, von Aulock S , Wendel A (1999). Effect of filgrastim treatment on inflammatory cytokines and lymphocyte functions. *Clinical Pharmacology & Therapeutics*. **66**, 415-424.

He T, Lu T, d'Uscio LV, Lam CF, Lee HC , Katusic ZS (2008). Angiogenic function of prostacyclin biosynthesis in human endothelial progenitor cells. *Circulation Research*. **103**, 80-88.

Hedrich CM, Rauen T, Crispin JC, Koga T, Ioannidis C, Zajdel M, Kyttaris VC , Tsokos GC (2013). cAMP responsive element modulator (CREM)alpha trans-represses the transmembrane glycoprotein CD8 and contributes to the generation of CD3+CD4-CD8- T cells in health and disease. *The Journal of Biological Chemistry*.

Herbert CB, Nagaswami C, Bittner GD, Hubbell JA , Weisel JW (1998). Effects of fibrin micromorphology on neurite growth from dorsal root ganglia cultured in three-dimensional fibrin gels. *Journal of Biomedical Materials Research*. **40**, 551-559.

Herink AK, Kothe L, Girndt M , Keysser G (2010). [Treatment options of acral ulcers in MCTD]. *Medizinische Klinik (Munich, Germany: 1983)*. **105**, 837-840.

Herrmann M, Zeiter S, Eberli U, Hildebrand M, Camenisch K, Menzel U, Alini M, Verrier S , Stadelmann VA (2018). Five Days Granulocyte Colony-Stimulating Factor Treatment Increases Bone Formation and Reduces Gap Size of a Rat Segmental Bone Defect: A Pilot Study. *Frontiers in Bioengineering and Biotechnology*. **6**, 5.

Higuchi M, Zeng D, Shizuru J, Gworek J, Dejbakhsh-Jones S, Taniguchi M , Strober S (2002). Immune tolerance to combined organ and bone marrow transplants after fractionated lymphoid irradiation involves regulatory NK T cells and clonal deletion. *Journal of Immunology*. **169**, 5564-5570.

Hoff P, Gaber T, Schmidt-Bleek K, Senturk U, Tran CL, Blankenstein K, Lutkecosmann S, Bredahl J, Schuler HJ, Simon P, Wassilew G, Unterhauser F, Burmester GR, Schmidmaier G, Perka C, Duda GN , Buttgereit F (2011). Immunologically restricted patients exhibit a pronounced inflammation and inadequate response to hypoxia in fracture hematomas. *Immunologic Research*.

Hoff P, Maschmeyer P, Gaber T, Schutze T, Raue T, Schmidt-Bleek K, Dziurla R, Schellmann S, Lohanatha FL, Rohner E, Ode A, Burmester GR, Duda GN, Perka C , Buttgereit F (2013). Human immune cells' behavior and survival under bioenergetically restricted conditions in an in vitro fracture hematoma model. *Cellular & Molecular Immunology*. **10**, 151-158.

Holler E (2005). Laminin isoform expression in breast tumors. *Breast Cancer Research*. **7**, 166-167.

Honczarenko M, Le Y, Swierkowski M, Ghiran I, Glodek AM , Silberstein LE (2006). Human bone marrow stromal cells express a distinct set of biologically functional chemokine receptors. *Stem Cells*. **24**, 1030-1041.

Hoogduijn MJ, Popp F, Verbeek R, Masoodi M, Nicolaou A, Baan C , Dahlke MH (2010). The immunomodulatory properties of mesenchymal stem cells and their use for immunotherapy. *International Immunopharmacology*. **10**, 1496-1500.

Huang H, Zhao N, Xu X, Xu Y, Li S, Zhang J , Yang P (2011). Dose-specific effects of tumor necrosis factor alpha on osteogenic differentiation of mesenchymal stem cells. *Cell Proliferation*. **44**, 420-427.

Huang S, Wettlaufer SH, Hogaboam C, Aronoff DM , Peters-Golden M (2007). Prostaglandin E(2) inhibits collagen expression and proliferation in patient-derived normal lung fibroblasts via E prostanoid 2 receptor and cAMP signaling. *American Journal of Physiology. Lung Cellular and Molecular Physiology*. **292**, L405-413.

Hung CH, Chu YT, Suen JL, Lee MS, Chang HW, Lo YC , Jong YJ (2009). Regulation of cytokine expression in human plasmacytoid dendritic cells by prostaglandin I2 analogues. *European Respiratory Society*. **33**, 405-410.

Ishida K, Matsumoto T, Sasaki K, Mifune Y, Tei K, Kubo S, Matsushita T, Takayama K, Akisue T, Tabata Y, Kurosaka M , Kuroda R (2010). Bone regeneration properties of granulocyte colony-stimulating factor via neovascularization and osteogenesis. *Tissue Engineering. Part A*. **16**, 3271-3284.

Jaffar Z, Wan KS , Roberts K (2002). A key role for prostaglandin I2 in limiting lung mucosal Th2, but not Th1, responses to inhaled allergen. *Journal of Immunology*. **169**, 5997-6004.

Jager M, Tillmann FP, Thornhill TS, Mahmoudi M, Blondin D, Hetzel GR, Zilkens C , Krauspe R (2008). Rationale for prostaglandin I2 in bone marrow oedema--from theory to application. *Arthritis Research & Therapy*. **10**, R120.

Jain N , Weinstein RS (2009). Giant osteoclasts after long-term bisphosphonate therapy: diagnostic challenges. *Nature Reviews Rheumatology*. **5**, 341-346.

Ji W, Yang F, van den Beucken JJ, Bian Z, Fan M, Chen Z , Jansen JA (2010). Fibrous scaffolds loaded with protein prepared by blend or coaxial electrospinning. *Acta Biomaterialia*. **6**, 4199-4207.

Jia B, Madsen L, Petersen RK, Techer N, Kopperud R, Ma T, Doskeland SO, Ailhaud G, Wang J, Amri EZ , Kristiansen K (2012). Activation of protein kinase A and exchange protein directly activated by cAMP promotes adipocyte differentiation of human mesenchymal stem cells. *PLOS ONE*. **7**, e34114.

Jorres A, Dinter H, Topley N, Gahl GM, Frei U , Scholz P (1997). Inhibition of tumour necrosis factor production in endotoxin-stimulated human mononuclear leukocytes by the prostacyclin analogue iloprost: cellular mechanisms. *Cytokine*. **9**, 119-125.

Kanakaris NK, Petsatodis G, Tagil M , Giannoudis PV (2009). Is there a role for bone morphogenetic proteins in osteoporotic fractures? *Injury*. **40 Suppl 3**, S21-26.

Kanczler JM , Oreffo RO (2008). Osteogenesis and angiogenesis: the potential for engineering bone. *European Cells & Materials*. **15**, 100-114.

Kawabe J, Yuhki K, Okada M, Kanno T, Yamauchi A, Tashiro N, Sasaki T, Okumura S, Nakagawa N, Aburakawa Y, Takehara N, Fujino T, Hasebe N, Narumiya S , Ushikubi F (2010). Prostaglandin I2 promotes recruitment of endothelial progenitor cells and limits vascular remodeling. *Arteriosclerosis, Thrombosis, and Vascular Biology*. **30**, 464-470.

Kawamoto T (2003). Use of a new adhesive film for the preparation of multi-purpose fresh-frozen sections from hard tissues, whole-animals, insects and plants. *Archives of Histology and Cytology*. **66**, 123-143.

Keating A (2012). Mesenchymal stromal cells: new directions. *Cell Stem Cell*. **10**, 709-716.

Keila S, Kelner A , Weinreb M (2001). Systemic prostaglandin E2 increases cancellous bone formation and mass in aging rats and stimulates their bone marrow osteogenic capacity in vivo and in vitro. *The Journal of Endocrinology*. **168**, 131-139.

Kemper O, Herten M, Fischer J, Haversath M, Beck S, Classen T, Warwas S, Tassemeier T, Landgraeber S, Lensing-Hohn S, Krauspe R , Jager M (2014). Prostacyclin suppresses twist expression in the presence of indomethacin in bone marrow-derived mesenchymal stromal cells. *Medical Science Monitor*. **20**, 2219-2227.

Keramaris NC, Calori GM, Nikolaou VS, Schemitsch EH , Giannoudis PV (2008). Fracture vascularity and bone healing: a systematic review of the role of VEGF. *Injury*. **39 Suppl 2**, S45-57.

Ketenjian AY , Arsenis C (1975). Morphological and biochemical studies during differentiation and calcification of fracture callus cartilage. *Clinical Orthopaedics and Related Research*, 266-273.

Khademhosseini A, Eng G, Yeh J, Fukuda J, Blumling J, 3rd, Langer R , Burdick JA (2006). Micromolding of photocrosslinkable hyaluronic acid for cell encapsulation and entrapment. *Journal of Biomedical Materials Research Part A*. **79**, 522-532.

Kim J, Park CS, Park CH, Jeoung DI, Kim YM , Choe J (2011). Beraprost enhances the APC function of B cells by upregulating CD86 expression levels. *Journal of Immunology*. **186**, 3866-3873.

Kim M, Kim C, Choi YS, Park C , Suh Y (2012). Age-related alterations in mesenchymal stem cells related to shift in differentiation from osteogenic to adipogenic potential: implication to age-associated bone diseases and defects. *Mechanisms of Ageing and Development*. **133**, 215-225.

Kingsley CI, Karim M, Bushell AR , Wood KJ (2002). CD25+CD4+ regulatory T cells prevent graft rejection: CTLA-4- and IL-10-dependent immunoregulation of alloresponses. *Journal of Immunology*. **168**, 1080-1086.

Kingsley CI, Nadig SN , Wood KJ (2007). Transplantation tolerance: lessons from experimental rodent models. *Transplant International*. **20**, 828-841.

Kitaori T, Ito H, Schwarz EM, Tsutsumi R, Yoshitomi H, Oishi S, Nakano M, Fujii N, Nagasawa T , Nakamura T (2009). Stromal cell-derived factor 1/CXCR4 signaling is critical for the recruitment of mesenchymal stem cells to the fracture site during skeletal repair in a mouse model. *Arthritis and Rheumatism*. **60**, 813-823.

Kitazawa H, Sato H, Adachi I, Masuko Y , Horikoshi I (1997). Microdialysis assessment of fibrin glue containing sodium alginate for local delivery of doxorubicin in tumor-bearing rats. *Biological & Pharmaceutical Bulletin*. **20**, 278-281.

Kjaergard HK , Weis-Fogh US (1994). Important factors influencing the strength of autologous fibrin glue; the fibrin concentration and reaction time--comparison of strength with commercial fibrin glue. *European Surgical Research*. **26**, 273-276.

Klein M, Vaeth M, Scheel T, Grabbe S, Baumgrass R, Berberich-Siebelt F, Bopp T, Schmitt E , Becker C (2012). Repression of cyclic adenosine monophosphate upregulation disarms and expands human regulatory T cells. *Journal of Immunology*. **188**, 1091-1097.

Knippenberg M, Helder MN, de Blieck-Hogervorst JM, Wuisman PI , Klein-Nulend J (2007). Prostaglandins differentially affect osteogenic differentiation of human adipose tissue-derived mesenchymal stem cells. *Tissue Engineering*. **13**, 2495-2503.

Kolaczkowska E , Kubes P (2013). Neutrophil recruitment and function in health and inflammation. *Nature Reviews Immunology*. **13**, 159-175.

Kolar P, Gaber T, Perka C, Duda GN , Buttgereit F (2011). Human early fracture hematoma is characterized by inflammation and hypoxia. *Clinical Orthopaedics and Related Research*. **469**, 3118-3126.

Kolar P, Schmidt-Bleek K, Schell H, Gaber T, Toben D, Schmidmaier G, Perka C, Buttgereit F , Duda GN (2010). The early fracture hematoma and its potential role in fracture healing. *Tissue Engineering. Part B, Reviews*. **16**, 427-434.

Kon T, Cho TJ, Aizawa T, Yamazaki M, Nooh N, Graves D, Gerstenfeld LC , Einhorn TA (2001). Expression of osteoprotegerin, receptor activator of NF-kappaB ligand (osteoprotegerin ligand) and related proinflammatory cytokines during fracture healing. *Journal of Bone and Mineral Research: the Official Journal of the American Society for Bone and Mineral Research*. **16**, 1004-1014.

Kong T, Wu J, Yeung KW, To MK, Shum HC , Wang L (2013). Microfluidic fabrication of polymeric core-shell microspheres for controlled release applications. *Biomicrofluidics*. **7**, 44128.

Konya V, Sturm EM, Schratl P, Beubler E, Marsche G, Schuligoi R, Lippe IT, Peskar BA , Heinemann A (2010). Endothelium-derived prostaglandin I(2) controls the migration of eosinophils. *Journal of Allergy and Clinical Immunology*. **125**, 1105-1113.

Kopp HG, Avecilla ST, Hooper AT , Rafii S (2005). The bone marrow vascular niche: home of HSC differentiation and mobilization. *Physiology (Bethesda)*. **20**, 349-356.

Kothapalli D, Flores-Stewart SA , Assoian RK (2005). Antimitogenic effects of prostacyclin on the G1 phase cyclin-dependent kinases. *Prostaglandins & Other Lipid Mediators*. **78**, 3-13.

Krampera M (2011). Mesenchymal stromal cell 'licensing': a multistep process. *Leukemia*. **25**, 1408-1414.

Krampera M, Glennie S, Dyson J, Scott D, Laylor R, Simpson E , Dazzi F (2003). Bone marrow mesenchymal stem cells inhibit the response of naive and memory antigen-specific T cells to their cognate peptide. *Blood*. **101**, 3722-3729.
Kratz F (2008). Albumin as a drug carrier: design of prodrugs, drug conjugates and nanoparticles. *Journal of Controlled Release: Official Journal of the Controlled Release Society*. **132**, 171-183.
Krause C, Korchynskyi O, de Rooij K, Weidauer SE, de Gorter DJ, van Bezooijen RL, Hatsell S, Economides AN, Mueller TD, Lowik CW , ten Dijke P (2010). Distinct modes of inhibition by sclerostin on bone morphogenetic protein and Wnt signaling pathways. *The Journal of Biological Chemistry*. **285**, 41614-41626.
Krauss S, Brand MD , Buttgereit F (2001). Signaling takes a breath--new quantitative perspectives on bioenergetics and signal transduction. *Immunity*. **15**, 497-502.
Kronenberg M (2005). Toward an understanding of NKT cell biology: progress and paradoxes. *Annual Review of Immunology*. **23**, 877-900.
Kuehl FA, Jr., Humes JL, Beveridge GC, Van Arman CG , Egan RW (1977). Biologically active derivatives of fatty acids: prostaglandins, thromboxanes, and endoperoxides. *Inflammation*. **2**, 285-294.
Kuhn NZ , Tuan RS (2010). Regulation of stemness and stem cell niche of mesenchymal stem cells: implications in tumorigenesis and metastasis. *Journal of Cellular Physiology*. **222**, 268-277.
Kumagai K, Vasanji A, Drazba JA, Butler RS , Muschler GF (2008). Circulating cells with osteogenic potential are physiologically mobilized into the fracture healing site in the parabiotic mice model. *Journal of Orthopaedic Research: Official Publication of the Orthopaedic Research Society*. **26**, 165-175.
Kuo CH, Lin CH, Yang SN, Huang MY, Chen HL, Kuo PL, Hsu YL, Huang SK, Jong YJ, Wei WJ, Chen YP , Hung CH (2012). Effect of prostaglandin I2 analogs on cytokine expression in human myeloid dendritic cells via epigenetic regulation. *Molecular Medicine*. **18**, 433-444.
Kusner LL, Yucius K, Sengupta M, Sprague AG, Desai D, Nguyen T, Charisse K, Kuchimanchi S, Kallanthottathil R, Fitzgerald K, Kaminski HJ , Borodovsky A (2019). Investigational RNAi Therapeutic Targeting C5 Is Efficacious in Pre-clinical Models of Myasthenia Gravis. *Molecular Therapy - Methods & Clinical Development*. **13**, 484-492.
Kuzushima M, Mogi M , Togari A (2006). Cytokine-induced nitric-oxide-dependent apoptosis in mouse osteoblastic cells: involvement of p38MAP kinase. *Archives of Oral Biology*. **51**, 1048-1053.
Lacey DC, Simmons PJ, Graves SE , Hamilton JA (2009). Proinflammatory cytokines inhibit osteogenic differentiation from stem cells: implications for bone repair during inflammation. *Osteoarthritis Cartilage*. **17**, 735-742.
Lad SP, Bagley JH, Karikari IO, Babu R, Ugiliweneza B, Kong M, Isaacs RE, Bagley CA, Gottfried ON, Patil CG , Boakye M (2013). Cancer after spinal fusion: the role of bone morphogenetic protein. *Neurosurgery*. **73**, 440-449.
Lafuma A , Quere D (2003). Superhydrophobic states. *Nature Materials*. **2**, 457-460.
Lagadic-Gossmann D, Huc L , Lecureur V (2004). Alterations of intracellular pH homeostasis in apoptosis: origins and roles. *Cell Death & Differentiation*. **11**, 953-961.
Le Blanc K , Mougiakakos D (2012). Multipotent mesenchymal stromal cells and the innate immune system. *Nature Reviews Immunology*. **12**, 383-396.
Le Blanc K, Tammik L, Sundberg B, Haynesworth SE , Ringden O (2003). Mesenchymal stem cells inhibit and stimulate mixed lymphocyte cultures and mitogenic responses independently of the major histocompatibility complex. *Scandinavian Journal of Immunology*. **57**, 11-20.
Lee IY, Ko EM, Kim SH, Jeoung DI , Choe J (2005). Human follicular dendritic cells express prostacyclin synthase: a novel mechanism to control T cell numbers in the germinal center. *Journal of Immunology*. **175**, 1658-1664.
Lee SF, Zhu XM, Wang YX, Xuan SH, You Q, Chan WH, Wong CH, Wang F, Yu JC, Cheng CH , Leung KC (2013). Ultrasound, pH, and magnetically responsive crown-ether-coated core/shell nanoparticles as drug encapsulation and release systems. *ACS Applied Materials & Interfaces*. **5**, 1566-1574.
Lee SK , Lorenzo J (2006). Cytokines regulating osteoclast formation and function. *Current Opinion in Rheumatology*. **18**, 411-418.
Lee YS , Chuong CM (1997). Activation of protein kinase A is a pivotal step involved in both BMP-2- and cyclic AMP-induced chondrogenesis. *Journal of Cellular Physiology*. **170**, 153-165.
Lehmann W, Edgar CM, Wang K, Cho TJ, Barnes GL, Kakar S, Graves DT, Rueger JM, Gerstenfeld LC , Einhorn TA (2005). Tumor necrosis factor alpha (TNF-alpha) coordinately regulates the expression of specific matrix metalloproteinases (MMPS) and angiogenic factors during fracture healing. *Bone*. **36**, 300-310.
Leibovich SJ , Ross R (1975). The role of the macrophage in wound repair. A study with hydrocortisone and antimacrophage serum. *The American Journal of Pathology*. **78**, 71-100.
Lekstrom-Himes JA , Gallin JI (2000). Immunodeficiency diseases caused by defects in phagocytes. *The New England Journal of Medicine.* **343**, 1703-1714.
Li RC, Cindrova-Davies T, Skepper JN , Sellers LA (2004). Prostacyclin induces apoptosis of vascular smooth muscle cells by a cAMP-mediated inhibition of extracellular signal-regulated kinase activity and can counteract the mitogenic activity of endothelin-1 or basic fibroblast growth factor. *Circulation Research*. **94**, 759-767.
Li W, Ren G, Huang Y, Su J, Han Y, Li J, Chen X, Cao K, Chen Q, Shou P, Zhang L, Yuan ZR, Roberts AI, Shi S, Le AD , Shi Y (2012). Mesenchymal stem cells: a double-edged sword in regulating immune responses. *Cell Death & Differentiation*. **19**, 1505-1513.
Lian WS, Cheng WT, Cheng CC, Hsiao FS, Chen JJ, Cheng CF , Wu SC (2011). In vivo therapy of myocardial infarction with mesenchymal stem cells modified with prostaglandin I synthase gene improves cardiac performance in mice. *Life Sciences*. **88**, 455-464.
Lienau J, Schmidt-Bleek K, Peters A, Haschke F, Duda GN, Perka C, Bail HJ, Schutze N, Jakob F , Schell H (2009). Differential regulation of blood vessel formation between standard and delayed bone healing. *Journal of Orthopaedic Research: Official Publication of the Orthopaedic Research Society*. **27**, 1133-1140.

Lienau J, Schmidt-Bleek K, Peters A, Weber H, Bail HJ, Duda GN, Perka C , Schell H (2010). Insight into the molecular pathophysiology of delayed bone healing in a sheep model. *Tissue Engineering. Part A*. **16**, 191-199.
Linhardt RJ, al-Hakim A, Liu JA, Hoppensteadt D, Mascellani G, Bianchini P , Fareed J (1991). Structural features of dermatan sulfates and their relationship to anticoagulant and antithrombotic activities. *Biochemical Pharmacology*. **42**, 1609-1619.
Liopeta K, Boubali S, Virgilio L, Thyphronitis G, Mavrothalassitis G, Dimitracopoulos G , Paliogianni F (2009). cAMP regulates IL-10 production by normal human T lymphocytes at multiple levels: a potential role for MEF2. *Molecular Immunology*. **46**, 345-354.
Liu J, Xu HH, Zhou H, Weir MD, Chen Q , Trotman CA (2013a). Human umbilical cord stem cell encapsulation in novel macroporous and injectable fibrin for muscle tissue engineering. *Acta Biomaterialia*. **9**, 4688-4697.
Liu W, Li H, Zhang X, Wen D, Yu F, Yang S, Jia X, Cong B , Ma C (2013b). Prostaglandin I2-IP signalling regulates human Th17 and Treg cell differentiation. *Prostaglandins, Leukotrienes & Essential Fatty Acids*. **89**, 335-344.
Liu Y, Wang L, Kikuiri T, Akiyama K, Chen C, Xu X, Yang R, Chen W, Wang S , Shi S (2011). Mesenchymal stem cell-based tissue regeneration is governed by recipient T lymphocytes via IFN-gamma and TNF-alpha. *Nature Medicine*. **17**, 1594-1601.
Lohse L, Nielsen J , Eriksen L (2006). Long-term treatment of pigs with low doses of monoclonal antibodies against porcine CD4 and CD8 antigens. *Acta Pathologica et Microbiologica Scandinavica*. **114**, 23-31.
Long F (2011). Building strong bones: molecular regulation of the osteoblast lineage. *Nature Reviews Molecular Cell Biology*. **13**, 27-38.
Lorand L (2007). Crosslinks in blood: transglutaminase and beyond. *FASEB Journal*. **21**, 1627-1632.
Lovgren AK, Jania LA, Hartney JM, Parsons KK, Audoly LP, Fitzgerald GA, Tilley SL , Koller BH (2006). COX-2-derived prostacyclin protects against bleomycin-induced pulmonary fibrosis. *American Journal of Physiology. Lung Cellular and Molecular Physiology*. **291**, L144-156.
Lu C, Xing Z, Wang X, Mao J, Marcucio RS , Miclau T (2012). Anti-inflammatory treatment increases angiogenesis during early fracture healing. *Archives of Orthopaedic and Trauma Surgery*. **132**, 1205-1213.
Lucarelli E, Beretta R, Dozza B, Tazzari PL, O'Connel SM, Ricci F, Pierini M, Squarzoni S, Pagliaro PP, Oprita EI , Donati D (2010). A recently developed bifacial platelet-rich fibrin matrix. *European Cells & Materials*. **20**, 13-23.
Ma J, Ge J, Zhang S, Sun A, Shen J, Chen L, Wang K , Zou Y (2005). Time course of myocardial stromal cell-derived factor 1 expression and beneficial effects of intravenously administered bone marrow stem cells in rats with experimental myocardial infarction. *Basic Research in Cardiology*. **100**, 217-223.
Maes C, Kobayashi T, Selig MK, Torrekens S, Roth SI, Mackem S, Carmeliet G , Kronenberg HM (2010). Osteoblast precursors, but not mature osteoblasts, move into developing and fractured bones along with invading blood vessels. *Developmental Cell*. **19**, 329-344.
Manigrasso MB , O'Connor JP (2008). Comparison of fracture healing among different inbred mouse strains. *Calcified Tissue International*. **82**, 465-474.
Mantovani A, Biswas SK, Galdiero MR, Sica A , Locati M (2013). Macrophage plasticity and polarization in tissue repair and remodelling. *The Journal of Pathology*. **229**, 176-185.
Manz RA, Thiel A , Radbruch A (1997). Lifetime of plasma cells in the bone marrow. *Nature*. **388**, 133-134.
Marsell R , Einhorn TA (2009). The role of endogenous bone morphogenetic proteins in normal skeletal repair. *Injury*. **40 Suppl 3**, S4-7.
Marsell R , Einhorn TA (2011). The biology of fracture healing. *Injury*. **42**, 551-555.
Martino MM, Briquez PS, Ranga A, Lutolf MP , Hubbell JA (2013). Heparin-binding domain of fibrin(ogen) binds growth factors and promotes tissue repair when incorporated within a synthetic matrix. *Proceedings of the National Academy of Sciences of the United States of America*. **110**, 4563-4568.
Marumo M , Wakabayashi I (2009). Sensitivity of thrombin-induced platelet aggregation to inhibition by ethanol. *Clinica Chimica Acta*. **402**, 156-159.
Masopust D, Vezys V, Marzo AL , Lefrancois L (2001). Preferential localization of effector memory cells in nonlymphoid tissue. *Science*. **291**, 2413-2417.
Matatall KA, Shen CC, Challen GA , King KY (2014). Type II interferon promotes differentiation of myeloid-biased hematopoietic stem cells. *Stem Cells*. **32**, 3023-3030.
Matsunaga YT, Morimoto Y , Takeuchi S (2011). Molding cell beads for rapid construction of macroscopic 3D tissue architecture. *Advanced Materials*. **23**, H90-94.
Matsuoka T , Narumiya S (2008). The roles of prostanoids in infection and sickness behaviors. *Journal of Infection and Chemotherapy*. **14**, 270-278.
Mazo IB, Honczarenko M, Leung H, Cavanagh LL, Bonasio R, Weninger W, Engelke K, Xia L, McEver RP, Koni PA, Silberstein LE , von Andrian UH (2005). Bone marrow is a major reservoir and site of recruitment for central memory CD8+ T cells. *Immunity*. **22**, 259-270.
Mediero A , Cronstein BN (2013). Adenosine and bone metabolism. *Trends in Endocrinology & Metabolism*. **24**, 290-300.
Mehta M, Strube P, Peters A, Perka C, Hutmacher D, Fratzl P , Duda GN (2010). Influences of age and mechanical stability on volume, microstructure, and mineralization of the fracture callus during bone healing: is osteoclast activity the key to age-related impaired healing? *Bone*. **47**, 219-228.
Melief SM, Schrama E, Brugman MH, Tiemessen MM, Hoogduijn MJ, Fibbe WE , Roelofs H (2013). Multipotent stromal cells induce human regulatory T cells through a novel pathway involving skewing of monocytes toward anti-inflammatory macrophages. *Stem Cells*. **31**, 1980-1991.
Merkle VM, Zeng L, Slepian MJ , Wu X (2014). Core-shell nanofibers: Integrating the bioactivity of gelatin and the mechanical property of polyvinyl alcohol. *Biopolymers*. **101**, 336-346.

Mia S, Warnecke A, Zhang XM, Malmstrom V , Harris RA (2014). An optimized protocol for human M2 macrophages using M-CSF and IL-4/IL-10/TGF-beta yields a dominant immunosuppressive phenotype. *Scandinavian Journal of Immunology*. **79**, 305-314.

Mirsaidi A, Tiaden AN , Richards PJ (2017). Prostaglandin E2 inhibits matrix mineralization by human bone marrow stromal cell-derived osteoblasts via Epac-dependent cAMP signaling. *Scientific Reports*. **7**, 2243.

Mo IF, Yip KH, Chan WK, Law HK, Lau YL , Chan GC (2008). Prolonged exposure to bacterial toxins downregulated expression of toll-like receptors in mesenchymal stromal cell-derived osteoprogenitors. *BMC Molecular and Cell Biology* **9**, 52.

Mo ZC, Ren K, Liu X, Tang ZL , Yi GH (2016). A high-density lipoprotein-mediated drug delivery system. *Advanced Drug Delivery Reviews*. **106**, 132-147.

Mohite A, Chillar A, So SP, Cervantes V , Ruan KH (2011). Novel mechanism of the vascular protector prostacyclin: regulating microRNA expression. *Biochemistry*. **50**, 1691-1699.

Moreno JJ (2017). Eicosanoid receptors: Targets for the treatment of disrupted intestinal epithelial homeostasis. *European Journal of Pharmacology*. **796**, 7-19.

Morton TJ, Furst W, van Griensven M , Redl H (2009). Controlled release of substances bound to fibrin-anchors or of DNA. *Drug Delivery*. **16**, 102-107.

Mosesson MW (1999). Fibrinogen and fibrin polymerization and functions. *Blood Coagulation & Fibrinolysis*. **10 Suppl 1**, S45-48.

Mountziaris PM , Mikos AG (2008). Modulation of the inflammatory response for enhanced bone tissue regeneration. *Tissue Engineering. Part B, Reviews*. **14**, 179-186.

Movat HZ (1955). Demonstration of all connective tissue elements in a single section; pentachrome stains. *A. M. A. Archives of Pathology*. **60**, 289-295.

Muller R, Hahn M, Vogel M, Delling G , Ruegsegger P (1996). Morphometric analysis of noninvasively assessed bone biopsies: comparison of high-resolution computed tomography and histologic sections. *Bone*. **18**, 215-220.

Munisso MC, Kang JH, Tsurufuji M , Yamaoka T (2012). Cilomilast enhances osteoblast differentiation of mesenchymal stem cells and bone formation induced by bone morphogenetic protein 2. *Biochimie*. **94**, 2360-2365.

Muramatsu R, Takahashi C, Miyake S, Fujimura H, Mochizuki H , Yamashita T (2012). Angiogenesis induced by CNS inflammation promotes neuronal remodeling through vessel-derived prostacyclin. *Nature Medicine*. **18**, 1658-1664.

Mutch NJ, Engel R, Uitte de Willige S, Philippou H , Ariens RA (2010). Polyphosphate modifies the fibrin network and down-regulates fibrinolysis by attenuating binding of tPA and plasminogen to fibrin. *Blood*. **115**, 3980-3988.

Nagao K, Tanaka H, Komai M, Masuda T, Narumiya S , Nagai H (2003). Role of prostaglandin I2 in airway remodeling induced by repeated allergen challenge in mice. *American Journal of Respiratory Cell and Molecular Biology*. **29**, 314-320.

Nakada D, Levi BP , Morrison SJ (2011). Integrating physiological regulation with stem cell and tissue homeostasis. *Neuron*. **70**, 703-718.

Nana-Sinkam SP, Lee JD, Sotto-Santiago S, Stearman RS, Keith RL, Choudhury Q, Cool C, Parr J, Moore MD, Bull TM, Voelkel NF , Geraci MW (2007). Prostacyclin prevents pulmonary endothelial cell apoptosis induced by cigarette smoke. *American Journal of Respiratory and Critical Care Medicine*. **175**, 676-685.

Narayanan S, Pavithran M, Viswanath A, Narayanan D, Mohan CC, Manzoor K , Menon D (2014). Sequentially releasing dual-drug-loaded PLGA-casein core/shell nanomedicine: design, synthesis, biocompatibility and pharmacokinetics. *Acta Biomaterialia*. **10**, 2112-2124.

Nathan C (2006). Neutrophils and immunity: challenges and opportunities. *Nature Reviews Immunology*. **6**, 173-182.

Nauta AJ, Kruisselbrink AB, Lurvink E, Willemze R , Fibbe WE (2006). Mesenchymal stem cells inhibit generation and function of both CD34+-derived and monocyte-derived dendritic cells. *Journal of Immunology*. **177**, 2080-2087.

Needleman P, Moncada S, Bunting S, Vane JR, Hamberg M , Samuelsson B (1976). Identification of an enzyme in platelet microsomes which generates thromboxane A2 from prostaglandin endoperoxides. *Nature*. **261**, 558-560.

Negrel R (1999). Prostacyclin as a critical prostanoid in adipogenesis. *Prostaglandins, Leukotrienes & Essential Fatty Acids*. **60**, 383-386.

Nehls V , Herrmann R (1996). The configuration of fibrin clots determines capillary morphogenesis and endothelial cell migration. *Microvascular Research*. **51**, 347-364.

Nemeth K, Mayer B , Mezey E (2010). Modulation of bone marrow stromal cell functions in infectious diseases by toll-like receptor ligands. *Journal of Molecular Medicine*. **88**, 5-10.

Nicodemus GD , Bryant SJ (2008). Cell encapsulation in biodegradable hydrogels for tissue engineering applications. *Tissue Engineering. Part B, Reviews*. **14**, 149-165.

Nicolaidou V, Wong MM, Redpath AN, Ersek A, Baban DF, Williams LM, Cope AP , Horwood NJ (2012). Monocytes induce STAT3 activation in human mesenchymal stem cells to promote osteoblast formation. *PLOS ONE*. **7**, e39871.

Nourissat G, Berenbaum F , Duprez D (2015). Tendon injury: from biology to tendon repair. *Nature Reviews Rheumatology*. **11**, 223-233.

Obata H, Sakai Y, Ohnishi S, Takeshita S, Mori H, Kodama M, Kangawa K, Aizawa Y , Nagaya N (2008). Single injection of a sustained-release prostacyclin analog improves pulmonary hypertension in rats. *American Journal of Respiratory and Critical Care Medicine*. **177**, 195-201.

Oh JH, Kim HJ, Kim TI, Baek JH, Ryoo HM , Woo KM (2012). The effects of the modulation of the fibronectin-binding capacity of fibrin by thrombin on osteoblast differentiation. *Biomaterials*. **33**, 4089-4099.

Ono T , Takayanagi H (2017). Osteoimmunology in Bone Fracture Healing. *Current Osteoporosis Reports*. **15**, 367-375.

Onoe H, Okitsu T, Itou A, Kato-Negishi M, Gojo R, Kiriya D, Sato K, Miura S, Iwanaga S, Kuribayashi-Shigetomi K, Matsunaga YT, Shimoyama Y , Takeuchi S (2013). Metre-long cell-laden microfibres exhibit tissue morphologies and functions. *Nature Materials*. **12**, 584-590.

Osathanon T, Giachelli CM , Somerman MJ (2009). Immobilization of alkaline phosphatase on microporous nanofibrous fibrin scaffolds for bone tissue engineering. *Biomaterials*. **30**, 4513-4521.

Ovanesov MV, Ananyeva NM, Panteleev MA, Ataullakhanov FI , Saenko EL (2005). Initiation and propagation of coagulation from tissue factor-bearing cell monolayers to plasma: initiator cells do not regulate spatial growth rate. *Journal of Thrombosis and Haemostasis*. **3**, 321-331.

Overgaard NH, Jung JW, Steptoe RJ , Wells JW (2015). CD4+/CD8+ double-positive T cells: more than just a developmental stage? *Journal of Leukocyte Biology*. **97**, 31-38.

Ozaki A, Tsunoda M, Kinoshita S , Saura R (2000). Role of fracture hematoma and periosteum during fracture healing in rats: interaction of fracture hematoma and the periosteum in the initial step of the healing process. *Journal of Orthopaedic Science: Official Journal of the Japanese Orthopaedic Association*. **5**, 64-70.

Pabinger C, Heu C, Frohner A , Dimai HP (2012). Pregnancy- and lactation-associated transient osteoporosis of both hips in a 32 year old patient with osteogenesis imperfecta. *Bone*. **51**, 142-144.

Pacifici R (2013). Osteoimmunology and its implications for transplantation. *American Journal of Transplantation.* **13**, 2245-2254.

Papotto PH, Ribot JC , Silva-Santos B (2017). IL-17(+) gammadelta T cells as kick-starters of inflammation. *Nature Immunology*. **18**, 604-611.

Parihar A, Eubank TD , Doseff AI (2010). Monocytes and macrophages regulate immunity through dynamic networks of survival and cell death. *Journal of Innate Immunity*. **2**, 204-215.

Parretta E, Cassese G, Barba P, Santoni A, Guardiola J , Di Rosa F (2005). CD8 cell division maintaining cytotoxic memory occurs predominantly in the bone marrow. *Journal of Immunology*. **174**, 7654-7664.

Patarroyo M, Tryggvason K , Virtanen I (2002). Laminin isoforms in tumor invasion, angiogenesis and metastasis. *Seminars in Cancer Biology*. **12**, 197-207.

Perez RA , Kim HW (2015). Core-shell designed scaffolds for drug delivery and tissue engineering. *Acta Biomaterialia.* **21**, 2-19.

Perez RA, Kim M, Kim TH, Kim JH, Lee JH, Park JH, Knowles JC , Kim HW (2014). Utilizing core-shell fibrous collagen-alginate hydrogel cell delivery system for bone tissue engineering. *Tissue Engineering. Part A*. **20**, 103-114.

Petje G, Radler C, Aigner N, Manner H, Kriegs-Au G , Grill F (2004). Pharmacological management of aseptic osteonecrosis in children. *Expert Opinion on Pharmacotherapy*. **5**, 1455-1462.

Phinney DG, Kopen G, Isaacson RL , Prockop DJ (1999). Plastic adherent stromal cells from the bone marrow of commonly used strains of inbred mice: variations in yield, growth, and differentiation. *Journal of Cellular Biochemistry*. **72**, 570-585.

Phinney DG , Pittenger MF (2017). Concise Review: MSC-Derived Exosomes for Cell-Free Therapy. *Stem Cells*. **35**, 851-858.

Pipan CM, Glasheen WP, Matthew TL, Gonias SL, Hwang LJ, Jane JA , Spotnitz WD (1992). Effects of antifibrinolytic agents on the life span of fibrin sealant. *The Journal of Surgical Research*. **53**, 402-407.

Pittenger MF, Mackay AM, Beck SC, Jaiswal RK, Douglas R, Mosca JD, Moorman MA, Simonetti DW, Craig S , Marshak DR (1999). Multilineage potential of adult human mesenchymal stem cells. *Science*. **284**, 143-147.

Plumas J, Chaperot L, Richard MJ, Molens JP, Bensa JC , Favrot MC (2005). Mesenchymal stem cells induce apoptosis of activated T cells. *Leukemia*. **19**, 1597-1604.

Polk BI , Rosenwasser LJ (2017). Biological Therapies of Immunologic Diseases: Strategies for Immunologic Interventions. *Immunology and Allergy Clinics of North America*. **37**, 247-259.

Pountos I, Georgouli T, Blokhuis TJ, Pape HC , Giannoudis PV (2008). Pharmacological agents and impairment of fracture healing: what is the evidence? *Injury*. **39**, 384-394.

Powell WF, Jr., Barry KJ, Tulum I, Kobayashi T, Harris SE, Bringhurst FR , Pajevic PD (2011). Targeted ablation of the PTH/PTHrP receptor in osteocytes impairs bone structure and homeostatic calcemic responses. *The Journal of Endocrinology*. **209**, 21-32.

Prabhala RH, Pelluru D, Fulciniti M, Prabhala HK, Nanjappa P, Song W, Pai C, Amin S, Tai YT, Richardson PG, Ghobrial IM, Treon SP, Daley JF, Anderson KC, Kutok JL , Munshi NC (2010). Elevated IL-17 produced by TH17 cells promotes myeloma cell growth and inhibits immune function in multiple myeloma. *Blood*. **115**, 5385-5392.

Qiu Y, Lam JK, Leung SW , Liang W (2016). Delivery of RNAi Therapeutics to the Airways-From Bench to Bedside. *Molecules*. **21**.

Raggatt LJ, Wullschleger ME, Alexander KA, Wu AC, Millard SM, Kaur S, Maugham ML, Gregory LS, Steck R , Pettit AR (2014). Fracture healing via periosteal callus formation requires macrophages for both initiation and progression of early endochondral ossification. *The American Journal of Pathology*. **184**, 3192-3204.

Raicevic G, Rouas R, Najar M, Stordeur P, Boufker HI, Bron D, Martiat P, Goldman M, Nevessignsky MT , Lagneaux L (2010). Inflammation modifies the pattern and the function of Toll-like receptors expressed by human mesenchymal stromal cells. *Human Immunology*. **71**, 235-244.

Ramaswamy G, Kim H, Zhang D, Lounev V, Wu JY, Choi Y, Kaplan FS, Pignolo RJ , Shore EM (2017). Gsalpha Controls Cortical Bone Quality by Regulating Osteoclast Differentiation via cAMP/PKA and beta-Catenin Pathways. *Scientific Reports*. **7**, 45140.

Ravichandran R, Venugopal JR, Sundarrajan S, Mukherjee S , Ramakrishna S (2011). Poly(Glycerol sebacate)/gelatin core/shell fibrous structure for regeneration of myocardial infarction. *Tissue Engineering. Part A*. **17**, 1363-1373.

Reagan WJ, Irizarry-Rovira A, Poitout-Belissent F, Bolliger AP, Ramaiah SK, Travlos G, Walker D, Bounous D , Walter G (2011). Best practices for evaluation of bone marrow in nonclinical toxicity studies. *Veterinary Clinical Pathology*. **40**, 119-134.

Reichert JC, Saifzadeh S, Wullschleger ME, Epari DR, Schutz MA, Duda GN, Schell H, van Griensven M, Redl H , Hutmacher DW (2009). The challenge of establishing preclinical models for segmental bone defect research. *Biomaterials*. **30**, 2149-2163.

Reinke S, Geissler S, Taylor WR, Schmidt-Bleek K, Juelke K, Schwachmeyer V, Dahne M, Hartwig T, Akyuz L, Meisel C, Unterwalder N, Singh NB, Reinke P, Haas NP, Volk HD , Duda GN (2013). Terminally differentiated CD8(+) T cells negatively affect bone regeneration in humans. *Science Translational Medicine*. **5**, 177ra136.

Ren G, Zhang L, Zhao X, Xu G, Zhang Y, Roberts AI, Zhao RC , Shi Y (2008). Mesenchymal stem cell-mediated immunosuppression occurs via concerted action of chemokines and nitric oxide. *Cell stem cell*. **2**, 141-150.

Rice JJ, Martino MM, De Laporte L, Tortelli F, Briquez PS , Hubbell JA (2013). Engineering the regenerative microenvironment with biomaterials. *Advanced Healthcare Materials*. **2**, 57-71.

Riemekasten G, Hoffmann U, Sunderkotter C, Weiss N , Kuhn A (2012). [Management of digital ulcers in patients with systemic sclerosis]. *Deutsche Medizinische Wochenschrift*. **137**, 34-40.

Riley JL, June CH , Blazar BR (2009). Human T regulatory cell therapy: take a billion or so and call me in the morning. *Immunity*. **30**, 656-665.

Ritchlin CT, Haas-Smith SA, Li P, Hicks DG , Schwarz EM (2003). Mechanisms of TNF-alpha- and RANKL-mediated osteoclastogenesis and bone resorption in psoriatic arthritis. *The Journal of Clinical Investigation*. **111**, 821-831.

Roch F , Bach MA (1991). Strain differences in mouse cellular responses to Mycobacterium lepraemurium and BCG subcutaneous infections. II. Production of interleukins 2, 4, and 6 and of interferon-gamma by draining lymph node cells. *Clinical Immunology and Immunopathology*. **60**, 443-454.

Roman A, Barbera JA, Escribano P, Sala ML, Febrer L, Oyaguez I, Sabater E , Casado MA (2012). Cost effectiveness of prostacyclins in pulmonary arterial hypertension. *Applied Health Economics and Health Policy*. **10**, 175-188.

Rowe SL, Lee S , Stegemann JP (2007). Influence of thrombin concentration on the mechanical and morphological properties of cell-seeded fibrin hydrogels. *Acta Biomaterialia*. **3**, 59-67.

Royce SM, Askari M , Marra KG (2004). Incorporation of polymer microspheres within fibrin scaffolds for the controlled delivery of FGF-1. *Journal of Biomaterials Science, Polymer Edition*. **15**, 1327-1336.

Ryaby JT (1998). Clinical effects of electromagnetic and electric fields on fracture healing. *Clinical Orthopaedics and Related Research*, S205-215.

Sahni A, Guo M, Sahni SK , Francis CW (2004). Interleukin-1beta but not IL-1alpha binds to fibrinogen and fibrin and has enhanced activity in the bound form. *Blood*. **104**, 409-414.

Sahni A, Odrljin T , Francis CW (1998). Binding of basic fibroblast growth factor to fibrinogen and fibrin. *The Journal of Biological Chemistry*. **273**, 7554-7559.

Sakaguchi S, Yamaguchi T, Nomura T , Ono M (2008). Regulatory T cells and immune tolerance. *Cell*. **133**, 775-787.

Sakiyama-Elbert SE , Hubbell JA (2000). Development of fibrin derivatives for controlled release of heparin-binding growth factors. *Journal of Controlled Release: Official Journal of the Controlled Release Society*. **65**, 389-402.

Sallusto F, Geginat J , Lanzavecchia A (2004). Central memory and effector memory T cell subsets: function, generation, and maintenance. *Annual Review of Immunology*. **22**, 745-763.

Sandberg O , Aspenberg P (2015). Different effects of indomethacin on healing of shaft and metaphyseal fractures. *Acta Orthopaedica*. **86**, 243-247.

Sandel PC, Gendelman M, Kelsoe G , Monroe JG (2001). Definition of a novel cellular constituent of the bone marrow that regulates the response of immature B cells to B cell antigen receptor engagement. *Journal of Immunology*. **166**, 5935-5944.

Sass FA, Fuchs M, Pumberger M, Geissler S, Duda GN, Perka C , Schmidt-Bleek K (2018). Immunology Guides Skeletal Muscle Regeneration. *International Journal of Molecular Sciences*. **19**.

Sawitzki B, Kieselbach B, Fisser M, Meisel C, Vogt K, Gaestel M, Lehmann M, Risch K, Grutz G , Volk HD (2004). IFN-gamma regulation in anti-CD4 antibody-induced T cell unresponsiveness. *Journal of the American Society of Nephrology*. **15**, 695-703.

Schell H, Duda GN, Peters A, Tsitsilonis S, Johnson KA , Schmidt-Bleek K (2017). The haematoma and its role in bone healing. *Journal of Experimental Orthopaedics*. **4**, 5.

Schell H, Thompson MS, Bail HJ, Hoffmann JE, Schill A, Duda GN , Lienau J (2008). Mechanical induction of critically delayed bone healing in sheep: radiological and biomechanical results. *Journal of Biomechanics*. **41**, 3066-3072.

Scheller EL, Doucette CR, Learman BS, Cawthorn WP, Khandaker S, Schell B, Wu B, Ding SY, Bredella MA, Fazeli PK, Khoury B, Jepsen KJ, Pilch PF, Klibanski A, Rosen CJ , MacDougald OA (2016). Corrigendum: Region-specific variation in the properties of skeletal adipocytes reveals regulated and constitutive marrow adipose tissues. *Nature Communications*. **7**, 13775.

Schindeler A, Liu R , Little DG (2009). The contribution of different cell lineages to bone repair: exploring a role for muscle stem cells. *Differentiation; Research in Biological Diversity*. **77**, 12-18.

Schirrmacher V, Feuerer M, Fournier P, Ahlert T, Umansky V , Beckhove P (2003). T-cell priming in bone marrow: the potential for long-lasting protective anti-tumor immunity. *Trends Mol Med*. **9**, 526-534.

Schlundt C, El Khassawna T, Serra A, Dienelt A, Wendler S, Schell H, van Rooijen N, Radbruch A, Lucius R, Hartmann S, Duda GN , Schmidt-Bleek K (2015). Macrophages in bone fracture healing: Their essential role in endochondral ossification. *Bone*.

Schmidt-Bleek K, Kwee BJ, Mooney DJ , Duda GN (2015). Boon and Bane of Inflammation in Bone Tissue Regeneration and Its Link with Angiogenesis. *Tissue Engineering. Part B, Reviews*. **21**, 354-364.

Schmidt-Bleek K, Petersen A, Dienelt A, Schwarz C , Duda GN (2014). Initiation and early control of tissue regeneration - bone healing as a model system for tissue regeneration. *Expert Opinion on Biological Therapy*. **14**, 247-259.

Schmidt-Bleek K, Schell H, Kolar P, Pfaff M, Perka C, Buttgereit F, Duda G , Lienau J (2009). Cellular composition of the initial fracture hematoma compared to a muscle hematoma: a study in sheep. *Journal of Orthopaedic Research: Official Publication of the Orthopaedic Research Society*. **27**, 1147-1151.

Schmidt-Bleek K, Schell H, Lienau J, Schulz N, Hoff P, Pfaff M, Schmidt G, Martin C, Perka C, Buttgereit F, Volk HD , Duda G (2012a). Initial immune reaction and angiogenesis in bone healing. *Journal of Tissue Engineering and Regenerative Medicine*.

Schmidt-Bleek K, Schell H, Schulz N, Hoff P, Perka C, Buttgereit F, Volk HD, Lienau J , Duda GN (2012b). Inflammatory phase of bone healing initiates the regenerative healing cascade. *Cell and Tissue Research*. **347**, 567-573.

Schmoekel HG, Weber FE, Schense JC, Gratz KW, Schawalder P , Hubbell JA (2005). Bone repair with a form of BMP-2 engineered for incorporation into fibrin cell ingrowth matrices. *Biotechnology and Bioengineering*. **89**, 253-262.

Scypinski S, Lanzano RL , Soltero RA (1990). Determination of iloprost in 5% dextrose in water solution by reversed-phase high performance liquid chromatography. *Journal of Pharmaceutical Sciences*. **79**, 934-937.

Shortman K , Heath WR (2010). The CD8+ dendritic cell subset. *Immunological Reviews*. **234**, 18-31.

Shouval DS, Ouahed J, Biswas A, Goettel JA, Horwitz BH, Klein C, Muise AM , Snapper SB (2014). Interleukin 10 receptor signaling: master regulator of intestinal mucosal homeostasis in mice and humans. *Advances in Immunology*. **122**, 177-210.

Sidney LE, Kirkham GR , Buttery LD (2014). Comparison of osteogenic differentiation of embryonic stem cells and primary osteoblasts revealed by responses to IL-1beta, TNF-alpha, and IFN-gamma. *Stem Cells and Development*. **23**, 605-617.

Sieber S, Wirth L, Cavak N, Koenigsmark M, Marx U, Lauster R , Rosowski M (2018). Bone marrow-on-a-chip: Long-term culture of human haematopoietic stem cells in a three-dimensional microfluidic environment. *Journal of Tissue Engineering and Regenerative Medicine*. **12**, 479-489.

Sierra DH (1993). Fibrin sealant adhesive systems: a review of their chemistry, material properties and clinical applications. *Journal of Biomaterials Applications*. **7**, 309-352.

Simon-Assmann P, Orend G, Mammadova-Bach E, Spenle C , Lefebvre O (2011). Role of laminins in physiological and pathological angiogenesis. *The International Journal of Developmental Biology*. **55**, 455-465.

Simon AM , O'Connor JP (2007). Dose and time-dependent effects of cyclooxygenase-2 inhibition on fracture-healing. *The Journal of Bone and Joint Surgery. American Volume*. **89**, 500-511.

Singh N, Karambelkar A, Gu L, Lin K, Miller JS, Chen CS, Sailor MJ , Bhatia SN (2011). Bioresponsive mesoporous silica nanoparticles for triggered drug release. *Journal of the American Chemical Society*. **133**, 19582-19585.

Sjogren K, Engdahl C, Henning P, Lerner UH, Tremaroli V, Lagerquist MK, Backhed F , Ohlsson C (2012). The gut microbiota regulates bone mass in mice. *Journal of Bone and Mineral Research*. **27**, 1357-1367.

Sjoland JA, Sidelmann JJ, Brabrand M, Pedersen RS, Pedersen JH, Esbensen K, Standeven KF, Ariens RA , Gram J (2007). Fibrin clot structure in patients with end-stage renal disease. *Journal of Thrombosis and Haemostasis*. **98**, 339-345.

Skovgaard C, Holm B, Troelsen A, Lunn TH, Gaarn-Larsen L, Kehlet H , Husted H (2013). No effect of fibrin sealant on drain output or functional recovery following simultaneous bilateral total knee arthroplasty: a randomized, double-blind, placebo-controlled study. *Acta Orthopaedica*. **84**, 153-158.

Soehnlein O , Lindbom L (2010). Phagocyte partnership during the onset and resolution of inflammation. *Nature Reviews Immunology*. **10**, 427-439.

Spaggiari GM, Capobianco A, Abdelrazik H, Becchetti F, Mingari MC , Moretta L (2008). Mesenchymal stem cells inhibit natural killer-cell proliferation, cytotoxicity, and cytokine production: role of indoleamine 2,3-dioxygenase and prostaglandin E2. *Blood*. **111**, 1327-1333.

Spicer PP , Mikos AG (2010). Fibrin glue as a drug delivery system. *Journal of Controlled Release: Official Journal of the Controlled Release Society*. **148**, 49-55.

Stagg J , Galipeau J (2013). Mechanisms of immune modulation by mesenchymal stromal cells and clinical translation. *Current Molecular Medicine*. **13**, 856-867.

Stitham J, Midgett C, Martin KA , Hwa J (2011). Prostacyclin: an inflammatory paradox. *Frontiers in Pharmacology*. **2**, 24.

Strassheim D, Riddle SR, Burke DL, Geraci MW , Stenmark KR (2009). Prostacyclin inhibits IFN-gamma-stimulated cytokine expression by reduced recruitment of CBP/p300 to STAT1 in a SOCS-1-independent manner. *Journal of Immunology*. **183**, 6981-6988.

Sun J, Song B, Zhang L, Shao Q, Liu Y, Yuan D, Zhang Y , Qu X (2016). Fucoidan inhibits CCL22 production through NF-kappaB pathway in M2 macrophages: a potential therapeutic strategy for cancer. *Scientific Reports*. **6**, 35855.

Suuronen R, Kontio R, Ashammakhi N, Lindqvist C , Laine P (2004). Bioabsorbable self-reinforced plates and screws in craniomaxillofacial surgery. *Bio-Medical Materials and Engineering*. **14**, 517-524.

Suzawa M, Takada I, Yanagisawa J, Ohtake F, Ogawa S, Yamauchi T, Kadowaki T, Takeuchi Y, Shibuya H, Gotoh Y, Matsumoto K , Kato S (2003). Cytokines suppress adipogenesis and PPAR-gamma function through the TAK1/TAB1/NIK cascade. *Nature Cell Biology*. **5**, 224-230.

Takayanagi H (2005). Inflammatory bone destruction and osteoimmunology. *Journal of Periodontal Research*. **40**, 287-293.

Teramoto T, Kiss A , Thorgeirsson SS (1998). Induction of p53 and Bax during TGF-beta 1 initiated apoptosis in rat liver epithelial cells. *Biochemical and Biophysical Research Communications*. **251**, 56-60.

Tillmann FP, Jager M, Blondin D, Schooldermann D, Voiculescu A, Sucker C, Grabensee B, Krauspe R , Hetzel GR (2007). Intravenous iloprost: a new therapeutic option for patients with post-transplant distal limb syndrome (PTDLS). *American Journal of Transplantation.* **7**, 667-671.

Tiwari SK, Tzezana R, Zussman E , Venkatraman SS (2010). Optimizing partition-controlled drug release from electrospun core-shell fibers. *International Journal of Pharmaceutics*. **392**, 209-217.

Toben D, Schroeder I, El Khassawna T, Mehta M, Hoffmann JE, Frisch JT, Schell H, Lienau J, Serra A, Radbruch A , Duda GN (2011). Fracture healing is accelerated in the absence of the adaptive immune system. *Journal of Bone and Mineral Research: the Official Journal of the American Society for Bone and Mineral Research*. **26**, 113-124.

Toskas G, Cherif C, Hund RD, Laourine E, Mahltig B, Fahmi A, Heinemann C , Hanke T (2013). Chitosan(PEO)/silica hybrid nanofibers as a potential biomaterial for bone regeneration. *Carbohydrate Polymers*. **94**, 713-722.

Tran DQ (2012). TGF-beta: the sword, the wand, and the shield of FOXP3(+) regulatory T cells. *J Mol Cell Biol*. **4**, 29-37.

Trandem K, Zhao J, Fleming E , Perlman S (2011). Highly activated cytotoxic CD8 T cells express protective IL-10 at the peak of coronavirus-induced encephalitis. *Journal of Immunology*. **186**, 3642-3652.

Tripp RA, Topham DJ, Watson SR , Doherty PC (1997). Bone marrow can function as a lymphoid organ during a primary immune response under conditions of disrupted lymphocyte trafficking. *Journal of Immunology*. **158**, 3716-3720.

Truchetet ME, Allanore Y, Montanari E, Chizzolini C , Brembilla NC (2012). Prostaglandin I(2) analogues enhance already exuberant Th17 cell responses in systemic sclerosis. *Annals of the Rheumatic Diseases*. **71**, 2044-2050.

Tsai MK, Hsieh CC, Kuo HF, Yang SN, Kuo CH, Huang MY, Tsai YM, Lee MS , Hung CH (2014). Effect of prostaglandin I2 analogs on macrophage inflammatory protein 1alpha in human monocytes via I prostanoid receptor and cyclic adenosine monophosphate. *Journal of Investigative Medicine*. **62**, 332-339.

Tsiridis E, Upadhyay N , Giannoudis P (2007). Molecular aspects of fracture healing: which are the important molecules? *Injury*. **38 Suppl 1**, S11-25.

Tsuji K, Bandyopadhyay A, Harfe BD, Cox K, Kakar S, Gerstenfeld L, Einhorn T, Tabin CJ , Rosen V (2006). BMP2 activity, although dispensable for bone formation, is required for the initiation of fracture healing. *Nature Genetics*. **38**, 1424-1429.

van de Vijver E, Maddalena A, Sanal O, Holland SM, Uzel G, Madkaikar M, de Boer M, van Leeuwen K, Koker MY, Parvaneh N, Fischer A, Law SK, Klein N, Tezcan FI, Unal E, Patiroglu T, Belohradsky BH, Schwartz K, Somech R, Kuijpers TW , Roos D (2012). Hematologically important mutations: leukocyte adhesion deficiency (first update). *Blood Cells, Molecules and Diseases*. **48**, 53-61.

van Maurik A, Herber M, Wood KJ , Jones ND (2002). Cutting edge: CD4+CD25+ alloantigen-specific immunoregulatory cells that can prevent CD8+ T cell-mediated graft rejection: implications for anti-CD154 immunotherapy. *Journal of Immunology*. **169**, 5401-5404.

Van Vlasselaer P, Borremans B, Van Den Heuvel R, Van Gorp U , de Waal Malefyt R (1993). Interleukin-10 inhibits the osteogenic activity of mouse bone marrow. *Blood*. **82**, 2361-2370.

Van Vlasselaer P, Borremans B, van Gorp U, Dasch JR , De Waal-Malefyt R (1994). Interleukin 10 inhibits transforming growth factor-beta (TGF-beta) synthesis required for osteogenic commitment of mouse bone marrow cells. *Journal of Cell Biology*. **124**, 569-577.

Ventura MT, Casciaro M, Gangemi S , Buquicchio R (2017). Immunosenescence in aging: between immune cells depletion and cytokines up-regulation. *Clinical and Molecular Allergy*. **15**, 21.

Volz M, Schaumburger J, Frick H, Grifka J , Anders S (2017). A randomized controlled trial demonstrating sustained benefit of Autologous Matrix-Induced Chondrogenesis over microfracture at five years. *International Orthopaedics*. **41**, 797-804.

Vremec D, Pooley J, Hochrein H, Wu L , Shortman K (2000). CD4 and CD8 expression by dendritic cell subtypes in mouse thymus and spleen. *Journal of Immunology*. **164**, 2978-2986.

Wagner W, Wiltfang J, Pistner H, Yildirim M, Ploder B, Chapman M, Schiestl N , Hantak E (2012). Bone formation with a biphasic calcium phosphate combined with fibrin sealant in maxillary sinus floor elevation for delayed dental implant. *Clinical Oral Implants Research*. **23**, 1112-1117.

Waldmann E, Vogt A, Crispin A, Altenhofer J, Riks I , Parhofer KG (2017). Effect of mipomersen on LDL-cholesterol in patients with severe LDL-hypercholesterolaemia and atherosclerosis treated by lipoprotein apheresis (The MICA-Study). *Atherosclerosis*. **259**, 20-25.

Walker LS , Sansom DM (2011). The emerging role of CTLA4 as a cell-extrinsic regulator of T cell responses. *Nature Reviews Immunology*. **11**, 852-863.

Wan C, Gilbert SR, Wang Y, Cao X, Shen X, Ramaswamy G, Jacobsen KA, Alaql ZS, Eberhardt AW, Gerstenfeld LC, Einhorn TA, Deng L , Clemens TL (2008). Activation of the hypoxia-inducible factor-1alpha pathway accelerates bone regeneration. *Proceedings of the National Academy of Sciences of the United States of America*. **105**, 686-691.

Wang H, Yang L , Rempel GL (2014). Preparation of pH-responsive polymer core-shell nanospheres for delivery of hydrophobic antineoplastic drug ellipticine. *Macromolecular Bioscience*. **14**, 166-172.

Wang SS, Yang MC , Chung TW (2008). Liposomes/chitosan scaffold/human fibrin gel composite systems for delivering hydrophilic drugs--release behaviors of tirofiban in vitro. *Drug Delivery*. **15**, 149-157.

Wang X, Friis T, Glatt V, Crawford R , Xiao Y (2017). Structural properties of fracture haematoma: current status and future clinical implications. *Journal of Tissue Engineering and Regenerative Medicine*. **11**, 2864-2875.

Wang X, Friis TE, Masci PP, Crawford RW, Liao W , Xiao Y (2016). Alteration of blood clot structures by interleukin-1 beta in association with bone defects healing. *Sci Rep*. **6**, 35645.

Waterman RS, Tomchuck SL, Henkle SL , Betancourt AM (2010). A new mesenchymal stem cell (MSC) paradigm: polarization into a pro-inflammatory MSC1 or an Immunosuppressive MSC2 phenotype. *PLOS ONE*. **5**, e10088.

Weinreb M, Rutledge SJ , Rodan GA (1997). Systemic administration of an anabolic dose of prostaglandin E2 induces early-response genes in rat bones. *Bone*. **20**, 347-353.

Wendeberg B (1961). Mineral metabolism of fractures of the tibia in man studied with external counting of Sr85. *Acta Orthopaedica Scandinavica. Supplementum*. **52**, 1-79.

Wendler S, Hartmann N, Hoppe B , Englert C (2015). Age-dependent decline in fin regenerative capacity in the short-lived fish Nothobranchius furzeri. *Aging Cell*. **14**, 857-866.

Wendler S, Schlundt C, Bucher CH, Birkigt J, Schipp CJ, Volk HD, Duda GN , Schmidt-Bleek K (2019). Immune Modulation to Enhance Bone Healing-A New Concept to Induce Bone Using Prostacyclin to Locally Modulate Immunity. *Frontiers in Immunology*. **10**, 713.

Weninger W, Crowley MA, Manjunath N , von Andrian UH (2001). Migratory properties of naive, effector, and memory CD8(+) T cells. *The Journal of Experimental Medicine*. **194**, 953-966.

Wiemer AJ, Hegde S, Gumperz JE , Huttenlocher A (2011). A live imaging cell motility screen identifies prostaglandin E2 as a T cell stop signal antagonist. *Journal of Immunology*. **187**, 3663-3670.

Wilson SR, Peters C, Saftig P , Bromme D (2009). Cathepsin K activity-dependent regulation of osteoclast actin ring formation and bone resorption. *The Journal of Biological Chemistry*. **284**, 2584-2592.

Woo EJ (2013). Adverse events after recombinant human BMP2 in nonspinal orthopaedic procedures. *Clinical Orthopaedics and Related Research*. **471**, 1707-1711.

Woo KM, Chen VJ , Ma PX (2003). Nano-fibrous scaffolding architecture selectively enhances protein adsorption contributing to cell attachment. *Journal of Biomedical Materials Research Part A*. **67**, 531-537.

Xia S, Zhang X, Zheng S, Khanabdali R, Kalionis B, Wu J, Wan W , Tai X (2016). An Update on Inflamm-Aging: Mechanisms, Prevention, and Treatment. *Journal of Immunology Research*. **2016**, 8426874.

Xing Z, Lu C, Hu D, Miclau T, 3rd , Marcucio RS (2010). Rejuvenation of the inflammatory system stimulates fracture repair in aged mice. *Journal of Orthopaedic Research*. **28**, 1000-1006.

Yang HS, La WG, Cho YM, Shin W, Yeo GD , Kim BS (2012). Comparison between heparin-conjugated fibrin and collagen sponge as bone morphogenetic protein-2 carriers for bone regeneration. *Experimental & Molecular Medicine*. **44**, 350-355.

Yang L, Tsang KY, Tang HC, Chan D , Cheah KS (2014). Hypertrophic chondrocytes can become osteoblasts and osteocytes in endochondral bone formation. *Proceedings of the National Academy of Sciences of the United States of America*. **111**, 12097-12102.

Yang X, Ricciardi BF, Hernandez-Soria A, Shi Y, Pleshko Camacho N , Bostrom MP (2007). Callus mineralization and maturation are delayed during fracture healing in interleukin-6 knockout mice. *Bone*. **41**, 928-936.

Yang Y, Li X, Qi M, Zhou S , Weng J (2008). Release pattern and structural integrity of lysozyme encapsulated in core-sheath structured poly(DL-lactide) ultrafine fibers prepared by emulsion electrospinning. *European Journal of Pharmaceutics and Biopharmaceutics*. **69**, 106-116.

Yin W, Pauza K, Olan WJ, Doerzbacher JF , Thorne KJ (2014). Intradiscal injection of fibrin sealant for the treatment of symptomatic lumbar internal disc disruption: results of a prospective multicenter pilot study with 24-month follow-up. *Pain Medicine*. **15**, 16-31.

Yoshida H, Yamaoka Y, Shinoyama M , Kamiya A (2000). Novel drug delivery system using autologous fibrin glue--release properties of anti-cancer drugs. *Biological & Pharmaceutical Bulletin*. **23**, 371-374.

Zaiss MM, Axmann R, Zwerina J, Polzer K, Guckel E, Skapenko A, Schulze-Koops H, Horwood N, Cope A , Schett G (2007). Treg cells suppress osteoclast formation: a new link between the immune system and bone. *Arthritis & Rheumatology*. **56**, 4104-4112.

Zaiss MM, Frey B, Hess A, Zwerina J, Luther J, Nimmerjahn F, Engelke K, Kollias G, Hunig T, Schett G , David JP (2010). Regulatory T cells protect from local and systemic bone destruction in arthritis. *Journal of Immunology*. **184**, 7238-7246.

Zeckey C, Mommsen P, Andruszkow H, Macke C, Frink M, Stubig T, Hufner T, Krettek C , Hildebrand F (2011). The aseptic femoral and tibial shaft non-union in healthy patients - an analysis of the health-related quality of life and the socioeconomic outcome. *The Open Orthopaedics Journal*. **5**, 193-197.

Zeng D, Hoffmann P, Lan F, Huie P, Higgins J , Strober S (2002). Unique patterns of surface receptors, cytokine secretion, and immune functions distinguish T cells in the bone marrow from those in the periphery: impact on allogeneic bone marrow transplantation. *Blood*. **99**, 1449-1457.

Zhao E, Wang L, Dai J, Kryczek I, Wei S, Vatan L, Altuwaijri S, Sparwasser T, Wang G, Keller ET , Zou W (2012a). Regulatory T cells in the bone marrow microenvironment in patients with prostate cancer. *OncoImmunology*. **1**, 152-161.

Zhao E, Xu H, Wang L, Kryczek I, Wu K, Hu Y, Wang G , Zou W (2012b). Bone marrow and the control of immunity. *Cellular & Molecular Immunology*. **9**, 11-19.

Zhou Q, Yang C , Yang P (2017). The Promotional Effect of Mesenchymal Stem Cell Homing on Bone Tissue Regeneration. *Current Stem Cell Research & Therapy*. **12**, 365-376.

Zhou W, Blackwell TS, Goleniewska K, O'Neal JF, Fitzgerald GA, Lucitt M, Breyer RM , Peebles RS, Jr. (2007a). Prostaglandin I2 analogs inhibit Th1 and Th2 effector cytokine production by CD4 T cells. *Journal of Leukocyte Biology*. **81**, 809-817.

Zhou W, Hashimoto K, Goleniewska K, O'Neal JF, Ji S, Blackwell TS, Fitzgerald GA, Egan KM, Geraci MW , Peebles RS, Jr. (2007b). Prostaglandin I2 analogs inhibit proinflammatory cytokine production and T cell stimulatory function of dendritic cells. *Journal of Immunology*. **178**, 702-710.

Zhou X, von der Mark K, Henry S, Norton W, Adams H , de Crombrugghe B (2014). Chondrocytes transdifferentiate into osteoblasts in endochondral bone during development, postnatal growth and fracture healing in mice. *PLOS Genetics*. **10**, e1004820.

Zhu H, Guo ZK, Jiang XX, Li H, Wang XY, Yao HY, Zhang Y , Mao N (2010). A protocol for isolation and culture of mesenchymal stem cells from mouse compact bone. *Nature Protocols*. **5**, 550-560.

Zhu H, Yu D, Zhou Y, Wang C, Gao M, Jiang H , Wang H (2013). Biological activity of a nanofibrous barrier membrane containing bone morphogenetic protein formed by core-shell electrospinning as a sustained delivery vehicle. *Journal of Biomedical Materials Research. Part B, Applied Biomaterials*. **101**, 541-552.

Zhu XH, Wang CH , Tong YW (2009). In vitro characterization of hepatocyte growth factor release from PHBV/PLGA microsphere scaffold. *Journal of Biomedical Materials Research Part A*. **89**, 411-423.

Ziegler SF (2016). Division of labour by CD4(+) T helper cells. *Nature Reviews Immunology.* **16**, 403.

Zou L, Barnett B, Safah H, Larussa VF, Evdemon-Hogan M, Mottram P, Wei S, David O, Curiel TJ , Zou W (2004). Bone marrow is a reservoir for CD4+CD25+ regulatory T cells that traffic through CXCL12/CXCR4 signals. *Cancer Research*. **64**, 8451-8455.

Zou W , Restifo NP (2010). T(H)17 cells in tumour immunity and immunotherapy. *Nature Reviews Immunology*. **10**, 248-256.